Turbulent Combustion Modeling

Denis VEYNANTE *
Laboratoire E.M2.C.
CNRS et Ecole Centrale Paris
Grande Voie des Vignes
92295 Châtenay-Malabry Cedex, France

Luc VERVISCH †
Institut National des Sciences Appliquées de Rouen
UMR CNRS 6614 / CORIA
Campus du Madrillet
Avenue de l'Université - BP 8
76801 Saint Etienne du Rouvray Cedex, France

Nota: Ce cours a été donné dans le cadre des Lecture Series du Von Karman Institute (Belgique) en 1999, 2001 et 2003. Une partie a fait l'objet d'un article de revue dans *Progress in Energy and Combustion Science* en 2002.

*e-mail : denis@em2c.ecp.fr ; Tel : +33 (0)1 41 13 10 80 ; Fax : +33 (0)1 47 02 80 35
†e-mail : vervisch@coria.fr ; Tel : +33 (0)2 32 95 97 85 ; Fax : +33 (0)2 32 95 97 80

Foreword

Numerical simulation of flames is a growing field bringing important improvements to our understanding of combustion. The main issues and related closures of turbulent combustion modeling are reviewed. Combustion problems involve strong coupling between chemistry, transport and fluid dynamics. The basic properties of laminar flames are first presented along with the major tools developed for modeling turbulent combustion. The links between the available closures are enlighted from a generic description of modeling tools. Then, examples of numerical models for mean burning rates are discussed for premixed turbulent combustion. The use of direct numerical simulation (DNS) as a research instrument is illustrated for turbulent transport occurring in premixed combustion, gradient and counter-gradient modeling of turbulent fluxes is addressed. Finally, a review of the models for nonpremixed turbulent flames is given.

Contents

1 Introduction

The number of combustion systems used in transformation and transportation industries is rapidly growing. This induces pollution and environmental problems becoming critical factors in our societies. The accurate control of turbulent flames therefore appears as a real challenge.

Computing is now truly on a par with experiment and theory as a research tool to produce multiscale information that is not available by using any other technique. Computational fluid dynamics (CFD) is efficiently used to improve the design of aerodynamical systems, and today no real progress in design can be made without using CFD. With the same objectives, much works have been devoted to turbulent combustion modeling, following a variety of approaches and distinct modeling strategies. This paper is intended to provide a generic review of these numerical models.

A wide range of coupled problems are involved in turbulent flames:

- The **fluid mechanical** properties of the combustion system must be well known to carefully describe the mixing between reactants and, more generally, all transfer phenomena occurring in turbulent flames (heat transfer, molecular diffusion, convection, turbulent transport...).
- **Detailed chemical reaction schemes** are necessary to estimate the consumption rate of the fuel, the formation of combustion products and pollutant species. A precise knowledge of the chemistry is absolutely required to predict ignition, stabilization or extinction of reaction zones together with pollution.
- **Two (liquid fuel) and three (solid fuel) phase systems** may be encountered. Liquid fuel injection is a common procedure and the three-dimensional spatial distribution of gaseous reactants depends on complex interactions between the breakdown of the liquid sheets, the vaporization of the liquid, turbulent mixing, and droplet combustion.
- **Radiative heat transfer** is generated within the flame by some species and carbon particles resulting from soot formation and transported by the flow motions. In furnaces, walls also interact with combustion through radiative transfer.

Turbulent combustion modeling is therefore a very broad subject. All the aspects of the problem are not addressed in the present review. We will only focus on the closure schemes developed and used to understand and calculate turbulent transport and mean burning rates in turbulent flames. The detail of chemistry, its reduction, tabulation, ... are not considered. However, the links existing between the models are evidenced, similitude which is sometimes much stronger than usually though.

Numerical modeling of flames is developed from the following steps (Fig. 1):

- Under assumptions such as high activation energy limit, **asymptotic analysis** [1, 2, 3] allows the analytical determination of flame properties in well-defined model problems (ignition, propagation of flame front, instabilities and acoustics, ...). This approach, limited to simplified situations, leads to analytical results exhibiting helpful scale factors (dimensionless numbers) and major flame behaviors. Asymptotic analysis is particularly well suited to perform quantitative comparison between various phenomena.
- **Simplified experiments** are useful to understand the basic properties of combustion (laminar flames, flame / vortex interactions,...) [4, 5]. These experiments are accompanied by **numerical simulations** of laminar flames incorporating complex chemistry and multi-species transports along with radiative heat losses [6].
- For given chemistry and transport model, in **direct numerical simulation** (DNS) all the scales of the turbulence (time and length) are calculated without resorting to closures for turbulent fluxes

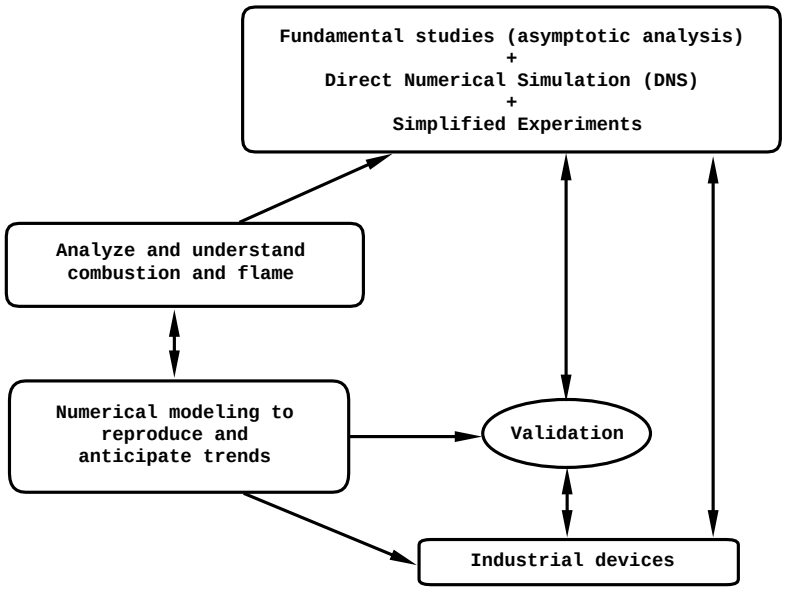

Figure 1: Combustion modeling steps

and mean burning rate. Turbulent flames are analyzed in simple configurations to extract data impossible to measure in experiments, and to isolate some specific phenomena (heat release, Lewis number, ...) [7, 8, 9, 10, 11].

Because of the large number of degrees of freedom involved in turbulent combustion, a full DNS of a practical system cannot be performed and averaging techniques leading to unclosed equations are necessary. **Models for turbulent flames** are then developed: closure techniques are proposed for unknown terms found in exact averaged balance equations. Once the models have been implemented in numerical codes, **validation procedures** are required. The numerical modeling is validated against measurements obtained from experiments. Configurations as close as possible to actual industrial systems are chosen for these tests. Then, the ultimate step is the simulation of a real combustion device.

The decomposition discussed in Fig. 1 is quite formal. Turbulent combustion modeling is actually a continuous ring between theoretical studies to analyze combustion, understand flames and improve models, implementation of these models into CFD, experimental measurements and comparison between these experimental data and the numerical results...

Following a short presentation of the balance equations for reactive flows (§ 2), a first part is devoted to a brief description of laminar flames (§ 3). After a presentation of the unsuccessful Taylor's expansion for closing the mean burning rate (§ 4), the physical analysis leading to turbulent combustion diagrams is developed (§ 5). Then, modeling tools available to derive turbulent combustion models are described and the relations between a priori quite different formalisms are evidenced (§ 6). The next three sections are devoted to combustion modeling in the context of Reynolds Averaged Navier-Stokes (RANS) equations. For premixed turbulent combustion, one reviews the available closures for the mean reaction rate (§ 7) and turbulent transport (§ 8). In a subsequent section (§ 9), the modeling of the mean burning rate in nonpremixed turbulent flames is addressed. The last section, § 10, is devoted to a brief introduction to large eddy simulation modeling.

2 Balance equations

2.1 Instantaneous balance equations

The basic set of balance equations comprises the classical Navier-Stokes, species and energy transport equations. These instantaneous local balance equations are, using the classical lettering [12, 13, 14]:

- **Mass**:

$$\frac{\partial \rho}{\partial t} + \frac{\partial \rho u_j}{\partial x_j} = 0 \tag{1}$$

- **Momentum** (i = 1, 2, 3):

$$\frac{\partial \rho u_i}{\partial t} + \frac{\partial \rho u_j u_i}{\partial x_j} = -\frac{\partial p}{\partial x_i} + \frac{\partial \tau_{ij}}{\partial x_j} + F_i \tag{2}$$

τ_{ij} denotes the viscous force tensor and F_i a body force.

- **Species** (N species with k = 1, ..., N):

$$\frac{\partial \rho Y_k}{\partial t} + \frac{\partial \rho u_j Y_k}{\partial x_j} = -\frac{\partial \mathcal{J}_j^k}{\partial x_j} + \dot{\omega}_k \tag{3}$$

$\mathcal{J}_j^k$ is the molecular diffusive flux of the species k and $\dot{\omega}_k$ the mass reaction rate of this species per unit volume.

- **Total enthalpy** $h_t = h + u_i u_i/2$:

$$\frac{\partial \rho h_t}{\partial t} + \frac{\partial \rho u_j h_t}{\partial x_j} = \frac{\partial p}{\partial t} + \frac{\partial}{\partial x_j}\left(\mathcal{J}_j^h + u_i \tau_{ij}\right) + u_j F_j \tag{4}$$

$u_i \tau_{ij}$ and $u_j F_j$ denote respectively the power due to viscous and body forces.

These equations are closed by expressions for the species molecular fluxes and the viscous forces. In practical situations, all fluids are assumed to be Newtonian, i.e. the viscous tensor is given by the Newton law:

$$\tau_{ij} = \mu_l \left(\frac{\partial u_i}{\partial x_j} + \frac{\partial u_j}{\partial x_i}\right) - \frac{2}{3}\mu_l \, \delta_{ij} \left(\frac{\partial u_k}{\partial x_k}\right) \tag{5}$$

where the laminar viscosity μ_l, depending on the fluid properties is introduced. δ_{ij} is the Kronecker symbol.

Species molecular diffusivities are generally described using the Fick law, assuming a major species:

$$\mathcal{J}_j^k = -\frac{\mu_l}{Sc_k}\frac{\partial Y_k}{\partial x_j} \tag{6}$$

Sc_k is the Schmidt number of the species k, defined as:

$$Sc_k = \frac{\mu_l}{\rho D_k} \tag{7}$$

D_k is the molecular diffusivity of the species k relatively to the major species.

More complex expressions may be used to describe multi-species molecular diffusion. Soret effect (species diffusion under temperature gradients) and molecular transport due to pressure gradients are usually neglected.

Enthalpy diffusion is described according to the Fourier law:

$$\mathcal{J}_j^h = -\frac{\mu_l}{Pr}\left[\frac{\partial h}{\partial x_j} + \sum_{k=1}^{N}\left(\frac{Pr}{Sc_k} - 1\right) h_k \frac{\partial Y_k}{\partial x_j}\right] \tag{8}$$

The Prandtl number Pr compares the diffusive transport of momentum (viscous forces) and temperature. In the previous expressions, radiative heat transfers and Dufour effect (enthalpy diffusion under mass fraction gradients) are neglected. The Prandtl number is written as a function of the thermal diffusivity λ and the constant pressure specific heat C_p:

$$Pr = \left(\frac{\mu_l C_p}{\lambda}\right) \tag{9}$$

Then, the Lewis number Le_k of the species k, comparing thermal and mass diffusivities is introduced:

$$Le_k = \left(\frac{Sc_k}{Pr}\right) = \left(\frac{\lambda}{\rho C_p D_k}\right) \tag{10}$$

Under the assumption of unity Lewis number, the enthalpy diffusive flux (Eq. 8) is simplified and mass fraction and enthalpy balance equations are formally identical. This assumption is generally made to simplify turbulent flame modeling. Nevertheless, thermo-diffusive instabilities occur in premixed systems when the Lewis number is lower than unity (for example for hydrogen). One direct consequence of these instabilities is an increase of the premixed flame area and of the global reaction rate [13, 15].

2.2 Reynolds and Favre averaging

Unfortunately, the full numerical solution of the instantaneous balance equations is limited to very simplified cases (DNS [8, 10, 11]), where the number of time and length scales present in the flow is not too great. To overcome this difficulty, an additive step is introduced by averaging the balance equations to describe only the mean flow field (local fluctuations and turbulent structures are integrated in mean quantities and these structures have no longer to be described in the simulation). Each quantity Q is split into a mean $\overline{Q}$ and a deviation from the mean noted Q':

$$Q = \overline{Q} + Q' \qquad \text{with} \qquad \overline{Q'} = 0 \tag{11}$$

Then, the previous instantaneous balance equations may be ensemble averaged to derive transport equations for the mean quantity $\overline{Q}$. This classical Reynolds averaging technique, widely used in non-reacting fluid mechanics, brings unclosed correlations such as $\overline{u'Q'}$ that are unknown and must be modeled. The numerical procedure is called Reynolds Averaged Navier-Stokes (RANS) modeling.

In turbulent flames, fluctuations of density are observed because of the thermal heat release, and Reynolds averaging induces some difficulties. Averaging the mass balance equation leads to:

$$\frac{\partial \overline{\rho}}{\partial t} + \frac{\partial}{\partial x_i}\left(\overline{\rho u}_i + \overline{\rho' u_i'}\right) = 0 \tag{12}$$

where the velocity / density fluctuations correlation $\overline{\rho' u_i'}$ appears. To avoid the explicit modeling of such correlations, a Favre (mass weighted, [16]) average $\widetilde{Q}$ is introduced and any quantity is then decomposed into $Q = \widetilde{Q} + Q''$:

$$\boxed{\widetilde{Q} = \frac{\overline{\rho Q}}{\overline{\rho}} \qquad ; \qquad \widetilde{Q''} = \frac{\overline{\rho\left(Q - \widetilde{Q}\right)}}{\overline{\rho}} = 0} \tag{13}$$

The Favre averaged continuity equation:

$$\frac{\partial \overline{\rho}}{\partial t} + \frac{\partial \overline{\rho}\widetilde{u}_i}{\partial x_i} = 0 \tag{14}$$

is then formally identical to the Reynolds averaged continuity equation for constant density flows. This result is true for any balance equations (momentum, energy, mass fractions...). Nevertheless, Favre averaging is **only a mathematical formalism**:

- There is no simple relation between Favre, $\widetilde{Q}$, and Reynolds, $\overline{Q}$, averages. A relation between $\widetilde{Q}$ and $\overline{Q}$ requires the knowledge of density fluctuations correlations $\overline{\rho' Q'}$ remaining hidden in Favre averaging (see § 7.3.4):

$$\overline{\rho}\widetilde{Q} = \overline{\rho}\overline{Q} + \overline{\rho' Q'} \tag{15}$$

- Comparisons between numerical simulations, providing Favre averaged quantities $\widetilde{Q}$, with experimental results are not obvious. Most experimental techniques determine Reynolds averaged data $\overline{Q}$ and differences between $\widetilde{Q}$ and $\overline{Q}$ may be significant (§ 7.3.4 and Fig. 17).

2.3 Favre averaged balance equations

Averaging instantaneous balance equations yields:

- **Mass**:

$$\frac{\partial \overline{\rho}}{\partial t} + \frac{\partial \overline{\rho}\widetilde{u}_j}{\partial x_j} = 0 \tag{16}$$

- **Momentum** (i = 1, 2, 3):

$$\frac{\partial \overline{\rho}\widetilde{u}_i}{\partial t} + \frac{\partial \overline{\rho}\widetilde{u}_j\widetilde{u}_i}{\partial x_j} = -\frac{\partial \overline{\rho}\widetilde{u_i'' u_j''}}{\partial x_j} - \frac{\partial \overline{p}}{\partial x_i} + \frac{\partial \overline{\tau}_{ij}}{\partial x_j} + \overline{F}_i \tag{17}$$

- **Chemical species** (for N species, k = 1, ..., N):

$$\frac{\partial \overline{\rho}\widetilde{Y}_k}{\partial t} + \frac{\partial \overline{\rho}\widetilde{u}_j\widetilde{Y}_k}{\partial x_j} = -\frac{\partial \overline{\rho}\widetilde{u_j'' Y_k''}}{\partial x_j} - \frac{\partial \overline{\mathcal{J}_j^k}}{\partial x_j} + \overline{\dot{\omega}}_k \tag{18}$$

- **Total enthalpy** $\widetilde{h}_t$:

$$\frac{\partial \overline{\rho}\widetilde{h}_t}{\partial t} + \frac{\partial \overline{\rho}\widetilde{u}_j\widetilde{h}_t}{\partial x_j} = -\frac{\partial \overline{\rho}\widetilde{u_j'' h_t''}}{\partial x_j} + \frac{\partial \overline{p}}{\partial t} + \frac{\partial}{\partial x_j}\left(\overline{\mathcal{J}_j^h} + \overline{u_i \tau_{ij}}\right) + \overline{u_j F_j} \tag{19}$$

The objective of turbulent combustion modeling is to propose closures for the unknown quantities appearing in the averaged balance equations, such as:

Reynolds stresses $\widetilde{u_i'' u_j''}$**.** The turbulence model provides an approximation for this term. The closure may be done directly or by deriving balance equations for these Reynolds stresses. However, most combustion works are based on turbulence modeling developed for non-reacting flows, such as $k-\varepsilon$, simply rewritten in terms of Favre averaging, and heat release effects on the Reynolds stresses are generally not explicitly included.

Species ($\widetilde{u_j''Y_k''}$) and temperature ($\widetilde{u_j''T}$) turbulent fluxes. These fluxes are usually closed using a gradient transport hypothesis:

$$\overline{\rho}\widetilde{u_j''Y_k''} = -\frac{\mu_t}{Sc_{kt}}\frac{\partial \widetilde{Y}_k}{\partial x_j} \tag{20}$$

where μ_t is the turbulent viscosity, estimated from the turbulence model, and Sc_{kt} a turbulent Schmidt number for the species k.

Nonetheless, theoretical and experimental works have evidenced that this assumption may be wrong in some premixed turbulent flames and counter-gradient turbulent transport may be observed [17, 18] (i.e. in an opposite direction compared to the one predicted by Eq. (20), see § 7.3.5 and § 8).

Laminar diffusive fluxes $\overline{\mathcal{J}_j^k}$, $\overline{\mathcal{J}_j^h}$,... are usually small compared to turbulent transport, assuming a sufficiently large turbulence level (large Reynolds numbers limit).

Species chemical reaction rates $\overline{\dot{\omega}}_k$. Turbulent combustion modeling generally focuses on the closure of these mean burning rates.

These equations, closed with appropriate models, allow only for the determination of mean quantities, that may differ from the instantaneous ones. Strong unsteady mixing effects, resulting from the rolling up of shear layers, are observed in turbulent flame, and the knowledge of steady statistical means is indeed not always sufficient to describe turbulent combustion. An alternative is to use large eddy simulation (LES).

2.4 Filtering and Large Eddy Simulation

The objective of Large Eddy Simulation (LES) is to explicitly compute the largest structures of the flow (typically the structures larger than the computational mesh size), while the effects of the smaller one are modeled. LES is widely studied in the context of non-reactive flows [19, 20, 21, 22], its application to combustion modeling is still at an early stage [23]. As in RANS, the complex coupling between micromixing and chemical reactions occurring at unresolved scales needs models, however, LES possesses some attracting properties:

- Large structures in turbulent flows generally depend on the geometry of the system. In opposition, smaller scales feature more universal properties. Accordingly, turbulence models may be more efficient when they have to describe only the smallest structures.
- Turbulent mixing controls most of global flame properties. In LES, unsteady large scale mixing (between fresh and burnt gases in premixed flames or between fuel and oxidizer in nonpremixed burners) is simulated, instead of being averaged.
- Most reacting flows exhibit large scale coherent structures [24], also especially observed when combustion instabilities occur. These instabilities result from the coupling between heat release, hydrodynamic flow field and acoustic waves. They need to be avoided because they induce noise, variations of the system main properties, large heat transfers and, even in some extreme cases, the destruction of the device. LES may be a powerful tool to predict the occurrence of such instabilities [25] and consequently improve passive or active control systems.
- With LES, large structures are explicitly computed and instantaneous fresh and burnt gases zones, with different turbulence characteristics (§ 8.7) are clearly identified. This may help to describe some properties of flame/turbulence interaction.

In LES, the relevant quantities Q are filtered in the spectral space (components greater than a given cut-off frequency are suppressed) or in the physical space (weighted averaging in a given volume). The filtered operation is defined by:

$$\boxed{\overline{Q}(\mathbf{x}) = \int Q(\mathbf{x}^*)\, F(\mathbf{x}-\mathbf{x}^*)\, d\mathbf{x}^*} \tag{21}$$

where F is the LES filter. Standard filters are:

- **A cut-off filter in the spectral space**:

$$\overline{F}\,(k) = \begin{cases} 1 & \text{if } k \leq \pi/\Delta \\ 0 & \text{otherwise} \end{cases} \tag{22}$$

  where k is the spatial wave number. This filter preserves the length scales greater than the cut-off length scale 2Δ.

- **A box filter in the physical space**:

$$F\,(\mathbf{x}) = F\,(x_1, x_2, x_3) = \begin{cases} 1/\Delta^3 & \text{if} \quad |x_i| \leq \Delta/2,\ i = 1,2,3 \\ 0 & \text{otherwise} \end{cases} \tag{23}$$

  where (x_1, x_2, x_3) are the spatial coordinates of the location $\mathbf{x}$. This filter corresponds to an averaging of the quantity Q over a box of size Δ.

- **A Gaussian filter in the physical space**:

$$F\,(\mathbf{x}) = F\,(x_1, x_2, x_3) = \left(\frac{6}{\pi\Delta^2}\right)^{3/2} \exp\left[-\frac{6}{\Delta^2}\left(x_1^2 + x_2^2 + x_3^2\right)\right] \tag{24}$$

All these filters are normalized:

$$\int_{-\infty}^{+\infty}\int_{-\infty}^{+\infty}\int_{-\infty}^{+\infty} F\,(x_1, x_2, x_3)\ dx_1 dx_2 dx_3 = 1 \tag{25}$$

In combusting flows, a mass-weighted, Favre filtering, is introduced as:

$$\boxed{\overline{\rho}\,\widetilde{Q}(\mathbf{x}) = \int \rho\, Q(\mathbf{x}^*)\, F(\mathbf{x}-\mathbf{x}^*)\, d\mathbf{x}^*} \tag{26}$$

Instantaneous balance equations (§ 2) may be filtered to derived balance equations for the filtered quantities $\overline{Q}$ or $\widetilde{Q}$. This derivation should be carefully conducted:

- Any quantity Q may be decomposed into a filtered component $\overline{Q}$ and a "fluctuating" component Q', according to: $Q = \overline{Q} + Q'$. But, in disagreement with classical Reynolds averaging (ensemble average), $\overline{Q'}$ may be non zero:

$$\begin{aligned} \overline{Q'}(\mathbf{x}) &= \int \left(Q(\mathbf{x}^*) - \overline{Q}(\mathbf{x}^*)\right) F(\mathbf{x}-\mathbf{x}^*)\, d\mathbf{x}^* \\ &= \int Q(\mathbf{x}^*) F(\mathbf{x}-\mathbf{x}^*)\, d\mathbf{x}^* - \int \overline{Q}(\mathbf{x}^*) F(\mathbf{x}-\mathbf{x}^*)\, d\mathbf{x}^* \\ &= \overline{Q}(\mathbf{x}) - \overline{\overline{Q}}(\mathbf{x}) \end{aligned} \tag{27}$$

where

$$\begin{aligned}\overline{\overline{Q}}(\mathbf{x}) &= \int \left[\int Q(\mathbf{x}^+) F(\mathbf{x}^* - \mathbf{x}^+)\, d\mathbf{x}^+ \right] F(\mathbf{x} - \mathbf{x}^*)\, d\mathbf{x}^* \\ &= \int\int Q(\mathbf{x}^+) F(\mathbf{x}^* - \mathbf{x}^+) F(\mathbf{x} - \mathbf{x}^*)\, d\mathbf{x}^+\, d\mathbf{x}^* \\ &\neq \overline{Q}(\mathbf{x}) \end{aligned} \tag{28}$$

To summarize:

$$\boxed{\overline{\overline{Q}} \neq \overline{Q} \quad ; \quad \overline{Q'} \neq 0 \qquad ; \qquad \widetilde{\widetilde{Q}} \neq \widetilde{Q} \quad ; \quad \widetilde{Q''} \neq 0} \tag{29}$$

The relations used in RANS $\overline{\overline{Q}} = \overline{Q}$, $\overline{Q'} = 0$, $\widetilde{\widetilde{Q}} = \widetilde{Q}$, $\widetilde{Q''} = 0$ are true when a cut-off filter in the spectral space is chosen (Eq. 22). Then, all the frequency components greater than a cut-off wave number $k_c = \pi/\Delta$ vanish.

- The derivation of balance equations for the filtered quantities $\overline{Q}$ or $\widetilde{Q}$ requires the exchange of filtering and derivation operators. This exchange is theoretically valid only under restrictive assumptions and is wrong, for example, when the filter size varies (filter size corresponding to the mesh size, depending on the spatial location). This point has been carefully investigated [26]. In most simulations, the uncertainties due to this operator exchange are neglected and assumed to be incorporated in subgrid scale modeling.

Filtering the instantaneous balance equations leads to equations formally similar to the Reynolds averaged balance equations given in § 2.3:

• **mass**:

$$\frac{\partial \overline{\rho}}{\partial t} + \frac{\partial \overline{\rho}\widetilde{u}_j}{\partial x_j} = 0 \tag{30}$$

• **momentum** (for i = 1, 2, 3):

$$\frac{\partial \overline{\rho}\widetilde{u}_i}{\partial t} + \frac{\partial \overline{\rho}\widetilde{u}_j\widetilde{u}_i}{\partial x_j} = -\frac{\partial}{\partial x_j}\left[\overline{\rho}\left(\widetilde{u_i u_j} - \widetilde{u}_i\widetilde{u}_j\right)\right] - \frac{\partial \overline{p}}{\partial x_i} + \frac{\partial \overline{\tau}_{ij}}{\partial x_j} + \overline{F}_i \tag{31}$$

• **Chemical species** (N species, k = 1, ..., N):

$$\frac{\partial \overline{\rho}\widetilde{Y}_k}{\partial t} + \frac{\partial \overline{\rho}\widetilde{u}_j\widetilde{Y}_k}{\partial x_j} = -\frac{\partial}{\partial x_j}\left[\overline{\rho}\left(\widetilde{u_j Y_k} - \widetilde{u}_j\widetilde{Y}_k\right)\right] + \overline{\dot{\omega}}_k \tag{32}$$

• **Total enthalpy** $h_t = h + u_i u_i/2$:

$$\frac{\partial \overline{\rho}\widetilde{h}_t}{\partial t} + \frac{\partial \overline{\rho}\widetilde{u}_j\widetilde{h}_t}{\partial x_j} = -\frac{\partial}{\partial x_j}\left[\overline{\rho}\left(\widetilde{u_j h_t} - \widetilde{u}_j\widetilde{h}_t\right)\right] + \frac{\partial \overline{p}}{\partial t} + \frac{\partial}{\partial x_j}\left(\overline{\mathcal{J}_j^h} + \overline{u_i\tau_{ij}}\right) + \overline{u_j F_j} \tag{33}$$

where $\overline{Q}$ and $\widetilde{Q}$ denote LES filtered quantities instead of ensemble means.

The unknown quantities are:

- *Unresolved Reynolds stresses* $(\widetilde{u_i u_j} - \widetilde{u}_i\widetilde{u}_j)$, requiring a subgrid scale turbulence model.
- *Unresolved species fluxes* $\left(\widetilde{u_j Y_k} - \widetilde{u}_j\widetilde{Y}_k\right)$ and enthalpy fluxes $\left(\widetilde{u_j h_t} - \widetilde{u}_j\widetilde{h}_t\right)$.
- *Filtered laminar diffusion fluxes* $\overline{\mathcal{J}_j^k}$, $\overline{\mathcal{J}_j^h}$.

- *Filtered chemical reaction rate* $\overline{\dot{\omega}}_k$.

These filtered balance equations, coupled to subgrid scale models may be numerically solved to simulate the unsteady behavior of the filtered fields. Compared to direct numerical simulations (DNS), part of the information contained in the unresolved scales is lost (and should be modeled). Compared to RANS, LES provides a valuable information on the large resolved motions.

Either using RANS or LES, combustion occurs at the unresolved scales of the computations. Then, the basic tools and formalism of turbulent combustion modeling are somehow the same for both techniques. Most of the RANS combustion models can be modified and adapted to LES modeling (see § 10).

3 Major properties of premixed, nonpremixed and partially premixed flames

3.1 Laminar premixed flames

The structure of a laminar premixed flame is displayed in Fig. 2. Fresh gases (fuel and oxidizer mixed at the molecular level) and burnt gases (combustion products) are separated by a thin reaction zone (typical thermal flame thickness, δ_l, are about 0.1 to 1 mm). A strong temperature gradient is observed (typical ratios between burnt and fresh gases temperatures are about 5 to 7). Another characteristic of a premixed flame is its ability to propagate towards the fresh gases. Because of the temperature gradient and the corresponding thermal fluxes, fresh gases are preheated and then start to burn. The local imbalance between diffusion of heat and chemical consumption leads to the propagation of the front. The propagation speed S_L of a laminar flame depends on various parameters (fuel and oxidizer compositions, fresh gases temperature,...) and is about 0.1 to 1 m/s. There is an interesting relation between the thermal flame thickness, δ_l, the laminar flame speed, S_L and the kinematic viscosity of the fresh gases, ν:

$$Re_f = \frac{\delta_l S_L}{\nu} \approx 4 \tag{34}$$

The flame Reynolds number, Re_f, is then almost constant. This relation, derived, for example, from the Zeldovich / Frank-Kamenetskii (ZFK) theory [13, 14] is often implicitly used in theoretical derivation of models for premixed turbulent combustion.

For a one-step irreversible simple chemical scheme:

$$Reactants \longrightarrow Products$$

the flame is described using a progress variable c, such as $c = 0$ in the fresh gases and $c = 1$ in the fully burnt ones. This progress variable may be defined as a reduced temperature or a reduced mass fraction:

$$c = \frac{T - T_u}{T_b - T_u} \qquad \text{or} \qquad c = \frac{Y_F - Y_F^u}{Y_F^b - Y_F^u} \tag{35}$$

where T, T_u and T_b are respectively the local, the unburnt gases and the burnt gases temperatures. Y_F, Y_F^u and Y_F^b are respectively the local, unburnt gases and burnt gases fuel mass fractions. Y_F^b is non-zero for a rich combustion (fuel in excess). For an unity Lewis number (same molecular and thermal diffusivities), without heat losses (adiabatic combustion) and compressibility effects, the two definitions (35) are equivalent and mass and energy balance equations reduce to a single balance equation for the progress variable:

$$\frac{\partial \rho c}{\partial t} + \nabla \cdot (\rho \mathbf{u} c) = \nabla \cdot (\rho D \nabla c) + \dot{\omega} \tag{36}$$

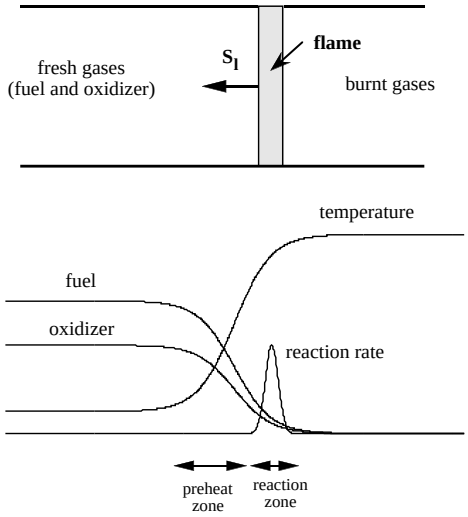

Figure 2: Structure of a laminar plane premixed flame.

The previous equation (36) may be recast under a propagative form, introducing the displacement speed w of the iso-c surface:

$$\frac{\partial c}{\partial t} + \mathbf{u} \cdot \nabla c = \underbrace{\frac{1}{\rho} \left[\frac{\nabla \cdot (\rho D \nabla c) + \dot{\omega}}{|\nabla c|} \right]}_{\text{displacement speed}} |\nabla c| = w \, |\nabla c| \tag{37}$$

Equation (36) then describes the displacement of an iso-c surface with the displacement speed w measured relatively to the flow. Introducing the vector $\mathbf{n}$ normal to the iso-c surface and pointing towards fresh gases ($\mathbf{n} = -\nabla c / |\nabla c|$), the displacement speed may be split into three contributions:

$$\begin{aligned} w &= \frac{1}{\rho |\nabla c|} \mathbf{n}\mathbf{n} : \nabla (\rho D \nabla c) - D \nabla \cdot \mathbf{n} + \frac{1}{\rho |\nabla c|} \dot{\omega} \\ w &= \underbrace{- \frac{1}{\rho \, |\nabla c|} \frac{\partial}{\partial n} (\rho D \, |\nabla c|)}_{w_n} \underbrace{- D \, \nabla \cdot \mathbf{n}}_{w_c} + \underbrace{\frac{1}{\rho \, |\nabla c|} \dot{\omega}}_{w_r} \end{aligned} \tag{38}$$

where $\partial / \partial n = \mathbf{n} \cdot \nabla$ denotes a normal derivative. w_n corresponds to molecular diffusion normal to iso-c surface, w_c is related to the curvature $\nabla \cdot \mathbf{n}$ of this surface and corresponds to tangential diffusion. w_r is due to the reaction rate $\dot{\omega}$. In a first approximation, $w_n + w_r$ may be modeled with the laminar flame

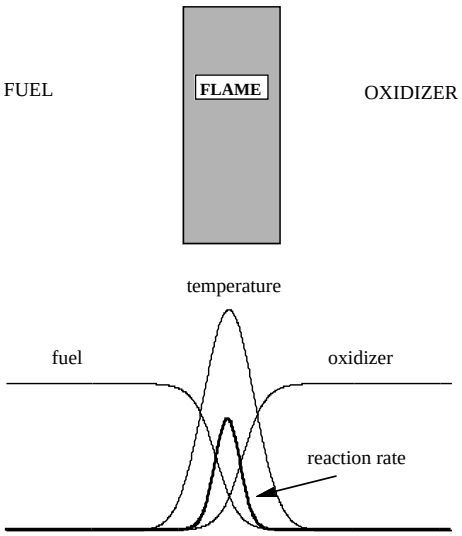

Figure 3: Generic structure of a laminar diffusion flame.

speed, S_L, whereas w_c incorporates wrinkling surface effects and may be expressed using Markstein lengths [27].

The propagation of reactive fronts has been the subject of various developments and more discussion may be found in [2] and references therein.

3.2 Laminar diffusion flames

In laminar diffusion flames, fuel and oxidizer are on both sides of a reaction zone where the heat is released. The burning rate is controlled by the molecular diffusion of the reactants toward the reaction zone (Fig. 3). In a counter-flowing fuel and oxidizer flame (Fig. 4), the amount of heat transported away from the reaction zone is exactly balanced by the heat released by combustion. A steady planar diffusion flame with determined thickness may be observed in the vicinity of the stagnation point. Increasing the jets velocity, quenching occurs when the heat fluxes leaving the reaction zone are greater than the chemical heat production. The structure of a steady diffusion flame therefore depends on ratios between characteristic times representative of molecular diffusion and chemistry [28]. The thicknesses of the mixing zone and of the reaction zone vary with these characteristic times. In opposition with premixed flames:

- Diffusion flames do not benefit from a self-induced propagation mechanism, but are mainly mixing controlled.
- The thickness of a diffusion flame is not constant, but depends on the local flow properties.

Let us consider the irreversible single step chemical reaction between fuel and oxidizer:

$$F + s\,O \rightarrow (1+s)\,P$$

where s is the mass stoichiometric coefficient. In term of mass fraction, this chemical reaction may be written:

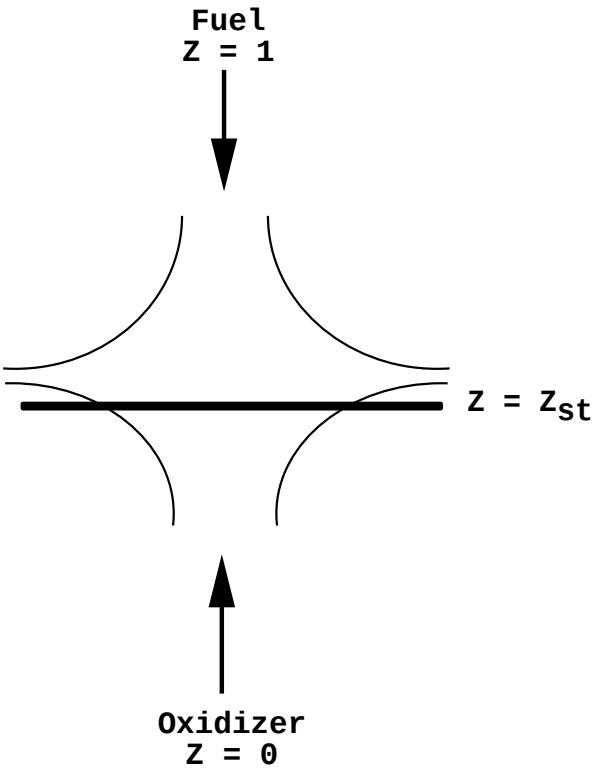

Figure 4: Sketch of a counter-flowing fuel and oxidizer diffusion flame.

$$\nu_F Y_F + \nu_o Y_o \rightarrow \nu_P Y_P$$

where Y_F, Y_O and Y_P are the mass fractions of the fuel, the oxidizer and the product respectively. ν_i are the stoichiometric molar coefficients of the reaction, W_i denotes the species molar weight and $\dot{\omega}$ is the reaction rate. The balance equations for mass fractions and temperature are necessary to identify the properties of the flame :

$$\begin{aligned}
\frac{\partial \rho Y_F}{\partial t} + \nabla \cdot (\rho \mathbf{u} Y_F) &= \nabla \cdot (\rho D_F \nabla Y_F) - \nu_F W_F \, \dot{\omega} \\
\frac{\partial \rho Y_O}{\partial t} + \nabla \cdot (\rho \mathbf{u} Y_O) &= \nabla \cdot (\rho D_O \nabla Y_O) - \nu_F W_O \, \dot{\omega} \\
\frac{\partial \rho T}{\partial t} + \nabla \cdot (\rho \mathbf{u} T) &= \nabla \cdot \left(\frac{\lambda}{C_p} \nabla T \right) + \nu_F W_F \left(\frac{Q}{C_p} \right) \dot{\omega}
\end{aligned}$$

The molecular diffusion is expressed using the Fick law, the chemical rate of fuel and oxidizer are respectively $\dot{\omega}_F = \nu_F W_F \, \dot{\omega}$ and $\dot{\omega}_O = \nu_O W_O \dot{\omega}$. Q is the amount of heat released by the combustion of an unit mass of fuel.

The internal structure of diffusion flames is usually discussed using the extent of mixing between fuel and oxidizer. It is first assumed that fuel and oxidizer molecular diffusivities are equal (i.e. $D_F = D_O = D$). Combining the transport equation for Y_F and Y_O, a conserved scalar (quantity that does not see the chemical reaction, a Schwab-Zeldovitch variable) $\varphi(Y_F, Y_O) = Y_F - Y_O/s$ is introduced, with the mass stoichiometric coefficient $s = (\nu_O W_O / \nu_F W_F)$. The mixture fraction Z is then defined by

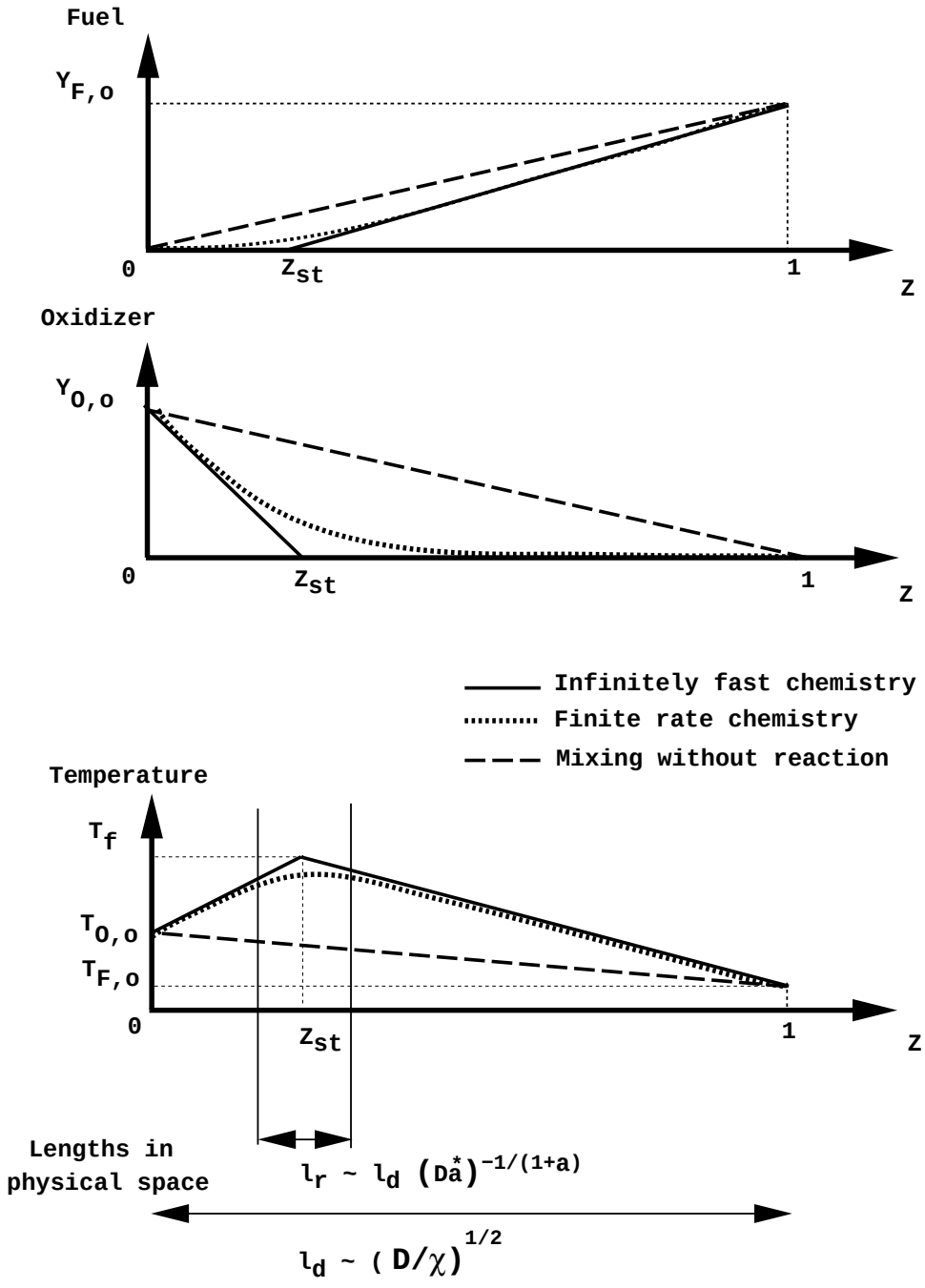

Figure 5: Inner structure of nonpremixed flames. The distribution in mixture fraction space of fuel, oxidizer and temperature lies between the infinitely fast chemistry limit and the pure mixing case. The thickness of the diffusive zone l_d is estimated from the scalar dissipation rate χ at the stoichiometric surface, whereas the characteristic thickness of the reaction zone l_r depends on both l_d and the Damköhler number. From [11].

normalizing φ using values in the fuel and oxidizer streams. Z evolves through the diffusive layer from zero (oxidizer) to unity (fuel):

$$Z = \frac{\phi \dfrac{Y_F}{Y_{F,o}} - \dfrac{Y_O}{Y_{O,o}} + 1}{\phi + 1} \tag{39}$$

$Y_{F,o}$ is the fuel mass fraction in the fuel feeding stream. Similarly, $Y_{O,o}$ is the oxidizer mass fraction in the oxidizer stream (for instance, in air, $Y_{O,o} \approx 0.23$), ϕ is the equivalence ratio of the nonpremixed flame:

$$\phi = \frac{sY_{F,o}}{Y_{O,o}} \tag{40}$$

The mixture fraction follows the balance equation:

$$\frac{\partial \rho Z}{\partial t} + \nabla \cdot (\rho \mathbf{u} Z) = \nabla \cdot (\rho D \nabla Z) \tag{41}$$

Other Schwab-Zeldovitch variables $\varphi(Y_F, T)$ and $\varphi(Y_O, T)$ (conserved scalars) may be derived by combining the variables (Y_F, T) and (Y_O, T). The mixture fraction and these additional conserved scalars are linearly related and one may write:

$$Y_O(\underline{x}, t) = \underbrace{Y_{O,o}(1 - Z(\underline{x}, t))}_{\text{Mixing}} + \underbrace{\frac{\nu_O W_O}{\nu_F W_F} \left(\frac{C_p}{Q}\right) \Big[Z(\underline{x}, t)(T_{F,o} - T_{O,o}) + (T_{O,o} - T(\underline{x}, t)) \Big]}_{\text{Combustion}} \tag{42}$$

$$Y_F(\underline{x}, t) = \overbrace{Z(\underline{x}, t) \quad Y_{F,o}} \quad + \overbrace{\frac{C_p}{Q} \Big[Z(\underline{x}, t)(T_{F,o} - T_{O,o}) + (T_{O,o} - T(\underline{x}, t)) \Big]} \tag{43}$$

where $T_{O,o}$ and $T_{F,o}$ are the temperatures of the fuel and oxidizer streams respectively. Using these algebraic relations, the diffusion flame is fully determined when the mixture fraction Z and either one of T, Y_F, or Y_O is known.

The conserved scalar approach may still be useful when fuel and oxidizer molecular diffusivities differ, but an additional mixture fraction:

$$Z_L = \frac{\Phi \dfrac{Y_F}{Y_{F,o}} - \dfrac{Y_O}{Y_{O,o}} + 1}{\Phi + 1} \tag{44}$$

should be introduced, verifying [29]:

$$\rho \frac{DZ}{Dt} = \frac{1}{\mathcal{L}} \nabla . \left(\frac{\lambda}{C_p} \nabla Z_L \right) \tag{45}$$

where:

$$\mathcal{L} = Le_O(1 + \phi)/(1 + \Phi) \quad \text{with} \quad \Phi = (Le_O/Le_F)\phi \tag{46}$$

where Le_i is the Lewis number of the species i. The relations between Z and Z_L are given in Table 1. When $Le_O = Le_F$, $Z_L = Z$. In experiments or in simulations involving complex chemistry, the mixture fraction is defined from mass fractions of atomic elements [30].

Mass fractions and temperature balance equations may be reorganized into a new frame where Z is one of the coordinates (see for instance [13] or [31]). A local orthogonal coordinate system attached to

Oxidizer side	**Fuel side**
$Z < Z_{st}$ and $Z_L < Z_{L_{st}}$	$Z > Z_{st}$ and $Z_L > Z_{L_{st}}$
$Z = Z_L(1+\Phi)/(1+\phi)$ $Y_F = 0$ $Y_O = Y_{O,o}(1 - Z(1+\phi))$ $T = (T_f - T_{O,o})Z(\phi+1) + T_{O,o}$	$Z = (\phi(Z_L(1+\Phi) - 1)/\Phi + 1)/(1+\phi)$ $Y_O = 0$ $Y_F = Y_{F,o}(Z(1+\phi) - 1)/\phi$ $T = (T_{F,o} - T_f)(Z(\phi+1) - 1)/\phi + T_f$

Table 1: Piecewise relations for infinitely fast chemistry including non-unity Lewis number. $Z_{st} = 1/(1+\phi)$ and $Z_{L_{st}} = 1/(1+\Phi)$ (see Eq. 46). The subscript $_o$ denotes a quantity measured in pure fuel or oxidizer, T_f is the flame temperature.

the surface of stoichiometric mixture is introduced and the derivatives in the stoichiometric plane are denoted $_\perp$. For unity Lewis number and using Eq. (41), the species transport equation writes:

$$\rho\frac{\partial Y_i}{\partial t} + \rho\mathbf{u}_\perp \cdot \nabla_\perp Y_i = \rho\chi\frac{\partial^2 Y_i}{\partial Z^2} + \nabla_\perp \cdot (\rho D \nabla_\perp Y_i) - \rho D \nabla_\perp (\ln|\nabla Z|) \cdot \nabla_\perp Y_i + \dot{\omega}_i \tag{47}$$

In Eq. (47), χ is the scalar dissipation rate of the mixture fraction Z:

$$\chi = D\left(\frac{\partial Z}{\partial x_j}\frac{\partial Z}{\partial x_j}\right) = D|\nabla Z|^2 \tag{48}$$

measuring the inverse of a diffusive time $\tau_\chi = \chi^{-1}$. As this time decreases, mass and heat transfers through the stoichiometric surface are enhanced.

When iso-Z surface curvatures are not too strong, the gradients measured along the stoichiometric surface are smaller than the gradients in the direction Z perpendicular to the stoichiometric surface, the balance equation for the mass fractions reduces to:

$$\rho\frac{\partial Y_i}{\partial t} = \rho\chi\frac{\partial^2 Y_i}{\partial Z^2} + \dot{\omega}_i \tag{49}$$

Neglecting unsteady effects, the time derivative vanishes and for unity Lewis numbers, the flame structure is fully described by:

$$\rho\chi\frac{\partial^2 Y_i}{\partial Z^2} + \dot{\omega}_i = 0 \qquad \text{and} \qquad \rho\chi\frac{\partial^2 T}{\partial Z^2} + \dot{\omega}_T = 0 \tag{50}$$

showing that the chemical reaction rate is directly related to the function $T(Z,\chi)$. Under these hypothesis, the diffusion flame is completely determined as a function of the mixture fraction Z and the scalar dissipation rate χ (or ∇Z):

$$Y_i = Y_i(Z,\chi) \quad ; \quad T = T(Z,\chi)$$

Expression for $\chi(Z,t)$ and full solutions for various laminar flames may be derived from asymptotic developments [28, 32], or solving Eq. (50) leading to Fig. 5.

Diffusion combustion is limited by two regimes corresponding to pure mixing of the reactants and infinitely fast chemistry (Fig. 5). When the chemistry is infinitely fast, the temperature depends on mixing through Z, but not on the rate of mixing χ [33]. Then, piecewise relationships exist between Z,

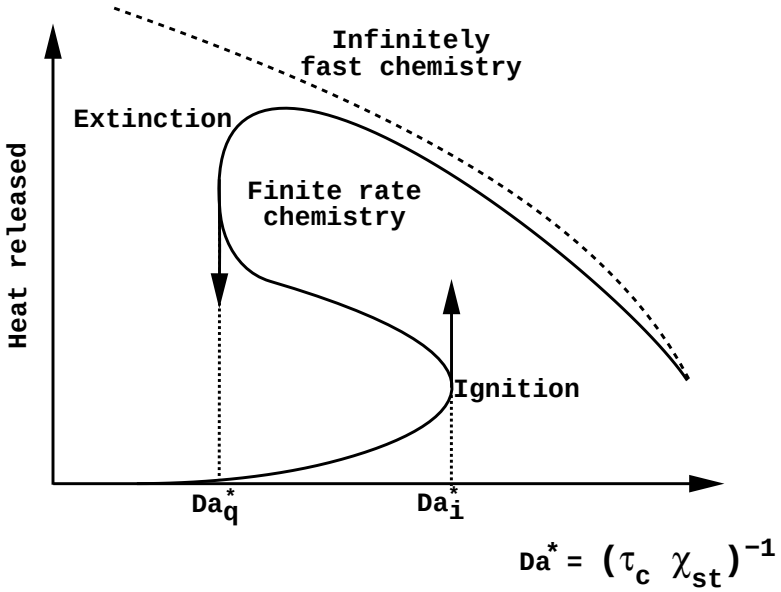

Figure 6: Generic response of the heat released by a one-dimensional strained diffusion flame versus Damkhöhler number. The dash line denotes infinitely fast chemistry. Da_q^* and Da_i^* are the critical values of $Da^* = (\tau_c \chi_{st})^{-1}$ at quenching and ignition respectively. τ_c is a given chemical time and $\chi_{st} = D|\nabla Z|^2_{Z=Z_{st}}$ is the scalar dissipation rate under stoichiometric conditions.

Z_L, species mass fractions and temperature, summarized in Table 1. Eq. (43) provides the maximum flame temperature T_f obtained when $Y_F = Y_O = 0$ and $Z = Z_{st} = 1/(1+\phi)$

$$T_f = \frac{T_{F,o} + T_{O,o}\phi + Y_{F,o}\dfrac{Q}{C_p}}{1+\phi}$$

In many combustion systems, the infinitely fast chemistry hypothesis cannot be invoked everywhere. For example in ignition problems or in the vicinity of stabilization zones, and more generally when large velocity gradients are found. The characterization of diffusion flames from the infinitely fast chemistry situation to the quenching limit is therefore of fundamental interest for turbulent combustion. The counterflow diffusion flame (Fig. 4) is a generic configuration well suited to reproduce and to understand the structure and the extinction of laminar diffusion flames. These extinction phenomena have been theoretically described using asymptotic developments [28, 32, 34]. A diffusive time $\tau_\chi \approx \chi_{st}^{-1} = (D|\nabla Z|^2)^{-1}_{Z=Z_{st}}$ and a chemical time τ_c are combined to build a Damköhler number $Da^* = (\tau_\chi/\tau_c) \approx (\tau_c \chi_{st})^{-1}$. The response of the burning rate to variations of Da^* leads to the so-called "S" curve (Fig. 6) [13]. Starting from a situation where the chemistry is fast, decreasing Da^* (increasing χ) makes the burning rate and transport through the stoichiometric surface greater, until chemistry cannot keep up with the large heat fluxes. Then, extinction develops. The value of the Damköhler Da_q^* at the extinction point may be estimated by quantifying the leakage of fuel (or oxidizer) through the stoichiometric surface [35].

Two limit cases are thus important for nonpremixed turbulent combustion modeling: pure mixing without combustion ($Da^* \to 0$) and infinitely fast chemistry ($Da^* \to \infty$). These cases delineate the domain where flames may develop in planes (Z, Y_F), (Z, Y_O) and (Z, T) (Fig. 5). Moreover, for a given location within a diffusion flame, by traveling along the normal to the stoichiometric surface, $T(Z)$ can

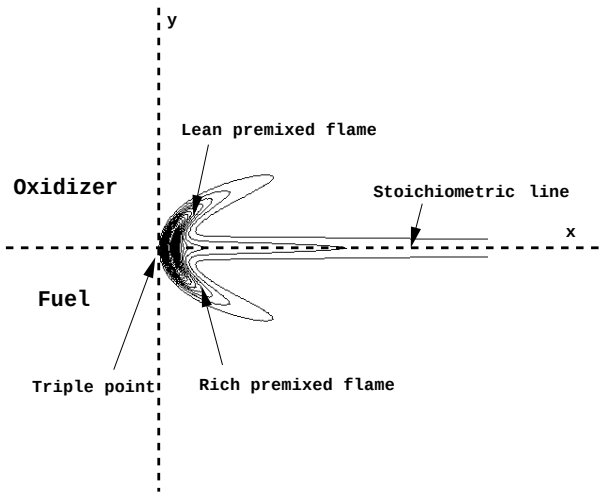

Figure 7: Schematic of a freely propagating triple flame.

be constructed and characterizes the combustion regime (i.e. fast or slow chemistry, Fig. 5). Many turbulent combustion models are based on this description of diffusion flame ; when the flow is turbulent, $T(Z)$ is replaced by the mean temperature calculated for a given value of Z, i.e. for a given state in the mixing between fuel and oxidizer.

3.3 Partially premixed flames

In nonpremixed combustion, some partial premixing of the reactants may exist before the reaction zone develops. Then, the pure diffusive / reactive layer, as observed in a laminar diffusion flame, may not be the unique relevant model problem. Furthermore, many flames in burners are stabilized by the recirculation of burnt gases, leading to stabilization mechanisms controlled by the mixing between fuel, oxidizer, and burnt gases. The mixtures feeding the reaction zone are then not always pure fuel and pure oxidizer.

There are situations where partial premixing is clearly important:

- Auto-ignition in a non-homogeneous distribution of fuel and oxidizer, where the reactants can be mixed before auto-ignition occurs.
- Laminar or turbulent flame stabilization, when combustion does not start at the very first interface between fuel and oxidizer in the vicinity of burner exit, so that fuel and oxidizer may mix without burning.
- After quenching of the reaction zone, the reactants may mix leading to possibility of re-ignition and combustion in a partially premixed regime [36].

The triple flame is an interesting model problem to approach partially premixed combustion. In a laminar shear layer where the mixing between cold fuel and oxidizer develops, a diffusion flame may be stabilized at the splitter plate by the combination of heat losses with viscous flow effects, or, further downstream [37]. In this latter case, combustion starts in a region where fuel and oxidizer have been mixed in stoichiometric proportion. The resulting premixed kernel tends to propagate towards fresh gases and contributes to the stabilization of the trailing diffusion flame. In a mixing layer configuration, the stoichiometric premixed kernel evolves to a rich partially premixed flame in the direction of the fuel

stream, while a lean partially premixed flame develops on the air side (Fig. 7). These two premixed flames are curved because their respective propagation velocities decrease when moving away from the stoichiometric condition. The overall structure, composed of two premixed flames and of a diffusion flame, is usually called "triple flame". Such triple flames have been firstly experimentally observed by Phillips [38]. Since this pioneer work, more recent experiments have confirmed the existence of triple flames in laminar flows [39, 40, 41]. Theoretical studies [42, 43, 44, 45, 46] and numerical simulations [47, 48, 49, 50, 51] have been devoted to triple flames. The propagation speed of triple flames is controlled by two parameters: the curvature of the partially premixed front, increasing with the scalar dissipation rate imposed in front of the flame, and the amount of heat release. The effect of heat release is to deviate the flow upstream of the triple flame, making the triple flame speed greater than the propagation speed of a planar stoichiometric flame. This deviation also induces a decrease of the mixture fraction gradient in the trailing diffusion flame. The triple flame velocity decreases when increasing the scalar dissipation rate at the flame tip. Triple flame velocity response to variations of scalar dissipation rate may be derived approximating the flame tip by a parabolic profile and using results from expansions in parabolic-cylinder coordinates. This analysis was used by Ghosal and Vervisch to include small but finite heat release and gas expansion, the triple flame velocity U_{TF} may be written [45]:

$$U_{TF} \approx S_L\,(1+\alpha) - \frac{\beta}{Z_{st}(1+\alpha)\sqrt{4\nu_F - 2}}\sqrt{\frac{\lambda}{\rho C_p}\chi_{st}} \tag{51}$$

where $\alpha = (T_{burnt} - T_{fresh})/T_{burnt}$ is defined from the temperatures on both sides of a stoichiometric premixed flame for the same mixture, β is the Zeldovitch number [13], ν_F the stoichiometric coefficient of the fuel and χ_{st} is measured far upstream in the mixing layer where the triple flame propagates. The value of the scalar dissipation rate at the triple point is of the order of $\chi_{st}/(1+\alpha)^2$ [45]. These relations are valid for small values of α and moderate, but non-zero, values of χ_{st}. The triple flame velocity given by Eq. (51) may be combined with Landau-Squire solution for nonreacting laminar round jet to construct a stability diagram for lift-off and blowout of jet laminar diffusion flames [52].

A variety of studies suggest that finite rate chemistry and quenching in nonpremixed combustion are somehow linked to partially premixed combustion [53].

4 A direct analysis: Taylor's expansion

A direct approach to describe turbulent combustion is first discussed in this section. This simple formalism, based on series expansion, illustrates the difficulties arising from the non-linear character of chemical sources.

Consider a simple irreversible reaction between fuel (F) and oxidizer (O):

$$F + s\,O \rightarrow (1+s)P$$

where the fuel mass reaction rate $\dot{\omega}_F$ is expressed from the Arrhenius law as:

$$\dot{\omega}_F = -A\rho^2 T^b Y_F Y_O \exp\left(-\frac{T_A}{T}\right) \tag{52}$$

A is the pre-exponential constant, T_A is the activation temperature.

As the reaction rate is highly non-linear, the averaged reaction rate $\overline{\dot{\omega}}_F$ cannot be easily expressed as a function of the mean mass fractions $\widetilde{Y}_F$ and $\widetilde{Y}_O$, the mean density $\overline{\rho}$ and the mean temperature $\widetilde{T}$. The first simple idea is to expand the mean reaction rate $\overline{\dot{\omega}}_F$ as a Taylor series:

$$\exp\left(-\frac{T_A}{T}\right) = \exp\left(-\frac{T_A}{\widetilde{T}}\right)\left(1 + \sum_{n=1}^{+\infty} P_n \frac{T''^n}{\widetilde{T}^n}\right) \quad ; \quad T^b = \widetilde{T}^b\left(1 + \sum_{n=1}^{+\infty} Q_n \frac{T''^n}{\widetilde{T}^n}\right) \tag{53}$$

where P_n and Q_n are given by:

$$P_n = \sum_{k=1}^{n} (-1)^{n-k} \frac{(n-1)!}{(n-k)! \left[(k-1)!\right]^2 k} \left(\frac{T_A}{\widetilde{T}}\right)^k \quad ; \quad Q_n = \frac{b(b+1)...(b+n-1)}{n!} \tag{54}$$

The mean reaction rate, $\overline{\dot{\omega}}_F$ becomes [54]:

$$\overline{\dot{\omega}}_F = -A\overline{\rho}^2 \widetilde{T}^b \widetilde{Y}_F \widetilde{Y}_O \exp\left(-\frac{T_A}{\widetilde{T}}\right) \left[1 + \frac{\widetilde{Y''_F Y''_O}}{\widetilde{Y}_F \widetilde{Y}_O} + (P_1+Q_1)\left(\frac{\widetilde{Y''_F T''}}{\widetilde{Y}_F \widetilde{T}} + \frac{\widetilde{Y''_O T''}}{\widetilde{Y}_O \widetilde{T}}\right) + (P_2+Q_2+P_1Q_1)\left(\frac{\widetilde{Y''_F T''^2}}{\widetilde{Y}_F \widetilde{T}^2} + \frac{\widetilde{Y''_O T''^2}}{\widetilde{Y}_O \widetilde{T}^2}\right) + ... \right] \tag{55}$$

Equation (55) leads to various difficulties. First, new quantities such as $\widetilde{Y''_k T''^n}$ have to be closed using algebraic expressions or transport equations. Because of non linearities, large errors exist when only few terms of the series expansion are retained. Expression (55) is quite complicated, but is only valid for a simple irreversible reaction and cannot be easily extended to realistic chemical schemes (at least 9 species and 19 reactions for hydrogen combustion, several hundred species and several thousand reactions for hydrocarbon combustion...). For these reasons, reaction rate closures in turbulent combustion are not based on (55). Models are rather derived from physical analysis as discuss below.

Nevertheless, this approach is used in some simulations of supersonic reacting flows [55] or to describe reaction in atmospheric boundary layer where the temperature T may be roughly assumed to be constant [56]. In these situations, only the first two terms in the series expansion are kept. A segregation factor, α_{FO}, is then introduced:

$$\alpha_{FO} = -\frac{\widetilde{Y''_F Y''_O}}{\widetilde{Y}_F \widetilde{Y}_O} = -\left(1 - \frac{\widetilde{Y_F Y_O}}{\widetilde{Y}_F \widetilde{Y}_O}\right) \tag{56}$$

to characterize the mixing between the reactants F and O. If they are perfectly separated $\widetilde{Y_F Y_O} = 0$ and $\alpha_{FO} = -1$. On the other hand, a perfect mixing ($\widetilde{Y''_F Y''_O} = 0$) leads to $\alpha_{FO} = 0$. This segregation factor may be either postulated or provided by a balance equation (see [57] in a large eddy simulation context). Then, the mean reaction rate becomes:

$$\overline{\dot{\omega}}_F = -A\ (1-\alpha_{FO})\ \overline{\rho}^2 \widetilde{T}^b \widetilde{Y}_F \widetilde{Y}_O \exp\left(-\frac{T_A}{\widetilde{T}}\right) \tag{57}$$

5 Scales and diagrams for turbulent combustion

5.1 Introduction

As the mean burning rate $\overline{\dot{\omega}}$ cannot be found from an averaging of Arrhenius laws, a physical approach is required to derive models for turbulent combustion. Turbulent combustion involves various lengths, velocity and time scales describing turbulent flow field and chemical reactions. The physical analysis is mainly based on comparison between these scales.

The turbulent flow is characterized by a Reynolds number comparing turbulent transport to viscous forces:

$$Re = \frac{u' l_t}{\nu} \tag{58}$$

where u' is the velocity rms (related to the square root of the turbulent kinetic energy k), l_t is the turbulence integral length scale and ν the kinematic viscosity of the flow.

The Damköhler number compares the turbulent (τ_t) and the chemical (τ_c) time scales:

$$Da = \frac{\tau_t}{\tau_c} \tag{59}$$

In the limit of high Damköhler numbers ($Da \gg 1$), the chemical time is short compared to the turbulent one, corresponding to a thin reaction zone distorted and convected by the flow field. The internal structure of the flame is not strongly affected by turbulence and may be described as a laminar flame element called "flamelet". The turbulent structures wrinkle and strain the flame surface. On the other hand, a low Damköhler number ($Da \ll 1$) corresponds to a slow chemical reaction. Reactants and products are mixed by turbulent structures before reaction. In this *perfectly stirred reactor* limit, the mean reaction rate may be expressed from Arrhenius laws using mean mass fractions and temperature, corresponding to the first term of the Taylor's expansion (55).

In turbulent flames, as long as quenching does not occur, most practical situations correspond to high or medium values of the Damköhler numbers. It is worth noting that various chemical time scales may be encountered: fuel oxidation generally corresponds to short chemical time scales ($Da \gg 1$) whereas pollutant production or destruction such as CO oxidation or NO formation are slower.

5.2 Turbulent premixed combustion diagram

5.2.1 Introduction

The objective is to analyze premixed turbulent combustion regimes by comparing turbulence and chemical characteristic length and time scales. This analysis leads to combustion diagrams where various regimes are presented as function of various dimensionless numbers [58, 59, 60, 13, 61, 27]. These diagrams could be a support to select and develop the relevant combustion model for a given situation. A formalism combining recent analysis [60, 27] is retained here.

For turbulent premixed flames, the chemical time scale, τ_c, may be estimated as the ratio of the thickness δ_l and the propagation speed S_L of the laminar flame[1]. Estimating the turbulent time from turbulent integral scale characteristics ($\tau_t = l_t/u'$), the Damköhler number becomes:

$$Da = \frac{\tau_t}{\tau_c} = \frac{l_t}{\delta_l}\frac{S_L}{u'} \tag{60}$$

where a velocity ratio (u'/S_L) and a length scale ratio (l_t/δ_l) are evidenced.

5.2.2 Combustion regimes

For large values of the Damköhler number ($Da \gg 1$), the flame front is thin and its inner structure is not affected by turbulence motions which only wrinkle the flame surface. This *flamelet regime* or *thin wrinkled flame regime* (Fig. 8a) occurs when the smallest turbulence scales (i.e. the Kolmogorov scales), have a turbulent time τ_k larger than τ_c (turbulent motions are too slow to affect the flame structure). This transition is described in term of the Karlovitz number Ka:

$$Ka = \frac{\tau_c}{\tau_k} = \frac{\delta_l}{l_k}\frac{u_k}{S_L} \tag{61}$$

[1]This chemical time τ_c corresponds to the time required for the flame to propagate over a distance equal to its own thickness. This time may also be viewed as a diffusive time scale, using Eq. (34):

$$\tau_c = \frac{\delta_l}{S_L} = \frac{1}{Re_f}\frac{\delta_l^2}{\nu}$$

The size l_k and the velocity u_k of Kolmogorov structures are given by [62]:

$$l_k = \left(\frac{\nu^3}{\varepsilon}\right)^{1/4} \quad ; \quad u_k = (\nu\varepsilon)^{1/4} \tag{62}$$

where ε is the dissipation of the turbulent kinetic energy k. The integral length scale l_t may be written:

$$l_t = \left(\frac{u'^3}{\varepsilon}\right) \tag{63}$$

using $\nu = \delta_l S_L$, corresponding to an unity flame Reynolds number Re_f (Eq. 34), yields

$$\boxed{Ka = \left(\frac{u'}{S_L}\right)^{3/2} \left(\frac{l_t}{\delta_l}\right)^{-1/2}} \tag{64}$$

Reynolds, Re, Damköhler, Da, and Karlovitz, Ka, numbers are related as:

$$\boxed{Re = Da^2 Ka^2} \tag{65}$$

and a set of two parameters (Re, Da), (Re, Ka) or (Da, Ka) are necessary to discuss regimes in the case of premixed reactants.

The Karlovitz number also compares the flame and the Kolmogorov length scales according to:

$$Ka = \left(\frac{\delta_l}{l_k}\right)^2 \tag{66}$$

The Karlovitz number is used to define the *Klimov-Williams criterion*, corresponding to $Ka = 1$, delineating between two combustion regimes. This criterion was first interpreted as the transition between the flamelet regime ($Ka < 1$), previously described, and the *distributed combustion regime* where the flame inner structure is strongly modified by turbulence motions. A recent analysis [27] has shown that, for Karlovitz numbers larger than unity ($Ka > 1$), turbulent motions become able to affect the flame inner structure but not necessarily the reaction zone. This reaction zone, where heat is released, has a thickness δ_r quite lower that the thermal thickness δ_l of the flame ($\delta_r \approx 0.1\delta_l$). The Karlovitz number based on this reaction thickness is:

$$Ka_r = \left(\frac{\delta_r}{l_k}\right)^2 = \left(\frac{\delta_r}{\delta_l}\right)^2 \left(\frac{\delta_l}{l_k}\right)^2 \approx \frac{1}{100}\left(\frac{\delta_l}{l_k}\right)^2 \approx \frac{Ka}{100} \tag{67}$$

Then, the following turbulent premixed flame regimes are proposed [27]:

- $Ka < 1$: **Flamelet regime** or **thin wrinkled flame regime** (Fig. 8a). Two subdivisions may be proposed depending on the velocity ratio u'/S_L:
  - $(u'/S_L) < 1$: *wrinkled flame*. As u' may be viewed as the rotation speed of the larger turbulent motions, turbulent structures are unable to wrinkle the flame surface up to flame front interactions. The laminar propagation is predominant and turbulence / combustion interactions remain limited.
  - $(u'/S_L) > 1$: *wrinkled flame with pockets* ("corrugated flames"). In this situation, larger structures become able to induce flame front interactions leading to pockets.
- $1 < Ka \leq 100$ ($Ka_r < 1$) : **Thickened wrinkled flame regime** or **thin reaction zone**. In this case, turbulent motions are able to affect and to thicken the flame preheat zone, but cannot modify the reaction zone which remains thin and close to a laminar reaction zone (Fig. 8b).

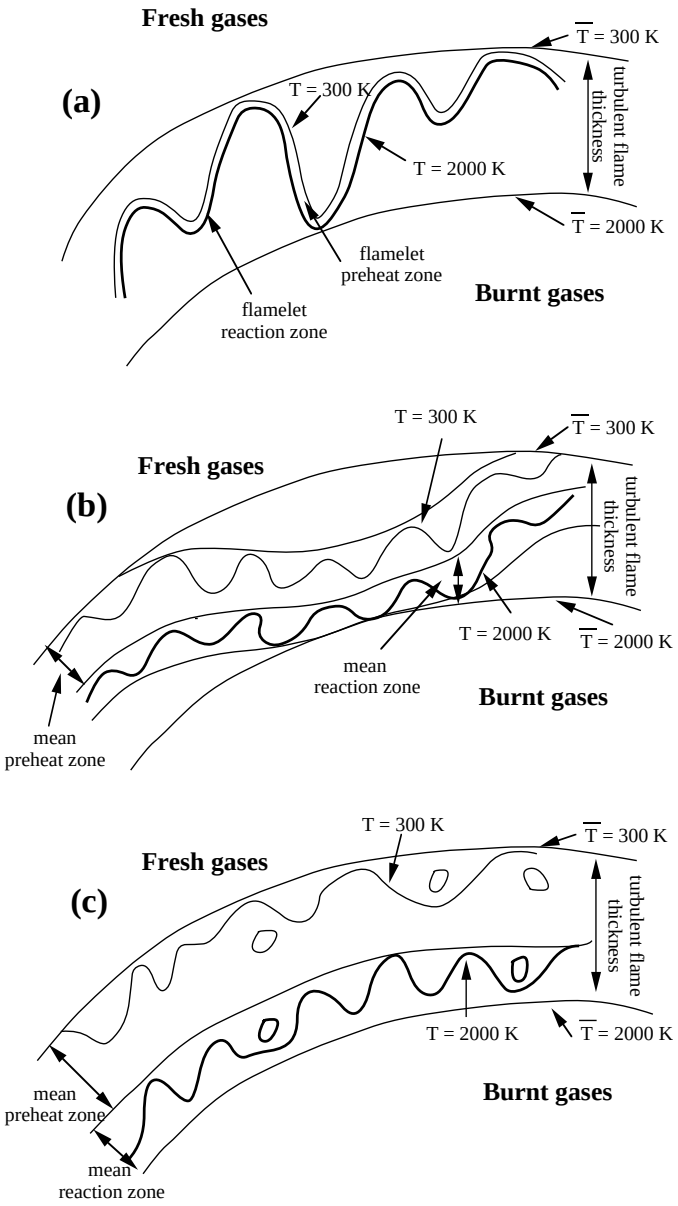

Figure 8: Turbulent premixed combustion regimes as identified by Borghi and Destriau (1995). (a) flamelet (thin wrinkled flame). (b) thickened wrinkled flame regime. (c) thickened flame regime.

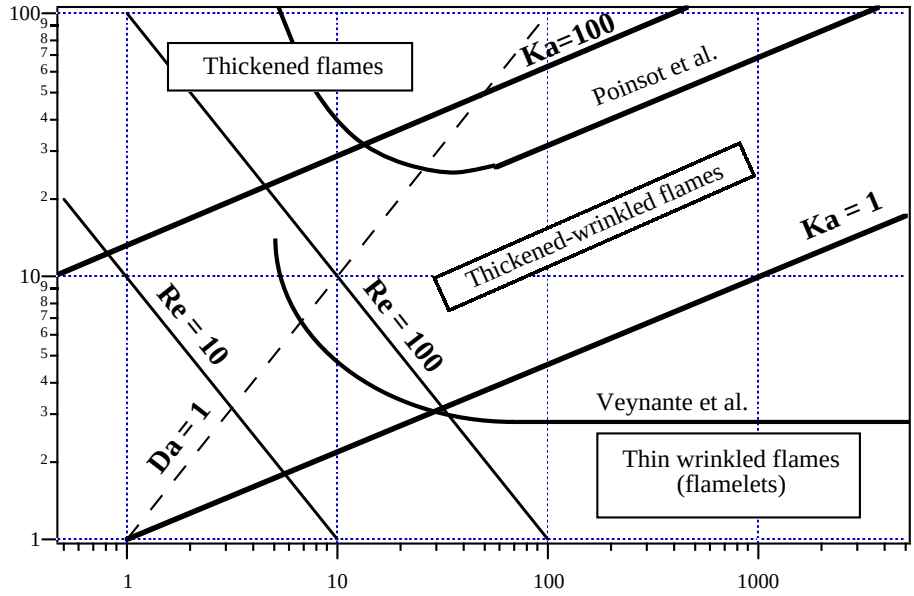

Figure 9: Turbulent premixed combustion diagram [60, 27]. Combustion regimes are identified using the length scale (l_t/δ_l) and the velocity (u'/S_L) ratii. The Klimov-Williams criterion ($Ka = 1$) corresponds to a flame thickness δ_l equal to the Kolmogorov scale l_k. Below this line, the flame is thinner than any turbulent scale. Below the line delineating the Peters criterion ($Ka = 100$ or $Ka_r = 1$), the reaction zone thickness, δ_r, is thinner than any turbulent scale and is not affected by turbulent motions (the criterion is plotted assuming $\delta_r \approx 0.1\,\delta_l$). The flamelet regime limit devised by Poinsot *et al.* [63] from direct numerical simulations is also displayed. The criterion proposed in [64] to delineate between gradient (above) and counter-gradient (below) turbulent transport is displayed assuming a heat release factor $\tau = T_b/T_u - 1 = 6$ where T_u and T_b are respectively the fresh and the burnt gases temperature (see § 8).

- $Ka > 100$ ($Ka_r > 1$) : **Thickened flame regime** or **well-stirred reactor**. In this situation, preheat and reaction zones are strongly affected by turbulent motions and no laminar flame structure may be identified (Fig. 8c).

These various regimes are generally displayed on a logarithmic diagram (u'/S_L ; l_t/δ_l), similar to the one presented on Fig. 9.

5.2.3 Comments

This analysis, leading to a rough classification of combustion regimes as a function of characteristic numbers, has been developed as a support to derive and choose turbulent combustion models. Following this classification, most practical applications correspond to *flamelet* or *thickened wrinkled flame* regimes. Nevertheless, **such analysis are only qualitative and should be used with great care**. A diagram such as the one displayed on Fig. 9 cannot be readily used to determine the combustion regime of a practical system from (u'/S_L) and (δ_l/l_t) ratii:

- The analysis is based on the assumption of an homogeneous and isotropic turbulence unaffected by heat release, which is not the case in combustion systems.
- Some used quantities are not clearly defined. For example, the flame thickness δ_l may be based on the thermal thickness or on the diffusive thickness. Accordingly, the limits between the various regimes may noticeably change.
- All regime limits are based on order of magnitude estimations and not on precise derivations. For example, the flamelet regime limit could correspond to a Karlovitz number $Ka = 0.1$ or $Ka = 10$, rather than $Ka = 1$.
- Various effects are not taken into account. Unsteady and curvature effects play an important role neglected here. Turbulent premixed combustion diagrams were analyzed using direct numerical simulations of flame / vortex interactions [63]. Results show that the flamelet regime seems to extend over the Klimov-Williams criterion (see Fig. 9). DNS has revealed that small turbulent scales, which are supposed in classical theories to have the strongest effects on flames, have small lifetimes because of viscous dissipation and therefore only limited effects on combustion, results recovered experimentally [65]. Peters [27] shows that the criterion $Ka = 100$ (i.e. $Ka_r = 1$) is in quite good agreement with the transition proposed in [63], at least when the length scale ratio, l_t/δ_l, is sufficiently large.
- Additive length scales have been introduced in the literature. For instance the Gibson scale l_G, to characterize the size of the smaller vortex able to affect the flame front was used [61]. This length was defined as the size of the vortex having the same velocity than the laminar flame speed S_L.
- All these analysis are implicitly based on a single step irreversible reaction. In actual turbulent combustion, a large number of chemical species and reactions are involved (several hundred species and several thousand reactions for propane burning in air). These reactions may correspond to a large range of chemical time scales. For example, the propane oxidation may assumed to be fast compared to turbulent time scale. On the other hand, the CO_2 formation from carbon monoxide (CO) and OH radical in the burnt gases is quite slower with chemical time of the same order than turbulent times.

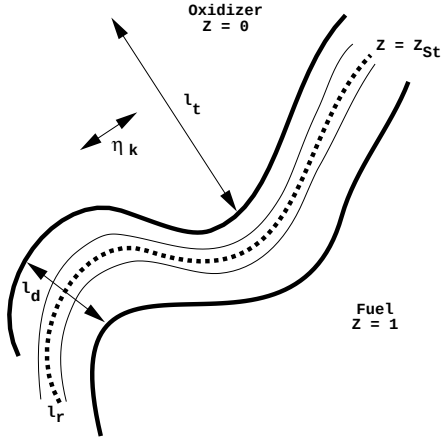

Figure 10: Sketch of a nonpremixed turbulent flame. Z is the mixture fraction, l_d the diffusive thickness, l_r the reaction zone thickness, l_t the turbulence integral length scale and l_k the Kolmogorov micro-scale.

5.3 Nonpremixed turbulent combustion diagram

5.3.1 Introduction

Two numbers, a length and a velocity ratii, have been used to identify premixed turbulent combustion regimes. The problem is more difficult in nonpremixed turbulent combustion because diffusion flames do not propagate and, therefore, exhibit no intrinsic characteristic speed. In addition, the thickness of the flame depends on the aerodynamics controlling the thickness of the local mixing layers developing between fuel and oxidizer (§ 3.2) and no fixed reference length scale can be easily identified for diffusion flames. This difficulty is well illustrated in the literature, where various characteristic scales have been retained depending on the authors [66, 67, 31, 68, 69, 70]. These classifications of nonpremixed turbulent flames may be organized in three major groups:

- The turbulent flow regime is characterized by a Reynolds number, whereas a Damköhler number is chosen for the reaction zone [71].
- The mixture fraction field is retained to describe the turbulent mixing using $\widetilde{Z''^2}$ and a Damköhler number (ratio of Kolmogorov to chemical time) characterizes the flame [31].
- A velocity ratio (turbulence intensity to flame speed) and a length ratio (integral scale to flame thickness) may be constructed [67] to delineate between regimes.

Additional lengths have also been introduced, using for instance thicknesses of profiles in mixture fraction space [66].

A laminar diffusion flame is fully determined from a Damköhler number $Da^* = (\tau_c \chi_{st})^{-1}$, where the value of the chemical time τ_c depends on the fuel chemistry [28] (§ 3.2). In this number, the scalar dissipation rate under stoichiometric condition ($Z = Z_{st}$), $\chi_{st} = D|\nabla Z|^2_{st}$, measures at the same time a mechanical time, $\tau_\chi = \chi_{st}^{-1}$, and, a characteristic mixing length, $l_d = (D/\chi_{st})^{1/2}$. According to asymptotic developments [28], the reaction zone thickness is of the order of $l_r \approx l_d \, (Da^*)^{-1/(a+1)}$, where a is the order of a global one-step reaction. Because diffusion flames do not feature a fixed reference length, a main difficulty arises when effects of unsteadiness need to be quantified. In a steady laminar flame the local rate of strain is directly related to χ_{st} (and to a flame thickness), however, when the velocity field fluctuates, unsteadiness in diffusion flames develops at two levels [72]:

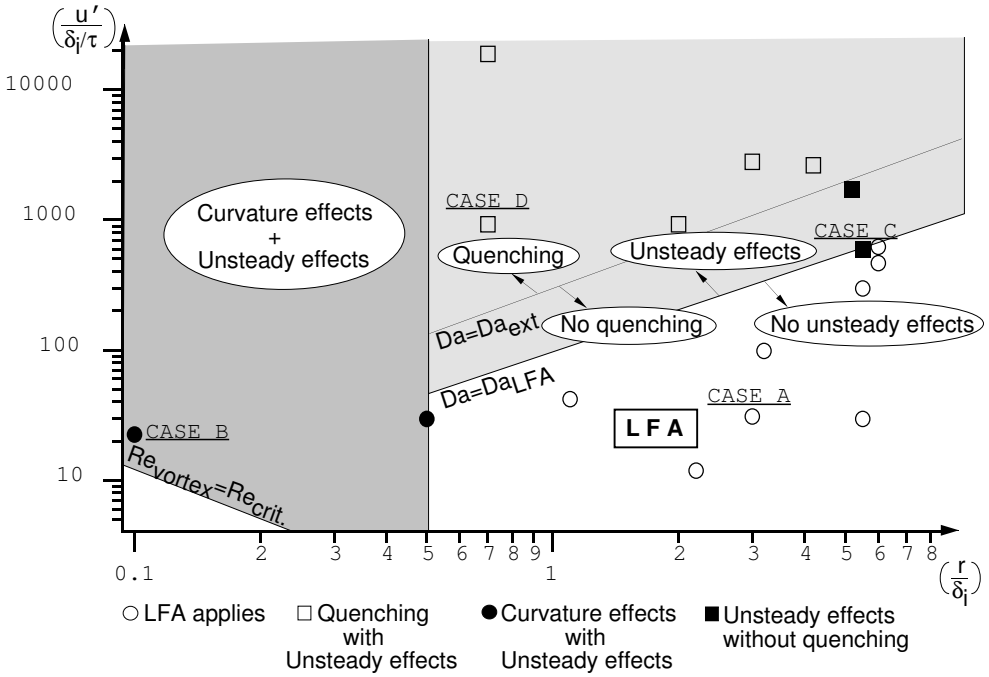

Figure 11: Nonpremixed flame/vortex interaction regimes by Cuenot and Poinsot [69]. This diagram delineates the steady Laminar Flamelet Assumption (LFA) validity regions, the quenching limits and the zone where unsteady and curvature effects are important during flame vortex interaction. $u^{'}$ is the level of velocity fluctuations, $\delta_i = l_d$ is the flame thickness ($\approx |\nabla Z|^{-1}$), τ is a chemical time and r the characteristic size of the vortices.

- The mixture fraction field Z does not respond immediately to velocity fluctuations, leading to a distribution of χ_{st} for given rates of strain. Because a strong correlation exists between χ_{st} and velocity gradients taken along the stoichiometric line [73], this effect is not the dominant one when finite rate chemistry occurs.
- For finite rate chemistry, the burning rate does not follow immediately variations of χ_{st}, leading to a second level of unsteadiness, modifying the burning rate (Eq. 68).

$$u^{'} \rightarrow \Big[\text{Unsteadiness in mixing}\Big] \rightarrow \chi_s \rightarrow \Big[\dot{\omega}_i \text{ unsteadiness (for } Da^* < \infty)\Big] \tag{68}$$

Summarizing these effects in a generic diagram is an arduous task. A diagram for laminar flames submitted to curvature associated to a time varying strain rate was obtained by Cuenot and Poinsot from DNS results of flame/vortex interaction [69]. In this diagram presented on Fig. 11, the flame thickness is $\delta_i \approx l_d$, whereas r and $u^{'}$ denote respectively the characteristic size and velocity of the vortex pair. This analysis evidences two limiting Damköhler numbers, Da_{LFA} and Da_{ext}. When Da^* is larger than Da_{LFA}, the flame front may be viewed as a steady laminar flame element and its inner structure is not affected by vortices. On the other hand, when $Da^* \leq Da_{ext}$, flame extinction occurs. In the intermediate Damköhler number range (i.e. $Da_{ext} < Da^* < Da_{LFA}$), strong unsteadiness effects are observed. In a nonpremixed turbulent flame, the reaction zones develop within a mean mixing zone whose thickness

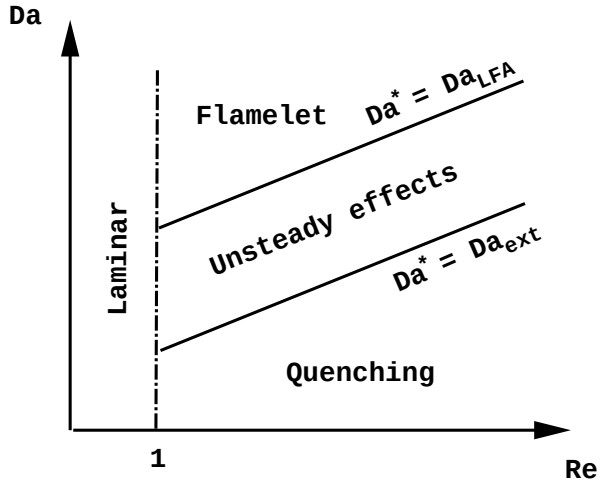

Figure 12: Schematic of nonpremixed turbulent combustion regimes as function of the Damköhler number $Da = \tau_t/\tau_c$ (constructed from the turbulent integral time scale τ_t and chemical time τ_c) and Re the turbulent Reynolds number.

l_z is of the order of the turbulent integral length scale l_t (Fig. 10):

$$l_z \approx |\nabla \widetilde{Z}|^{-1} \approx l_t \approx \left(\frac{k^{3/2}}{\varepsilon}\right) \tag{69}$$

Turbulent small scale mixing mainly depends on both velocity fluctuations, transporting the iso-Z surfaces (stirring), and diffusion between these iso-surfaces that compose the mixing layer of thickness l_d, with

$$l_d \approx \left(\frac{D}{\widetilde{\chi}_{st}}\right)^{1/2} \tag{70}$$

where $\widetilde{\chi}_{st}$ denotes the conditional value of the scalar dissipation rate χ for $Z = Z_{st}$.

When transport of species and heat by velocity fluctuations is faster than transfer in the diffusion flame, a departure from laminar flamelet is expected. Also, when the Kolmogorov scale l_k is of the order of the flame thickness, the inner structure of the reaction zone may be modified by the turbulence. As diffusion flame scales strongly depend on the local flow motions, one may write:

$$l_d \approx \alpha_1 l_k \text{ and } \widetilde{\chi}_{st} \approx \frac{\alpha_2}{\tau_k} \tag{71}$$

where $\alpha_1 \geq 1$ and $\alpha_2 \leq 1$ (the maximum local strain rate would correspond to $l_d = l_k$).

Then using $\tau_t/\tau_k = \sqrt{Re}$, the Damköhler number comparing turbulent flame scale and chemical flame scale is recast as:

$$Da = \frac{\tau_t}{\tau_c} = \frac{\tau_t}{\tau_k}\frac{\tau_k}{\tau_c} \approx \frac{\tau_t}{\tau_k}\frac{\alpha_2}{\widetilde{\chi}_{st}\tau_c} \approx \alpha_2\sqrt{Re}Da^* \tag{72}$$

Constant Damköhler numbers Da^* correspond to lines of slope $1/2$ in a log-log (Da, Re). When the chemistry is sufficiently fast (large Da values), the flame is expected to have a laminar flame structure. This condition may be simply expressed as $Da^* \geq Da_{LFA}$ On the other hand, for large chemical times (i.e. when $Da^* \leq Da_{ext}$), extinction occurs. Laminar flames are encountered for low Reynolds numbers ($Re < 1$). Results are summarized in Fig. 12.

In a practical combustion devices, α_1 and α_2 would evolve in space and time according to flow fluctuations, velocity and scalar energetic spectra. In a given burner, it is likely that one may observe at different locations, or consequently, flamelet behavior and strong unsteadiness, or even quenching.

As the classification of premixed turbulent flames, these considerations are limited by the numerous hypothesis necessary to derive the regimes.

6 Tools for turbulent combustion modeling

6.1 Introduction

The mean heat release rate is one of the main quantities of practical interest that should be approximated by turbulent combustion models. The simplest and more direct approach is to develop the chemical rate in Taylor series as a function of species mass fractions and temperature (Eq. 55). This analysis is limited by its low accuracy and by the rapidly growing complexity of the chemistry (§ 4). It is then concluded that the non-linear character of the problem requires the introduction of new tools.

These new tools must be designed to describe turbulent flames and have to provide estimation of mean production or consumption rates of chemical species. They also need to be based on known quantities (mean flow characteristics, for example) or on quantities that may be easily modeled or obtained from closed balance equations. In this section, a generic description of the main concepts used to model turbulent combustion is proposed. Relations between the various approaches are also emphasized, but the discussion of the closure strategy is postponed to subsequent sections.

The basic ingredients to describe turbulent flames remain the quantities introduced for laminar flame analysis: the progress variable c for premixed combustion ($c = 0$ in fresh gases and $c = 1$ in burnt gases, see § 3.1), and, the mixture fraction Z for nonpremixed flames (Z is a passive scalar, with $Z = 0$ in pure oxidizer and $Z = 1$ in pure fuel, see § 3.2). The flame position would correspond to values of the progress variable c lying between 0 and 1, or, to Z taking on values in the vicinity of $Z = Z_{st}$.

Three main types of approaches are summarized on Fig. 13:

- The burning rate may be quantified in terms of **turbulent mixing**. When the Damköhler number $Da = \tau_t/\tau_c$, comparing turbulent (τ_t) and chemical (τ_c) characteristic times, is large (a common assumption in combustion modeling), the reaction rate is limited by turbulent mixing, described in terms of scalar dissipation rates [74]. The small scale dissipation rate of species controls the mixing of the reactants and, accordingly, play a dominant role in combustion modeling, even for finite rate chemistry.

- In the **geometrical analysis**, the flame is described as a geometrical surface, this approach is usually linked to a flamelet assumption (the flame is thin compared to all flow scales). Following this view, scalar fields (c or Z) are studied in terms of dynamics and physical properties of iso-value surfaces defined as flame surfaces (iso-c^* or iso-Z_{st}). The flame is then envisioned as an interface between fuel and oxidizer (nonpremixed) or between fresh and burnt gases (premixed). A flame normal analysis is derived by focusing the attention on the structure of the reacting flow along the normal to the flame surface. This leads to flamelet modeling when this structure is compared to one-dimensional laminar flames. The density of flame surface area per unit volume is also useful to estimate the burning rate.

- The **statistical properties** of scalar fields may be collected and analyzed for any location within the flow. Mean values and correlations are then extracted via the knowledge of one-point probability density functions (pdf). The determination of these pdfs leads to pdf modeling. A one-point statistical analysis restricted to a particular value of the scalar field is related to the study of conditional statistics. Conditional statistics which are obviously linked to the geometrical analysis and to flame surfaces when the conditioning value is c^* or Z_{st}.

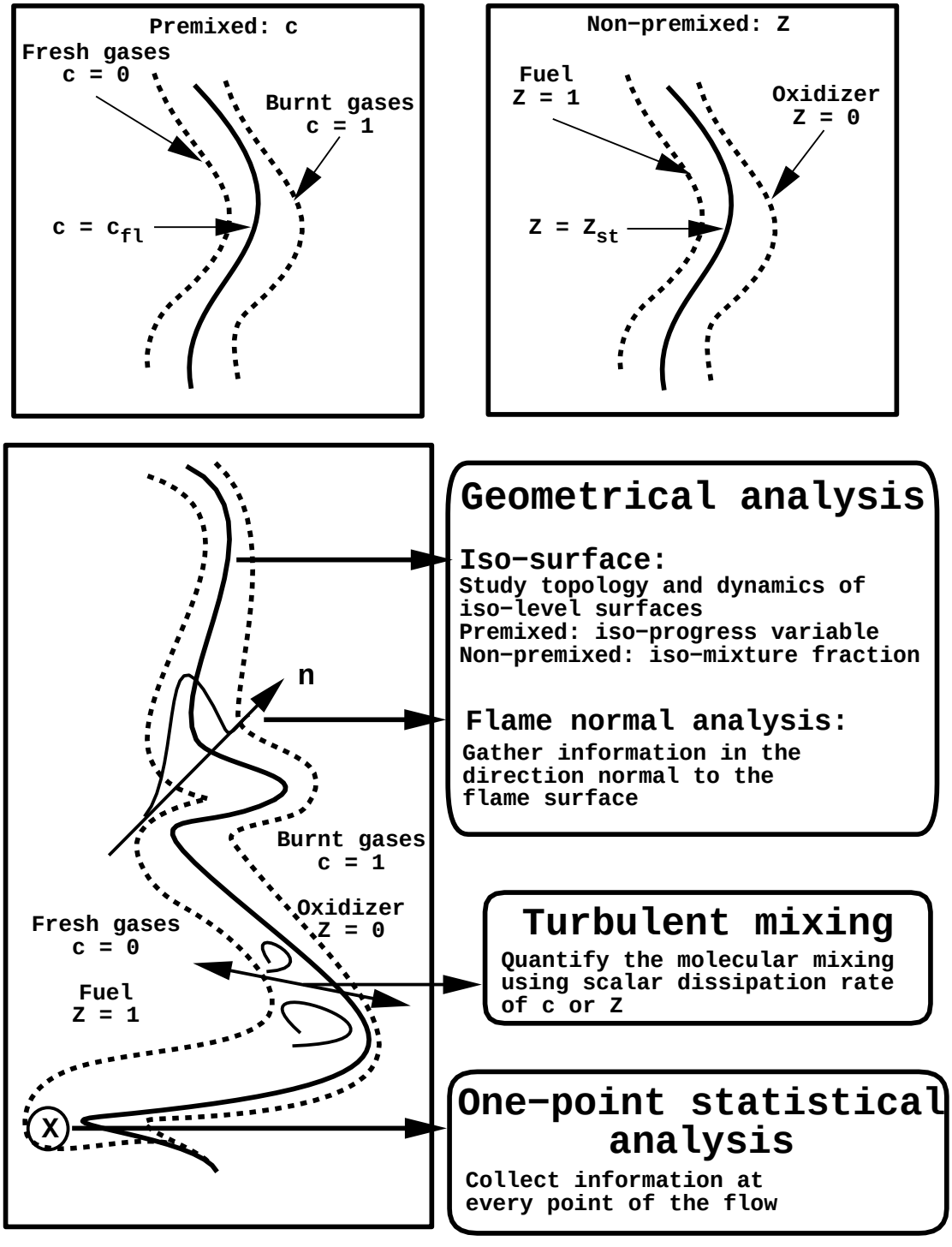

Figure 13: Three types of analysis for premixed or nonpremixed turbulent flames.

6.2 Scalar dissipation rate

In a first step, the transport equation for $\widetilde{c''^2}$ or $\widetilde{Z''^2}$ are derived, these fluctuations characterize non-homogeneities and intermittencies. In the case of the progress variable, the variance $\widetilde{c''^2}$ is defined as:

$$\overline{\rho}\widetilde{c''^2} = \overline{\rho\left(c-\widetilde{c}\right)^2} = \overline{\rho}\left(\widetilde{c^2}-\widetilde{c}^2\right) = \overline{\rho c^2} - \overline{\rho}\widetilde{c}^2 \tag{73}$$

Starting from the balance equation for the progress variable (Eq. 36), c is decomposed into $c = \widetilde{c} + c''$, then the new equation is multiplied by c'' and averaged. After straightforward manipulations, the exact transport equation for $\widetilde{c''^2}$ reads:

$$\begin{aligned}\frac{\partial\overline{\rho}\widetilde{c''^2}}{\partial t} + \nabla\cdot\left(\overline{\rho}\widetilde{\mathbf{u}}\widetilde{c''^2}\right) + \nabla\cdot\left(\overline{\rho}\widetilde{\mathbf{u}''c''^2}\right) = \nabla\cdot\left(\overline{\rho D\nabla c''^2}\right) + 2\overline{c''\nabla\cdot(\rho D\nabla\widetilde{c})} \\ \underbrace{-2\overline{\rho}\widetilde{u''c''}\cdot\nabla\widetilde{c}}_{\text{Production}} \underbrace{-2\overline{\rho D\nabla c''\cdot\nabla c''}}_{\text{Dissipation}} + \underbrace{2\overline{\dot{\omega}c''}}_{\text{Source}}\end{aligned} \tag{74}$$

In addition to the two diffusive terms $\nabla\cdot\left(\overline{\rho D\nabla c''^2}\right)$ and $2\overline{c''\nabla\cdot(\rho D\nabla\widetilde{c})}$, which are non zero, but expected small for large Reynolds number flows (especially the second one), two important terms are found: The fluctuating part of the scalar dissipation rate $2\overline{\rho D\nabla c''\cdot\nabla c''}$ and a correlation $\overline{\dot{\omega}c''}$ involving the chemical source.

In the literature, various expressions have been associated to the terminology *scalar dissipation rate* (in laminar flame theory, it actually quantifies a diffusion speed § 3.2). It may include the density ρ, a factor 2 and be written in term of instantaneous (c) or fluctuating (c'') values of the concentration species. Thereafter:

$$\overline{\rho}\widetilde{\chi} = \overline{\rho D\,\nabla c\cdot\nabla c} = \overline{\rho D}\,\nabla\widetilde{c}\cdot\nabla\widetilde{c} + 2\overline{\rho D\,\nabla c''}\cdot\nabla\widetilde{c} + \overline{\rho D\nabla c''\cdot\nabla c''}$$

leading to, when mean gradients are neglected:

$$\overline{\rho}\widetilde{\chi} \approx \overline{\rho D\nabla c''\cdot\nabla c''} \tag{75}$$

Then, $\overline{\rho}\widetilde{\chi}$ is the dissipation rate of the fluctuations of the scalar field.

In the simplified case of homogeneous flames (no $\widetilde{c}$ or $\widetilde{Z}$ gradient), the time evolution of the scalar variances are governed by:

$$\begin{aligned}\text{Premixed combustion:} \quad & \frac{d\overline{\rho}\widetilde{c''^2}}{dt} = -2\overline{\rho D\nabla c''\cdot\nabla c''} + 2\overline{\dot{\omega}c''} \\ \text{Nonpremixed combustion:} \quad & \frac{d\overline{\rho}\widetilde{Z''^2}}{dt} = -2\overline{\rho D\nabla Z''\cdot\nabla Z''}\end{aligned}$$

These equations have important implications:

- The scalar dissipation rate directly measures the decaying speed of fluctuations via turbulent micromixing. Since the burning rate depends on the contact between the reactants, in any models, the scalar dissipation rate enters directly or indirectly the expression for the mean burning rate. For instance, when assuming very fast chemistry and a combustion limited by mixing, the mean burning rate is proportional to the scalar dissipation rate of Z or c.

- Within a premixed system, turbulent mixing occurs between fresh and burnt gases. One may then expect a very strong coupling between mixing phenomena and chemical reaction. This is observed in the equation for $\widetilde{c''^2}$ where, at the same time, $\widetilde{\chi}$ and the chemical source $\widetilde{\dot{\omega}c''}$ are involved.
- In a nonpremixed flame, fresh fuel and fresh oxidizer have to be mixed at the molecular level for reacting and the flame is mainly controlled by turbulent mixing occurring between the fresh gases. In consequence, there is no chemical source acting on the evolution of $\widetilde{Z''^2}$. The mixture fraction Z is sensitive to chemistry only via density change, making the coupling between chemistry and mixing different than in the case of premixed combustion.

This preliminary analysis shows that **dissipation rate of scalars is a very key concept of turbulent combustion** and, directly or indirectly, χ appears in any tools used to model flames. The main stumbling block in turbulent combustion modeling and bridges between the various modeling concepts emerge through the scalar dissipation rate.

6.3 Geometrical description

The flame front is here described as a geometrical entity. This analysis is generally linked to the assumption of a sufficiently thin flame, viewed as an interface between fresh and burnt gases in premixed combustion or as an interface between fuel and oxidizer in nonpremixed situations. Two formalisms have been proposed: field equation or flame surface density concept.

6.3.1 G-field equation

The balance equation for the progress variable may be written:

$$\frac{\partial c}{\partial t} + \mathbf{u} \cdot \nabla c = \frac{1}{\rho} \left(\nabla \cdot (\rho D \nabla c) + \dot{\omega} \right) = w \left| \nabla c \right| \qquad \text{or} \qquad \frac{\partial c}{\partial t} + \mathbf{u}_c \cdot \nabla c = 0 \tag{76}$$

where $\mathbf{u}_c$ is the absolute propagation velocity of the progress variable field. This velocity is easily decomposed into the flow velocity $\mathbf{u}$ and w the relative velocity of the iso-c surface measured with respect to the flow, leading to $\mathbf{u}_c = \mathbf{u} + w\,\mathbf{n}$, where $\mathbf{n} = -(\nabla c / \left| \nabla c \right|)$ is the local normal vector to the iso-c surface, pointing toward the fresh gases. The relative displacement speed w is given by Eq. (37).

In laminar flames, a G field whose level $G = G_0$ represents the flame surface, was introduced to simulate the propagation of fronts [75]. The "G-equation" may be written:

$$\frac{\partial G}{\partial t} + \mathbf{u}_c \cdot \nabla G = 0 \qquad \text{or} \qquad \frac{\partial G}{\partial t} + \mathbf{u} \cdot \nabla G = w \left| \nabla G \right| \tag{77}$$

This kinematic description of premixed combustion possesses some attractive aspects:

- The internal flame front structure does not need to be resolved on the computational mesh. Only the G-field, generally quite thicker than the flame front, needs to be resolved. Usually, $G(\underline{x})$ is defined as the distance of the given location $\underline{x}$ to the flame front [76].
- Under the assumption of constant density (thermodiffusive assumption), the G-equation may be used for low cost direct numerical simulations. Each G iso-surface is then related to a flame front, and one may argue that a single simulation corresponds to the computation of several flames.

In non constant density flows where thermal heat release is included, the displacement speed w of the G-iso-surface is affected by thermal expansion and should be corrected for density variations,

even in the case of a steady laminar flame propagating at the constant laminar flame speed S_L, defined relatively to the unburnt gases. This correction is:

$$w = \frac{\rho_u}{\rho} w_u \tag{78}$$

where w_u is the flame displacement speed relative to the unburnt gases of density ρ_u.

A more difficult point is the coupling required between the G-equation and the species or energy balance equations. The G-equation provides a kinematic description of the flame front and involves its displacement speed w. The reactant consumption and the heat release rate are controlled by the consumption speed S_c:

$$\rho_u S_c = \int_{-\infty}^{\infty} \dot{\omega} d\xi \tag{79}$$

where ρ_u in the fresh gases density and ξ the spatial coordinate along the normal direction to the flame front. Of course, w and S_c are related but may be quite different, especially in high flame front curvature zones [77]. The displacement speed w may also be quite different from the laminar flame speed S_L.

The coupling between the consumption speed S_c and the displacement speed w is a very key point in G-field modeling. Three approaches have been proposed to overcome this difficulty:

- **Flame front tracking technique**: The displacement of the flame front is evaluated from the displacement speed w, leading to an estimation of the volume of burnt gases produced along with the thermal heat release [78, 79]. Based on a purely geometric approach, this technique is well suited to two dimensional simulations, but its extension to 3D cases may not be straightforward.

- **Temperature (or energy) reconstruction**: The temperature field is directly estimated from the G field as [80]:

  $$T = T_u + \frac{Q}{C_p} H\left(G - G^*\right) \tag{80}$$

  where T_u is the temperature of unburnt gases, Q the reaction heat release and H denotes the Heaviside function (the Heaviside function is smoothed on the mesh of the simulation). This approach does not require a balance equation for the energy but is not applicable when heat losses or compressibility effects (for example in an internal combustion engines) occur.

- **Estimation of the heat release rate from the G-field**: The G-field is used to estimate the heat release rate to be incorporated in the balance energy equation from a formulation similar to Eq. (80) [81]. Accordingly, any other effects (heat losses, compressibility) may be included.

This formalism may be extended to turbulent flames. Averaging the progress variable equation (76) leads to:

$$\frac{\partial \widetilde{c}}{\partial t} + \widetilde{\mathbf{u}} \cdot \nabla \widetilde{c} = \frac{\rho_u}{\overline{\rho}} \underbrace{\left[\frac{-\nabla \cdot \left(\overline{\rho} \widetilde{\mathbf{u}'' \mathbf{c}''} \right) + \overline{\rho w \left| \nabla c \right|}}{\left| \nabla \widetilde{c} \right|} \right]}_{S_T} \left| \nabla \widetilde{c} \right| \tag{81}$$

where the turbulent flame speed, S_T, has to be modeled. The G-equation becomes:

$$\frac{\partial \widetilde{G}}{\partial t} + \widetilde{\mathbf{u}} \cdot \nabla \widetilde{G} = \frac{\rho_u}{\overline{\rho}} S_T \left| \nabla \widetilde{G} \right|$$

The mean turbulent flame brush is then located at the points where $\widetilde{G} = G_0$. The G-equation does not required thin flame elements per se. The overall turbulent flame is only viewed as a propagating surface

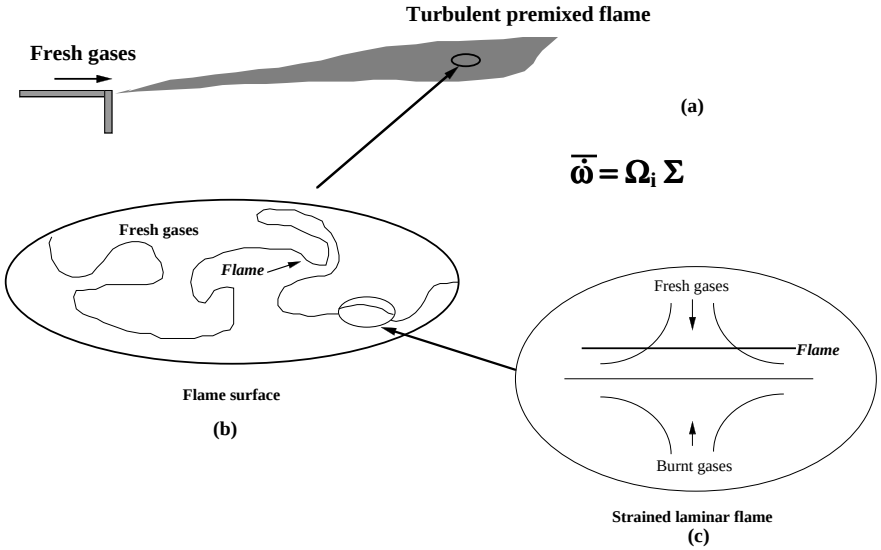

Figure 14: Flame surface density modeling

without solving for the internal flame structure. This formalism is therefore a good candidate for the numerical simulation of large systems where the knowledge of the internal structure of the flame brush is not required [78]. Nevertheless, a model has to be supplied for S_T, when doing so, turbulent transport and propagation may be separated to carefully model the effect of turbulence on w, the instantaneous displacement speed of the premixed front [31, 27].

6.3.2 Flame surface density description

The flame is identified as a surface and the flame surface density Σ is introduced, Σ measures the available flame area δA per unit volume δV. The mean burning rate of a species i is then modeled as:

$$\overline{\dot{w}}_i = \dot{\Omega}_i \Sigma \tag{82}$$

where $\dot{\Omega}_i$ is the mean local burning rate per unit of flame area integrated along the normal direction to the flame surface. $\dot{\Omega}_i$ is related to the properties of the local flame front and is generally estimated from a prototype laminar flame, incorporating more or less complexity. For instance, one may consider a planar laminar flame, submitted or not to a steady strain, a laminar flame where curvature effects have been introduced, or even a laminar unsteady strained and curved flame. The main advantage of this formulation, summarized on Fig. 14, is to decouple the chemical description (Ω_i) from the flame/turbulence interaction (Σ). The flame surface is convected, diffused, curved and strained by the velocity field [82, 15]. The flame surface density Σ may be estimated either from algebraic relations (see § 7.4.2) or as a solution of a balance equation. Using a phenomenological analysis, this balance equation was first proposed by Marble and Broadwell [83] for nonpremixed turbulent combustion. More rigorous derivations were obtained from geometrical considerations [84, 15] and from a statistical description [85, 86, 87] leading to an exact, but unclosed, balance equation. The derivation using statistical tools is now briefly summarized.

In premixed combustion, the flame surface density Σ of the iso-c^* surface is estimated from the conditional gradient of the progress variable c [85]:

$$\boxed{\Sigma(c^*) = \overline{|\nabla c|\,\delta(c-c^*)} = \left(\overline{|\nabla c|\,|c=c^*}\right)\,\overline{P}(c^*)} \tag{83}$$

where $\delta\,(c-c^*)$ is a local measure of the probability (see § 6.4.3), $\left(\overline{|\nabla c|\,|c=c^*}\right)$ is the conditional average of $|\nabla c|$ for $c=c^*$ and $\overline{P}(c^*)$ is to the probability to find $c=c^*$ at the given location. From this definition and the balance equation for the progress variable c, an exact equation for the flame surface density Σ may be derived according to the following steps [86]:

1. Derivation of an equation for $|\nabla c|$ from the equation for the instantaneous progress variable c.
2. Derivation of an equation for $|\nabla c|\,\delta(c-c^*)$ by conditioning the previous $|\nabla c|$ balance equation.
3. Averaging the $|\nabla c|\,\delta(c-c^*)$ balance equation leading to an exact equation for the flame surface density $\Sigma = \overline{|\nabla c|\,\delta(c-c^*)}$.

This derivation is valid for any iso-scalar surface (c^* can take any values between zero and unity) and $\Sigma(c^*,\underline{x},t)$ is also called a **surface density function**, the derivation of its balance equation is quite tedious [86] and similar to the derivation of a balance equation for the probability density function (§ 6.4.3), detail are not given here. Two equivalent forms of the progress variable equation may be used:

- A classical reaction/diffusion formulation:

$$\frac{\partial c}{\partial t} + \mathbf{u}\cdot\nabla c = \frac{1}{\rho}\left[\nabla\cdot(\rho D\nabla c) + \dot{\omega}\right] \tag{84}$$

- A propagative form:

$$\frac{\partial c}{\partial t} + \mathbf{u}\cdot\nabla c = w\,|\nabla c| \tag{85}$$

  where the displacement speed w of the flame front relatively to the flow was introduced (Eq. 37). This equation corresponds to the *G*-equation [76] (§ 6.3.1).

Two different types of equation for Σ are associated to these two formulations of the progress variable balance equation.

- A reaction/diffusion formulation:

$$\boxed{\begin{array}{rll} \dfrac{\partial\Sigma}{\partial t} + \nabla\cdot\left(\langle\mathbf{u}\rangle_s\Sigma\right) = & & \langle\nabla\cdot\mathbf{u} - \mathbf{nn}:\nabla\mathbf{u}\rangle_s\Sigma \\ & - & \left\langle\dfrac{1}{|\nabla c|}\dfrac{\partial}{\partial n}\left(\dfrac{1}{\rho}\left[\nabla\cdot(\rho D\nabla c)+\dot{\omega}\right]\right)\right\rangle_s\Sigma \\ & - & \dfrac{\partial}{\partial c^*}\left[\left\langle\dfrac{1}{\rho}\left[\nabla\cdot(\rho D\nabla c)+\dot{\omega}\right]\right\rangle_s\Sigma\right] \end{array}} \tag{86}$$

- A propagative formulation:

$$\boxed{\frac{\partial\Sigma}{\partial t} + \nabla\cdot\left(\langle\mathbf{u}\rangle_s\Sigma\right) = \langle\nabla\cdot\mathbf{u} - \mathbf{nn}:\nabla\mathbf{u}\rangle_s\Sigma - \nabla\cdot\left[\langle w\mathbf{n}\rangle_s\Sigma\right] + \langle w\nabla\cdot\mathbf{n}\rangle_s\Sigma} \tag{87}$$

where $\mathbf{n}$ is the unit vector normal to the $c = c^*$ surface and pointing towards the fresh gases ($\mathbf{n} = -\nabla c/|\nabla c|$). $\nabla \cdot \mathbf{n}$ corresponds to the flame front curvature. $\partial/\partial n = \mathbf{n} \cdot \nabla$ is a normal to the flame front derivative. $\partial/\partial c^*$ is a derivative in the sample space c^*. The surface averaged of Q, $\langle Q \rangle_s$, is defined as:

$$\langle Q \rangle_s = \frac{\overline{Q\,|\nabla c|\,\delta(c-c^*)}}{\overline{|\nabla c|\,\delta(c-c^*)}} = \frac{\left(\overline{Q|\nabla c| \Big| c = c^*}\right)}{\left(\overline{|\nabla c| \Big| c = c^*}\right)} \tag{88}$$

Here the notation $\langle Q \rangle_s$ implicitly indicates that the mean is taken for $c = c^*$, and $\langle Q \rangle_s$ is a function of c^*. The propagative formulation is often written in term of total stretch $\mathcal{A}_{c^*}$ of the iso-c^* surface

$$\frac{1}{\Sigma}\left(\frac{\partial \Sigma}{\partial t} + \nabla \cdot (\langle \mathbf{u} + w\mathbf{n} \rangle_s \Sigma)\right) = \mathcal{A}_{c^*} = \langle \underbrace{\nabla \cdot \mathbf{u} - \mathbf{nn} : \nabla \mathbf{u}}_{\text{tangential strain rate}} + \overbrace{w \nabla \cdot \mathbf{n}}^{\text{Curvature}} \rangle_s \tag{89}$$

The LHS terms in the two balance equations (86) and (87) correspond to unsteady effects and to the flame surface convection. The first term in the RHS expresses the action of the tangential strain rate on the flame surface. The last two terms in Eq. (86) describe respectively reaction/diffusion effects along the flame normal direction and fluxes in the sample space c^*. The last two terms in the RHS of the propagative equation (87) correspond to front convection due to a normal propagation and combined propagation/curvature effects.

These two formulations of the Σ balance equation induce the following comments:

- The two balance equations (86) and (87) are mathematically strictly equivalent but the problem is not expressed in the same way. In the propagative form (Eq. 87), many effects are incorporated in the flame front propagation speed, w, that may differ from the laminar flame speed S_L [77]. On the other hand, a flux term in the sample space is found in the reaction/diffusion derivation. In Eq. (87) the imbalance between diffusion and reaction is cast in the form of the propagation velocity w, Eq. (86) recalls that transfer phenomena between iso-surfaces are involved in this propagation.
- The derivation of the balance equation (86) and (87) implicitly forgets some mathematical singularities that may become important in particular situations. For example, the normal vector $\mathbf{n}$ is assumed to be well defined and having a finite derivative. This may not be the case when two close flame fronts interacts.
- In combustion modeling, a single iso-c^* surface is assumed to correspond to the flame front. This is a priori true when the flame is infinitely thin, assuming that the local reaction rate per unit flame area, $\dot{\Omega}_i$, describes whether the flame is actually burning or not. However in real turbulent flames, the local burning zone is not infinitely thin and the flame front, identified as the location of the maximum reaction, may differ from the c^* iso-surface. This may be for instance the case when analyzing data of direct numerical simulations where the flame front has to be resolved on the computational grid.
- Using the Favre decomposition ($\mathbf{u} = \widetilde{\mathbf{u}} + \mathbf{u}''$), the convection flux term may be decomposed into mean and turbulent components:

$$\langle \mathbf{u} \rangle_s \Sigma = \widetilde{\mathbf{u}} \Sigma + \langle \mathbf{u}'' \rangle_s \Sigma \tag{90}$$

  The strain rate term is also split into a contribution due to the mean flow and a contribution due to turbulent velocity fluctuations:

$$\langle \nabla \cdot \mathbf{u} - \mathbf{nn} : \nabla \mathbf{u} \rangle_s \Sigma = \underbrace{\left(\nabla \cdot \widetilde{\mathbf{u}} - \langle \mathbf{nn} \rangle_s : \nabla \widetilde{\mathbf{u}}\right)}_{A_T} \Sigma + \underbrace{\langle \nabla \cdot \mathbf{u}'' - \mathbf{nn} : \nabla \mathbf{u}'' \rangle_s}_{a_T} \Sigma \tag{91}$$

All these definitions may be extended to flame fronts which are not infinitely thin. Integrating Eq. (83) across iso-surface levels leads to:

$$\int_0^1 \Sigma(c^*)\, dc^* = \int_0^1 \left(\overline{|\nabla c||c=c^*}\right) \overline{P}(c^*)\, dc^* = \overline{|\nabla c|} \tag{92}$$

that is a direct estimation of the inverse of the mean local flame thickness δ ($\delta = (\overline{|\nabla c|})^{-1}$) and may be viewed as a "generalized flame surface density", $\overline{|\nabla c|}$ follows a balance equation similar to the $\Sigma(c^*)$ balance equation (87), where surface averages $\langle Q \rangle_s$ are replaced by "generalized surface averages" $\overline{\langle Q \rangle}_s$ which do not depend on c^*:

$$\overline{\langle Q \rangle}_s = \frac{1}{\overline{|\nabla c|}} \int_0^1 \langle Q \rangle_s \Sigma(c^*)\, dc^* \tag{93}$$

In flame surface density models, under a flamelet assumption, for any values of c^*, the flame surface is assumed to behave such as $\Sigma(c^*) \approx \overline{|\nabla c|} = \overline{\Sigma}$.

All balance equations remain formally the same but have to be closed. The same modeling issues emerge using the G-equation formalism [88]. One needs to develop closures for the turbulent flux of flame surface, for the propagation velocity of the surface, as well as for the effects of curvature and strain rate.

6.3.3 Flame wrinkling description

The previous formalism may be recast in term of flame surface wrinkling. The basic idea is to introduce the ratio $\Xi(c^*)$ of the flame surface to its projection in the direction of propagation $\mathbf{n_p}$:

$$\Xi(c^*) = \frac{\Sigma(c^*)}{\mathbf{n_p} \cdot \left(\overline{\mathbf{n}\, |\nabla c|\, \delta(c-c^*)}\right)} = \frac{\left(\overline{|\nabla c| \Big| c=c^*}\right) \overline{P}(c^*)}{\mathbf{n_p} \cdot \left(\overline{\mathbf{n}\, |\nabla c|\, \delta(c-c^*)}\right)} = \frac{\left(\overline{|\nabla c|\, |c=c^*}\right)}{\mathbf{n_p} \cdot \left(\overline{\mathbf{n}\, |\nabla c|\, |c=c^*}\right)} \tag{94}$$

where $\mathbf{n}$ and $\mathbf{n_p}$ are the unit vectors normal to the instantaneous flame front and to the mean propagating direction respectively. These vectors are chosen pointing towards the fresh gases and are given by:

$$\mathbf{n} = -\frac{\nabla c}{|\nabla c|} \qquad ; \qquad \mathbf{n_p} = -\frac{\left(\overline{\nabla c|c=c^*}\right)}{\left|\left(\overline{\nabla c|c=c^*}\right)\right|} \tag{95}$$

Then:

$$\Xi(c^*) = \frac{\left(\overline{|\nabla c|\, |c=c^*}\right)}{\left|\left(\overline{\nabla c|c=c^*}\right)\right|} = \frac{\Sigma(c^*)}{\left|\left(\overline{\nabla c|c=c^*}\right)\right| \overline{P}(c^*)} \tag{96}$$

As in the previous section, a generalized flame surface wrinkling, $\overline{\Xi}$, is introduced:

$$\overline{\Xi} = \frac{\displaystyle\int_0^1 \Sigma(c^*)\, dc^*}{\displaystyle\int_0^1 \left|\left(\overline{\nabla c|c=c^*}\right)\right| \overline{P}(c^*)\, dc^*} = \frac{\overline{|\nabla c|}}{|\nabla \overline{c}|} = \frac{\overline{\Sigma}}{|\nabla \overline{c}|} \tag{97}$$

For an infinitely thin flame front, $\Xi(c^*) = \overline{\Xi}$ for any c^* value.

Flame surface density and flame wrinkling factor are closely related. Balance equations may also be derived and closed for $\Xi(c^*)$ or $\overline{\Xi}$. These equations are quite more complicated than flame surface density balance equations, but the wrinkling factor may be more convenient for initial and/or boundary conditions ($\overline{\Xi} \geq 1$ everywhere). This approach has been explored by Weller *et al* [89, 90].

6.4 Statistical approaches: Probability density function

6.4.1 Introduction

Predictions of radicals and intermediate species such as OH, or pollutants like CO, require the description of the flame front internal structure, for intermediate states between fresh and burnt gases in premixed flames or between fuel and oxidizer in nonpremixed flames. Even-though G field and density of flame surface Σ need some statistical treatments, they are initially based on a geometrical view describing the flame as a thin interface. In probability density function methods, one wishes to relax this assumption by focussing on the statistical properties of intermediate states within the flame front.

The probability density function (pdf) $\overline{P}(Y^*; \underline{x}, t)$ quantifies the probability to find, for a given location $\underline{x}$ and a time t, a variable Y (mass fraction, temperature, velocity...) within the range $[Y^* - \Delta Y/2, Y^* + \Delta Y/2]$. This probability is equal to $\overline{P}(Y^*; \underline{x}, t)\, \Delta Y$ [91, 92, 93, 94, 95]. The pdf verifies the following simple relations:

$$\begin{aligned} \int_Y \overline{P}(Y^*; \underline{x}, t)\, dY^* &= 1 \\ \int_Y Y^* \overline{P}(Y^*; \underline{x}, t)\, dY^* &= \overline{Y}(\underline{x}, t) \\ \int_Y (Y^* - \overline{Y})^2 \overline{P}(Y^*; \underline{x}, t)\, dY^* &= \overline{Y'^2}(\underline{x}, t) \end{aligned}$$

where Y^* is the sample space variable corresponding to the random variable Y. When more than one variable is required to capture the flame structure, a joint probability density function $\overline{P}(Y_1^*, ..., Y_N^*; \underline{x}, t)$ is introduced [96]. The mean burning rate (or any mean quantity) is then estimated as:

$$\overline{\dot{w}}_{Y_1}(\underline{x}, t) = \int_{Y_1} ... \int_{Y_N} \dot{w}_{Y_1}(Y_1^*, ..., Y_N^*) \overline{P}(Y_1^*, ..., Y_N^*; \underline{x}, t)\, dY_1^* ... dY_N^* \tag{98}$$

Conditional statistics have been used to defined the flame surface density (§ 6.3.2), these conditional means are also useful in a pdf context. Consider a nonpremixed flame where the chemistry is reduced to a single step reaction, and where radiative heat losses are neglected. Laminar combustion would be parameterized with two variables, for example, fuel mass fraction Y_F and mixture fraction Z (see § 3.2). The turbulent flame is then fully described by the joint pdf of mixture fraction and fuel mass fraction, $\overline{P}(Y_F^*, Z^*; \underline{x}, t)$. For such flames, it is interesting to focus on the statistical properties of the fuel mass fraction Y_F for a given value of the mixture fraction Z (§ 3.2 and Fig. 5). The conditional pdf $\overline{P}_c(Y_F^* | Z^*; \underline{x}, t)$ is introduced and defined for a given value of Z^* as:

$$\overline{P}(Y_F^*, Z^*; \underline{x}, t) = \overline{P}_c(Y_F^* | Z^*; \underline{x}, t)\, \overline{P}(Z^*; \underline{x}, t)$$

The conditional mean is readily defined from:

$$\left(\overline{Y_F \Big| Z(\underline{x}, t) = Z^*} \right) = \int_0^1 Y_F^*\, \overline{P}_c(Y_F^* | Z^*; \underline{x}, t)\, dY_F^*$$

In this decomposition, $\overline{P}(Z^*;\underline{x},t)$ describes the statistical properties of fuel/air mixing, whereas $\overline{P}_c(Y_F^*|Z^*;\underline{x},t)$ and $\left(\overline{Y_F|Z(\underline{x},t)=Z^*}\right)$ are linked to the internal structure of the flame front.

Two main directions may be chosen to built numerical models from pdf:

- To presume the pdf shape from available mean quantities.
- To solve a balance equation for the pdf.

6.4.2 Presumed probability density functions

The simplest approach to the mixing between fuel and oxidizer in a nonpremixed flame is to presume the shape of the pdf $\overline{P}(Z^*;\underline{x},t)$, usually with a Beta function [71]:

$$\widetilde{P}(Z^*;\underline{x},t) = \frac{Z^{*a-1}(1-Z^*)^{b-1}}{\int_0^1 Z^{+a-1}(1-Z^+)^{b-1}dZ^+}$$

This presumed pdf should reproduce the mean of the mixture fraction $\widetilde{Z}$ and its variance $\widetilde{Z''^2}$:

$$\begin{aligned}\widetilde{Z} &= \int_0^1 Z^*\widetilde{P}(Z^*;\underline{x},t)\,dZ^* \\ \widetilde{Z''^2} &= \int_0^1 (Z^*-\widetilde{Z})^2\widetilde{P}(Z^*;\underline{x},t)\,dZ^*\end{aligned}$$

and using the relation [97]:

$$\int_0^1 Z^{*n}\widetilde{P}(Z^*;\underline{x},t)dZ^* = \frac{a(a+1)...(a+(n-1))}{(a+b)(a+b+1)...(a+b+(n-1))}$$

The two-parameters a and b are determined as:

$$\begin{aligned}a &= \widetilde{Z}\left(\frac{\widetilde{Z}\left(1-\widetilde{Z}\right)}{\widetilde{Z''^2}}-1\right) \geq 0 \\ b &= a\left(\frac{1}{\widetilde{Z}}-1\right) \geq 0\end{aligned}$$

This technique requires the solving of a balance equation for the mean and the variance of Z (§ 9.2). $\widetilde{Z''^2}$ vanishes when reactants are perfectly mixed and reaches its maximum value, $\widetilde{Z}\left(1-\widetilde{Z}\right)$, when fuel and oxidizer are completely segregated (§ 5.3), then the pdf takes the form of a double peak function, with peaks located at $Z=0$ and $Z=1$. This approach is also used in premixed flames replacing the mixture fraction Z by the progress variable c [98].

6.4.3 Pdf balance equation

The pdf balance equation is first written for the progress variable c. The time evolution of a probability density function is easily derived by expressing the pdf as the average of a function $\delta\left(c^* - c(\underline{x},t)\right)$ defined as [99]:

$$\begin{array}{lll} \delta\left(c^* - c(\underline{x},t)\right) = 1/\Delta c^* & \text{if} & c^* - \Delta c^*/2 < c < c^* + \Delta c^*/2 \\ \delta\left(c^* - c(\underline{x},t)\right) = 0 & \text{otherwise} & \end{array}$$

By definition:

$$\overline{P}(c^*;\underline{x},t) = \overline{\delta\left(c^* - c(\underline{x},t)\right)} \tag{99}$$

The time evolution of the reactive species $c(\underline{x},t)$ is given by:

$$\frac{\partial c}{\partial t} = -\mathbf{u}\cdot\nabla c + \frac{1}{\rho}\Big[\nabla\cdot(\rho D\nabla c(\underline{x},t)) + \dot{\omega}\Big] \tag{100}$$

and $\delta\left(c^* - c(\underline{x},t)\right)$ verifies:

$$\frac{\partial}{\partial\Psi}\Big[\delta\left(c^* - c(\underline{x},t)\right)\Big] = \frac{\partial}{\partial c}\Big[\delta\left(c^* - c(\underline{x},t)\right)\Big]\frac{\partial c(\underline{x},t)}{\partial\Psi} = -\frac{\partial}{\partial c^*}\Big[\delta\left(c^* - c(\underline{x},t)\right)\Big]\frac{\partial c(\underline{x},t)}{\partial\Psi} \tag{101}$$

where Ψ can either be time or any spatial coordinates. This relation and Eq. (99) are key relations, useful to obtain all equations discussed in this section.

After simple manipulations combining Eq. (100) with Eq. (101), the transport equation for the pdf may be written:

$$\frac{\partial}{\partial t}\Big[\overline{P}(c^*;\underline{x},t)\Big] = -\frac{\partial}{\partial c^*}\left[\left(\overline{\frac{\partial c(\underline{x},t)}{\partial t} \mid c(\underline{x},t) = c^*}\right)\overline{P}(c^*;\underline{x},t)\right] \tag{102}$$

where conditional averaging

$$\overline{Q(c)\,\delta\left(c^* - c(\underline{x},t)\right)} = \left(\overline{Q(c) \mid c(\underline{x},t) = c^*}\right)\overline{P}(c^*;\underline{x},t)$$

is introduced.

Equation (102) shows that the time evolution of the pdf is controlled by a flux in the sample space c^*. This flux is driven by a velocity equal to the conditional mean of the time evolution of the progress variable c. In other words, when the mean of $(\partial c(\underline{x},t)/\partial t)$ is non zero for the value $c = c^*$, the probability of finding the occurrence $c = c^*$ is modified. Because the probability to find all the possible values is constant and equal to unity:

$$\int_0^1 \overline{P}(c^*;\underline{x},t)\,dc^* = 1$$

an increase or a decrease of the density of probability for $c = c^*$ implies a modification of this density for other values of c^*, justifying the convective term in sample space. This term insures that the density of probability is transported from point to point in the sample space c^* in a conservative manner. The flux depends on the conditional mean of the time evolution of the progress variable given by Eq. (100):

$$\begin{aligned} \left(\overline{\frac{\partial c}{\partial t} \mid c(\underline{x},t) = c^*}\right) &= \left(\overline{-\mathbf{u}\cdot\nabla c \mid c(\underline{x},t) = c^*}\right) \\ &+ \left(\overline{\frac{1}{\rho}\Big[\nabla\cdot(\rho D\nabla c(\underline{x},t))\Big] \mid c(\underline{x},t) = c^*}\right) + \left(\overline{\dot{\omega} \mid c(\underline{x},t) = c^*}\right) \end{aligned} \tag{103}$$

In Eq. (104), the conditional value of the source term is a function of c defined in one-point and is exactly known since:

$$\left(\overline{\dot{\omega}(c) \mid c(\underline{x},t)=c^*}\right) = \dot{\omega}\left(c^*\right)$$

The main advantage of pdfs in turbulent combustion lies in this availability to deal with chemistry, any term defined in one-point (as chemical source) is closed. Nonetheless, this advantage is offset by the fact that reactants are brought to the reaction zone by diffusion, and the conditional mean of $\partial c(\underline{x},t)/\partial t$ also includes a conditional diffusive term:

$$\left(\overline{\frac{1}{\rho}\left(\nabla\cdot(\rho D\nabla c)\right) \mid c(\underline{x},t)=c^*}\right) \tag{104}$$

named *micromixing term* and remaining unclosed (as any term involving spatial derivatives). This micromixing term may be rewritten with the scalar dissipation rate, $\chi = D|\nabla c|^2$, assuming $\rho D \approx cst$:

$$\begin{aligned}\frac{\partial}{\partial c^*}\left[\left(\overline{D\nabla^2 c \mid c(\underline{x},t)=c^*}\right)\overline{P}(c^*;\underline{x},t)\right] = & - D\nabla^2\overline{P}(c^*;\underline{x},t) \\ & + \frac{\partial^2}{\partial c^{*2}}\left[\left(\overline{\chi \mid c(\underline{x},t)=c^*}\right)\overline{P}(c^*;\underline{x},t)\right]\end{aligned}$$

The first term in the RHS, $D\nabla^2\overline{P}(c^*;\underline{x},t)$ is usually negligible compared to the transport due to velocity fluctuations. The total dissipation rate, $\overline{\chi}$ is recovered as:

$$\overline{\chi} = \int_0^1 \left(\overline{\chi \mid c(\underline{x},t)=c^*}\right)\overline{P}(c^*;\underline{x},t)\,dc^*$$

Using diffusion or scalar dissipation rate, the probability density function balance equation may be organized in two different forms:

- In term of molecular diffusion:

$$\begin{aligned}&\frac{\partial}{\partial t}\left[\overline{P}(c^*;\underline{x},t)\right] = \\ &\quad -\frac{\partial}{\partial c^*}\left[\left(\left(\overline{-\mathbf{u}\cdot\nabla c + \frac{1}{\rho}\Big(\nabla\cdot(\rho D\nabla c)\Big) \mid c(\underline{x},t)=c^*}\right) + \dot{\omega}(c^*)\right)\overline{P}(c^*;\underline{x},t)\right]\end{aligned} \tag{105}$$

- In term of scalar dissipation rate:

$$\begin{aligned}\frac{\partial}{\partial t}\left[\overline{P}(c^*;\underline{x},t)\right] = & - \frac{\partial}{\partial c^*}\left[\left(\left(\overline{-\mathbf{u}\cdot\nabla c \mid c(\underline{x},t)=c^*}\right) + \dot{\omega}(c^*)\right)\overline{P}(c^*;\underline{x},t)\right] \\ & - \frac{\partial^2}{\partial c^{*2}}\left[\left(\overline{\chi \mid c(\underline{x},t)=c^*}\right)\overline{P}(c^*;\underline{x},t)\right]\end{aligned}$$

The convective term may be split into mean, $\overline{\mathbf{u}}\cdot\nabla\overline{P}(c^*;\underline{x},t)$, and fluctuating components. Using an eddy viscosity model, the fluctuating part becomes: $-\nu_t\nabla\overline{P}(c^*;\underline{x},t)$, leading to the pdf balance equation:

$$\begin{aligned}\frac{\partial}{\partial t}\left[\overline{P}(c^*;\underline{x},t)\right] + \overline{\mathbf{u}}\cdot\nabla\overline{P}(c^*;\underline{x},t) = & \ \nu_t\nabla\overline{P}(c^*;\underline{x},t) - \frac{\partial}{\partial c^*}\left[\dot{\omega}(c^*)\overline{P}(c^*;\underline{x},t)\right] \\ & - \frac{\partial^2}{\partial c^{*2}}\left[\left(\overline{\chi \mid c(\underline{x},t)=c^*}\right)\overline{P}(c^*;\underline{x},t)\right]\end{aligned} \tag{106}$$

Weighted, or Favre, averages are also introduced in pdfs, for instance when $\rho = \rho(c)$:

$$\overline{\rho}\,\widetilde{P}(c^*;\underline{x},t) = \overline{\rho(c^*)\delta(c(\underline{x},t)-c^*)} = \rho\,(c^*)\,\overline{P}\,(c^*,\underline{x},t)$$

When more than one species are taken into account, the pdf balance equation is derived using the same formalism with [92]

$$\overline{\rho}\widetilde{P}(Y_1^*,...,Y_N^*) = \overline{\rho(Y_1,...,Y_N^*)\delta(Y_1-Y_1^*)\cdots\delta(Y_N-Y_N^*)}$$

leading to:

$$\begin{aligned}
&\overline{\rho}\frac{\partial}{\partial t}\widetilde{P}(Y_1^*,...,Y_N^*;\underline{x},t) = \\
&\quad - \quad \overline{\rho}\sum_{i=1}^{N}\frac{\partial}{\partial Y_i^*}\left[\left(\overline{\left(-\mathbf{u}\cdot\nabla Y_i\middle|\underline{Y}(\underline{x},t)=\underline{Y}^*\right)}+\dot{\omega}_i^*\right)\widetilde{P}(Y_1^*,...,Y_N^*;\underline{x},t)\right] \\
&\quad - \quad \overline{\rho}\sum_{i=1}^{N}\sum_{j=1}^{N}\frac{\partial}{\partial Y_i^*}\frac{\partial}{\partial Y_j^*}\left[\left(\overline{D\frac{\partial Y_i}{\partial x_k}\frac{\partial Y_j}{\partial x_k}\middle|\underline{Y}(\underline{x},t)=\underline{Y}^*}\right)\widetilde{P}(Y_1^*,...,Y_N^*;\underline{x},t)\right]
\end{aligned} \tag{107}$$

The same terms are identified on the RHS: convection by the conditional velocity and by the chemical source, and micromixing. As done in Eq. (106), the convective term in physical space can be decomposed into mean and fluctuating parts.

6.4.4 Joint velocity/concentrations pdf

To avoid the gradient transport assumption for the turbulent flux, $\left(\overline{u'.\nabla c\middle|c(\underline{x},t)=c^*}\right)$, the joint velocity/concentration pdf is introduced. Once this joint pdf is known, turbulence model, as $k-\varepsilon$, are, a priori, no longer required for the mean flow. However, an equation for ε is still needed to estimate a characteristic mixing time, except when the frequency of mixing is also included in the joint pdf [100]. The transport equation for this joint composition/velocity pdf is given below for the progress variable c, where the RHS contains the unclosed terms.

$$\begin{aligned}
\frac{\partial}{\partial t}\left[\overline{P}(\mathbf{u}^*,c^*;\underline{x},t)\right] \quad &+ \quad \mathbf{u}^*.\nabla\overline{P}(\mathbf{u},c;\underline{x},t) + \left(\nu\nabla^2\overline{u}_i - \frac{1}{\overline{\rho}}\frac{\partial\overline{p}}{\partial x_i}\right)\frac{\partial}{\partial u_i^*}\left[\overline{P}(\mathbf{u}^*,c^*;\underline{x},t)\right] \\
&+ \quad \frac{\partial}{\partial c^*}\left[\dot{\omega}(c^*)\overline{P}(\mathbf{u}^*,c^*;\underline{x},t)\right] = \\
&\quad \underbrace{\frac{\partial}{\partial u_i^*}\left[\left(\overline{\frac{1}{\rho}\frac{\partial p'}{\partial x_i}\mid\mathbf{u}=\mathbf{u}^*,c=c^*}\right)\overline{P}(\mathbf{u}^*,c^*;\underline{x},t)\right]}_{\text{Pressure fluctuations}} \\
&- \quad \underbrace{\frac{\partial}{\partial u_i^*}\left[\left(\overline{\nu\nabla^2 u_i'\mid\mathbf{u}=\mathbf{u}^*,c=c^*}\right)\overline{P}(\mathbf{u}^*,c^*;\underline{x},t)\right]}_{\text{Viscous dissipation}} \\
&- \quad \underbrace{\frac{\partial}{\partial c^*}\left[\left(\overline{\frac{1}{\rho}D\nabla^2 c\mid\mathbf{u}=\mathbf{u}^*,c=c^*}\right)\overline{P}(\mathbf{u}^*,c^*;\underline{x},t)\right]}_{\text{Molecular diffusion}}
\end{aligned} \tag{108}$$

The LHS terms are closed and represent respectively accumulation, convection in physical space by the random velocity field (incorporating turbulent transport), convection of the pdf in velocity space, here

the convective velocity is the mean of the viscous dissipation and the mean pressure gradient, and finally the closed chemical source. The unclosed terms (RHS) are the pressure fluctuations, the fluctuating part of the viscous dissipation and micromixing. All these phenomena remain to be closed.

6.4.5 Conditional Moment Closure (CMC)

Conditional Moment Closure modeling was first proposed in [101, 102]. As with pdf, the idea is to focus on particular states between fresh gases and fully burnt product in premixed flames, or, between fuel and oxidizer in nonpremixed combustion. However, here only conditional moments $\left(\overline{\rho Y_i | c=c^*}\right)$ are considered. In premixed flames, the conditional quantity is the progress variable c, whereas for nonpremixed combustion, the mixture fraction is used. In premixed flames, the mean value, $\widetilde{Y}_i$ of Y_i may be estimated as:

$$\overline{\rho}\widetilde{Y}_i = \int_0^1 \left(\overline{\rho Y_i | c=c^*}\right) \overline{P}\left(c^*; \underline{x}, t\right) dc^* \tag{109}$$

One may solve a balance equation for the conditional quantities $Q_i(c^*)$ defined as:

$$Q_i(c^*) = \frac{\left(\overline{\rho Y_i | c=c^*}\right)}{\left(\overline{\rho | c=c^*}\right)}$$

This balance equation is [103, 104]:

$$\left(\overline{\rho \mid c^*}\right) \frac{\partial Q_i}{\partial t} = -\left(\overline{\rho u_i \mid c^*}\right) \frac{\partial Q_i}{\partial x_i} + \left(\overline{\rho\chi \mid c^*}\right) \frac{\partial^2 Q_i}{\partial {c^*}^2} + \left(\overline{\dot{\omega}_i \mid c^*}\right) + E_{Q_i} + E_{Y_i} \tag{110}$$

The two last terms of Eq. (110) are usually neglected, E_{Q_i} appears from molecular diffusion along with differential diffusion effects across the iso-c surface, E_{Y_i} represents the effects of turbulent fluctuations on the deviation from the conditional mean. The three first terms on the right hand side are unclosed, they describe convective transport, micromixing (χ enters this term) and chemical source. Closures for the conditional values of the scalar dissipation rate, but also for the conditional value of the chemical source of Y_i, calculated for a given value of the progress variable c^* or the mixture fraction Z, are required [105, 106]. One equation has to be solved for each value of c^* retained. The number of these values is determined from the accuracy required to estimate both the mean from Eq. (109) and the second order derivative in the sample space (i.e. $\partial/\partial {c^*}^2$) found in Eq. (110). On the other hand, the probability density function entering expression (109), $\overline{P}\left(c^*; \underline{x}, t\right)$ is presumed.

CMC may also be viewed as a multi-surface description, any conditional quantity $\left(\overline{\rho Y_i | c=c^*}\right)$ corresponding to the conditional average of Y_i along the iso-surface $c = c^*$.

6.5 Similarities and links between the tools

Major links between the tools used in turbulent combustion modeling are now developed. Without loss of the generic character of the discussion, we consider the case of a turbulent premixed flame represented with a progress variable c. To describe this turbulent flame, three quantities are useful:

- The scalar dissipation rate of the progress variable $\overline{\rho}\widetilde{\chi} = \overline{\rho D \nabla c \cdot \nabla c}$.
- The pdf of the progress variable $\overline{P}(c^*; \underline{x}, t)$.
- The flame surface density Σ or the mean field $\overline{G}$.

	Scalar dissipation rate $\overline{\rho}\widetilde{\chi}$	Probability density function $\overline{P}(c^*)$	Flame surface density $\Sigma(c^*)$
$\overline{\rho}\widetilde{\chi}$	–	$\int_0^1 \left(\overline{\rho D\|\nabla c\|^2 \| c=c^*}\right) \overline{P}(c^*)\, dc^*$	$\int_0^1 \langle \rho D\|\nabla c\| \rangle_s \Sigma(c^*) dc^*$
$\overline{P}(c^*)$	$\left(\overline{\chi \| c=c^*}\right)$ via PDF Eq.	–	$\Sigma(c^*)/\left(\overline{\|\nabla c\| \| c=c^*}\right)$
$\Sigma = \overline{\|\nabla c\|}$	$\frac{\overline{\rho}\widetilde{\chi}}{\langle \rho D\|\nabla c\| \rangle_s}$	$\int_0^1 \left(\overline{\|\nabla c\| \| c^*}\right) \overline{P}(c^*)\, dc^*$	$\int_0^1 \Sigma(c^*)\, dc^*$

Table 2: Exact relations between mean scalar dissipation rate, $\widetilde{\chi}$, probability density function, $\overline{P}(c^*)$ or surface density, $\Sigma(c^*)$ of iso-surface $c = c^*$ and generalized flame surface density $\Sigma = \overline{|\nabla c|}$. Connections with the G-equation are readily obtained with Eq. (113). $\langle Q \rangle_s$ is a surface average (Eq. 88), $\overline{\langle Q \rangle}_s$ corresponds to generalized surface average and is defined in Eq. (93). c is the conditional variable (progress variable in premixed flames, mixture fraction in nonpremixed combustion).

Simple links exist between these quantities:

- The conditional value of the scalar dissipation rate enters the pdf transport equation (Eq. 106), therefore there is a direct connection between $\overline{P}(c^*; \underline{x}, t)$ and $\widetilde{\chi}$.
- The surface density function $\Sigma(c^*; \underline{x}, t)$, or flame surface, is related to the pdf via the conditional value of $|\nabla c|$, $\Sigma = \left(\overline{|\nabla c|\, | c=c^*}\right) \overline{P}(c^*)$ (Eq. 83).

Since χ is proportional to $|\nabla c|$, the flame surface Σ, the pdf $\overline{P}(c^*)$ and the dissipation rate $\widetilde{\chi}$ are very strongly related. Using the joint pdf of c and χ, the flame surface density may be written:

$$\Sigma(c^*; \underline{x}, t) = \left(\overline{\sqrt{\frac{\chi}{D}} \Big| c=c^*}\right) \overline{P}(c^*, \underline{x}, t) = \int_\chi \sqrt{\frac{\chi^*}{D}} \overline{P}(c^*, \chi^*; \underline{x}, t)\, d\chi^* \tag{111}$$

and characteristic length scales $\delta_c = \sqrt{D/\chi}$ of the iso-c distribution are embedded within $\Sigma(c^*)$.

Combining Eq. (83) and Eq. (88) with Eq. (93), the mean c-scalar dissipation rate is also a function of surface densities:

$$\overline{\rho}\widetilde{\chi} \;=\; \overline{\rho D|\nabla c|^2} = \int_0^1 \langle \rho D|\nabla c| \rangle_s \Sigma(c^*)\, dc^* \;=\; \overline{\langle \rho D|\nabla c| \rangle}_s \overline{|\nabla c|} \tag{112}$$

where the generalized surface average $\overline{\langle Q \rangle}_s$ is defined by Eq. (93). Relations between flame surface densities and scalar dissipation rates were anticipated by Borghi [107]. In premixed combustion, using a $G-$ field equation, the flame front is identified to a given level $G = G_0$ [27]. The flame surface density is then:

$$\Sigma(G_0) = \left(\overline{|\nabla G| | G=G_0}\right) \overline{P}(G_0) \tag{113}$$

Hence, previous relations may be recast in terms of the G-equation.

The CMC formalism (see § 6.4.5) may be reorganized in term of flame surface density:

$$\overline{\rho}\widetilde{Y_i} = \int_0^1 \left(\overline{\rho Y_i | c=c^*}\right)\, \overline{P}\,(c^*; \underline{x}, t)\; dc^* = \int_0^1 \left\langle \frac{\rho Y_i}{|\nabla c|} \right\rangle_s \Sigma(c^*)\, dc^* \tag{114}$$

Tool	Averaged reaction rate
Scalar dissipation	$\overline{\rho}\dfrac{\int_0^1 \left\langle \dfrac{\dot{\omega}}{\lvert\nabla c\rvert} \right\rangle_s \Sigma(c^*)\, dc^*}{2\int_0^1 \langle \rho D \lvert\nabla c\rvert \rangle_s \Sigma(c^*)\, dc^*} \widetilde{\chi} = \overline{\rho}\dfrac{\overline{\left\langle \dfrac{\dot{\omega}}{\lvert\nabla c\rvert} \right\rangle_s}}{2\overline{\langle \rho D \lvert\nabla c\rvert \rangle_s}} \widetilde{\chi}$
Probability density function	$\int_0^1 \dot{\omega}(c^*)\overline{P}(c^*)\, dc^*$
Flame surface density	$\int_0^1 \left\langle \dfrac{\dot{\omega}}{\lvert\nabla c\rvert} \right\rangle_s \Sigma(c^*)\, dc^* = \overline{\left\langle \dfrac{\dot{\omega}}{\lvert\nabla c\rvert} \right\rangle_s} \overline{\lvert\nabla c\rvert}$

Table 3: Exact expressions for the averaged reaction rate as a function of the mean scalar dissipation, $\widetilde{\chi}$, probability density function, $\overline{P}(c^*)$ or surface density, $\Sigma(c^*)$ of iso-surface $c = c^*$. Connections with the G-equation are readily obtained with Eq. (113). $\langle Q \rangle_s$ is a surface average (Eq. 88), $\overline{\langle Q \rangle}_s$ corresponds to generalized surface average and is defined in Eq. (93).

where the conditional mean $Q_i(c^*)$ may be written:

$$Q_i(c^*) = \frac{\left(\overline{\rho Y_i | c = c^*}\right)}{\left(\overline{\rho | c = c^*}\right)} = \frac{\langle \rho Y_i / |\nabla c| \rangle_s}{\langle \rho / |\nabla c| \rangle_s} \tag{115}$$

and appears as directly related to $c = c^*$ surface averaged quantities.

The links between the combustion modeling tools are summarized in Table 2. The mean burning rate is given by:

$$\overline{\dot{\omega}} = \int_0^1 \dot{\omega}(c^*)\overline{P}(c^*)\, dc^* \tag{116}$$

Using relations (83), (88) and Eq. (112), this expression becomes:

$$\begin{aligned} \overline{\dot{\omega}} &= \int_0^1 \left(\overline{\dot{\omega} | c = c^*}\right) \overline{P}(c^*)\, dc^* = \int_0^1 \left\langle \frac{\dot{\omega}}{|\nabla c|} \right\rangle_s \Sigma(c^*)\, dc^* = \overline{\left\langle \frac{\dot{\omega}}{|\nabla c|} \right\rangle_s} \overline{|\nabla c|} \\ &= \overline{\left\langle \frac{\dot{\omega}}{\sqrt{\chi / D}} \right\rangle_s} \Sigma = \frac{1}{\overline{\langle \rho D |\nabla c| \rangle_s}} \overline{\left\langle \frac{\dot{\omega}}{|\nabla c|} \right\rangle_s} \overline{\rho} \widetilde{\chi} \end{aligned} \tag{117}$$

Models based on probability density functions, conditional means, flame surface density function and generalized flame surface density are then related via the scalar dissipation rate.

These expressions are extended to burning rate depending on many species using multi-dimensional pdfs and conditional averaging. When the local reaction rate is a function of various quantities (species

Description	Tools	Modeling issues
Geometrical	**G-Field** with $G = G^*$ at the flame $\partial\widetilde{G}/\partial t + \widetilde{\mathbf{u}} \cdot \nabla\widetilde{G} = (\rho_u/\overline{\rho}) S_T \left\lvert \nabla\widetilde{G} \right\rvert$ **Flame surface** Σ Algebraic closure or Transport equation	Propagation speed S_T $\overline{\dot{\omega}}_i = \underset{Combustion}{\dot{\Omega}_i} \overset{Turbulence}{\Sigma}$ Total Stretch = Curvature + Strain rate
Small scales	**Scalar dissipation rate** $\overline{\rho}\widetilde{\chi} = \overline{\rho D \lvert\nabla Y\rvert^2}$ Algebraic closure or Transport equation	- Fast Chemistry $\widetilde{\dot{\omega}} \approx \widetilde{\chi}$ - Provide the rate of micromixing
Statistical	**Probability density function** $\widetilde{P}(Y_F^*, Z^*; \underline{x}, t)$ (1) Presumed + Flamelets (2) Transport Equation **Conditional mean, CMC, Presumed PDF** $\left(\overline{Y_F \left\lvert Z(\underline{x}, t) = Z^*\right.}\right) = \int_0^1 Y_F^* \overline{P}_c(Y_F^* \lvert Z^*; \underline{x}, t) dY_F^*$	Micromixing (1) Strategy to generate the pdf (2) Solve $(\partial\widetilde{P}/\partial t) = \ldots$ Micromixing and conditional source

Fundamental links : $\Sigma(\underline{x}, t) = \left(\overline{|\nabla c| | c = c^*}\right) \overline{P}(c^*; \underline{x}, t)$ and $\overline{\rho}\widetilde{\chi} = \overline{\langle \rho D \, |\nabla c| \rangle_s} \overline{|\nabla c|}$

Table 4: Tools for turbulent combustion modeling.

mass fractions, temperature,...), Y_i and a sampling scalar c:

$$\begin{aligned} \overline{\dot{\omega}}_i &= \int_{Y_1} \cdots \int_{Y_N} \int_0^1 \dot{\omega}_i(Y_1^*, \cdots, Y_N^*, c^*) \overline{P}(Y_1^*, \cdots, Y_N^*, c^*) \, dY_1^* \cdots dY_N^* \, dc^* \\ &= \int_0^1 \underbrace{\left[\int_{Y_1} \cdots \int_{Y_N} \dot{\omega}_i(Y_1^*, \cdots, Y_N^*, c^*) \overline{P}_c(Y_1^*, \cdots, Y_N^* | c^*) \, dY_1^* \cdots dY_N^* \right]}_{\left(\overline{\dot{\omega}_i(Y_1, \cdots, Y_N, c) | c = c^*}\right)} \overline{P}(c^*) \, dc^* \end{aligned} \tag{118}$$

decomposing the joint-pdf as $\overline{P}(Y_1^*, \cdots, Y_N^*, c^*) = \overline{P}_c(Y_1^*, \cdots, Y_N^* | c^*) \overline{P}(c^*)$.

The fundamentals of turbulent combustion modeling clearly rely on **pdf**, **flame surface density**, **G-field** and **scalar dissipation rate** concepts. The previous relations may be used to carefully compare the proposed closure schemes and Table 4 summarizes the tools and their related modeling issues. Various expressions for mean reaction rates are displayed in Table 3. Major differences between the various approaches only appear when closing the unknown quantities, but at the light of these relations, many closures are actually somehow equivalent.

7 Reynolds-averaged models for turbulent premixed combustion

7.1 Turbulent flame speed

Turbulent premixed flames may be described in terms of a global turbulent flame speed S_T. From experimental data [108, 109] or theoretical analysis (Renormalization Group Theory, [110]), the following

expression has been proposed:

$$\frac{S_T}{S_L} = 1 + \alpha \left(\frac{u'}{S_L} \right)^n \tag{119}$$

where α and n are two model constants of the order of unity. u' is the turbulent velocity (i.e the RMS velocity).

Unfortunately, the turbulent flame speed S_T is not a fully well defined quantity [111]. Experimental data exhibit a large scatter because they depend on various parameters (chemistry characteristics, turbulence scales, flow geometry,...). While this global approach is not particularly well suited to close Favre averaged transport equations, it may be of interest in the context of Large Eddy Simulation [78, 112].

7.2 Eddy-Break-Up model

Devised in [113], this model is based on a phenomenological analysis of turbulent combustion assuming high Reynolds ($Re \gg 1$) and Damköhler ($Da \gg 1$) numbers. The reaction zone is viewed as a collection of fresh and burnt gases pockets. Following the Kolmogorov cascade, turbulence leads to a break down of fresh gases structures. Accordingly, the mean reaction rate is mainly controlled by the turbulent mixing time τ_t. When oxidizer is in excess, the mean reaction rate is expressed as:

$$\overline{\dot{\omega}}_F = -C_{EBU}\, \overline{\rho}\, \frac{\sqrt{\widetilde{Y_F''^2}}}{\tau_t} \tag{120}$$

where Y_F'' denotes the fuel mass fraction fluctuations and C_{EBU} is a model constant of the order of unity. The turbulent mixing time, τ_t is estimated from the turbulence kinetic energy k and its dissipation rate ε according to:

$$\tau_t = \frac{k}{\varepsilon}$$

as an approximation of the characteristic time of the integral length scales of the turbulent flow field.

The reaction rate may be recast in terms of progress variable, c, as:

$$\overline{\dot{\omega}} = C_{EBU}\, \overline{\rho}\, \frac{\sqrt{\widetilde{c''^2}}}{\tau_t} \tag{121}$$

Mass fraction fluctuations $\widetilde{Y_F''^2}$ (or progress variable fluctuations $\widetilde{c''^2}$) must be modeled and may be estimated from a balance equation (see Eq. 74). Assuming an infinitely thin flame front (i.e. $c = 0$ or $c = 1$), $\widetilde{c''^2}$ is easily estimated because $c^2 = c$:

$$\overline{\rho}\widetilde{c''^2} = \overline{\rho\,(c - \widetilde{c})^2} = \overline{\rho}\left(\widetilde{c^2} - \widetilde{c}^2\right) = \overline{\rho}\,\widetilde{c}\,(1 - \widetilde{c}) \tag{122}$$

The square root has been introduced for dimension reasons in Eq. (120) and (121) but, unfortunately, Eq. (121) and (122) lead to inconsistencies because the $\widetilde{c}$ derivative of $\overline{\dot{\omega}}$, $d\overline{\dot{\omega}}/d\widetilde{c}$, is infinite both in $\widetilde{c} = 0$ and $\widetilde{c} = 1$ (Borghi, private communication, 1999). Then, a corrected version of the Eddy-Break-Up model, without square root, is used for practical simulations:

$$\overline{\dot{\omega}} = C_{EBU}\, \overline{\rho}\, \frac{\varepsilon}{k} \widetilde{c}(1 - \widetilde{c}) \tag{123}$$

or, in terms of fuel mass fraction:

$$\boxed{\overline{\dot{\omega}}_F = -C_{EBU}\, \overline{\rho}\, \frac{\varepsilon}{k} \frac{\widetilde{Y}_F}{Y_F^0} \left(1 - \frac{\widetilde{Y}_F}{Y_F^0}\right)} \tag{124}$$

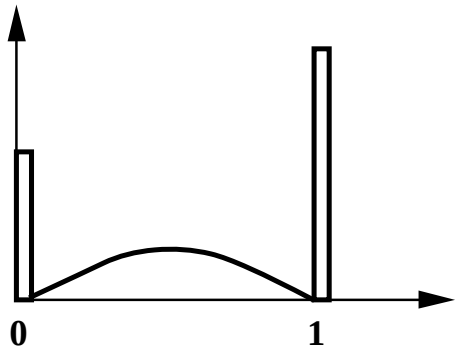

Figure 15: Probability density function in premixed turbulent combustion.

where Y_F^0 is the initial fuel mass fraction in the reactant stream, assuming excess of oxidizer.

The EBU model was found attractive because the reaction rate is simply written as a function of known quantities without any additional transport equation and is available in most commercial CFD codes. The modeled reaction rate does not depend on chemical characteristics and assumes an homogeneous and isotropic turbulence. Some adjustments of the model constant C_{EBU} have been proposed to mimic chemical features [114]. Eddy-Break-Up modeling tends to overestimate the reaction rate, especially in highly strained regions, where the ratio ε/k is large (flame-holder wakes, walls,...).

7.3 Bray-Moss-Libby (BML) model

7.3.1 Introduction

Known under the initials of its authors, Bray, Moss and Libby, or, from the involved physical hypothesis, BiModal Limit, this model, first proposed in 1977 [115], has been the subject of a large amount of works leading to many improvements (see papers by Bray, Moss and Libby, and then by Bray, Champion and Libby). Combining a statistical approach using probability density functions and a physical analysis, this model has evidenced some special features of turbulent premixed combustion (counter-gradient turbulent transport, flame turbulence generation, ...). The presentation is mainly limited here to basic concepts of the BML formulation.

A one-step, irreversible chemical reaction between two reacting species, fresh gases (R) and combustion products (P) is considered:

$$R \rightarrow P$$

Classical assumptions are made to simplify the formulation: perfect gases, incompressible flows, constant chemical properties, unity Lewis numbers,...). A progress variable, c, of the chemical reaction is introduced and is such as $c = 0$ in fresh gases and $c = 1$ in fully burnt gases, as described in Section 3.1. The basic idea of the BML formulation is to presume the probability density function of the progress variable c at a given location $(\underline{x}, t)$ as a sum of fresh, fully burnt and burning gases contributions (Fig. 15):

$$\overline{P}(c, \underline{x}, t) = \underbrace{\alpha(\underline{x}, t)\delta(c)}_{\text{fresh gases}} + \underbrace{\beta(\underline{x}, t)\delta(1-c)}_{\text{burnt gases}} + \underbrace{\gamma(\underline{x}, t)\, f(c, \underline{x}, t)}_{\text{burning gases}} \tag{125}$$

where α, β and γ respectively denotes the probability to have, at location $(\underline{x}, t)$, fresh gases, burnt gases and reacting mixture. $\delta(c)$ and $\delta(1-c)$ are respectively the Dirac delta functions corresponding to fresh gases ($c = 0$) and fully burnt ones ($c = 1$).

Normalization of the probability density function:

$$\int_0^1 \overline{P}(c,\underline{x},t)\,dc = 1 \tag{126}$$

leads to the following relations:

$$\alpha+\beta+\gamma = 1 \tag{127}$$

$$\int_0^1 f(c,\underline{x},t)\,dc = 1 \tag{128}$$

with $f(0)=f(1)=0$.

The balance equation for the progress variable c may be written:

$$\frac{\partial \rho c}{\partial t} + \nabla\cdot(\rho \mathbf{u} c) = \nabla\cdot(\rho D \nabla c) + \dot{\omega} \tag{129}$$

This equation is averaged and the mean reaction rate, at the location $(\underline{x},t)$ is:

$$\overline{\dot{\omega}}(\underline{x},t) = \int_0^1 \dot{\omega}(c)\overline{P}(c,\underline{x},t)\,dc \tag{130}$$

leading to (125):

$$\overline{\dot{\omega}}(\underline{x},t) = \gamma(\underline{x},t)\int_0^1 \dot{\omega}(c) f(c,\underline{x},t)\,dc \tag{131}$$

All studies devoted to this line of models are based on such a formulation. The objective is now to determine the unknown functions α, β, γ and the probability density function f.

Using the Damköhler number, Da, comparing turbulence and chemical time scales, and, the turbulent Reynolds number Re, two particular cases emerge:

1. $Re \gg Da \gg 1$. The combustion is controlled by the turbulent transport and the reaction zone may be assumed to be infinitely thin. Accordingly, $\gamma \ll 1$ (i.e. $\alpha \gg \gamma$ and $\beta \gg \gamma$). This simplification leads to the well-known BML model and will be the only case considered here.

2. $Re \gg Da > 1$ or $Re > Da \gg 1$. In the first case, the flame thickness is not negligible and in the second one, the chemical reaction cannot be assumed infinitely fast compared to the turbulent transport. These situations correspond to "flamelet models". The reaction zone is then analyzed as a collection of laminar flame elements, of which properties need to be incorporated into the estimation of the overall reaction rate.

7.3.2 BML model analysis

This model is developed under the assumption that $Re \gg Da \gg 1$, corresponding to $\gamma \ll 1$. At a given location in the flow, an intermittency between fresh gases ($c=0$) and fully burnt ones ($c=1$) is observed and the probability density function of the progress variable c reduces to:

$$\overline{P}(c,\underline{x},t) = \alpha(\underline{x},t)\delta(c) + \beta(\underline{x},t)\delta(1-c) \tag{132}$$

Then at the point $\underline{x},t$ inside the reaction zone, c is a telegraphic signal as displayed in Fig. 16.

Under this assumption, α and β are easily determined as a function of the Favre average progress variable $\widetilde{c}$:

$$\overline{\rho c} = \overline{\rho}\widetilde{c} = \int_0^1 \rho c \overline{P}(c)dc = \rho_b \beta \tag{133}$$

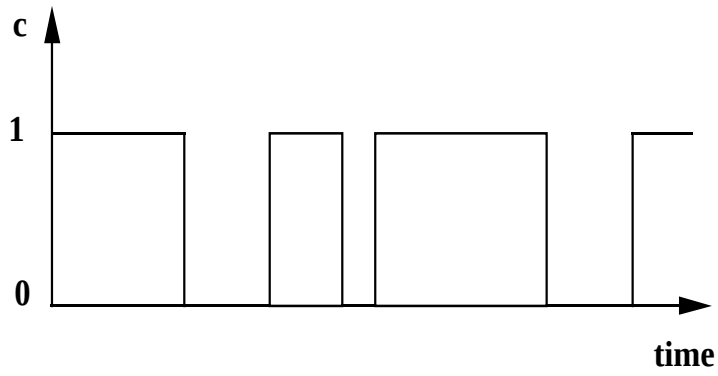

Figure 16: Intermittency between fresh and fully burnt gases at a given location in the reaction zone. This signal corresponds to a bimodal ($c = 0$ and $c = 1$) probability density function.

where ρ_b is the burnt gases density.

$$\beta = \frac{\overline{\rho c}}{\rho_b} \qquad \text{and} \qquad \alpha = 1 - \frac{\overline{\rho c}}{\rho_b} \tag{134}$$

The mean density $\overline{\rho}$ may be written:

$$\overline{\rho} = \int_0^1 \rho \, dc = \alpha \rho_u + \beta \rho_b = \left(1 - \frac{\overline{\rho c}}{\rho_b}\right) \rho_u + \frac{\overline{\rho c}}{\rho_b} \rho_b \tag{135}$$

One may also introduce the reaction heat release factor τ, defined as:

$$\tau = \frac{\rho_u}{\rho_b} - 1 = \frac{T_b}{T_u} - 1 \tag{136}$$

leading to:

$$\rho_u = (1 + \tau) \, \rho_b = \overline{\rho} \, (1 + \tau \widetilde{c}) \tag{137}$$

corresponding to the perfect gases state law, assuming a constant pressure P.

Then, the probabilities α and β become:

$$\boxed{\alpha = \frac{1 - \widetilde{c}}{1 + \tau \widetilde{c}} \quad ; \quad \beta = \frac{(1 + \tau) \, \widetilde{c}}{1 + \tau \widetilde{c}}} \tag{138}$$

The probability density function $\overline{P}(c)$ is determined and depends only on the mean progress variable $\widetilde{c}$ (and on the heat release factor, τ, which is fixed for a given chemical reaction). The BML model involves a presumed pdf (Eq. 131), however, the mean reaction rate cannot be calculated from the pdf since γ was neglected in Eq. (125).

Starting from the conservative and non-conservative forms of the progress variable c balance equations:

$$\begin{aligned} \frac{\partial \rho c}{\partial t} + \nabla \cdot (\rho \mathbf{u} c) &= \nabla \cdot (\rho D \nabla c) + \dot{\omega} \\ \rho \frac{\partial c}{\partial t} + \rho \mathbf{u} \cdot \nabla c &= \nabla \cdot (\rho D \nabla c) + \dot{\omega} \end{aligned}$$

and multiplying by c and adding these equations:

$$\frac{\partial \rho c^2}{\partial t} + \nabla \cdot \left(\rho \mathbf{u} c^2\right) \quad = \quad \nabla \cdot \left(\rho D \nabla c^2\right) - 2\rho D \, \nabla c \cdot \nabla c + 2c\dot{\omega} \tag{139}$$

Subtracting the balance equation for c^2 (139) to the balance equation for the progress variable c (129) leads to a balance equation for $c(1-c)$:

$$\frac{\partial}{\partial t}\left[\rho c(1-c)\right] + \nabla \cdot \left[\rho \mathbf{u} c(1-c)\right] = \nabla \cdot \left(\rho D \nabla \left[c(1-c)\right]\right) + 2\rho D \, \nabla c \cdot \nabla c - 2c\,\dot{\omega} + \dot{\omega} \tag{140}$$

Under the assumption of the BML model, the progress variable c is equal to zero or to unity. Accordingly, $c(1-c) = 0$ and the balance equation (140) reduces to:

$$2\rho D \, \nabla c \cdot \nabla c = 2c\dot{\omega} - \dot{\omega} \tag{141}$$

leading to, after averaging:

$$2\overline{\rho D \, \nabla c \cdot \nabla c} = (2c_m - 1)\,\overline{\dot{\omega}} \tag{142}$$

where a progress variable c_m, defined as:

$$c_m = \frac{\displaystyle\int_0^1 c\dot{\omega} f(c) dc}{\displaystyle\int_0^1 \dot{\omega} f(c) dc} \tag{143}$$

has been introduced and characterizes the chemical reaction.

The mean reaction rate $\overline{\dot{\omega}}$ becomes:

$$\boxed{\overline{\dot{\omega}} = 2\frac{\overline{\rho\chi}}{2c_m - 1}} \tag{144}$$

where $\overline{\rho\chi}$ is the scalar dissipation rate of the progress variable c.

$$\overline{\rho\chi} = \overline{\rho}\widetilde{\chi} = \overline{\rho D \, \nabla c \cdot \nabla c} = \overline{\rho D \frac{\partial c}{\partial x_i} \frac{\partial c}{\partial x_i}} \tag{145}$$

The mean reaction rate $\overline{\dot{\omega}}$ is then related to the dissipation rate $\widetilde{\chi}$, describing the turbulent mixing, and to c_m, characterizing the chemical reaction. A transport equation for the scalar dissipation rate may be written and solved [116], or one may postulate a linear relaxation of the fluctuations generated by micromixing (§ 9.2.2), leading to:

$$\overline{\rho\chi} = \frac{\overline{\rho c''^2}}{\tau_t} \tag{146}$$

where a turbulent time scale, τ_t is introduced. Assuming an intermittency between fresh and burnt gases ($c = 0$ or $c = 1$), $\widetilde{c''^2}$ is given by Eq. (122). Then:

$$\boxed{\overline{\dot{\omega}} = \frac{2}{2c_m - 1}\frac{\overline{\rho}\widetilde{c}\,(1-\widetilde{c})}{\tau_t}} \tag{147}$$

The Eddy-Break-Up model expression (Eq. 123) is recovered (§ 7.2). The BML model may then be viewed as a theoretical derivation, where the assumptions made are clearly stated, of the Eddy-Break-Up (EBU) model, initially based on a phenomenological approach.

7.3.3 Recovering mean reaction rate from tools relations

The analysis developed in section § 7.3.2 is the usual derivation of the BML model. However, expression (144) linking mean reaction rate and scalar dissipation may also be recovered from the general relations between modeling tools (Eq. 117):

$$\overline{\dot{\omega}} = \frac{1}{\overline{\langle \rho D |\nabla c| \rangle_s}} \overline{\left\langle \frac{\dot{\omega}}{|\nabla c|} \right\rangle_s} \overline{\rho}\widetilde{\chi} \tag{148}$$

To link mean reaction rate and scalar dissipation rate using the flamelet analysis, Eq. (148) requires estimates for $\dot{\omega}/|\nabla c|$ and $\rho D\ |\nabla c|$, averaging of these quantities along iso-surface $c = c^*$ and integration over all the possible c^* values. Assuming that infinitely thin flame elements may be viewed as one-dimensional, steady state, premixed laminar flame propagating at a given laminar flame speed S_L, the balance equation for the progress variable c in this 1D flame is:

$$\rho_0 S_L \nabla \cdot c = \nabla \cdot (\rho D \nabla c) + \dot{\omega} \tag{149}$$

where ρ_0 denotes the density in the fresh gases. Integrating Eq. (149) across all the flame front from fresh gases to burnt gases ($-\infty \leq x \leq +\infty$) and up to a given location x_0, corresponding to a progress variable c_0 ($-\infty \leq x \leq x_0$), leads to:

$$\rho_0 S_L = \int_{-\infty}^{+\infty} \dot{\omega}\, dx = \int_0^1 \frac{\dot{\omega}}{|\nabla c|}\, dc \tag{150}$$

$$(\rho D \nabla c)_{x_0} = \rho_0 S_L c_0 - \int_{-\infty}^{x_0} \dot{\omega}\, dx = \left[\int_0^1 \frac{\dot{\omega}}{|\nabla c|}\, dc \right] c_0 - \int_0^{c_0} \frac{\dot{\omega}}{|\nabla c|}\, dc \tag{151}$$

As the flame front is supposed to be thin and planar, all c^* iso-surfaces have the same surface and all quantities are constant along these surfaces, moreover the flame is supposed locally one-dimensional and $|\nabla c| = \nabla c$. Then:

$$\begin{aligned} \frac{\int_0^1 \langle \dot{\omega}/|\nabla c| \rangle_s\, dc^*}{\int_0^1 \langle \rho D\ |\nabla c| \rangle_s\, dc^*} &= \frac{\int_0^1 \dot{\omega}/|\nabla c|\, dc}{\int_0^1 \rho D\ |\nabla c|\ dc} = \frac{\int_{-\infty}^{+\infty} \dot{\omega}\, dx}{\int_{-\infty}^{+\infty} \dot{\omega}\, dx \int_0^1 c\, dc - \int_0^1 \int_0^{c_0} (\dot{\omega}/|\nabla c|)\ dc\, dc_0} \\ &= \frac{2 \int_{-\infty}^{+\infty} \dot{\omega}\, dx}{2 \int_{-\infty}^{+\infty} c\, \dot{\omega}\, dx - \int_{-\infty}^{+\infty} \dot{\omega}\, dx} = \frac{2}{2c_m - 1} \end{aligned} \tag{152}$$

where c_m is defined as:

$$c_m = \frac{\int_{-\infty}^{+\infty} c\, \dot{\omega}\, dx}{\int_{-\infty}^{+\infty} \dot{\omega}\, dx} \tag{153}$$

Then, from Eq. (148):

$$\overline{\dot{\omega}} = 2 \frac{\overline{\rho\chi}}{2c_m - 1} \tag{154}$$

recovering Eq. (144). This second analysis leads to the following comments:

- The definition of c_m is slightly different in Eq. (144) and Eq. (154). In the first one, the integration is performed over all possible values of the progress variable c at a **given location** $(\underline{x}, t)$. In the second analysis, the integration is performed along a normal direction to the flame front, assumed to be a laminar one-dimensional premixed flame. For an infinitely thin flame front, one may expect the probability to find $c \neq 0$ and $c \neq 1$ ($0 < c < 1$) roughly constant and $f(c) = 1$ in Eq. (143).
- This second derivation clearly exhibits how a flamelet model works (the turbulent flame is viewed as a collection of thin laminar flame elements). The c_m parameter is related to the inner structure of the flame front and to the properties of the chemical reaction.
- Making use of the flame surface density Σ as defined by Eq. (112), the expression for the mean burning rate becomes:

$$\overline{\dot{\omega}} = \rho_0 S_L \Sigma \tag{155}$$

where

$$\Sigma = \frac{2}{2c_m - 1} \frac{1}{\rho_0 S_L} \overline{\rho} \widetilde{\chi} \approx \frac{2}{2c_m - 1} \frac{1}{\rho_0 S_L} \overline{\rho} \frac{\widetilde{c}\,(1 - \widetilde{c})}{\tau_t} \tag{156}$$

- The BML model has been developed starting from a statistical analysis (two peaks pdf), the mean reaction rate was written in terms of the scalar dissipation rate of the progress variable c, which may be recast in terms of flame surface density, exhibiting simple links between modeling tools.

7.3.4 Reynolds and Favre averaging

Assuming a bimodal distribution of the progress variable c, Reynolds ($\overline{c}$) and Favre ($\widetilde{c}$) averages are easily related. From:

$$\overline{c} = \int_0^1 c \overline{P}(c)\, dc = \beta \tag{157}$$

$$\overline{\rho c} = \overline{\rho} \widetilde{c} = \int_0^1 \rho c \overline{P}(c)\, dc = \rho_b \beta = \rho_b \overline{c} \tag{158}$$

together with expressions (137) and (138), one easily obtains:

$$\boxed{\overline{c} = \frac{(1 + \tau)\, \widetilde{c}}{1 + \tau \widetilde{c}}} \tag{159}$$

corresponding to a model for the density / progress variable correlations (Eq. 15):

$$\overline{\rho' c'} = -\overline{\rho} \frac{\tau \widetilde{c}\,(1 - \widetilde{c})}{1 + \tau \widetilde{c}} \tag{160}$$

Reynolds ($\overline{c}$) and Favre ($\widetilde{c}$) averages of the instantaneous progress variable c are compared on Fig. 17 for various values of the heat release factor τ. The discrepancy between the two quantities strongly increases with τ. $\overline{\rho' c'}$ is plotted as a function of $\widetilde{c}$ on Fig. 18.

7.3.5 Conditional averaging - Counter-gradient turbulent transport

The analysis of intermittency between fresh gases ($c = 0$) and fully burnt gases ($c = 1$) leads to the introduction of conditional averaging. The Favre average $\widetilde{Q}$ of any quantity Q may be expressed as a function of the fresh gases ($\overline{Q}^u$) and fully burnt products ($\overline{Q}^b$) conditional averages:

$$\overline{\rho} \widetilde{Q} = \overline{\rho Q} = \int_0^1 \rho\, Q \overline{P}(c)\, dc = \alpha \rho_u \overline{Q}^u + \beta \rho_b \overline{Q}^b \tag{161}$$

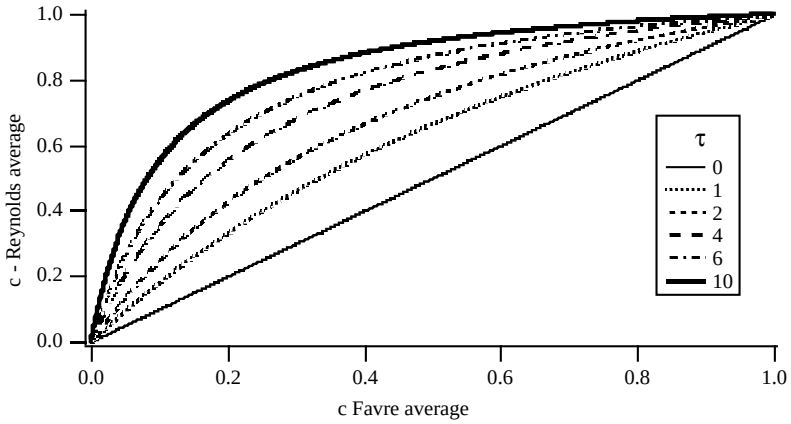

Figure 17: The Reynolds average $\overline{c}$ of the progress variable c is plotted as a function of the Favre average $\widetilde{c}$ for various values of the heat release factor τ, assuming a bimodal distribution ($c = 0$ or $c = 1$) of c (Eq. 159).

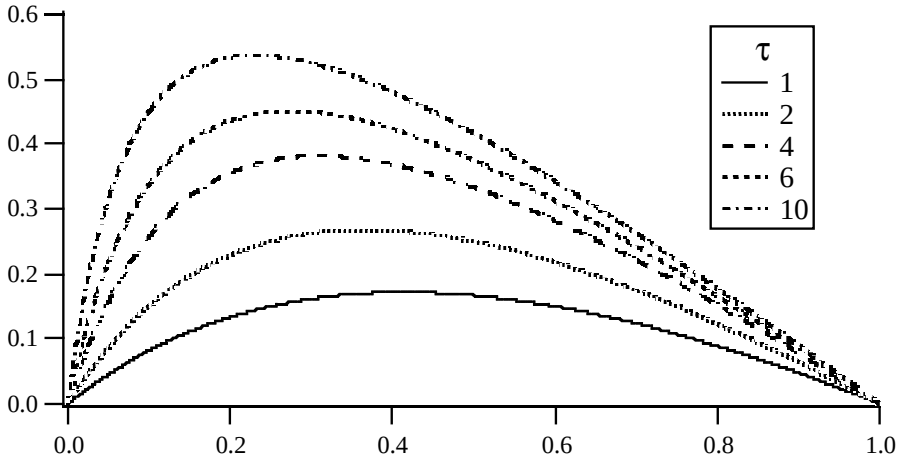

Figure 18: Correlation $-\overline{\rho' c'}/\overline{\rho}$ as a function of the Favre averaged progress variable $\widetilde{c}$ for various values of the heat release factor τ, assuming a bimodal distribution ($c = 0$ or $c = 1$) of c (Eq. 160).

using Eq. (137) and (138):

$$\boxed{\widetilde{Q} = (1-\widetilde{c})\ \overline{Q}^u + \widetilde{c}\,\overline{Q}^b} \tag{162}$$

where $\overline{Q}^u$ and $\overline{Q}^b$ are defined as:

$$\begin{aligned} \overline{Q}^u &= \int_{-\infty}^{+\infty} Q\overline{P}_c(Q|c=0)\,dQ \\ \overline{Q}^b &= \int_{-\infty}^{+\infty} Q\overline{P}_c(Q|c=1)\,dQ \end{aligned}$$

$\overline{P}_c(Q|c)$ is the pdf of Q for the given value c of the progress variable (conditional pdf see § 6.4.1).

The components $\widetilde{u}_k$ of the mean velocity vector $\widetilde{\mathbf{u}}$ may be written as a linear combination of their conditional fresh and burnt gases averages:

$$\widetilde{u}_i = (1-\widetilde{c})\ \overline{u}_i^u + \widetilde{c}\,\overline{u}_i^b \tag{163}$$

Then:

$$\overline{\rho}\widetilde{u_i''c''} = \overline{\rho}\,(\widetilde{u_i c} - \widetilde{u}_i\widetilde{c}) = \overline{\rho}\,\left(\widetilde{c}\,\overline{u}_i^b - \widetilde{u}_i\widetilde{c}\right) = \overline{\rho}\,\widetilde{c}(1-\widetilde{c})(\overline{u}_i^b - \overline{u}_i^u) \tag{164}$$

which is the scalar turbulent flux, generally modeled using a gradient assumption:

$$\overline{\rho}\widetilde{u_i''c''} = -\frac{\mu_t}{S_c}\left(\frac{\partial\widetilde{c}}{\partial x_i}\right) \tag{165}$$

The two expressions (164) and (165) may describe opposite fluxes: Consider a left-traveling one dimensional turbulent flame, because of thermal expansion the conditional velocity in the burnt gases, $\overline{u}_i^b$, is expected to be larger than the conditional velocity in the fresh gases, $\overline{u}_i^u$. According to Eq. (164), the turbulent flux, $\widetilde{u_i''c''}$ is expected to be positive. On the other hand, as the mean progress variable gradient is also positive, Eq. (165) leads to a negative value of $\widetilde{u_i''c''}$. This situation, called "counter-gradient turbulent transport", is a key point of the BML analysis and will be further discussed in § 8.

The Reynolds stresses $\widetilde{u_i''u_j''}$ may also be decomposed using the same formalism:

$$\widetilde{u_i''u_j''} = (1-\widetilde{c})\overline{u_i'u_j'}^u + \widetilde{c}\overline{u_i'u_j'}^b + \underbrace{\widetilde{c}(1-\widetilde{c})(\overline{u}_i^b - \overline{u}_i^u)(\overline{u}_j^b - \overline{u}_j^u)}_{intermittency} \tag{166}$$

where one may note a weighted mean between the Reynolds stresses in the fresh ($\overline{u_i'u_j'}^u$) and in the burnt gases ($\overline{u_i'u_j'}^b$) representative of turbulent motions. The additional term represents the intermittency between fresh and burnt gases.

7.4 Models based on the flame surface area estimation

7.4.1 Introduction

Several flame surface density models are now discussed. Their derivation and their histories differ, but they are all based on similar concepts, described in section § 6.3.2. These models assume that the chemical reaction occurs in thin layers separating fresh gases from fully burnt ones (high Damköhler number limit). The reaction zone may then be viewed as a collection of laminar flame elements called *flamelets*.

The flame surface density is here introduced at the light of experimental data from [117, 118]. The experimental burner is displayed on Fig. 19. A turbulent premixed propane/air flame is stabilized

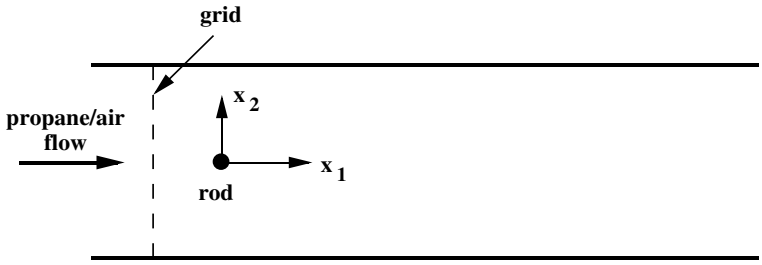

Figure 19: Experimental burner. A propane/air premixed flow is injected in a rectangular burner through a grid. The turbulent flame is stabilized behind a small cylinder (blockage ratio of 6 %). From [117, 118].

behind a small cylinder (blockage ratio of 6 %). Flow rates are about 35 to 100 g/s, corresponding to inlet velocities between 10 to 30 m/s (turbulence levels from 5 to 10 %). Equivalence ratio ϕ are in the range 0.7 to 1.1. Velocity (laser Doppler velocimetry), CH and C_2 radical emission (reaction rate estimation) and high-speed laser tomography (flame front characteristics) measurements have been performed and are described in [117, 118, 119, 120].

In Fig. 20 (half burner), flame surface density profiles are plotted as a function of the transverse coordinate for various downstream locations and for two equivalence ratios.

7.4.2 Algebraic expressions for the flame surface density Σ

Assuming intermittency between fresh and burnt gases (§ 7.3), Bray, Moss, Libby and their coworkers have proposed to describe the mean reaction rate $\overline{\dot{\omega}}$ as the product of a flame crossing frequency ν and a local reaction rate per flame crossing, w_F:

$$\overline{\dot{\omega}} = w_F \, \nu \tag{167}$$

Because $c(t)$ may be viewed as a telegraphic signal (Fig. 16), this crossing frequency is derived from a statistical analysis of the telegraph equation, leading to:

$$\nu = \frac{2\,\overline{c}\,(1-\overline{c})}{\widehat{T}} \tag{168}$$

where $\widehat{T}$ is time scale for the fluctuations of c.

This analysis is attractive because the crossing frequency ν may be easily obtained in experiments, for example from time-resolved local temperature measurements (thermocouple). On the other hand, the flame surface density Σ and the local reaction rate per flame crossing (w_F) are not obvious to estimate. Eq. (168) is generally closed estimating $\widehat{T}$ from a characteristic turbulent time τ_t. The reaction rate per crossing flame, w_F (Eq. 167), is usually modeled as:

$$w_F = \frac{\rho_0 S_L}{\delta_l / t_t} \tag{169}$$

where ρ_0 is the unburnt gases density, S_L and δ_l are respectively the speed and the thickness of the laminar flame. The flame transit time t_t measures the averaged time spend by a point in the flow to cross a flame front and corresponds to the mean transition time between $c = 0$ and $c = 1$ levels of the progress variable, as shown in Fig. 21 (in practice, the c-signal is not exactly bimodal).

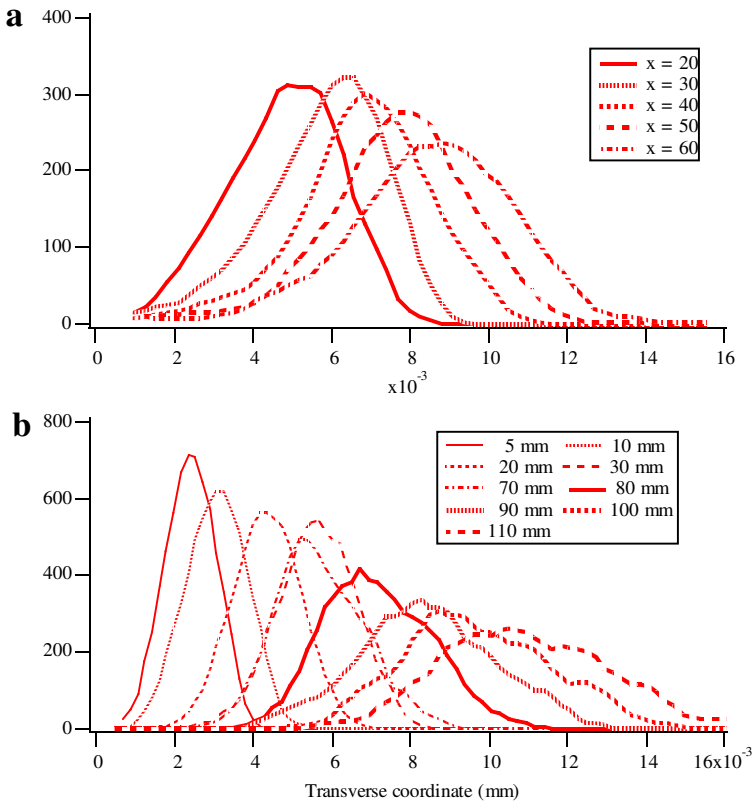

Figure 20: Transverse flame surface density (Σ) profiles (m^{-1}) plotted as a function of the transverse location for various downstream locations (mm downstream the rod). (a) $\phi = 0.78$; (b) $\phi = 0.9$. Flow rate: 35 g/s. From [118].

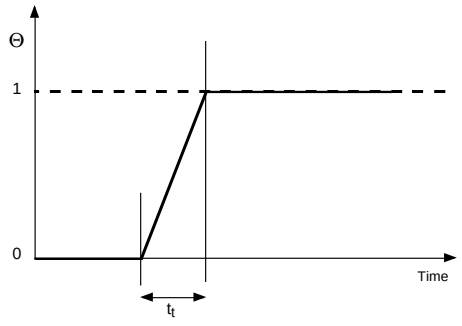

Figure 21: Definition of the flame transit time t_t is the flame crossing frequency BML model.

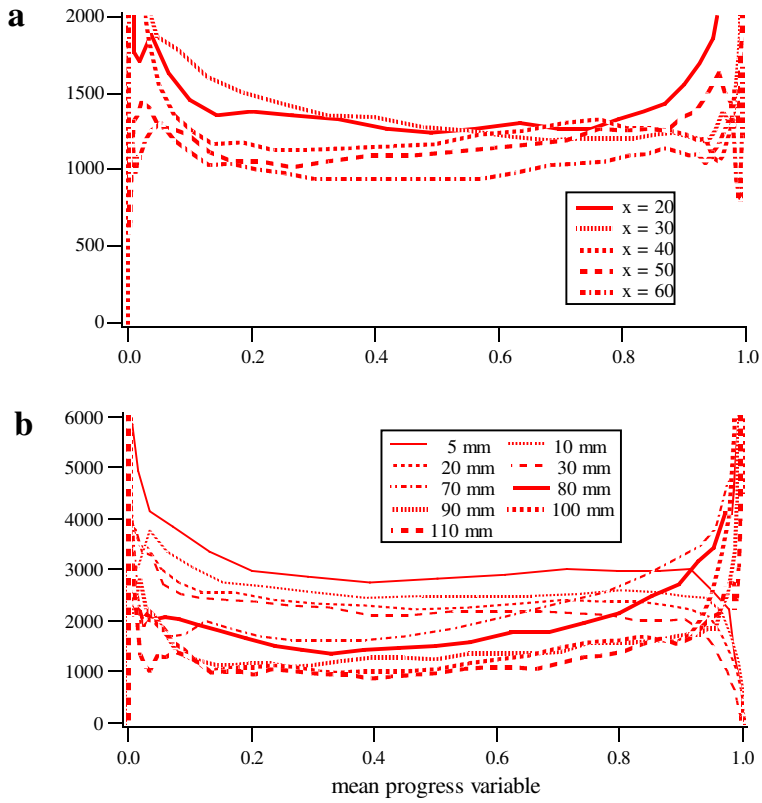

Figure 22: $\Sigma/(\overline{c}(1-\overline{c}))$ transverse profiles in mm^{-1} corresponding to $g/(\sigma_y L_y)$ in the Bray, Champion, Libby model (Eq. 170), plotted as the function of the mean progress variable $\overline{c}$ for several locations downstream from the rod. (a) $\phi = 0.78$; (b) $\phi = 0.9$. From [118].

This model has been latter rewritten in term of flame surface density, leading to the algebraic expression [121]:

$$\boxed{\Sigma = g\frac{\overline{c}(1-\overline{c})}{\sigma_y L_y} = \frac{g}{\sigma_y L_y}\frac{1+\tau}{(1+\tau\widetilde{c})^2}\widetilde{c}(1-\widetilde{c})} \tag{170}$$

where g is a constant of order unity. σ_y is a flamelet orientation factor measuring the mean angle of the instantaneous flame front with the $\overline{c}$-surface and assumed to be an universal model constant ($\sigma_y \approx 0.5$). L_y is a flame front wrinkling length scale and Eq. (159) has been used to replace $\overline{c}$ as a function of $\widetilde{c}$. A submodel is required to describe the wrinkling length scale L_y, generally assumed to be proportional to the integral length scale l_t:

$$L_y = C_l l_t \left(\frac{S_L}{u'}\right)^n \tag{171}$$

where C_l and n are two constants of the order of unity [74].

The agreement between this BML model and the experimental data is very good, as displayed on Fig. 22 where the ratio $\Sigma/\left[\overline{c}\,(1-\overline{c})\right]$, corresponding to $g/\sigma_y L_y$ and assumed to be constant, is displayed. Nevertheless, a submodel is required for the wrinkling length scale which increases with the downstream location in our experiment.

Estimating the local reaction rate per unit flame area $\dot{\Omega}_c$ from the laminar flame speed S_L ($\dot{\Omega}_c = \rho_0\, S_L$,

where ρ_0 is the fresh gases density) the mean reaction rate becomes, when $n = 1$:

$$\overline{\dot{\omega}} = \rho_0 \frac{g}{\sigma_y C_l} \frac{u'}{l_t} \overline{c}(1 - \overline{c}) = \rho_0 \frac{g}{\sigma_y C_l} \frac{u'}{l_t} \frac{(1+\tau)\,\widetilde{c}(1-\widetilde{c})}{(1+\tau\widetilde{c})^2} \tag{172}$$

As $\tau_t = l_t/u'$ is a turbulence characteristic time scale, the mean reaction rate $\overline{\dot{\omega}}$ is proportional to the intermittency between fresh and burnt gases, determined from $\widetilde{c}(1-\widetilde{c})$ or $\overline{c}(1-\overline{c})$, and inversely proportional to τ_t. The physical analysis leading to the Eddy-Break-Up model is recovered and a similar expression for the reaction rate is found. The previous expression is slightly different than the one proposed in § 7.3.3. The discrepancies are easily explained by the crude model used for the scalar dissipation of the progress variable to derive Eq. (156). In Eq. (172), u'/l_t is generally modeled from the turbulence $k - \varepsilon$ model as ε/k. The ITNFS efficiency function Γ_k [126] may be introduced in the turbulent time scale to account for the reduced ability of small turbulent structures to wrinkle the flame front. ITNFS is one of the closure schemes for the flame surface density balance equation (see § 7.4.3 and Table 5). The mean reaction rate is then [127, 128, 129]:

$$\overline{\dot{\omega}} = \alpha \rho_0 \Gamma_k \left(\frac{l_t}{\delta_l}, \frac{u'}{S_L} \right) \frac{\varepsilon}{k} \overline{c}(1 - \overline{c}) \tag{173}$$

where α is a model constant and the efficiency function Γ_k depends on the length scale (l_t/δ_l) and the velocity (u'/S_L) ratii comparing the turbulence and the laminar flame characteristics. The efficiency function has been fitted from DNS data [126, 123]:

$$\log_{10}(\Gamma_k) = -\frac{1}{s+0.4} \exp\left[-(s+0.4)\right] + \left(1 - \exp\left[-(s+0.4)\right]\right) \left(\sigma_1 \left(\frac{u'}{S_L} \right)\ s - 0.11 \right) \tag{174}$$

where

$$s = \log_{10}\left(\frac{l_t}{\delta_l} \right) \quad \text{and} \quad \sigma_1 \left(\frac{u'}{S_L} \right) = \frac{2}{3} \left(1 - \frac{1}{2} \exp\left[-\left(\frac{u'}{S_L} \right)^{\frac{1}{3}} \right] \right) \tag{175}$$

When the length scale ratio l_t/δ_l tends towards zero, Γ_k also decreases, reducing the effective flame strain rate, as displayed on Fig. 23. Γ_k only slightly depends on the velocity ratio u'/S_L. The efficiency function does not reach a constant level when l_t/δ_l increases since increasing l_t/δ_l, keeping u'/S_L constant, corresponds to an implicit increase of the turbulent Reynolds number Re.

Because the efficiency function Γ_k tends to counterbalance the known trend of Eddy-Break-Up modeling to overestimate the mean reaction rate in highly strained regions, this simple approach improves the accuracy of the numerical predictions.

The BML model proposes a simple algebraic expression to estimate the flame surface density Σ and the corresponding reaction rate, but Bray, Moss, Champion and Libby have mainly focused their attention to a careful description of the turbulent fluxes using the balance equations for the Reynolds stresses $\overline{\rho}\widetilde{u_i'' u_j''}$ and the scalar fluxes $\overline{\rho}\widetilde{u_i'' c''}$ to take into account the possible occurrence of counter-gradient transport and flame turbulence generation [130, 131].

The flame surface density may also be derived from fractal theories, leading to [132]:

$$\boxed{\Sigma = \frac{1}{L_{outer}} \left(\frac{L_{outer}}{L_{inner}} \right)^{D-2}} \tag{176}$$

where L_{inner} and L_{outer} are respectively the inner and outer cut-off length scales (the flame surface is assumed to be fractal between these two scales). D is the fractal dimension of the flame surface. The cut-off scales are generally estimated for the turbulence Kolmogorov l_k and the integral l_t length scales.

MODEL	$S_1 = \kappa_m \Sigma$	$S_2 = \kappa_t \Sigma$	S_3	D
CPB [122]	$A_{ik}\frac{\partial \overline{u}_k}{\partial x_i}\Sigma$	$\alpha_0 C_A \left(\frac{\varepsilon}{\nu}\right)^{1/2}\Sigma$		$\alpha_0 S_L \frac{2+e^{-aR}}{3(1-\overline{c})}\Sigma^2$ $R = \frac{(1-\overline{c})\varepsilon}{\Sigma S_L k}$
CFM1 CFM2-a CFM2-b [123]	$A_{ik}\frac{\partial \overline{u}_k}{\partial x_i}\Sigma$ $A_{ik}\frac{\partial \overline{u}_k}{\partial x_i}\Sigma$ $A_{ik}\frac{\partial \overline{u}_k}{\partial x_i}\Sigma$	$\alpha_0 \frac{\varepsilon}{k}\Sigma$ $\alpha_0 \Gamma_K \frac{\varepsilon}{k}\Sigma$ $\alpha_0 \Gamma_K \frac{\varepsilon}{k}\Sigma$		$\beta_0 \frac{S_L + C\sqrt{k}}{1-\overline{c}}\Sigma^2$ $\beta_0 \frac{S_L + C\sqrt{k}}{1-\overline{c}}\Sigma^2$ $\beta_0 \frac{S_L + C\sqrt{k}}{\overline{c}(1-\overline{c})}\Sigma^2$
MB [116]	$E\frac{\overline{u_i' u_k'}}{k}\frac{\partial \overline{u}_k}{\partial x_i}\Sigma$	$\alpha_0\sqrt{Re}\frac{\varepsilon}{k}\Sigma$	$\frac{F}{S_L}\frac{\varepsilon}{k}\overline{u_i' c'}\frac{\partial \overline{c}}{\partial x_i}$	$\beta_0 \frac{S_L\sqrt{Re}}{\overline{c}(1-\overline{c})\left(1+d\frac{S_L}{\sqrt{k}}\right)^{2\gamma}}\Sigma^2$
CD [124]		$\alpha_0\lambda\frac{\varepsilon}{k}\Sigma$ for $\kappa_t \leq \alpha_0 K \frac{S_L}{\delta_L}$		$\beta_0 \frac{S_L}{1-\overline{c}}\Sigma^2$
CH1 CH2 [125]		$\alpha_0 \left(\frac{\varepsilon}{15\nu}\right)^{1/2}\Sigma$ $\alpha_0 \frac{u'}{l_{tc}}\Sigma$		$\beta_0 \frac{S_L}{\overline{c}(1-\overline{c})}\Sigma^2$ $\beta_0 \frac{S_L}{\overline{c}(1-\overline{c})}\Sigma^2$

Table 5: Comparison of source (S_i) and consumption (D) terms in the flame surface density balance equation in different turbulent premixed combustion models (details in text). k and ε denote respectively the turbulent kinetic energy and its dissipation. Re is the turbulent Reynolds number. α_0, β_0, γ, λ, C_A, a, d, C, E and K are model constants Γ_k is the efficiency function in the ITNFS model [126] and depends on the length scale (l_t/δ_l) and the velocity (u'/S_L) ratii comparing the turbulence and the laminar flame characteristics. In the Choi model (CH) [125], u' denotes the rms turbulent velocity and l_{tc} is an arbitrary length scale introduced for dimensional consistency and combined to α_0 as a single arbitrary constant.

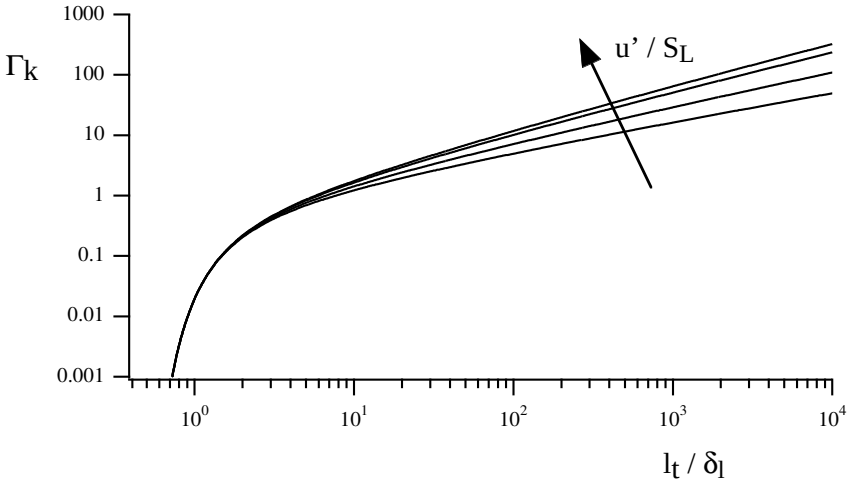

Figure 23: ITNFS efficiency function Γ_k (Eq. 174) as a function of the length scale ratio l_t/δ_l for several values of the velocity ratio u'/S_L (0.1; 1.0; 10.; $+\infty$).

7.4.3 Flame surface density balance equation closures

The previously described balance equations for Σ (Eqs. 86 and 87) are unclosed and require modeling. In Table 5, various closures found in the literature are compared where S_1 is the strain rate acting on the surface and induced by the mean flow field. S_2 is the strain rate due to the turbulent motions (Eq. 91) and the third source term, S_3, occurs only in the derivation proposed in [116]. D describes the consumption of flame area. The modeled balance equation is rewritten as:

$$\frac{\partial \Sigma}{\partial t} + \nabla \cdot (\widetilde{U}\Sigma) = \nabla \cdot \left(\frac{\nu_t}{\sigma_\Sigma} \nabla \Sigma \right) + S_1 + S_2 + S_3 - D \tag{177}$$

In this expression, the turbulent flux of flame surface density is expressed using a classical gradient assumption, ν_t is the turbulent viscosity and σ_Σ a flame surface turbulent Schmidt number. Five main closures are summarized:

- **The CPB model [122]** is derived from the exact transport equation for the flame surface density. The strain rate due to the turbulent fluctuations is estimated from the time scale $\sqrt{\nu/\varepsilon}$ of the Kolmogorov structures. The turbulent strain rate is probably overestimated. Despite the Kolmogorov structures contain the highest energy, their lifetime is too short (because of viscous effects) to actually affect the flame front [63].

- **The Coherent Flame Model (CFM)**, developed by Candel and his coworkers following the initial work of Marble of Broadwell [83]. Three versions are presented in Table 5. In the initial version (CFM1), the strain rate due to the turbulent fluctuations is estimated from the characteristic time of the integral length scale (k/ε). In the two succeeding formulations (CFM2), the expression of the turbulent strain rate acting on the flame front is improved from direct numerical simulations and multi-fractal analysis (ITNFS model, Eq. (174) [126]). The destruction term differs in these two last formulations (CFM2a and CFM2b).

- **The MB model [116]** is based on an exact equation for the scalar dissipation rate $\widetilde{\chi}$:

$$\overline{\rho}\widetilde{\chi} = \overline{\rho D \frac{\partial c''}{\partial x_i} \frac{\partial c''}{\partial x_i}} \tag{178}$$

assuming a constant density ρ. The transport equation is rewritten as a flame surface density transport equation under the flamelet assumption (see § 6.5, Eq. 112). This approach leads to a different expression for the source term S_1 and an additive source term S_3 is found. In a first analysis, this term S_3, which does not depend on the available flame surface density Σ, might be viewed as an ignition term [133] involving a gradient of the mean fuel mass fraction or of the mean temperature (i.e. fresh gases are ignited by heat transfers). However, this analysis does not hold because the flame surface density balance equation is derived assuming an established flame surface. In fact, as shown below, S_3 corresponds to an anisotropic contribution of the turbulent strain rate a_T (see Eq. 195). S_3 seems to be negligible in practical simulations, at least to describe the flame front propagation in an homogeneous and isotropic turbulent flow field.

- **The CD model [124]** is similar to the first version of the Coherent Flame Model (CFM1). An additional term is proposed to take into account flame extinction under excessively high strain rates. Such a term was tested in the Coherent Flame Model but the choice of the critical strain rate is somewhat arbitrary. Moreover, this critical strain rate cannot be deduced from planar strained laminar flame studies because, due to curvature and unsteady effects, a flame is able to sustain higher strain rates than expected.

- **The CH model [125]** has been devised for spark-ignited engines to recover experimental data obtained in a closed vessel [134]. The consumption term D is similar to the one proposed in CFM2-b model whereas two formulations of the strain rate induced by turbulent motions are proposed. The first expression (CH1) corresponds to the closure in CPB model, based on the Kolmogorov turbulent time scale. In CH2, the strain rate is only proportional to the turbulence intensity u' and an arbitrary length scale, l_{tc}, is incorporated in the model constant.

Despite these comments, all these closures exhibit strong similarities. For example, the consumption term D is always proportional to Σ^2. A comparison between these models to predict turbulent flame speed S_T may be found in [123]. In the case of a statistically one-dimensional turbulent flame propagating in a frozen turbulence, a KPP (Kolmogorov - Petroski - Piskunov) analysis was used to analytically determine the turbulent flame speed S_T as a function of the model parameters. It was found that only the CFM-2 formulation is able to predict the so-called bending phenomenon, where the turbulent flame speed decreases before the occurrence of flame extinction when the turbulence level increases, as experimentally evidenced [109].

A recent work, [133] has compared CPB, CFM1, MB and CD models to predict a turbulent premixed jet flame. The CD predicts extremely high temperatures whereas CFM1, MB and CPB provide reasonable predictions of mean velocities and temperatures. A slight overestimate (respectively underestimate) of temperature is pointed out for CPB (respectively MB) and is probably due to the expression for the strain rate. The MB closure [116] is found to be more sensitive to the inlet turbulent quantities than CFM1 but CFM2 models, incorporating an efficiency function including the inability of small vortices to wrinkle the flame surface, have not been tested. Flame surface density models are extended to non-isenthalpic flows (premixed reactants injected in a co-flow of air [135]). A pioneering work has been first conducted [129] extending the algebraic flame surface density BML model to non-isenthalpic flows, using similar concepts. A presumed pdf for a mixture fraction Z, determined from mean and rms values of Z, is incorporated to account for dilution phenomena.

7.4.4 Analysis of the flame surface density balance equation

Following the description of the exact balance equation for the flame surface density Σ (section 6.3.2) and the summary of the most popular closures (section 7.4.3), the aim of this section is to carefully

analyze this balance equation. This analysis may be based on direct numerical simulations [15] or on experimental data [117, 118].

Starting from the "propagative" form (Eq. 87):

$$\begin{aligned}\frac{\partial \Sigma}{\partial t} + \nabla \cdot (\widetilde{\mathbf{u}}\Sigma) + \nabla \cdot (\langle \mathbf{u}'' \rangle_s \Sigma) = \quad & \underbrace{\left(\nabla \cdot \widetilde{\mathbf{u}} - \langle \mathbf{nn} \rangle_s : \nabla \widetilde{\mathbf{u}}\right)}_{A_T} \Sigma + \underbrace{\langle \nabla \cdot \mathbf{u}'' - \mathbf{nn} : \nabla \mathbf{u}'' \rangle_s}_{a_T} \Sigma \\ - \quad & \underbrace{\nabla \cdot [\langle w\mathbf{n} \rangle_s \Sigma]}_{\text{propagation}} + \underbrace{\langle w \nabla \cdot \mathbf{n} \rangle_s \Sigma}_{\text{curvature}}\end{aligned} \tag{179}$$

each unclosed term may be investigated as follow:

Turbulent transport

The turbulent flux of flame surface density is generally expressed using gradient transport:

$$\langle \mathbf{u}'' \rangle_s \Sigma = -\frac{\nu_t}{\sigma_\Sigma} \nabla \mathbf{\Sigma} \tag{180}$$

Bidaux and Bray (1994, unpublished work, see for example [74, 64]) have shown from a simple BML-type approach that the turbulent fluxes of the mean progress variable ($\widetilde{c}$) and of the flame surface density (Σ) are closely related. Assuming that the conditional velocity on the flame surface, $\langle \widetilde{\mathbf{u}} \rangle_s$ is a linear function of the conditional fresh ($\overline{\mathbf{u}}^u$) and burnt ($\overline{\mathbf{u}}^b$) gases velocities:

$$\langle \widetilde{\mathbf{u}} \rangle_s = \overline{\mathbf{u}}^u + c^* \left(\overline{\mathbf{u}}^b - \overline{\mathbf{u}}^u \right) \tag{181}$$

where c^* denotes the c-level chosen to define the flame front. The BML relation (Eq. 163):

$$\widetilde{\mathbf{u}} = (1 - \widetilde{c})\, \overline{\mathbf{u}}^u + \widetilde{c}\, \overline{\mathbf{u}}^b \tag{182}$$

leads to:

$$\langle \mathbf{u}'' \rangle_s = \langle \mathbf{u} \rangle_s - \widetilde{\mathbf{u}} = (c^* - \widetilde{c}) \left(\overline{\mathbf{u}}^b - \overline{\mathbf{u}}^u \right) \tag{183}$$

From Eq. (164) the flame surface density turbulent flux becomes:

$$\boxed{\langle \widetilde{\mathbf{u}''} \rangle_s \Sigma = \frac{(c^* - \widetilde{c})}{\widetilde{c}\,(1 - \widetilde{c})} \widetilde{\mathbf{u}'' c''}\, \Sigma} \tag{184}$$

This relation, confirmed by direct numerical simulations [64], shows that turbulent fluxes of $\widetilde{c}$ and Σ are closely related. A counter-gradient turbulent transport will be observed simultaneously for these two scalar fields.

Strain rate induced by the mean flow field, A_T

The only unclosed quantities in the strain rate due to the mean flow field, A_T, are the orientation factors $\langle \mathbf{nn} \rangle_s$. Following [122], the vector normal to the flame front, $\mathbf{n}$ may be split in a mean, $\mathbf{M}$, and a fluctuating, $\mathbf{m}$, components:

$$\mathbf{n} = \mathbf{M} + \mathbf{m} \qquad \text{with} \qquad \langle \mathbf{n} \rangle_s = \mathbf{M} \quad \text{et} \quad \langle \mathbf{m} \rangle_s = 0 \tag{185}$$

Then, the orientation factors become:

$$\langle \mathbf{nn} \rangle_s = \mathbf{M}\,\mathbf{M} + \langle \mathbf{mm} \rangle_s \tag{186}$$

Using the definition $\mathbf{n}|\nabla c| = -\nabla c$ and assuming an infinitely thin flame front lead after averaging to [136, 122]:

$$\langle \mathbf{n} \rangle_s \Sigma = \mathbf{M}\Sigma = -\nabla \overline{c} \tag{187}$$

where $\overline{c}$ and $\widetilde{c}$ are related using the BML relation $\overline{\rho}\widetilde{c} = \rho^b \overline{c}$ (Eq. 133). Then, only the fluctuation cross products $\langle \mathbf{mm} \rangle_s$ remain unclosed. Several closure schemes have been proposed:

- In [122] one assumes an isotropic distribution of the fluctuating components of the normal vector $\mathbf{n}$:

$$\langle m_i m_j \rangle_s = \frac{\delta_{ij}}{3} \left(1 - M_k M_k\right) \tag{188}$$

- In [116], a relation between orientation factors and Reynolds stresses is indirectly proposed:

$$\langle n_i n_j \rangle_s = \frac{\widetilde{u_i'' u_j''}}{2k} \tag{189}$$

  where k is the turbulent kinetic energy.

- From experimental data, [117] a quite more complicated model is proposed that will not be described here because its practical implementation is probably not so easy. These authors have also shown that the isotropic assumption made in [122] is clearly wrong for the turbulent flame stabilized downstream a small rod. On the other hand, a slight modification of [116] leads to very good results [118]:

$$\langle n_i n_i \rangle_s = \frac{\sum_{k \neq i} \widetilde{u_k''}^2}{4k}, \quad \langle n_i n_{j \neq i} \rangle_s = \frac{\widetilde{u_i'' u_j''}}{2k} \tag{190}$$

These orientation factors have very important effects and may lead to surprising results. In the flame-holder stabilized turbulent flame investigated in [118], the main velocity gradient is the transverse gradient of the mean axial velocity, corresponding to the mixing layer shear stress. But, because of the low value of the corresponding orientation factor, its contribution to the strain rate A_T induced by the mean flow field is not that important. The strain rate A_T is dominated by the axial gradient of the mean axial velocity, induced by the thermal expansion due to the combustion heat release, as illustrated in Fig. 24. Notice also that the strain rate A_T cannot be reduced to the simplified expression firstly proposed [83]:

$$A_T = \left| \nabla \widetilde{U} \right| \tag{191}$$

Recent works [137] have shown that $\left| \nabla \widetilde{U} \right|$ may probably be viewed as a model for the total strain rate $A_T + a_T$ and not only for the strain rate A_T due to the mean flow. This finding explains why, in previous versions of the Coherent Flame Model where the orientation factors $\langle n_i n_j \rangle_s$ were not incorporated, the mean strain rate A_T was not included because the simple expression (191) clearly overestimates A_T.

Strain rate a_T due to turbulent motions

The source term due to the strain rate a_T is:

$$a_T \Sigma = \langle \nabla \cdot \mathbf{u}'' - \mathbf{nn} : \nabla \mathbf{u}'' \rangle_s \Sigma = \langle \delta_{ij} \frac{\partial u''_i}{\partial x_j} - n_i n_j \frac{\partial u''_i}{\partial x_j} \rangle_s \Sigma \tag{192}$$

In most models, this term is generally assumed to be proportional to the inverse of a turbulent time scale, either the Kolmogorov time scale (CPB model) or the integral time scale ε/k (CFM, MB and CD models). This turbulent time may corrected with the efficiency function, Γ_k, of the ITNFS closure (Eq. 174). Nevertheless, a_T is always modeled being isotropic despite the orientation factors $\mathbf{nn}$ occurring in expression (192).

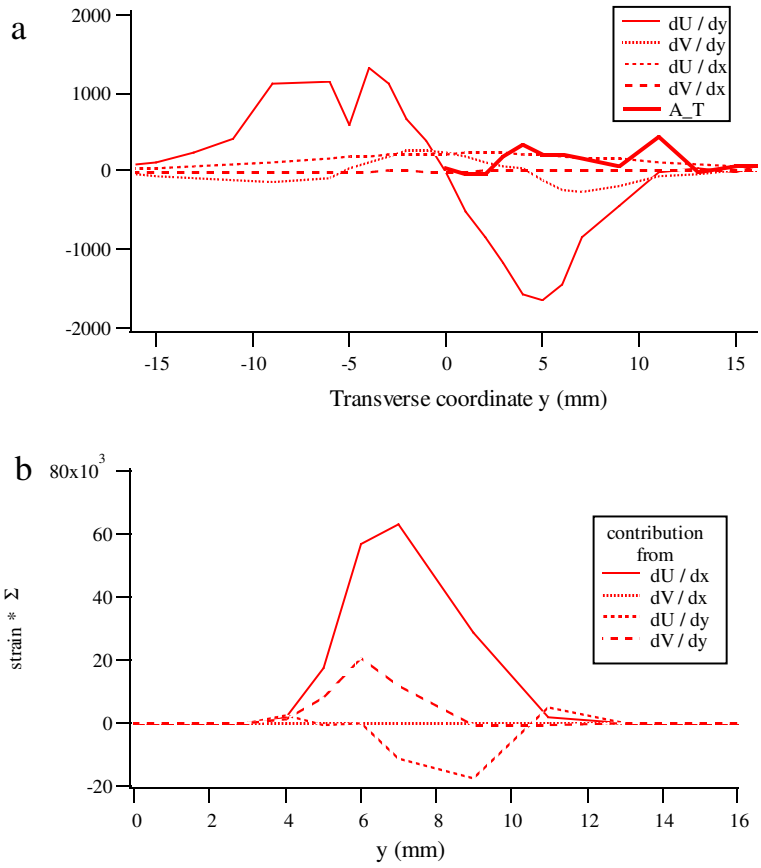

Figure 24: (a) Transverse profiles of the mean velocity gradients and the corresponding strain rate A_T. (b) Components of the source term $A_T\Sigma$ due to the strain rate induced by the mean flow field. Data are plotted as a function of the transverse coordinate y for $x = 80\ mm$ and $\phi = 0.9$. From [118].

Using the previous splitting of the normal vector to the flame front, **n**, combined with the geometrical relation (187), leads to:

$$\begin{aligned} a_T\Sigma = \langle \delta_{ij} \frac{\partial u''_i}{\partial x_j} \rangle_s \Sigma &- \frac{1}{\Sigma} \langle \frac{\partial u''_i}{\partial x_j} \rangle_s \frac{\partial \overline{c}}{\partial x_i} \frac{\partial \overline{c}}{\partial x_j} + \langle m_j \frac{\partial u''_i}{\partial x_j} \rangle_s \frac{\partial \overline{c}}{\partial x_i} \\ &+ \langle m_i \frac{\partial u''_i}{\partial x_j} \rangle_s \frac{\partial \overline{c}}{\partial x_j} - \langle m_i m_j \frac{\partial u''_i}{\partial x_j} \rangle_s \Sigma \end{aligned} \tag{193}$$

This interesting relation decomposes the source term due to the strain rate induced by turbulent motions, $a_T\Sigma$, into two parts: a contribution depending only on turbulent characteristics that may be assumed to be isotropic (first and last terms) and an anisotropic contribution, where the mean flame surface orientation occurs through the gradient of the mean progress variable (second, third and fourth terms). A priori, this last part is not proportional to the available flame surface density Σ.

When velocity and normal vector fluctuations are supposed uncorrelated (this assumption is well verified in direct numerical simulation data), the previous expression may be reduced using:

$$\langle m_j \frac{\partial u''_i}{\partial x_j} \rangle_s = \langle m_j \rangle_s \langle \frac{\partial u''_i}{\partial x_j} \rangle_s = 0 \tag{194}$$

from the m_j definition. Then:

$$a_T\Sigma = \underbrace{\langle \delta_{ij} \frac{\partial u''_i}{\partial x_j} \rangle_s \Sigma - \langle m_i m_j \frac{\partial u''_i}{\partial x_j} \rangle_s \Sigma}_{\text{isotropic contribution}} - \underbrace{\frac{1}{\Sigma} \langle \frac{\partial u''_i}{\partial x_j} \rangle_s \frac{\partial \overline{c}}{\partial x_i} \frac{\partial \overline{c}}{\partial x_j}}_{\text{anisotropic contribution}} \tag{195}$$

This simple analysis explains the third source term, S_3 found in [116] from the derivation of a balance equation for the scalar dissipation rate $\widetilde{\chi}$ of the progress variable c. This term S_3 corresponds to an anisotropic contribution depending on $\nabla\overline{c}$ and on the strain rate due to turbulent motions. Assuming a gradient type closure for the turbulent transport of the fresh gases, S_3 is proportional to $\nabla\overline{c} \cdot \nabla\overline{c}$ and appears as a model for the anisotropic contribution of the turbulent strain rate. Nonetheless, Mantel and Borghi [116] have shown that this term is negligible in numerical simulations of a flame propagating in an homogeneous and isotropic turbulent flow field. This finding is probably questionable in other configurations and further investigations are required.

Propagation and curvature terms

These two terms are analyzed together because they derive from the laminar flame propagation and are related to the flame front displacement speed w. The modeling of these terms requires the description of the displacement speed w that may have values far from the laminar flame speed S_L [77]. This stands as the main difficulty of the propagative approach for the flame surface density balance equation because various effects are incorporated in w (strain rate, curvature effects,...).

Assuming a constant displacement speed w equal to the laminar flame speed S_L, the **normal propagation term** becomes:

$$\nabla \cdot [\langle w\mathbf{n} \rangle_s \Sigma] = S_L \nabla \cdot [\langle \mathbf{n} \rangle_s \Sigma] = S_L \nabla \cdot [-\nabla\overline{c}] = -S_L \nabla^2\overline{c} \tag{196}$$

where the geometrical relation (187) is used.

This term is generally neglected in models (see Table 5). Experimental data from [117, 118] in a V-shape turbulent flame show that it is not always negligible and is of the same order than the curvature term. The **propagation / curvature term** becomes:

$$\langle w\nabla \cdot \mathbf{n} \rangle_s \Sigma = S_L \langle \nabla \cdot \mathbf{n} \rangle_s \Sigma \tag{197}$$

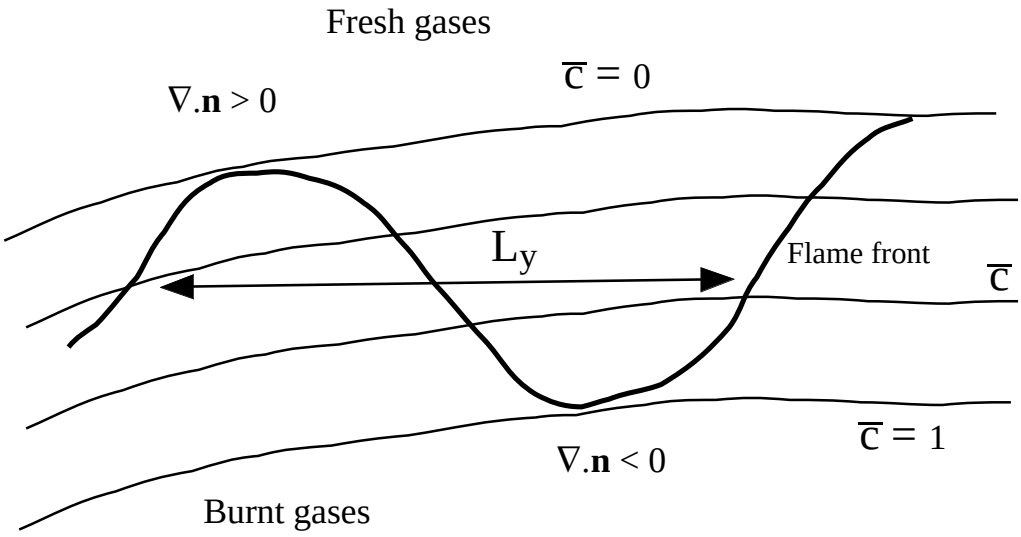

Figure 25: Flame front curvature analysis

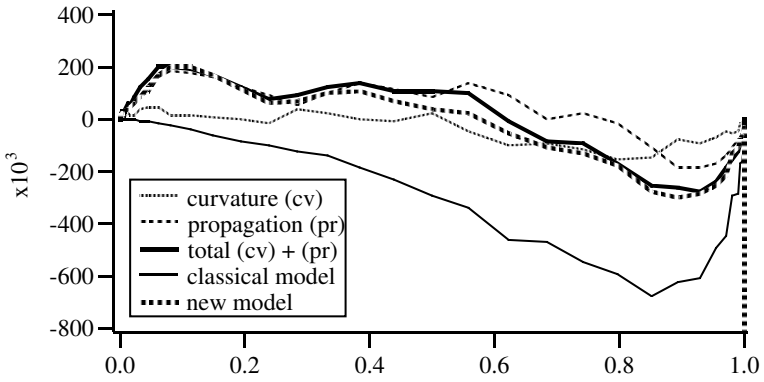

Figure 26: Transverse profiles of propagation ($\nabla\cdot[\langle\mathbf{n}\rangle_s\Sigma]$), curvature ($\langle\nabla.\mathbf{n}\rangle_s\Sigma$) and combined ($\langle\nabla.\mathbf{n}\rangle_\mathbf{s}\Sigma-\nabla.[\langle\mathbf{n}\rangle_s\Sigma]$) terms ($m^{-2}$) in the flame surface density balance equation plotted as a function of the mean progress variable $\overline{c}$. The consumption term modeled as $-\Sigma^2/(1-\overline{c})$ and the new proposed closure, $\nabla^2\overline{c}+\beta(c^*-\overline{c})\Sigma^2/\overline{c}(1-\overline{c})$ where $\beta=0.4$ and $c^*=0.5$ are also displayed. $\phi=0.90$, $x=80\ mm$. From [118].

where the only unknown is the mean flame front curvature $\langle\nabla\cdot\mathbf{n}\rangle_s$. The curvature is positive when the flame front is convex towards the fresh gases, which is, a priori, the case when the mean progress variable $\overline{c}$ is close to zero (see Fig. 25). On the other hand, curvatures are probably negative (flame convex towards the burnt gases) when $\overline{c}\approx 1$. Assuming that the mean curvature is of the order of the inverse of the wrinkling length scale L_y, we have:

$$\lim_{\overline{c}\to 0}\langle\nabla\cdot\mathbf{n}\rangle_s=\frac{1}{L_y}\quad\text{and}\quad\lim_{\overline{c}\to 1}\langle\nabla\cdot\mathbf{n}\rangle_s=-\frac{1}{L_y}$$

Then, a simple linear model may be proposed:

$$\langle\nabla\cdot\mathbf{n}\rangle_s\approx\frac{c^*-\overline{c}}{L_y}\tag{198}$$

Replacing L_y by its value as a function of the flame surface density Σ from BML modeling (Eq. 170) leads to the following model for the curvature term in the Σ-equation:

$$\langle w\nabla\cdot\mathbf{n}\rangle_s\Sigma\approx\beta\,S_L\,\frac{c^*-\overline{c}}{\overline{c}\,(1-\overline{c})}\Sigma^2\tag{199}$$

where β is a model constant. This term is positive in the fresh gases side of the turbulent flame brush and becomes negative in the burnt gases side. This trend is in agreement with the findings of direct numerical simulations [15] and experimental measurements [117, 118], as displayed in Fig. 26. The expression differs from classical closure where $\langle w\nabla\cdot\mathbf{n}\rangle_s$ is always negative (term D in Table 5).

A linear relaxation is retained to model the mean curvature $\langle\nabla\cdot\mathbf{n}\rangle_s$ (Eq. 198). This type of closure is common in turbulent reacting flows and possesses similarities with the relaxation model used for the scalar dissipation rate (§ 9.2) or for the pdf balance equation (§ 9.8.2). The links between these closures are further discussed in § 9.8.5.

The previous analysis was based on both a theoretical analysis of the exact Σ-balance equation and

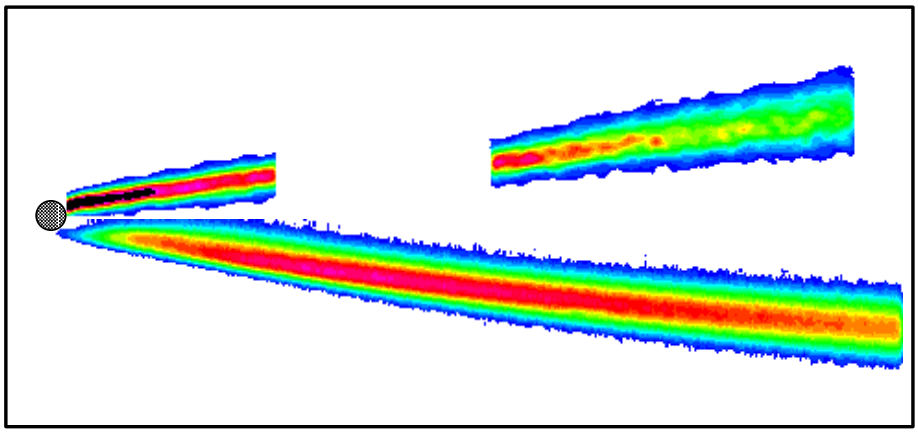

Figure 27: Flame surface density (half top) and mean reaction rate, estimated form CH radical emission (half bottom) fields are compared for $\phi = 0.90$. Flame surface density data, extracted from two different data sets, are not available from 30 mm to 70 mm downstream the rod. From [118].

experimental data [117, 118]. An improved version of the closed balance equation may be proposed:

$$\frac{\partial \Sigma}{\partial t} + \nabla.(\widetilde{\mathbf{u}}\Sigma) + \nabla.(\langle \mathbf{u}'' \rangle_s \Sigma) = \quad (\nabla.\widetilde{\mathbf{u}} - \langle \mathbf{nn} \rangle_s \,:\, \nabla \widetilde{\mathbf{u}})\,\Sigma + \Gamma_k \left(\frac{u'}{S_L}, \frac{l_t}{\delta_l} \right) \frac{\varepsilon}{k} \Sigma$$
$$+ \quad S_L \nabla^2 \overline{c} + \beta\, S_L\, (c^* - \overline{c})\, \frac{\Sigma^2}{\overline{c}\,(1-\overline{c})} \tag{200}$$

where Γ_k is the ITNFS efficiency function [126]. Orientation factors, $\langle n_i n_j \rangle_s$, may be described using a formulation previously discussed. The turbulent flux $\langle \mathbf{u}'' \rangle_s \Sigma$ is described using a classical gradient expression.

7.4.5 Flame stabilization modeling

In Fig. 27 are compared the flame surface density fields obtained from laser tomography and the mean reaction rate estimated from CH radical emission. According to Eq. (82), reaction rate and flame surface density are roughly proportional, excepted close to the stabilization rod, the flame surface density Σ is high whereas the mean reaction rate remains low. In this zone, fresh and burnt gases are separated by an interface (high surface densities) where combustion has started but is not yet fully established. This finding displays one of the difficulty of flame surface density models. In their present formulations, these models are unable to describe the flame stabilization because the Σ-equation (Eq. 179) is derived assuming that the flame does exist. All source terms in this equation are proportional to Σ or to Σ^2 and the equation cannot generate flame surface when there is no initial flame surface. In addition, an initiation effect must also be incorporated to account for ignition time delay in the local reaction rate per unit surface, Ω_i (Eq. 82), to recover the observed results.

7.4.6 A related approach: G-equation

As described in § 6.3.1, the premixed turbulent flame may be described using a level set approach. Most of the modeling issues discussed above are then recast in terms of G-equation and modeling for the

turbulent burning velocity S_T [88].

8 Turbulent transport in premixed combustion

8.1 Introduction

Turbulent fluxes of the progress variable c, $\overline{\rho}\,\widetilde{u_i''c''}$, are generally modeled using a gradient transport hypothesis as for inert scalars (§ 7):

$$\overline{\rho}\,\widetilde{u_i''c''} = -\frac{\mu_t}{Sc_t}\left(\frac{\partial \widetilde{c}}{\partial x_i}\right) \tag{201}$$

where μ_t is the turbulent viscosity given by the turbulence model and Sc_t is a turbulent Schmidt number. Theoretical [138] and experimental studies [17, 18] have evidenced in some turbulent premixed flames counter-gradient turbulent transport where the turbulent fluxes $\overline{\rho}\,\widetilde{u_i''c''}$ and the mean progress variable $\widetilde{c}$ gradient, $\partial\widetilde{c}/\partial x_i$, have the same sign in some regions and cannot be approximated with Eq. (201). This phenomenon is known as **counter-gradient turbulent transport** or **counter-gradient turbulent diffusion**.

This surprising finding was explained by the work of Bray, Moss and Libby discussed in section § 7.3. In their formulation, the turbulent fluxes of the progress variable c are directly connected to fresh ($\overline{u}_i^u$) and burnt gases ($\overline{u}_i^b$) conditional velocities (Eq. 164, § 7.3.5):

$$\overline{\rho}\widetilde{u_i''c''} = \overline{\rho}\,\widetilde{c}\,(1-\widetilde{c})(\overline{u}_i^b - \overline{u}_i^u) \tag{202}$$

Even though conditional velocities are not obvious quantities, this expression is useful to explain counter-gradient turbulent transport: Because of the thermal expansion due to combustion heat release, the burnt gases conditional velocity, $\overline{u}_i^b$, is likely to be greater than the fresh gases conditional velocity, $\overline{u}_i^u$. Then, in opposition with the modeled expression (Eq. 201), the turbulent fluxes of the progress variable c have the same sign than the mean gradient $(\partial\widetilde{c}/\partial x_i)$. Counter-gradient transport also increases when the heat release factor τ, defined by Eq. (136), increases [139].

The various versions of this BML model propose an algebraic closure for the mean reaction rate of the progress variable c, but focus the attention on the scalar turbulent transport (closure schemes for the turbulent fluxes $\overline{\rho}\widetilde{u_i''c''}$ balance equations), whereas other models may lead to more sophisticated reaction rate formulations, retaining a simple gradient closure (Eq. 201) for these fluxes.

The occurrence of counter-gradient turbulent transport have been analyzed using direct numerical simulation (DNS) [64]. The results demonstrate the power of DNS to help in the modeling of turbulent combustion. This section is devoted to these results, obtained from a direct solution, without any closure models, of the instantaneous balance equations.

8.2 Direct numerical simulation analysis of turbulent transport

8.2.1 Introduction

Gradient and counter-gradient turbulent scalar transport were observed in DNS of premixed flame / tridimensional turbulence interaction [140, 141]. Then, simulations of two-dimensional flame / turbulence interactions were reported [64]. The reduced costs of 2D simulations allow the investigation of a large range of flame and turbulence parameters. In these simulations, a planar and laminar premixed flame is firstly superimposed to an homogeneous and isotropic turbulent flow field (Fig. 28). The flame front is progressively wrinkled by turbulent motions, and the turbulence decays in time. After a time of the order of the eddy-turnover time of the largest turbulence structures, the flame may be assumed to be in equilibrium with the turbulent flow field and relevant modeling informations are extracted

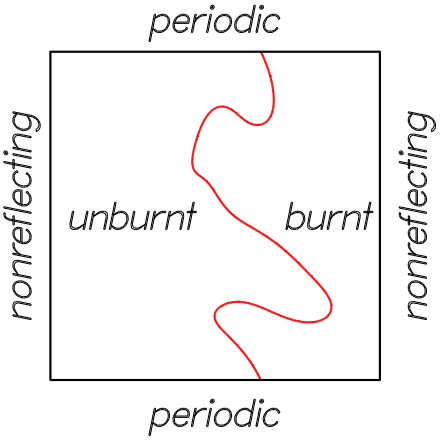

Figure 28: Numerical configuration. A plane laminar premixed flame is initially superimposed to an homogeneous and isotropic turbulence.

from DNS. As the numerical configuration is statistically one-dimensional in the propagating direction, quantities such as mean progress variable or mean turbulent fluxes may be extracted from averaging in the perpendicular direction.

8.2.2 Results

Turbulent fluxes $\overline{\rho u'' c''}$ extracted from the direct numerical simulations conducted by A. Trouvé [140] (denoted CTR) and C. Rutland [141] are displayed on Fig. 29. The first database clearly exhibits gradient turbulent transport, whereas the second one corresponds to a counter-gradient situation. The main discrepancy between the two databases lies in the initial turbulence level which is higher in the CTR simulation ($u'_0/S_L = 10$) than in the C. Rutland database ($u'_0/S_L = 1$).

Mean and conditional average velocities across the turbulent flame brush are displayed on Fig. 30 for the two DNS simulations. These results lead to the following comments:

- As expected, in the Rutland database, the burnt gases conditional velocity, $\overline{u}^b$, is higher than the fresh gases conditional velocity, $\overline{u}^u$, leading to a counter-gradient turbulent transport in agreement with expression (202).
- On the other hand, in the CTR database, the fresh gases conditional velocity is higher than the burnt gases conditional velocity. This result is first surprising: $\overline{u}^b$ is expected to be larger than $\overline{u}^u$ because of thermal expansion due to the heat release. However, this observation is in agreement with expression (202) and a gradient turbulent transport. Notice that Eq. (202) overestimates the turbulent flux $\widetilde{u''c''}$ (see Fig. 29) because, due to the flame thickness that must be resolved in the numerical simulation, the progress variable c is not fully bimodal ($c = 0$ or $c = 1$). In both cases, the Bray-Moss-Libby model remains able to predict the turbulent flux type (gradient or counter-gradient).

The two-dimensional simulations conducted in [64], referenced as CRCT in Fig. 31 have been used to analyze the occurrence of counter-gradient turbulent transport. The gradient turbulent transport is clearly enhanced by an increase of the turbulence level u'/S_L and decreasing values of the heat release factor τ. The "increase", in terms of velocity ratio u'/S_L, of the line delimiting gradient and counter-gradient turbulent transport when l_t/δ_l decreases is due to the reduced ability of small scale turbulence

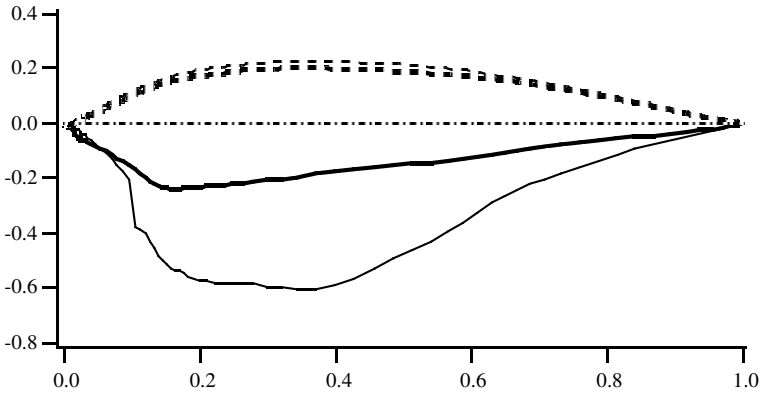

Figure 29: Turbulent flux $\overline{\rho u'' c''}$ displayed as a function of the mean progress variable $\widetilde{c}$ (bold lines) in the tri-dimensional direct numerical simulations from CTR (———) and Rutland (- - - -). Positive (respectively negative) values of $\overline{\rho u'' c''}$ denote a counter-gradient (respectively gradient) turbulent transport. The corresponding turbulent fluxes estimated using the BML expression (Eq. 202) are displayed for comparison using thin lines. Velocities are made dimensionless using the laminar flame speed S_L [64].

motions to wrinkle the flame front. This phenomenon has been already evidenced [63] and included in the ITNFS model [126]. Three and two dimensional direct numerical simulations lead to very similar results for this problem.

8.3 Physical analysis

A simple physical analysis is now reported to derive a criterion predicting the occurrence of counter-gradient turbulent diffusion [64].

Following Bidaux & Bray (1994) (unpublished work already presented in the BML model context § 7.4.4), turbulent fluxes of the progress variable c, $\widetilde{u_i'' c''}$, are directly connected to the surface-averaged fluctuating velocity, $\langle u_i'' \rangle_s$ (Eq. 184). Thus, a model for $\widetilde{u_i'' c''}$ may be deduced from a model for $\langle u_i'' \rangle_s$ involving the conditional fresh and burnt gases mean velocities:

$$\langle u_i'' \rangle_s = \langle u_i \rangle_s - \widetilde{u}_i = (c^* - \widetilde{c}) \left(\overline{u}_i^b - \overline{u}_i^u \right) \tag{203}$$

In the following, the flow field is assumed to be statistically one-dimensional and only the turbulent transport in the propagating direction, $\widetilde{u'' c''}$ will be described. Our analysis is based on the two limiting cases pictured in Fig. 32:

Low turbulence level The flame front remains smooth and the velocity jump between fresh and burnt gases, $\overline{u}_b - \overline{u}_u$, is determined primarily by thermal expansion and its value is close to the one obtained in a plane and laminar flame ($\overline{u}_b - \overline{u}_u \approx \tau s_L$). Eq. (203) becomes:

$$\langle u'' \rangle_s = (c^* - \widetilde{c})\ \tau\ S_L \tag{204}$$

High turbulence level Due to strong viscous dissipation of turbulent eddies in the hot burnt gas, the flame front motions are assumed to be dominated by the turbulence properties taken upstream of the flame.

- At the leading edge of the turbulent flame (near $\widetilde{c} = 0$), the flame front is convected towards the fresh gases with a mean velocity estimated by $-u'$ (see Fig. 32). Then:

$$\overline{u}^b - \overline{u}^u \approx -u' \tag{205}$$

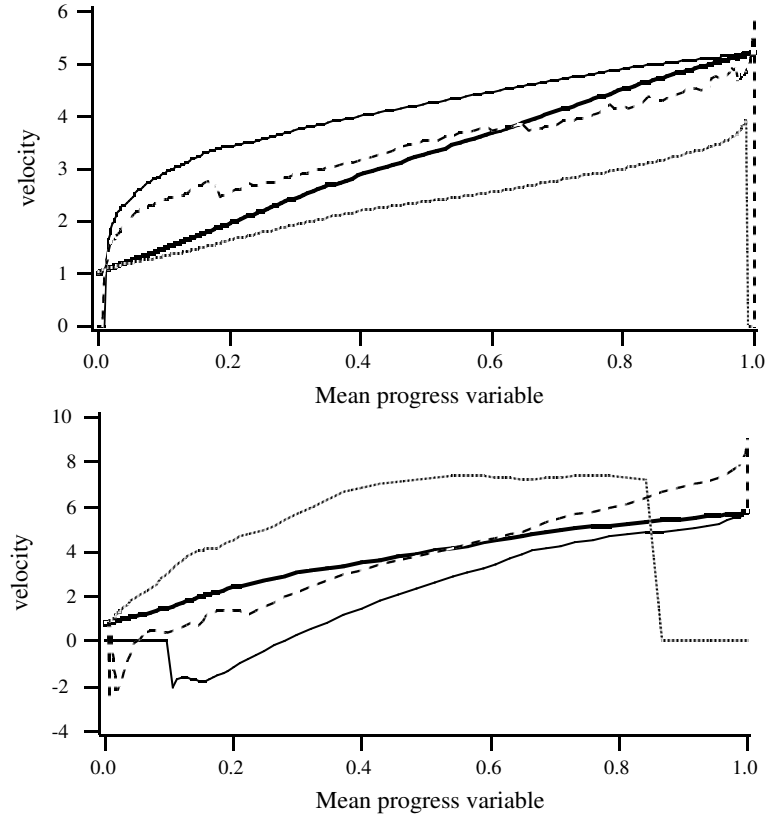

Figure 30: Conditional velocities across the turbulent flame brush displayed as a function of the mean progress variable $\widetilde{c}$ in the Rutland (top) and the CTR (bottom) databases. Favre averaged velocity, $\widetilde{u}$ (——), fresh gases conditional velocity, $\overline{u}^u$ (·····), burnt gases conditional velocity, $\overline{u}^b$ (——) and flame front conditional velocity, $\langle u \rangle_S$ (– – – –). Velocities are made dimensionless using the laminar flame speed S_L [64].

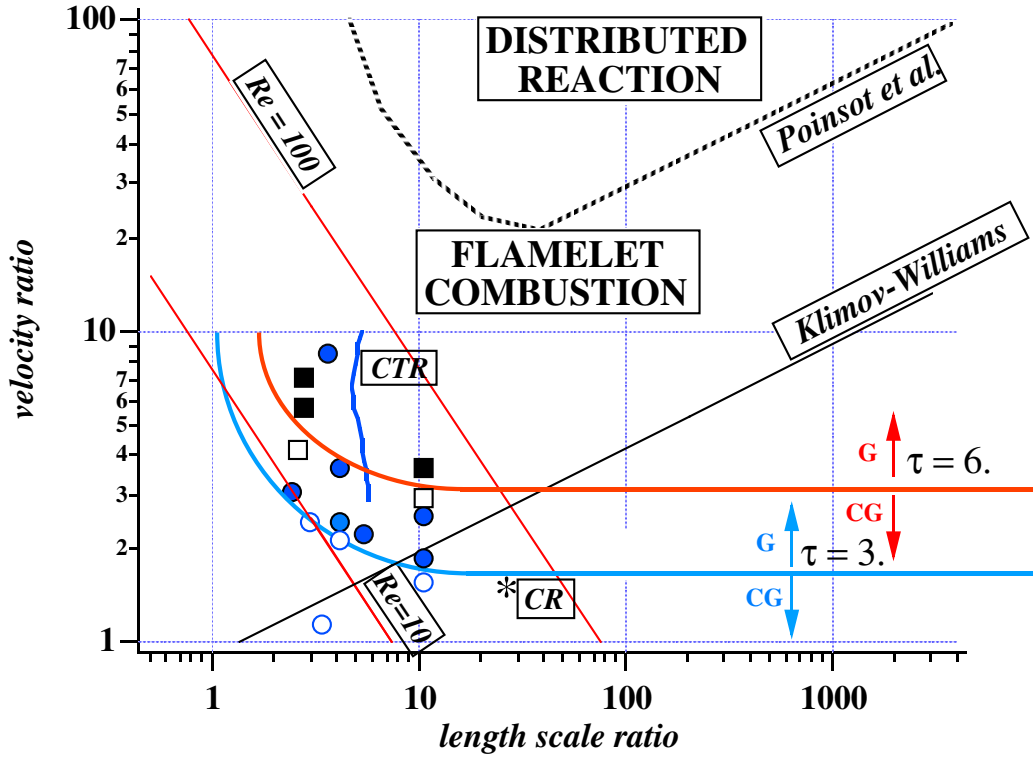

Figure 31: Premixed turbulent combustion diagram. The DNS flame-flow conditions are plotted as a function of the velocity ratio, u'/S_L, and length-scale ratio, l_t/δ_L. The Classical Klimov-Williams criterion and the criterion from [63] are given to show the domain of validity of flamelet combustion. Also plotted are the DNS conditions of the Rutland (CR, $\tau = 2.3$) and CTR ($\tau = 3$) simulations. As the turbulence is decaying in the CTR simulation, CTR conditions are displayed as an almost vertical line. The symbols $\circ$ ($\tau = 3$) and $\square$ ($\tau = 6$) correspond to the CRCT DNS. In 2D DNS, the turbulence decay is smaller and is not represented. Filled (open) symbols denote gradient (counter-gradient) turbulent diffusion. The transition criterion, $N_B \equiv \tau s_L/2\alpha u' = 1$ (Eq. 210), separating CGD (below) from GD (above) is plotted for $\tau = 3$ and $\tau = 6$ ([64]).

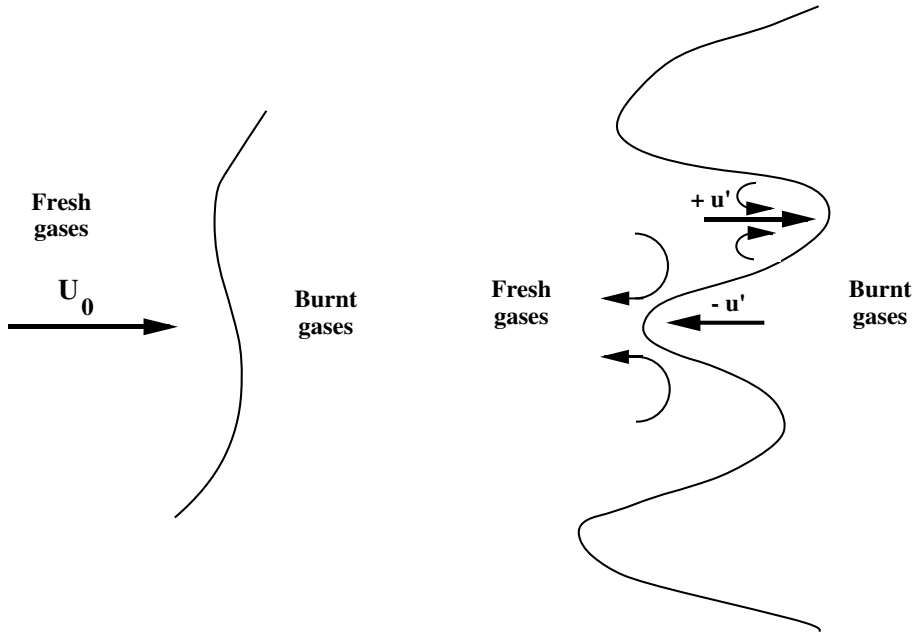

Figure 32: Two limiting cases: counter-gradient transport promoted by thermal expansion (left) ; gradient transport due to turbulent motions (right).

where u' denotes the rms velocity in the fresh gases.

- At the trailing edge of the flame brush ($\widetilde{c} \approx 1$), the flame front is convected by turbulent motions towards the burnt gases with a mean speed estimated by $+u'$ (see Fig. 32):

$$\overline{u}^b - \overline{u}^u \approx +u' \tag{206}$$

leading to the simple linear model:

$$\langle u'' \rangle_s = -2\ (c^* - \widetilde{c})\ \alpha\, u' \tag{207}$$

where α is an efficiency function, similar to the ITNFS model [126], accounting for the weak ability of small scale turbulent motions to wrinkle and convect the flame front. α is expected to be of order unity for large turbulent length scales and vanishes when turbulent eddies are too small to affect the flame front. The factor 2 has been introduced assuming $c^* \approx 0.5$.

Then, modeling $\langle u'' \rangle_s$ as a sum of these two contributions leads to:

$$\langle u'' \rangle_s = (c^* - \widetilde{c})\ (\tau\, S_L - 2\alpha u') \tag{208}$$

and the turbulent flux becomes:

$$\boxed{\widetilde{u''c''} = \widetilde{c}\ (1 - \widetilde{c})\ (\tau\, S_L - 2\alpha u')} \tag{209}$$

This simple model is well verified in direct numerical simulations [64]. The turbulent flux may be viewed as the sum of two contributions acting in opposite directions, one induced by turbulent motions and the other by thermal expansion. Then, the turbulent transport are analyzed as follow: for a sufficiently high turbulence level, the flame is unable to impose its own dynamics to the flow field and the

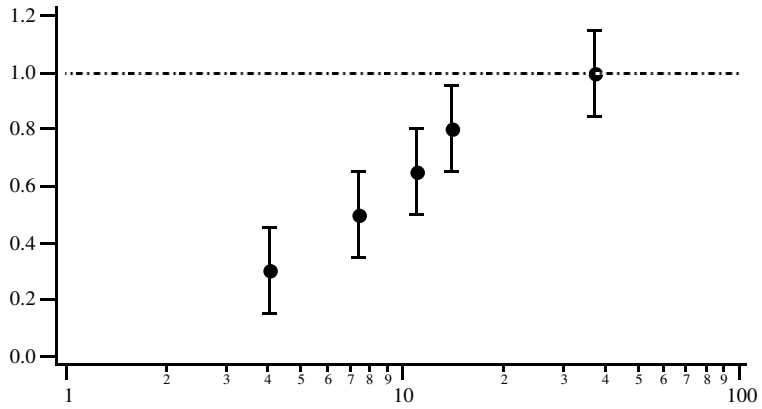

Figure 33: DNS estimated efficiency function α (Eq. 209) as a function of the length scale ratio l_t/δ_l comparing the integral turbulent length scale and the laminar flame thickness ([64]).

turbulent transport is of gradient type, as for any inert scalar. In counterpart, when the turbulence level remains low, the thermal expansion due to heat release dominates and the flame is able to impose its own dynamics leading to a counter-gradient turbulent transport. Counter-gradient turbulent diffusion occurs when $\widetilde{u''c''}$ is positive and expression (209) may be used to derive a criterion delineating gradient and counter-gradient regimes. The Bray number:

$$\boxed{N_B = \frac{\tau\, S_L}{2\,\alpha\, u'}} \tag{210}$$

is greater (respectively lower) than unity when a counter-gradient (respectively gradient) turbulent transport is expected. This criterion is well verified by direct numerical simulation results, as shown in Fig. 31. The efficiency function α has been estimated from DNS (Fig. 33). Recent experimental results [142] have confirmed these findings.

Comments:

- Following Fig. 31 and criterion (210), in practical applications turbulent transport may be counter-gradient, or close to the transition between gradient and counter-gradient regimes. In many cases, the heat release factor τ is about 5 to 7 leading to a transition between gradient and counter-gradient situations when u'/S_L is of the order of 3. Nevertheless, the possible occurrence of counter-gradient transport is generally neglected in modeling.

- The mean progress variable gradient may be estimated as:

$$\frac{\partial \widetilde{c}}{\partial x} \approx \frac{\widetilde{c}\,(1-\widetilde{c})}{\delta_b} \tag{211}$$

  where a length scale δ_b characterizing the flame brush is introduced. Then, the gradient type contribution in Eq. (209) corresponds to a Prandt-Kolmogorov turbulence modeling:

$$2\,\widetilde{c}\,(1-\widetilde{c})\delta_b\,\alpha\,u' \approx 2\,\alpha\,\delta_b\,\sqrt{k}\,\frac{\partial \widetilde{c}}{\partial x} \tag{212}$$

  where k is the turbulent kinetic energy and $u' = \sqrt{k}$.

- Recent works [143, 144] have reported regimes, corresponding to low turbulence levels, where combustion instabilities occur and wrinkle the flame front, acting in an opposite direction than counter-gradient diffusion reducing the flame front wrinkling. These instabilities should also be included in combustion models [145].
- Expression (209) has been derived to analyze the occurrence of counter-gradient transport, but is not suited for numerical simulations. For instance, such a simplified formulation is unable to predict a gradient transport in the vicinity of the leading edge ($\widetilde{c} \approx 0$) always observed, even in counter-gradient situations.

8.4 External pressure gradient effects

The previous analysis is completed by investigating the effects of externally imposed pressure gradients on turbulent premixed flames. Counter-gradient turbulent transport was first explained [17, 146] by differential buoyancy effects of pressure gradients on pockets of heavy and cold fresh gases and on pockets of light and hot burnt gases. In many combustion systems, flames are ducted and submitted to strong pressure gradients due to thermal expansion and leading to flow accelerations. In [18] it is experimentally shown that counter-gradient transports are enhanced in ducted flames. In [143, 147], the same type of DNS than [64] were conducted, introducing an externally imposed pressure gradient (in fact, due to technical reasons, a constant acceleration). The main conclusions, displayed in Fig. 34 and Fig. 35 are:

- A favorable pressure gradient, i.e. a pressure decrease from unburnt to burnt gases, is found to decrease the flame wrinkling (see Fig. 34), the flame brush thickness, and the turbulent flame speed S_T (Fig. 35). It also promotes counter-gradient turbulent transport.
- On the other hand, adverse pressure gradients tend to increase the flame brush thickness and turbulent flame speed (Fig. 35), and enhance classical gradient turbulent transport. As proposed in [148], the turbulent flame speed is modified by a buoyancy term linearly dependent on both the imposed pressure gradient and the integral length scale l_t.
- A corrected Bray criterion (Eq. 210) has been proposed to account for the pressure gradient effects. We do not give more details because this modified criterion needs to be validated and improved (length scale effects are not so clear and various analysis are possible, see [147]).

All these results suggest that counter-gradient turbulent transport should be expected in most ducted turbulent flames and some experimental observations are now reported.

8.5 Counter gradient transport - Experimental results

The V-shape turbulent flame was described in section § 7.4.1. The thermal expansion modifies the flame dynamics as it is clearly apparent on the high speed tomography films (scheme in Fig. 36, see also [118]): in the first part of the chamber (region 1), because of the rod wake, the coherent structures embedding the flame front turn clockwise (counterclockwise) in the upper (lower) flame sheet, as in classical Von Kármán vortex streets, except for their symmetry due to pressure waves. When the centerline velocity increases, because of thermal expansion in burnt gases (region 2), the upper (lower) coherent structures start to turn counterclockwise (clockwise). This phenomenon may be recast in terms of turbulent transport using a simple geometrical analysis based on the Bray - Moss - Libby relation (202) and summarized in Table 6. Accordingly, transverse turbulent flux $\widetilde{v''c''}$ is always of gradient type, but the change in structures rotation corresponds to a transition between gradient and counter-gradient transport for the downstream turbulent flux $\widetilde{u''c''}$. The turbulent fluxes are of gradient type just behind the

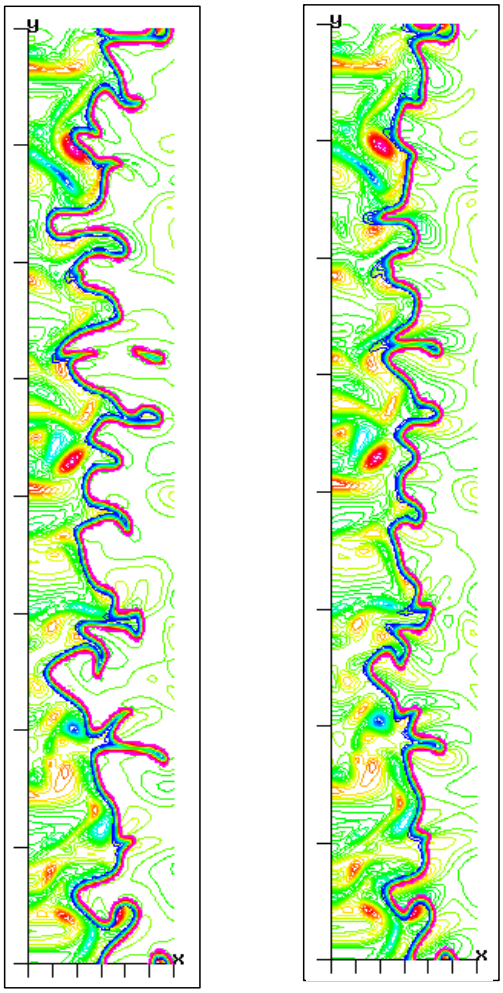

Figure 34: Superimposed instantaneous temperature and vorticity fields at the same time. (a) No imposed pressure gradient - gradient turbulent transport ; (b) Favorable imposed pressure gradient - counter-gradient turbulent transport. A planar laminar flame separating fresh gases (left) from burnt gases is initially superimposed to an homogeneous and isotropic turbulent flow field ($u'_0/S_L = 5.$). From [147].

Zone	$\overline{u}^b - \overline{u}^f$	$\frac{\partial \widetilde{c}}{\partial x}$	$\widetilde{u''c''}$	$\overline{v}^b - \overline{v}^f$ (when $y > 0$)	$\frac{\partial \widetilde{c}}{\partial y}$ (when $y > 0$)	$\widetilde{v''c''}$
1	< 0	> 0	G	> 0	< 0	G
2	> 0	> 0	CG	> 0	< 0	G

Table 6: Geometrical analysis of the scalar turbulent transport in a V-shape premixed flame (see Fig. 36). G and CG denote respectively a gradient and a counter-gradient turbulent diffusion.

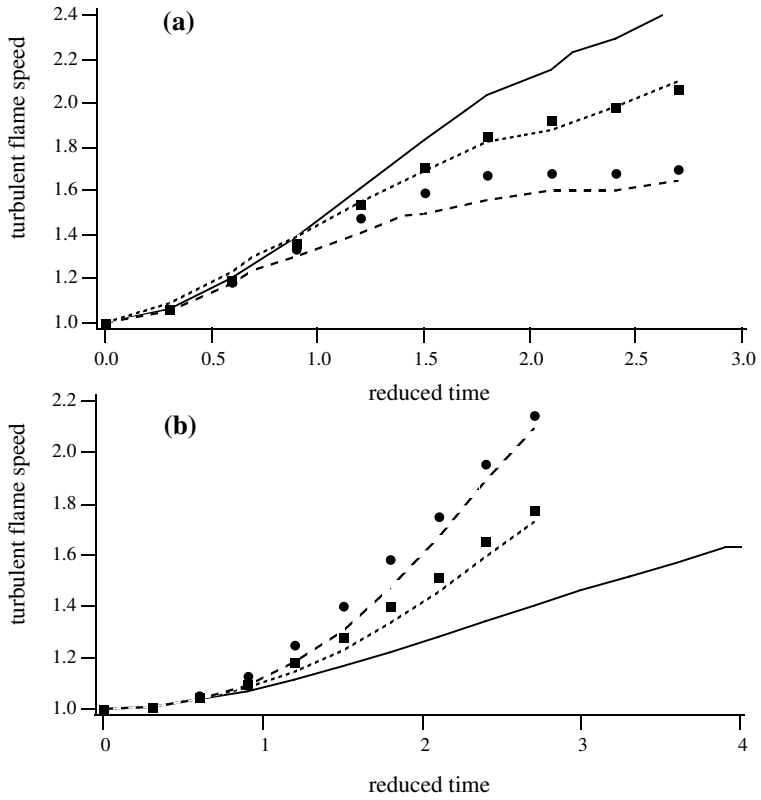

Figure 35: Reduced turbulent flame speed S_T/S_L plotted as a function of the reduced time $t/t_f = S_L t/\delta_L$, where $t_f = \delta_L/S_L$ is a flame time, for different values of the externally imposed pressure gradient. (a) initial turbulent level $u_0'/S_L = 5$; no pressure gradient (——) and increasing favorable pressure gradient (····· and – – – –); (b) initial turbulent level $u_0'/S_L = 2$; no pressure gradient (——) and increasing adverse pressure gradient (····· and – – – –). Markers correspond to the Libby theory [148]. From [147].

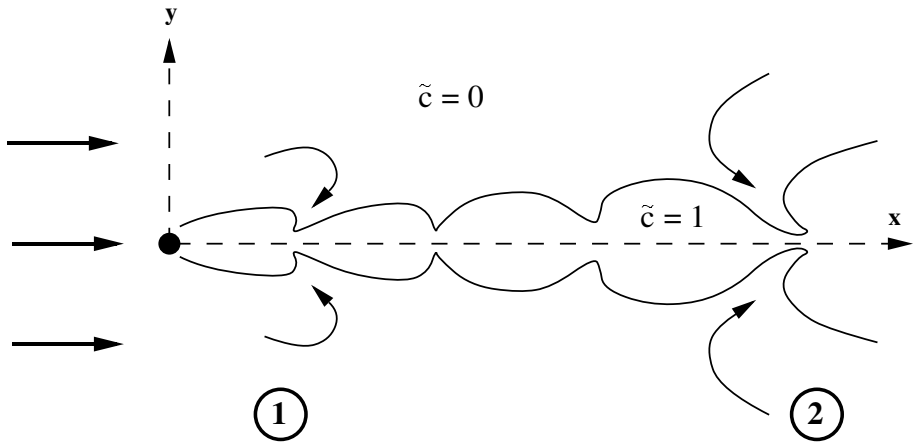

Figure 36: A rough scheme of the coherent structures dynamics observed using laser tomography [118].

rod, as expected to ensure the stabilization of the flame, and becomes of counter-gradient type further downstream.

8.6 To include counter-gradient turbulent transport in modeling

Excepted the works of Bray, Moss, Libby and their co-workers [17, 146, 127, 128, 131], very few works have been devoted to the effective modeling of counter gradient transport. The approach of Bray et al. is mainly based on second order modeling, using balance equations for the turbulent fluxes $\widetilde{u_i'' c''}$. These equations are easily derived from momentum and progress variable balance equations:

$$\begin{aligned}\underbrace{\frac{\partial \overline{\rho}\widetilde{u_i'' c''}}{\partial t}}_{(I)} + \underbrace{\frac{\partial \overline{\rho}\widetilde{u}_j \widetilde{u_i'' c''}}{\partial x_j}}_{(II)} = & - \underbrace{\frac{\partial \overline{\rho} u_j'' \widetilde{u_i'' c''}}{\partial x_j}}_{(III)} - \underbrace{\overline{\rho}\widetilde{u_i'' u_j''}\frac{\partial \widetilde{c}}{\partial x_j}}_{(IV)} - \underbrace{\overline{\rho}\widetilde{u_j'' c''}\frac{\partial \widetilde{u}_i}{\partial x_j}}_{(V)} - \underbrace{\overline{c''}\frac{\partial \overline{p}}{\partial x_i}}_{(VI)} - \underbrace{\overline{c''\frac{\partial p'}{\partial x_i}}}_{(VII)} \\ & - \underbrace{\overline{u_i''\frac{\partial \mathcal{J}_k}{\partial x_k}}}_{(VIII)} - \underbrace{\overline{u_i''\frac{\partial \tau_{ik}}{\partial x_k}}}_{(IX)} + \underbrace{\overline{\rho}\widetilde{u_i''\dot{\omega}}}_{(X)}\end{aligned} \tag{213}$$

where RHS terms correspond respectively to: $\overline{\rho}\widetilde{u_i'' c''}$ turbulent transport (III), $\widetilde{c}$-gradient effects (IV), mean velocity gradient effects (V), the action of mean (VI) and fluctuating (VII) pressure gradients, $\overline{\rho}\widetilde{u_i'' c''}$ turbulent dissipation ($VIII$ and IX) and reaction rate (X). This balance equation is, of course, unclosed and each term may be extracted from direct numerical simulations [64, 147, 131].

The discussion of the closure schemes for this equation is out of the scope of the present review and the reader may found relevant informations in [146, 127, 131]. Some comments may be made:

- The $\widetilde{u_i'' c''}$ turbulent transport (III) is generally modeled using a classical gradient expression (gradient turbulent transport at the third order).
- Mean progress variable gradient terms (IV) needs Reynolds stresses $\widetilde{u_i'' u_j''}$ modeling. Then, new balance equations are derived, and closed, for these quantities (second order turbulence model).

- The mean velocity gradient term (V) is closed because turbulent fluxes $\widetilde{u_j''c''}$ are provided by their balance equations.

- The mean pressure gradient term (VI) is easily known under a BML assumption (§ 7.3). Making use of Eq. (159) yields:

$$\overline{c''} = \overline{c} - \widetilde{c} = \tau \frac{\widetilde{c}\,(1-\widetilde{c})}{1+\tau\,\widetilde{c}} \tag{214}$$

- The fluctuating pressure term (VII) is more difficult to understand and to model. In [146] this term is neglected, however this assumption is not supported by DNS results [147]. The mean pressure term (VI) and the fluctuating pressure term (VII) probably need to be modeled together as $\overline{c''\partial p/\partial x_i}$. In [127] one carefully discusses the pressure gradient term closure. Recently, a model based on a partitioning of each pressure fluctuation covariance into contributions from reactants, products and thin flamelets was proposed [131]. The comparison of this new model with DNS results are encouraging and confirm the importance of the intermittency between the conditional mean pressure gradients in reactants and products.

- Turbulent dissipation terms ($VIII$ and IX) are generally expressed together using small scale dissipation rate assumptions [146].

Second order closures for turbulent fluxes and Reynolds stresses require 9 additive balance equations in 3D simulations (3 for progress variable fluxes, $\widetilde{u_i''c''}$, and 6 for Reynolds stresses, $\widetilde{u_i''u_j''}$). Because of very high computational costs, model closures and implementation difficulties, very few simulations have been conducted using the second order formulation. Recently [128], very promising results were obtained, particularly in predicting experimental results [18].

8.7 Towards a conditional turbulence modeling ?

The BML formulation (§ 7.3.5) directly distinguishes between the properties of fresh and burnt gases, this was achieved using conditional averaging (Eq. 162). This approach is very attractive because turbulence characteristics may differ in fresh and in burnt gases as shown on Fig. 37, where velocity histograms obtained using laser Doppler velocimetry in the V-shape turbulent flame (§ 7.4.1) are displayed. The velocity distribution is almost Gaussian in the unburnt and the burnt gases, but becomes clearly bimodal in the reaction zone denoting an intermittency between fresh and burnt gases, according to Eq. (166). This bimodal distribution does not correspond to the assumptions made in the derivation of most turbulence models, such as k-ε.

A conditional approach to determine the fresh ($\overline{Q}^u$) and burnt ($\overline{Q}^b$) gases conditional averages of a quantity Q is probably a promising way leading to a straightforward description of turbulent transport (Eq. 164 and 166). The objective is then to derive balance equations for quantities such as:

$$\overline{\rho c\, Q} = \overline{\rho}\widetilde{c}\,\overline{Q}^b \qquad ; \qquad \overline{\rho(1-c)\; Q} = \overline{\rho}\,(1-\widetilde{c})\;\overline{Q}^u$$

which is easy from c and Q balance equations [136]. These equations remain to be closed and few attempts have been conducted in this direction [149, 90, 143], but no clear conclusions may be found in literature.

All these works devoted to turbulent transport suggest that turbulence combustion modeling might probably be greatly improved by advancing the description of turbulent transport itself. This point motivates large eddy simulation (LES) for turbulent combustion modeling [150].

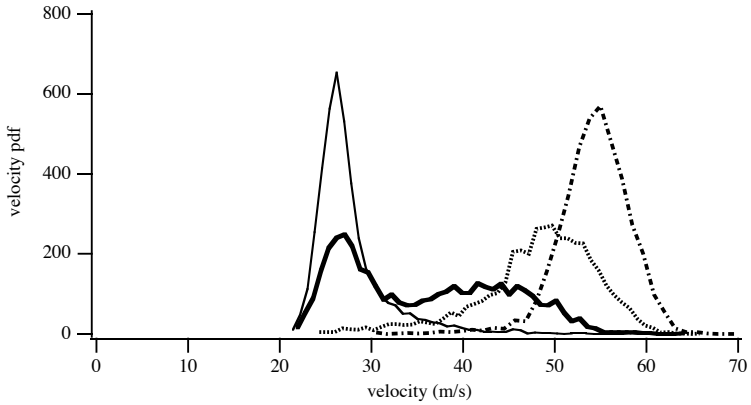

Figure 37: Axial velocity u histograms for four transverse locations 80 mm downstream the rod in the V-shape turbulent flame (Fig. 19): burnt gases (y = 0 mm, —·—) ; reaction zone (y = 5 mm, ····· and y = 12 mm, ———) ; unburnt gases (y = 18 mm, ———). From [118].

9 Reynolds averaged models for nonpremixed turbulent combustion

9.1 Introduction

Much works have been devoted to the numerical modeling of nonpremixed combustion systems, mainly assuming a chemistry much faster than mixing and molecular diffusion. This "mixed is burnt" regime is easily described from the turbulent mixing of conserved scalars (§ 3.2) and mixing problems were the subject of many discussions [151, 152, 153].

There exist strong motivations for improving nonpremixed and partially premixed turbulent combustion modeling:

- The development of new combustion technologies for aircraft engines, and more generally for gas turbines operating in the nonpremixed regime, implies the accurate determination of the position in the flow where combustion starts and the control of pollutants emission. Crucial points which cannot be addressed using infinitely fast chemistry hypothesis.
- Many practical systems include liquid injection of the fuel, followed by nonpremixed and partially premixed combustion.
- Even in burners operating in the premixed regime, the premixing of the reactants is not always complete at the molecular level and some partial premixing may be observed. Sometimes, partial premixing is even desirable to limit pollutant emissions (stratified charge engines).

As for premixed combustion (§ 7 and § 8), the modeling of turbulent diffusion flames relies on simplifying assumptions for both chemistry and transport. Depending on the simplifications made for these mechanisms, various approaches for laminar flames and models for turbulent flames are obtained (see Table 7). Hypothesis formulated to construct models for nonpremixed turbulent flames may be organized into three major groups:

- Assumption of infinitely fast chemistry (mixed is burnt).
- Finite rate chemistry assuming a local diffusive-reactive budget similar to the one observed in laminar flames (flamelet assumption).

Major assumptions	Flame structure in mixture fraction space	Turbulent combustion model
• Infinitely fast chemistry • Chemical equilibrium	Species are functions of Z: $Y_i = Y_i(Z^*)$ [33]	Presumed Pdf $\widetilde{P}(Z^*)$ from $\widetilde{Z}$ and $\widetilde{Z''^2}$ $\widetilde{Y}_i = \int_Z Y_i(Z^*)\widetilde{P}(Z^*)dZ^*$
• One-dimensional strained reaction zones • Diffusion balances chemistry as in a 1-D counter-flow flame • Single-step or complex chemistry • Constant ($Le_i = 1$) or complex transport properties ($Le_i \neq 1$)	Species are functions of Z and χ: $Y_i = Y_i(Z^*, \chi^*(t))$ Steady[61] or unsteady [154]	Flamelet modeling $\widetilde{Y}_i = \int_Z \int_\chi Y_i(Z^*, \chi^*)\widetilde{P}(Z^*, \chi^*)dZ^*d\chi^*$ [155]
	Total heat release is a function of χ: $\dot{\Omega}(\chi_{st}) = \int_{-\infty}^{+\infty} \dot{\omega}_T(\xi, \chi_{st})d\xi$ ξ coordinate across the flamelet [87]	Coherent flame model Solve for the density of flame surface Σ $\widetilde{\dot{\omega}}_T = \dot{\Omega}(\widetilde{\chi})\Sigma$ [83]
• Diffusion is captured via micromixing modeling • Simple transport properties $Le_i = 1$ • Single-step or complex chemistry • Chemical source is closed (only for pdf methods)	Solve for conditional moments: $\overline{Y}_i^C(Z^*) = \left(\overline{Y_i \mid Z = Z^*}\right)$	Conditional Moment Closure Presumed pdf $\widetilde{P}(Z^*)$ [101], [102] $\widetilde{Y}_i = \int_0^1 \overline{Y}_i^C(Z^*)\widetilde{P}(Z^*)dZ^*$
	Solve for representative PaSR: $dY_i/dZ = (\widetilde{Y}_i - Y_i + \tau_t\dot{\omega}_i^{PaSR})/(\widetilde{Z} - Z)$ to get $\dot{\omega}_i(Z, \tau_t)^{PaSR}$	Presumed pdf + PaSR modeling MIL/PEUL [67], [156] $\widetilde{\dot{\omega}}_i = \sum_k \int_Z \left(\dot{\omega}_i{}^{PaSR}(Z^*, \tau_t^*)\right)_k \widetilde{P}(Z^*, \tau_t^*)dZ^*d\tau_t$
	Solve for Monte-Carlo particles: $dY_i^k/dt = (\widetilde{Y}_i - Y_i^k)/\tau_t + \dot{\omega}_i^k$ to get $\widetilde{P}(Y_1^*, \cdots, Y_n^*)$	Pdf methods $\widetilde{Y}_i = \int_{Y_1} \cdots \int_{Y_n} Y_i^*\widetilde{P}(Y_1^*, \cdots, Y_n^*)dY_1^* \cdots dY_n^*$ [92]

Table 7: Modeling strategies for nonpremixed turbulent flames. Z is the mixture fraction, $\chi = D|\nabla Z|^2$ its scalar dissipation rate, $\widetilde{P}$ denotes pdfs, $\dot{\Omega}$ an integrated amount of heat release, Σ the density of flame surface and $\overline{Y}_i^C$ a conditional moment. PaSR stands for Partially Stirred Reactor, turbulent micromixing was expressed with a linear relaxation (IEM-LMSE) $D\nabla^2 Y_i \approx (\widetilde{Y}_i - Y_i)/\tau_t$ where $\tau_t \approx (k/\varepsilon)$ is an eddy break up mixing time, other formulation exist [95]. From [53].

- Finite rate chemistry with a separated treatment of molecular and heat transport from chemical reaction (CMC, pdf method; § 6). Diffusion is then addressed using turbulent micromixing modeling, while chemical sources can be dealt with in an exact and closed form (only for pdf).

The proposed closures are all based on a particular description of turbulent mixing, hence the basic concepts useful to capture fuel/air turbulent mixing are first presented.

9.2 Fuel/Air mixing modeling

9.2.1 Introduction

The mean value of the mixture fraction $\widetilde{Z}$ gives an indication of the local mean fuel/air mixing in turbulent flows. In addition, the structure and the properties of the flame depend on $\widetilde{Z''^2}$, measuring the degree of mixing between reactants. A simple description of turbulent mixing is thus obtained from the two fields: $\widetilde{Z}$ and $\widetilde{Z''^2}$. Introducing the classical gradient transport closure for the turbulent fluxes (§ 6), one may write:

$$\overline{\rho}\frac{\partial \widetilde{Z}}{\partial t} + \overline{\rho}\widetilde{\mathbf{u}}\cdot\nabla\widetilde{Z} = \overline{\rho}\nu_t\nabla^2\widetilde{Z} \tag{215}$$

$$\overline{\rho}\frac{\partial \widetilde{Z''^2}}{\partial t} + \overline{\rho}\widetilde{\mathbf{u}}\cdot\nabla\widetilde{Z''^2} = \overline{\rho}\nu_t\nabla^2\widetilde{Z''^2} + \underbrace{2\overline{\rho}\nu_t|\nabla\widetilde{Z}|^2}_{\text{Production}} - \underbrace{2\overline{\rho}\widetilde{\chi}}_{\text{Dissipation}} \tag{216}$$

The first term on the RHS is the turbulent transport, the second in (216) is the production of fluctuations by the mean gradients, the last is the scalar dissipation rate $\widetilde{\chi}$ remaining unclosed. $\overline{\rho}\widetilde{\chi} = \overline{\rho D|\nabla Z|^2}$ was discussed for premixed turbulent flames, in the EBU, BML and Σ models (§ 7).

9.2.2 Balance equation and simple relaxation model for $\widetilde{\chi}$

A transport equation may be derived for $\widetilde{\chi}$ from the Z balance equation (Eq. 41):

$$\begin{aligned}
&\frac{\partial\overline{\rho}\widetilde{\chi}}{\partial t} + \frac{\partial\overline{\rho}\widetilde{u}_j\widetilde{\chi}}{\partial x_j} + \frac{\partial}{\partial x_j}\left(\overline{\rho D u_j''\frac{\partial Z''}{\partial x_i}\frac{\partial Z''}{\partial x_i}}\right) = \\
&\underbrace{-2\frac{\partial}{\partial x_j}\left(\overline{\rho D u_j''\frac{\partial Z''}{\partial x_i}}\frac{\partial\widetilde{Z}}{\partial x_i}\right)}_{(I)} \underbrace{-2\frac{\partial\widetilde{Z}}{\partial x_i}\left(\overline{\rho D\frac{\partial Z''}{\partial x_j}\frac{\partial u_j''}{\partial x_i}}\right)}_{(II)} \underbrace{-2\frac{\partial\widetilde{Z}}{\partial x_j}\left(\overline{\rho D\frac{\partial Z''}{\partial x_i}\frac{\partial u_j''}{\partial x_i}}\right)}_{(III)} \\
&\underbrace{-2\frac{\partial\widetilde{u}_j}{\partial x_i}\left(\overline{\rho D\frac{\partial Z''}{\partial x_i}\frac{\partial Z''}{\partial x_j}}\right)}_{(IV)} \underbrace{-2\overline{\rho D\frac{\partial u_j''}{\partial x_i}\frac{\partial Z''}{\partial x_i}\frac{\partial Z''}{\partial x_j}}}_{(V)} \underbrace{-2\,\overline{D^2\rho\frac{\partial}{\partial x_j}\left(\frac{\partial Z''}{\partial x_i}\right)\frac{\partial}{\partial x_j}\left(\frac{\partial Z''}{\partial x_i}\right)}}_{(VI)} \\
&\underbrace{-\overline{\frac{2}{\rho}D\frac{\partial Z}{\partial x_i}\frac{\partial\rho}{\partial x_i}\frac{\partial}{\partial x_j}\left(\rho D\frac{\partial Z}{\partial x_j}\right)}}_{(VII)}
\end{aligned} \tag{217}$$

The term (I) on the RHS describes curvature effects of the mean mixture fraction field and, as (II) and (III), contains correlations between the Z field and the velocity field. Compared to other terms,

these correlations vanish for sufficiently large Reynolds numbers. (IV) corresponds to the correlations between mean flow motion and fluctuations. (V) is the strain rate of the scalar Z field, already discussed for flame surface density modeling in premixed flames (§ 7.4.4). (VI) is the dissipation rate of the scalar dissipation rate and (VII) is negligible when density gradients are kept small.

To derive a linear relaxation closure for the scalar dissipation rate, an homogeneous Z steady field in equilibrium (production = dissipation) is first considered. Then, Eq. (217) reduces to a balance between the straining rate of Z and the dissipation rate of the scalar dissipation rate:

$$-2\rho D\overline{\frac{\partial u_j^{''}}{\partial x_i}\frac{\partial Z''}{\partial x_i}\frac{\partial Z''}{\partial x_j}} = 2D^2\rho\overline{\frac{\partial}{\partial x_j}\left(\frac{\partial Z''}{\partial x_i}\right)\frac{\partial}{\partial x_j}\left(\frac{\partial Z''}{\partial x_i}\right)} \tag{218}$$

the fluctuating velocity gradient is assumed to be of the order of the inverse of the small scales characteristic time, i.e. $(\partial u_j^{''}/\partial x_i) \sim (1/\tau_k) \sim (\varepsilon/\nu)^{1/2}$. The remaining part of the strain rate term is proportional to $\widetilde{\chi}$, then:

$$-2\rho D\overline{\frac{\partial u_j^{''}}{\partial x_i}\frac{\partial Z''}{\partial x_i}\frac{\partial Z''}{\partial x_j}} \sim \frac{\overline{\rho}\widetilde{\chi}}{\tau_k} \sim R_\lambda\,\frac{\overline{\rho}\widetilde{\chi}}{(k/\varepsilon)}$$

where R_λ is a Reynolds number based on the Taylor micro-scale. A quadratic behavior in $\widetilde{\chi}$, with a direct dependence in $(\widetilde{Z''^2})^{-1}$ is anticipated for the dissipation rate of the scalar dissipation rate:

$$\overline{2\rho D^2\frac{\partial}{\partial x_j}\left(\frac{\partial Z''}{\partial x_i}\right)\frac{\partial}{\partial x_j}\left(\frac{\partial Z''}{\partial x_i}\right)} \sim R_\lambda\,\frac{\overline{\rho}\widetilde{\chi}^2}{\widetilde{Z''^2}}$$

The equilibrium condition (Eq. 218) leads to:

$$\boxed{\widetilde{\chi} = \frac{\widetilde{Z''^2}}{(k/\varepsilon)}} \tag{219}$$

recovering the widely used linear relaxation model.

Equation (219) is a very simplified description of micromixing. The scalar dissipation rate depends on the detail of the characteristics of the turbulence (velocity and scalar energetic spectrum), the linear relaxation is thus a first approximation that may be improved, for instance, by solving a modeled balanced equation for $\widetilde{\chi}$. Such a closed equation may be found in [157].

The knowledge of $\widetilde{Z}$ and $\widetilde{Z''^2}$ from their closed transport equation may be used to presume the pdf of Z, $\widetilde{P}(Z^*;\underline{x},t)$, with a beta-shape (see § 6.4.2). Because the internal structure of diffusion flames is easily obtained from conditional statistics as $(\overline{Y_i|Z=Z^*})$ (§ 3.2), many models (flamelet, CMC) incorporate a beta-pdf to calculate means quantities:

$$\widetilde{Y}_i(\underline{x},t) = \int_0^1 \underbrace{\left(\overline{Y_i|Z=Z^*}\right)}_{\text{Flame structure}} \overbrace{\widetilde{P}(Z^*;\underline{x},t)}^{\text{Mixing}}\,dZ^* \tag{220}$$

The simplest of these models invokes the infinitely fast chemistry assumption.

9.3 Models assuming infinitely fast chemistry

9.3.1 Eddy Dissipation Model

The eddy dissipation model (EDC) is a direct extension to nonpremixed flame of the Eddy Break Up (EBU) closure, initially devoted to turbulent premixed combustion [158] (§ 7.2). The fuel burning rate is

calculated according to:

$$\overline{\rho\dot{\omega}}_F = \alpha\,\overline{\rho}\,\frac{\varepsilon}{k}\min\left(\widetilde{Y}_F, \frac{\widetilde{Y}_O}{s}, \beta\frac{\widetilde{Y}_P}{(1+s)}\right) \tag{221}$$

where α and β are adjustable parameters of the closure. In Eq. (221), the reaction rate is limited by a deficient species. To account for the existence of burnt gases bringing the energy to ignite the fresh reactants, this species may be the reaction products (when β is non zero). A priori, this model does not respect the response of diffusion combustion in mixture fraction space and may generate mean fuel mass fraction values lower than $\widetilde{Y}_F^{IFCM}$. Actually, for large α, Eq. (221) is difficult to justify.

9.3.2 Presumed pdf: infinitely fast chemistry model (IFCM)

One of the first description of nonpremixed combustion was given in [33] who assumed an infinitely fast single step chemical reaction (§ 3.2). Considering the piecewise relations (Fig. 5, Table 1):

$$Y_F = Y_F^{IFCM}(Z) \quad ; \quad Y_O = Y_O^{IFCM}(Z) \quad ; \quad T = T^{IFCM}(Z) \tag{222}$$

relating the fuel and oxidizer mass fractions, and, the temperature to the mixture fraction in the case of infinitely fast chemistry, mean quantities may be directly obtained with a beta-pdf (§ 6.4.2) and Eq. (220):

$$\widetilde{Y}_F^{IFCM} = \int_0^1 Y_F^{IFCM}(Z^*)\widetilde{P}(Z^*;\underline{x},t)\,dZ^* \tag{223}$$

$$\widetilde{Y}_O^{IFCM} = \int_0^1 Y_O^{IFCM}(Z^*)\widetilde{P}(Z^*;\underline{x},t)\,dZ^* \tag{224}$$

$$\widetilde{T}^{IFCM} = \int_0^1 T^{IFCM}(Z^*)\widetilde{P}(Z^*;\underline{x},t)\,dZ^* \tag{225}$$

The mean flame structure is then known from an infinitely fast chemistry model (IFCM) without solving balance equations for mean thermochemical quantities. The inputs of this "mixed is burnt" closure are $\widetilde{Z}$ and $\widetilde{Z''^2}$ determining the beta-pdf chosen to capture the detail of fuel/air mixing. IFCM is therefore a two-equations model for nonpremixed turbulent combustion. It is very popular and is usually coupled with a low Mach number solution of the turbulent flow [159], so that the thermodynamics of the flow is fully known from Eq. (225). IFCM is an interesting first guess to provide the global flame structure for the maximum of heat that can be released, a valuable result for certain aspects of design. Notice that the piecewise relations are exact when the chemical time is infinitely small. Therefore, for very large Damköhler numbers (§ 3.2), IFCM is an accurate description of a turbulent diffusion flame. Unfortunately such a zero order model does not exist for premixed turbulent combustion. To handle multi-step chemistry, infinitely fast chemistry may be replaced by a chemical equilibrium condition [160].

This model lack of any prediction capacities when ignition, quenching or even small finite rate chemistry effects exist.

9.4 Flamelet modeling

9.4.1 Introduction

Experiments in jets flames and direct numerical simulations suggest that there exist situations in burners where the chemistry is fast, but not infinitely fast (see for example [161, 162]). In these measurements

and calculations, the response of the flame in mixture fraction space lies in the vicinity of the curves given by Y_i^{IFCM} (Fig. 38). Models have been proposed for such flames [155, 61]. For a given state of mixing in the turbulent flow, thus given values of Z and χ, flamelet models are derived assuming that the local balance between diffusion and reaction is similar to the one found in a prototype laminar flame for the same values of Z and χ. Flamelet models are therefore constructed from an asymptotic view of diffusive-reaction layers as given by Fig. 6. The two control parameters of planar and steady laminar strained flames are used: the mixture fraction Z and its scalar dissipation rate χ (§ 3.2). In a turbulent flow, these two quantities fluctuate in space and time, but when the joint pdf $\widetilde{P}(Z^*, \chi^*; \underline{x}, t)$ is known, the mean properties of the flame may be calculated as:

$$\widetilde{Y}_i = \int_{Z^*} \int_{\chi^*} Y_i^{SLFM}(Z^*, \chi^*) \widetilde{P}(Z^*, \chi^*; \underline{x}, t)\, d\chi^*\, dZ^* \tag{226}$$

$Y_i^{SLFM}(Z^*, \chi^*)$ is the local flame structure in mixture fraction space and $\widetilde{P}(Z^*, \chi^*; \underline{x}, t)$ captures the statistics of fuel/air mixing. SLFM stands for Steady Laminar Flamelet Model. This model may be viewed as a direct improvement of the infinitely fast chemistry model (IFCM), since it uses the same formalism, but with an additional parameter: the scalar dissipation rate χ, thereby including finite rate chemistry effects. For a given chemistry, and therefore a given chemical time τ_c, when the Damköhler number $Da^* = (\tau_c \chi_{st})^{-1}$ is large, IFCM is recovered. An increase of χ is followed by finite rate chemistry effects, or even quenching when χ becomes too large (Fig. 6), then, $Y_i^{SLFM}(Z^*, \chi^*)$ features mixing without reaction (Fig. 5).

The inputs of SLFM are similar to those of IFCM: $\widetilde{Z}$, $\widetilde{Z''^2}$ to which $\widetilde{\chi}$ is added. Two issues emerge:

1. $Y_i^{SLFM}(Z^*, \chi^*)$ must be determined and tabulated under particular hypothesis, choosing a given laminar flame prototype.
2. $\widetilde{P}(Z^*, \chi^*; \underline{x}, t)$ must be presumed using the mean values available to quantify fuel/air mixing (i.e. $\widetilde{Z}$, $\widetilde{Z''^2}$ and $\widetilde{\chi}$).

9.4.2 Flame structure in composition space, $Y_i^{SLFM}(Z^*, \chi^*)$

$Y_i^{SLFM}(Z^*, \chi^*)$ may be tabulated from solutions of counter-flow diffusion flames (Fig. 4; [61]), a flame configuration widely studied experimentally [163, 164]. Assuming within the turbulent flow thin quasi one-dimensional structures convected and stretched by the fluid motions, and neglecting higher order terms, the equations for the species and temperature become (§ 3.2):

$$\begin{aligned} \frac{\partial Y_i}{\partial t} &= \dot{\omega}_i + \left(\frac{\chi}{Le_i}\right)\left(\frac{\partial^2 Y_i}{\partial Z^2}\right) \\ \frac{\partial T}{\partial t} &= -\sum_{n=1}^{N} \frac{h_n \dot{\omega}_n}{C_p} + \chi \left(\frac{\partial^2 T}{\partial Z^2}\right) \end{aligned}$$

where $\chi = (\lambda/\rho C_p)|\nabla Z|^2$.

These equations were used to discuss laminar diffusion flames (see Eq. 47, Eq. 50 and § 3.2). Omitting the time derivative (steady flamelet), for a given value of χ corresponding to local micromixing condition, one has to solve for:

$$\dot{\omega}_i = -\frac{\chi}{Le_i}\frac{\partial^2 Y_i}{\partial Z^2} \tag{227}$$

The solution of this equation for given concentrations and temperatures boundary conditions, and various χ provides a *Flamelet Library* $Y_i(Z, \chi)$. A variety of techniques are available to build these libraries [165].

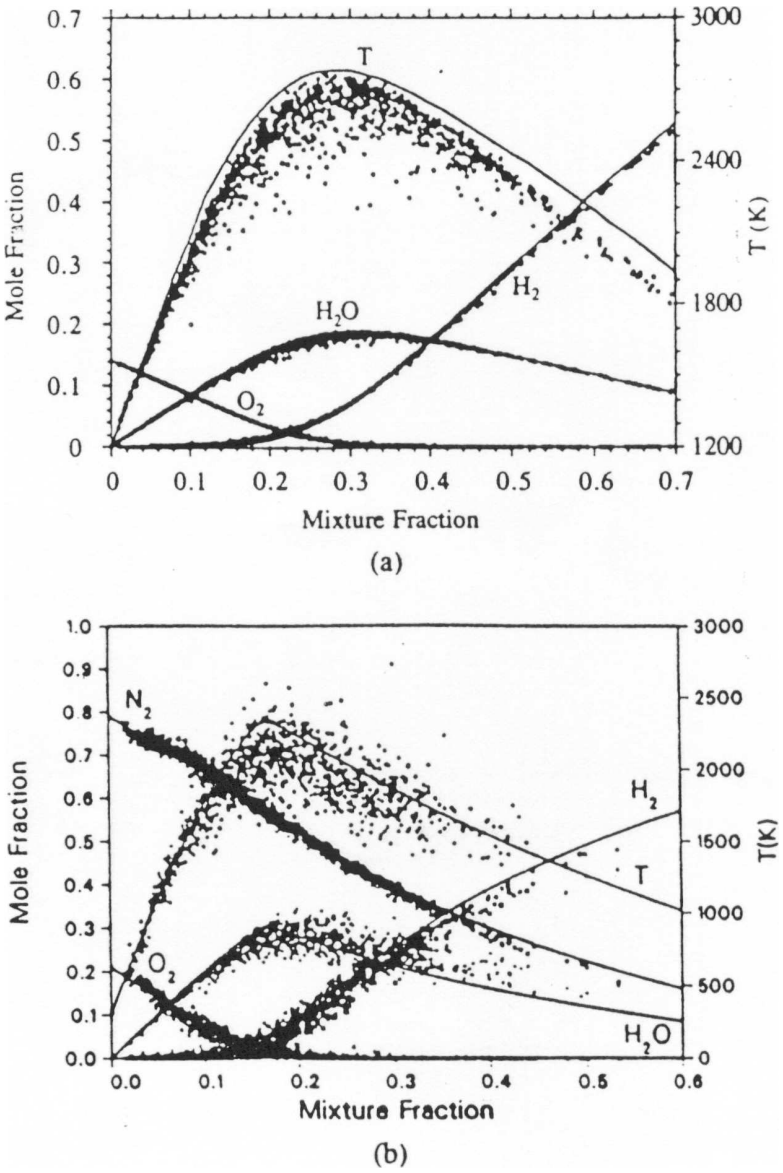

Figure 38: Scatter plots of major species mole fractions and temperature as functions of mixture fraction: (a) Data from three-dimensional direct numerical simulations of Montgomery et al (1993); (b) Raman scattering measurements of Barlow et al (1990) in H_2/Argon-air flame. *Solid lines* indicate chemical equilibrium.

In SLFM, the characteristic time required to balance diffusion and reaction is assumed to be much smaller than any other flow time scale of the problem. The hypotheses involved in SLFM can be disputed, leading to various improvements:

- Eq. (227) has been obtained neglecting diffusion in the direction tangential to the iso-Z_{st} surface, arguing that, when the mixing element is sufficiently thin and features weak curvature, the gradients measured along the stoichiometric surface are much smaller than those in the perpendicular direction (§ 3.2). Thus, when using Eq. (227) to describe a prototype flame of turbulent flamelets, one supposes that the mixing field may be reduced to a steady one-dimensional structure. In consequence the validity of Eq. (227) in a turbulent flow also depends on the properties of micromixing, and up to now, it is not obvious to draw conclusions since one would need to measure the scalar dissipation rate in turbulent flames. Some experimental results are available [166], but more works are required to conclude on the dimensionality of scalar micromixing in flames.

- There are other issues related to the multidimensional character of diffusion flames. Straining cannot be uniformly distributed along the flame sheet, leading to flamelet interactions when the distribution of χ is non-uniform on the iso-Z_{st}. This transverse loss or gain of heat modifies the structure of the flamelet in the normal direction to the stoichiometric surface [53].

- Reference states at infinity used to tabulate the flamelets may have to account for partial premixing [167, 168]. Consider the simple case of a jet flame, where close to the nozzle inlet, pure fuel and pure air react to form products. Moving downstream, turbulent diffusion mixes these products with air, on the air side, and with fuel, on the fuel side. Further downstream, the reactants feeding the reaction zone are not likely to be either pure fuel or pure air. This situation is strongly enhanced in flows where recirculation zones are found to stabilize combustion. In [168], this shortcoming of SLFM is overcome introducing *transient flamelets*, for which reference states at infinity vary according to the value of a progress variable $\widetilde{c}$.

- Flamelet libraries can be calculated in physical space or in mixture fraction space. It is usually observed that the decay of OH towards equilibrium is predicted by the flamelet solution in mixture fraction space using the scalar dissipation rate as a control parameter sensitive to species boundary conditions, trend that is not fully reproduced by the flamelet solution in physical space where the input parameter is the strain rate [168].

- Unsteadiness is also an important aspect. Time-dependent flamelets have been used to include unsteady effects [169, 170, 171]. As shown in [172], when a high value of the scalar dissipation rate is imposed to the flame for a sufficiently short period of time, extinction may not be completed, with a limiting frequency at which the flame almost behaves like a steady state flame. Unsteady flamelet were used [173] to simulate extinction and re-ignition in a turbulent jet flame, history effects were included using a Lagrangian time measured along the stoichiometric line. This work was pursued [154] introducing as an additional control parameter, the diffusion time needed to exchange mass and energy over a distance ΔZ in mixture fraction space.

  This is more generally related to questions arising concerning the determination of quenching limits along with the accuracy of quenching predictions using flamelets theory. Problem which can be addressed numerically, for instance by post-processing DNS databases to study the reactive / diffusive layer in terms of flamelets [174, 175, 176, 177, 69, 73]. Numerical simulations of flame/vortex interaction, used to construct a combustion diagram ([69], Fig. 11), show that when strong unsteadiness and/or curvature effects appear, the laminar flamelet assumption does not always predict quenching (Fig. 11). Two critical Damköhler numbers, Da_{LFA} and Da_{ext}, are easily derived from the simulations to find the limit conditions where unsteady (Da_{LFA}) and extinction (Da_{ext}) effects become important. These numbers are then compared with Da_q^*, the quenching Damköhler derived from asymptotic analysis [28]. It is found that $(Da_{LFA}/Da_q^*) \approx 2$ while

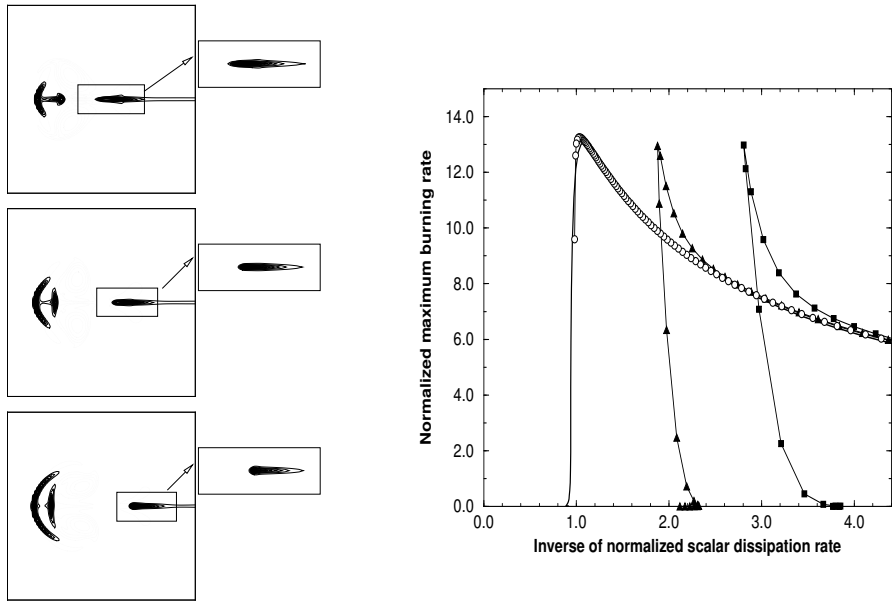

Figure 39: Three successive times of two-dimensional unsteady quenching of a planar diffusion flame pinched by a pair of vortices, configuration studied in [51]. Left, bold: iso-reaction rate, dotted: vorticity, zoom: region of the flow where the centerline response of the flame versus inverse mixture fraction dissipation rate is plotted. Right, Solid line: 1-D flamelet library, diamond: top left 2-D flame, square: middle left 2-D flame, triangle: bottom left 2-D flame.

$(Da_{ext}/Da_q^*) \approx 0.4$. Therefore, Eq. (227) is an interesting approximation for Da^* larger than Da_q^*, twice the asymptotic quenching value in these simulations. Below this value, even in the simple configuration of flame/vortex interaction, the time evolution of the reaction zone is fully dominated by unsteady effects.

- Another related point of interest in flamelet theory is the response of the turbulent flame when quenching zones develop. In other words, one may discuss the assumption that the occurrence of local extinction at some points does not prevent using flamelet response for the remaining part of the turbulent flame. Again using DNS, constant density flames near extinction were studied [178]. A critical Damköhler number at which extinction occurs is determined as a function of a flame thickness parameter, defined as the ratio between the rms mixture fraction and the reaction zone width in mixture fraction space. As expected for these flames featuring strong unsteadiness effects, the value of the critical extinction Damköhler number was different from the one predicted by laminar flame theory. This observation was explained by statistical variability. Consequently, an extinction may be observed with Damköhler numbers larger or smaller than Da_q^*. In this last study, the lower value of Da_{ext} differs from steady flamelets and exceeds the value Da_q^* given by flamelet theory. Other DNS results have shown that the scalar dissipation rate controlling the growth of the flame hole is lower than the one that should be applied to first quench the flame [36]. In Fig. 39, a DNS database is further analyzed [51] in which a diffusion flame is pinched by a pair of vortices. The value of χ when the flame extinguishes is in perfect agreement with χ_q measured in a laminar flamelet library (Fig. 39, top). But once a hole exists in the flame, the scalar dissipation rate $\chi_{q_{Ed}}$ at the quenching location is smaller than χ_q and varies depending on the structure of the edge flame. The fluxes of heat along the stoichiometric surface are responsible for this departure

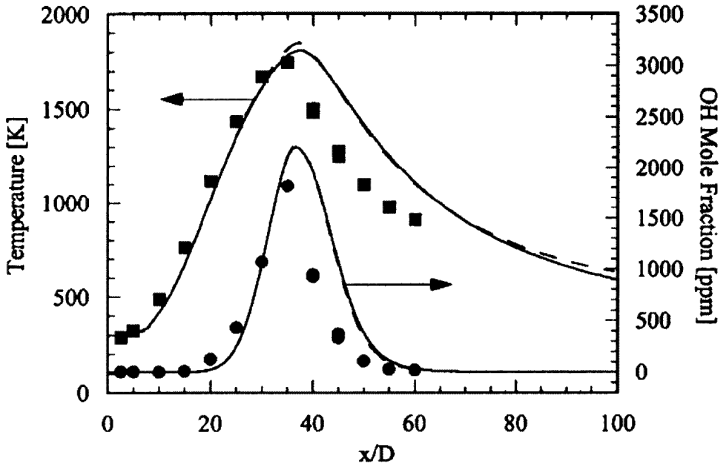

Figure 40: Top: Favre-averaged mean values of temperature and OH mole fraction along the centerline of a jet flame. Bottom: radial profiles of mean temperature and OH mole fraction. Comparison between experiments and flamelet modeling. From [154].

from one-dimensional flamelet behavior. When the diffusion flame and its extremity have reaction zones of the same thickness, for $\chi > \chi_q$ the response of the reaction rate follows the laminar flamelet one (Fig. 39, middle). Latter after quenching, $\chi_{q_{Ed}}$ decreases and a partially premixed front develops at the edge of the burning zone, then the reaction rate reaches values above the laminar flamelet behavior (Fig. 39, bottom). These values are representative of the existence of burning in a premixed regime at the extremity of the diffusion flame. Therefore, the quenching scalar dissipation rate χ_q is the relevant quantity to describe the quenching of a burning flamelet, but diffusion flame quenching leads to edge flame combustion (partially premixed flamelets).

Within the family of closures for nonpremixed turbulent flames, models based on Eq. (227) are a great progress compared to infinitely fast chemistry hypothesis. When the chemistry is fast enough with mixing elements featuring sheet like properties, they provide interesting results (Fig. 40) and further refinements of flamelets models are under development [179]. It is also worthwhile to note that with SLFM, the turbulent micromixing of chemical species does not need any particular treatment, since diffusion is directly included and coupled with chemistry in Eq. (227).

9.4.3 Mixing modeling in SLFM

In Steady Laminar Flamelet Models (SLFM), the fuel/air turbulent mixing is captured via the joint pdf $\widetilde{P}(Z^*, \chi^*; \underline{x}, t)$. Most of the flamelet models explicitly suppose that the mixture fraction and its dissipation rate are two uncorrelated quantities:

$$\widetilde{P}(Z^*, \chi^*; \underline{x}, t) \approx \widetilde{P}(Z^*; \underline{x}, t)\widetilde{P}(\chi^*; \underline{x}, t)$$

A beta function is assumed to presume $\widetilde{P}(Z^*; \underline{x}, t)$ (see § 6.4.2) and a log-normal distribution is used for $\widetilde{P}(\chi^*; \underline{x}, t)$ [61]:

$$\widetilde{P}(\chi^*; \underline{x}, t) = \frac{1}{\sqrt{2\pi}\chi^*\sigma(\underline{x}, t)} \exp\left(-\frac{1}{2\sigma^2(\underline{x}, t)}(\ln\chi^* - \gamma(\underline{x}, t))^2\right)$$

The two parameters σ and γ are provided by the first and second moments of the scalar dissipation rate:

$$\widetilde{\chi} = \exp(\gamma + \frac{\sigma^2}{2}) \quad \text{and} \quad \widetilde{\chi''^2} = \widetilde{\chi}^2(\exp(\sigma^2) - 1)$$

In [61] $\sigma^2 = 2$ is proposed.

Another alternative is to estimate a mean scalar dissipation rate under stoichiometric condition [88]. Starting from the solution of a steady strained planar counter-flow flame:

$$Z(\eta) = \frac{1}{2}\text{erfc}(\eta/\sqrt{2}) \quad \text{where} \quad \eta(\xi) = \sqrt{\frac{a}{D}}\int_0^\xi \frac{\rho(\xi^*)}{\rho_o} d\xi^*$$

a is the strain rate, ξ the coordinate normal to the stoichiometric plane and the assumption $\rho^2 D \approx cst = \rho_o^2 D_o$ was used. The corresponding scalar dissipation rate is given by:

$$\chi(Z) = \frac{a}{2\pi}\exp(-2[\text{erfc}^{-1}(2Z)]^2) = \chi_0 \frac{a}{2\pi}\exp(-2[\text{erfc}^{-1}(2Z)]^2) = \chi_0 F(Z) \tag{228}$$

erfc^{-1} denotes the reciprocal of the complementary error function and χ_0 is the maximum value of the scalar dissipation rate. Mean and conditional scalar dissipation rate are then related by:

$$\widetilde{\chi}_{st} = \widetilde{\chi}\mathcal{F}\left(\widetilde{Z}, \widetilde{Z''^2}\right) \tag{229}$$

where $\mathcal{F}$ is given by:

$$\mathcal{F}\left(\widetilde{Z}, \widetilde{Z''^2}\right) = \frac{F(Z_{st})}{\int_0^1 f(Z^*)\widetilde{P}(Z^*)\, dZ^*} \tag{230}$$

and to retain in the flamelet library the profiles $Y_i^{SLFM}(Z^*, \widetilde{\chi}_{st})$ for averaging with $\widetilde{P}(Z^*)$ (Eq. 226).

Here again, the stumbling block is the estimation of the mean scalar dissipation rate $\widetilde{\chi}$. The linear relaxation model may be written (Eq. 219):

$$\widetilde{\chi} = C_\chi \frac{\widetilde{Z''^2}}{(k/\varepsilon)}$$

where C_χ is a constant depending on the topological and spectral properties of the mixture fraction field. More recently, it was proposed to choose [31]:

$$\widetilde{\chi} = C_\chi \frac{(\Delta Z_F)^2}{(k/\varepsilon)}$$

$C_\chi \approx 2$, ΔZ_F is the thickness of the reaction zone of these laminar flame measured in mixture fraction space. The reaction zone is centered at the location $Z = Z_{st}$. As the stoichiometric surface is closed to the air side for hydrocarbon flame ($Z_{st} << 1$), one may write:

$$\Delta Z_F \sim 2Z_{st}$$

which provides an interesting approximation of this reaction thickness. This last expression was successful to model turbulent flame liftoff [180].

9.4.4 Conclusion

The laminar flamelet model presumes the conditional mean of species $\left(\overline{\rho Y_i | Z = Z^*}\right)$ averaging over the response of laminar prototype flames:

$$\left(\overline{\rho Y_i | Z = Z^*}\right) = \overline{\rho} \int_{\chi^*} Y_i^{SLFM}\left(Z^*, \chi^*\right) \widetilde{P}\left(\chi^*\right) \, d\chi^*$$

In our generic classification of turbulent combustion modeling (§ 6) and Eq. (220), SLFM may be viewed as a presumed pdf technique involving conditional mean values determined from laminar flame solutions. Another alternative is to build models where quantities are estimated introducing a direct treatment of micromixing and small scale diffusion (see § 9.6, § 9.7 and § 9.8).

9.5 Flame surface density modeling, Coherent Flame Model (CFM)

Flame surface density concepts were firstly introduced for the Coherent Flame Model (CFM) [83]. The balance equation for the flame surface density Σ was based on phenomenological considerations starting from balance equation for a material surface where combustion effects have been intuitively added [83, 181]. Recent works [182, 183, 87] have provided an exact balance equation, identifying the flame surface to the stoichiometric iso-surface $Z = Z_{st}$. The flame surface density is then defined as:

$$\Sigma = \overline{|\nabla Z| \, \delta\left(Z - Z_{st}\right)} = \left(\overline{|\nabla Z| \mid Z = Z_{st}}\right) \, \overline{P}(Z_{st}) \tag{231}$$

where $\overline{P}(Z_{st})$ denotes the probability of finding $Z = Z_{st}$. Starting from this definition and the balance equation for the mixture fraction Z (Eq. 41), an exact but unclosed, balance equation for the flame surface density Σ may be derived (§ 6.3.2).

In flame surface density models, under a flamelet assumption, it is assumed that the interface between fuel and oxidizer in nonpremixed burners behaves, for any values of Z, such as $\Sigma(Z^*) \approx \overline{|\nabla Z|} = \Sigma$ (§ 6.3.2). The mean burning rate $\overline{\dot{\omega}}_i$ is then expressed as the product of Σ by $\dot{\Omega}_i$ the local reaction rate per unit of flame area. Σ accounts for flame turbulence interaction and $\dot{\Omega}_i$ for the chemistry. According to Eq. (117)

$$\overline{\dot{\omega}}_i = \left\langle \frac{\dot{\omega}_i}{|\nabla Z|} \right\rangle_s \overline{|\nabla Z|} = \dot{\Omega}_i \Sigma \tag{232}$$

The local burning rate $\dot{\Omega}_i$ is estimated from a one-dimensional laminar flame as:

$$\dot{\Omega}_i = \left\langle \frac{\dot{\omega}_i}{|\nabla Z|} \right\rangle_s \approx \int_0^1 \frac{\dot{\omega}_i}{|\nabla Z|} \, dZ = \int_{-\infty}^{+\infty} \dot{\omega}_i \, d\xi \tag{233}$$

where ξ is the coordinate along the normal to the flame front.

In diffusion flamelets, where $\dot{\omega}_i$ depends on the mixture fraction Z and the scalar dissipation χ, expressions (93), (88) and the relation:

$$\left(\overline{\dot{\omega}_i | Z^*}\right) = \int_{\chi} \dot{\omega}_i\left(Z^*, \chi^*\right) \overline{P}_c(\chi^* \big| Z^*) \, d\chi^* \tag{234}$$

lead to:

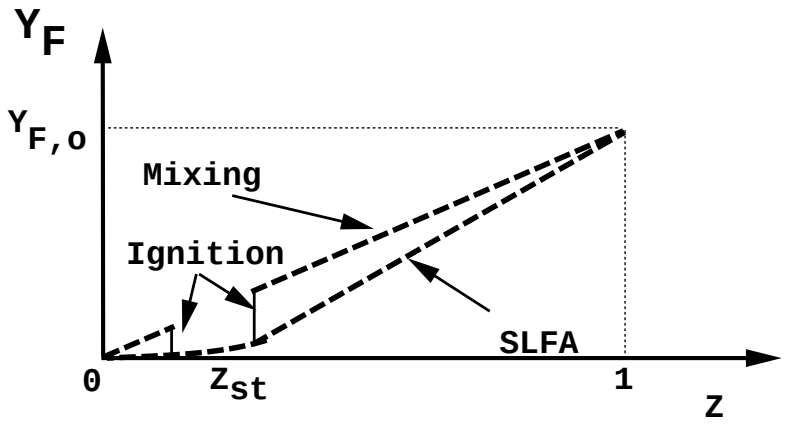

Figure 41: Sketch of MIL in mixture fraction space.

$$\dot{\Omega}_i = \frac{1}{\overline{|\nabla Z|}} \int_0^1 \int_\chi \dot{\omega}_i(Z^*, \chi^*) \overline{P}_c(\chi^*|Z^*) \overline{P}(Z^*)\, d\chi^*\, dZ^* \tag{235}$$

Then, using Eq. (233):

$$\dot{\Omega}_i \approx \int_{-\infty}^{+\infty} \int_\chi \dot{\omega}_i(\chi^*, \xi) \overline{P}_c(\chi^*|Z^*)\, d\chi^*\, d\xi \approx \int_\chi \underbrace{\left[\int_{-\infty}^{+\infty} \dot{\omega}_i(\chi^*, \xi)\, d\xi \right]}_{\dot{\Omega}_i(\chi^*)} \overline{P}(\chi^*)\, d\chi^* \tag{236}$$

The reaction rate per unit of flame area should, therefore, be estimated from the integrated reaction rate of a flamelet submitted to a scalar dissipation rate χ with the distribution $\overline{P}(\chi^*)$. In practice, $\dot{\Omega}_i$ is estimated as $\dot{\Omega}_i = \dot{\Omega}_i(\widetilde{\chi})$, where $\widetilde{\chi}$ is the averaged scalar dissipation rate. The Coherent Flame Model, then, corresponds to a simplified version of the Steady Laminar Flamelet Model.

The introduction of effects of unsteadiness was realized in [181], following the analysis proposed in [169] in the context of SLFM, a flame time response is then introduced when calculating $\dot{\Omega}_i$.

9.6 MIL model

MIL ("Modèle Intermittent Lagrangien" or Lagrangian Intermittent Model) was proposed by Borghi in [67]. As Steady Laminar Flamelet Model (SLFM) and Conditional Moment Closure (CMC), MIL incorporates the flame structure in Z space. Arguing that mixing occurs without reaction for large values of the scalar dissipation rate, corresponding to fast mixing, the flame structure is constructed dynamically from two possibilities of diffusion combustion: Mixing without reaction (before ignition) and infinitely fast chemistry (after ignition) (Fig. 41). The transition between mixing without combustion and a "mixed is burnt" regime is controlled by the position of an ignition time delay, τ_{ig}, within the distribution of fuel/air turbulent mixing times τ_t, with $\tau_k < \tau_t < +\infty$ where $\tau_k \simeq (\nu/\varepsilon)^{1/2}$ is the Kolmogorov time.

The ignition delay τ_{ig} is associated to a scalar dissipation rate χ_{ig} ($\tau_{ig} \approx \chi_{ig}^{-1}$). The main objective of MIL is to account for unsteadiness in the coupling between small scale diffusion and chemistry, by mean

of the spectral distribution of micromixing times. For a given value of $\tau_{ig} \approx {\chi_{ig}}^{-1}$, mixing times smaller than τ_{ig} ($\tau_t < \tau_{ig}$ or $\chi > \chi_{ig}$) prevent ignition and contribute to pure mixing. Whereas for $\chi < \chi_{ig}$, corresponding to $\tau_t > \tau_{ig}$, mixing is slower than chemistry and combustion develops.

The inputs of MIL are:

1. A table of ignition delay τ_{ig} depending on mixture fraction, fuel mass fraction and mean temperature, $\tau_{ig} = \tau_{ig}(\widetilde{T}, \widetilde{Y}_F, Z)$. This table look up is easily derived from Partially Stirred Reactors (PaSR) calculations, where $\widetilde{T}$ and $\widetilde{Y}_F$ are the mean conditions in the PaSR. Detailed chemistry can be used to construct such τ_{ig} [184].
2. The pdf of turbulent mixing times $\overline{P}(\tau_t; \underline{x}, t)$ (equivalent to the pdf of the inverse of χ).
3. The pdf of the mixture fraction $\widetilde{P}(Z^*; \underline{x}, t)$.
4. The mean concentration of fuel $\widetilde{Y}_F$.

The output is the mean burning rate $\widetilde{\dot{w}}_F$ to calculate new $\widetilde{Y}_F$ values, accounting for auto-ignition and transient in turbulent flames. Assuming that combustion occurs only when ignition is faster than turbulent fuel/air mixing, the probability to find ignition at a particular location is:

$$\alpha(Z; \underline{x}, t) = \int_{\tau_{ig}(Z;\underline{x},t)}^{+\infty} \overline{P}(\tau_t; \underline{x}, t) d\tau_t$$

where $\overline{P}(\tau_t; \underline{x}, t)$ is the pdf of the micromixing times having a mean value equal to the integral length scale time (k/ε). Since τ_{ig} depends on position in mixture fraction space and mean temperature, α is also a function of Z and of the local flow conditions through position and time. Once $\overline{P}(\tau_t; \underline{x}, t)$ and $\widetilde{P}(Z^*; \underline{x}, t)$ are known, the mean burning rate of fuel is estimated as:

$$\widetilde{\dot{\omega}}_F(\underline{x}, t) = \int_0^1 \int_{\tau_{ig}(Z^*;\underline{x},t)}^{+\infty} \dot{\omega}_F^{MIL}(Z^*, \tau_t^*) \widetilde{P}(Z^*; \underline{x}, t)\, \overline{P}(\tau_t^*; \underline{x}, t)\, d\tau_t^*\, dZ^* \tag{237}$$

A partially stirred reactor (PaSR), combining mixing and chemical effects, is introduced to calculate $\dot{\omega}_F^{MIL}(Z^*, \tau_t^*)$ [67], leading to:

$$\frac{dY_F^*}{dZ} = \frac{(\widetilde{Y}_F^* - Y_F) + \tau_t^*\, \dot{\omega}_F^{MIL}}{(\widetilde{Z} - Z^*)} \tag{238}$$

This technique is close to the one chosen in [185] for modeling NO_x production in turbulent jet flames. Eq. (238) describes a local flame element, where molecular diffusion, $D\nabla^2 Y_F$, is modeled as a linear relaxation term $(\widetilde{Y}_F - Y_F)/\tau_t$. Solving Eq. (238) with boundary conditions similar to the ones of flamelet libraries provides $\dot{\omega}_F^{MIL}(Z^*, \tau_t^*)$.

A generic shape for $\overline{P}(\tau_t; \underline{x}, t)$ was proposed [184, 156]:

$$\overline{P}(\tau_t; \underline{x}, t) = (q-1) \frac{\tau_t^{(q-1)}}{\tau_k^q} \exp\left(-\frac{(q-1)}{q} \left(\frac{\tau_t}{\tau_k} \right)^q \right)$$

$q(\underline{x}, t)$ is determined so that $\widetilde{Y}_F^{MIL}$ calculated along the MIL trajectory in mixture fraction space (Fig. 41), weighted by the beta pdf, reproduces the mean $\widetilde{Y}_F$.

Figure 42 displays an example of numerical simulation of a Lean Premixed Prevaporized (LPP) combustion chamber using MIL. The LPP system is divided into three parts: First, liquid fuel is injected and

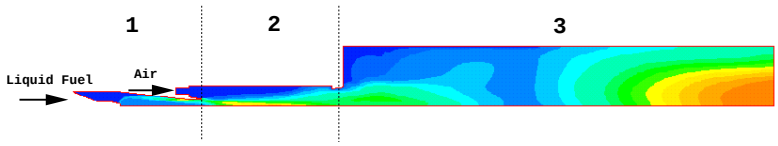

Figure 42: Snapshot of temperature in a TURBOMECA-ONERA LPP engine computed with MIL. From [156]. 1: Vaporized tube, 2: Premixed tube, 3: Flame tube. Combustion starts in the premixed tube.

vaporized (Prevaporized tube), then is mixed with air in the premixed tube before entering the main combustion chamber. Combustion is expected in a lean premixed regime to reduce pollutant emission. The premixed tube operates for a large range of inlet temperature (from 300 K to 800 K) and a large range of pressure (from 1 bar to 40 bar). For the highest temperature and pressure conditions, some undesirable effects, like auto-ignition or flash-back, may be observed in the premixed tube. These findings are reproduced with turbulent combustion closures like MIL describing strongly coupled micromixing and ignition phenomena [156].

9.7 Conditional Moment Closure (CMC)

Infinitely fast chemistry (IFCM), steady laminar flamelets (SLFM), and MIL suggest that nonpremixed turbulent flames may be conveniently studied using conditional averaging in the mixture fraction space. Instead of getting $Q_i = (\overline{\rho Y_i | Z = Z^*})/(\overline{\rho | Z = Z^*})$ from laminar flamelets, the CMC approach proposes to solve a balance equation for Q_i [101, 102, 104], which is written, neglecting two terms (Eq. 110):

$$\left(\overline{\rho \mid Z = Z^*}\right) \frac{\partial Q_i}{\partial t} = \underbrace{-\left(\overline{\rho u_i \mid Z = Z^*}\right) \frac{\partial Q_i}{\partial x_i}}_{(I)} + \underbrace{\left(\overline{\rho \chi \mid Z = Z^*}\right) \frac{\partial^2 Q_i}{\partial c^{*2}}}_{(II)} + \underbrace{\left(\overline{\dot{\omega}_i \mid Z = Z^*}\right)}_{(III)} \tag{239}$$

In addition to turbulent transport included in (I), micromixing (II) and the chemical source (III) are unclosed. In the simplest version of CMC, the fluctuations of chemical source in mixture fraction space are neglected leading to:

$$\left(\overline{\dot{\omega}_i \mid Z = Z^*}\right) = \dot{\omega}_i \left(\left(\overline{Y_1 \mid Z = Z^*}\right), \cdots, \left(\overline{Y_N \mid Z = Z^*}\right)\right) \tag{240}$$

As for any combustion models, the scalar dissipation rate is unknown (II). With CMC, the conditional average $\left(\overline{\rho \chi \mid Z = Z^*}\right)$ needs closure. This conditional mean is an important ingredient of the pdf transport equation and micromixing models are available (§ 9.8.1). Similarly, when the pdf is known via its presumed beta shape (§ 6.4.2), the conditional value of χ may be approximated from $\widetilde{P}(Z^*)$ to obtain $\left(\overline{\rho \chi \mid Z = Z^*}\right)$ [186].

CMC has been the subject of many works and refinements during the past years [104]. The following points have been addressed:

- The approximation of the conditional chemical source using Eq. (240) is much less restrictive than to write $\widetilde{\dot{\omega}}_i \approx \dot{\omega}_i(\widetilde{Y}_1, \cdots, \widetilde{Y}_N)$, but implies a weak level of fluctuations for a given value of Z. When calculating the chemical source, the conditional pdf $\overline{P}_c(Y_i | Z^*)$ is approximated by a peak located at $\left(\overline{Y_i | Z = Z^*}\right)$. Accordingly, this method is expected to provide interesting results for conditions not too far from infinitely fast chemistry.

- The estimation of $\left(\overline{\rho\chi \mid Z=Z^*}\right)$ from a beta-pdf is feasible for simple shapes of $\widetilde{P}(Z^*)$, but as shown from the pdf balance equation (Eq. 106), the detail of $\left(\overline{\rho\chi \mid Z=Z^*}\right)$ is linked to the detail of the shape of the pdf, that may not be correctly captured with a presumed pdf.
- Within an homogeneous field, the CMC equation reduces to:

$$\left(\overline{\rho \mid Z=Z^*}\right)\frac{\partial Q_i}{\partial t}=\left(\overline{\rho\chi \mid Z=Z^*}\right)\frac{\partial^2 Q_i}{\partial {Z^*}^2}+\left(\overline{\dot{\omega}_i \mid Z=Z^*}\right) \tag{241}$$

  This last formulation may be compared with the flamelet equation (Eq. 227) replacing Q_i by Y_i [106]. These two turbulent combustion models have similarities in term of their general formalism, but their underlying physical assumptions strongly differ. CMC incorporates diffusion as turbulent micromixing and decouples it from chemistry. On the other hand, the flamelet assumption deals with a coupled representation of diffusion and reaction as in a laminar flame for a given value of χ, and therefore, a given thickness of the laminar diffusive zone.

Once determined M the number of conditional values required to capture the conditional means of the N chemical species, CMC modeling requires the solution of $N \times M$ balance equations. CMC was also extended to reacting particles [187].

9.8 Pdf modeling

In premixed turbulent combustion modeling, BML and related closures assume a bimodal probability density function (pdf) of the progress variable. In nonpremixed flames, using infinitely fast chemistry (IFCM), steady laminar flamelet (SLFM), or conditional moment closure (CMC), the pdf of the mixture fraction was assigned a beta-shape. The objective of PDF modeling is to relax all hypothesis concerning the shape of pdfs. Once a methodology has been developed to calculate pdfs, it is possible to construct turbulent combustion closures in which all the values taken by species and temperature in mixture fraction space may be reached (Fig. 5 and 43). As in flamelet modeling and CMC, a detailed description of chemistry may be incorporated in the modeling. Differential diffusion is easily introduced in SLFM when tabulating counterflow flames, these preferential diffusion effects may be more difficult to introduce in CMC, in the context of pdfs, some works have been made in this direction [188, 189]. Two levels of complexity may be chosen:

- One may solve the balance equation for the joint pdf of the thermochemical variables, species, temperature..., (Eq. 107 in § 6):

$$\begin{aligned}
&\overline{\rho}\frac{\partial}{\partial t}\widetilde{P}(Z^*;\underline{x},t)= \\
&\quad - \quad \overline{\rho}\sum_{i=1}^{N}\frac{\partial}{\partial Y_i^*}\left[\left(\left(\overline{-\mathbf{u}\cdot\nabla Y_i \middle| \underline{Y}(\underline{x},t)=\underline{Y}^*}\right)+\dot{\omega}_i^*\right)\widetilde{P}(Z^*;\underline{x},t)\right] \\
&\quad - \quad \overline{\rho}\sum_{i=1}^{N}\sum_{j=1}^{N}\frac{\partial}{\partial Y_i^*}\frac{\partial}{\partial Y_j^*}\left[\left(\overline{D\frac{\partial Y_i}{\partial x_k}\frac{\partial Y_j}{\partial x_k}\middle| \underline{Y}(\underline{x},t)=\underline{Y}^*}\right)\widetilde{P}(Z^*;\underline{x},t)\right]
\end{aligned} \tag{242}$$

- Velocity field statistics may also be included into the pdf, then the balance equation for the joint pdf of velocity and species is resolved (Eq. 109). Recent developments have also included time scale information into the pdf [190, 191].

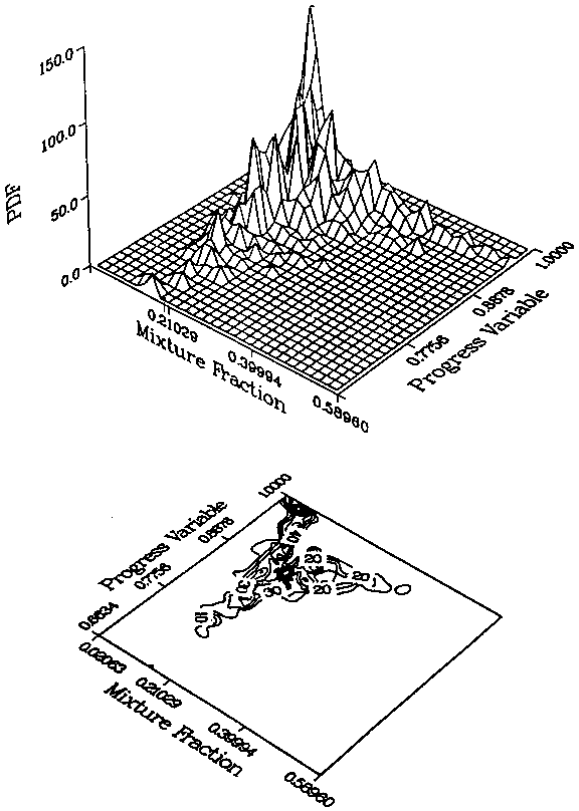

Figure 43: Two-dimensional pdf of mixture fraction and reaction progress variable for a round jet non-premixed flame. From [103].

There are two major issues with pdf modeling:

- Models must be proposed for capturing micromixing and viscous effects (the latter only when the velocity field is incorporated into the pdf).
- A new numerical treatment is required and leads to the decomposition of the pdf into a large number of computational particles required to succeed in the computational implementation of pdf methods [192, 92, 193]. The chemical composition and velocities of these particles evolve according to simple differential equations, resulting from a discrete Monte Carlo simulation of the continuous pdf equation.

The main advantage of pdf lies in the possibility of treating complex chemical sources directly (§ 6).

9.8.1 Turbulent micromixing

From the discussion of fundamentals properties of flames and of turbulent combustion models, the scalar dissipation rate appears as a key quantity in both premixed and nonpremixed turbulent systems. Using pdfs and CMC, one needs to express the conditional mean value of the scalar dissipation rate (or the conditional mean value of diffusion). This term represents turbulent micromixing [94, 95].

Using turbulence modeling, such as the $k-\varepsilon$ closure, a mean mechanical time $\tau_t \simeq (k/\varepsilon)$ and a micro-scale time $\tau_k \approx (\nu/\varepsilon)^{1/2}$ may be estimated. A global picture of mixing should therefore distinguish between macro and micromixing [194]:

- The **macromixing** is organized from a cascade mechanism between large and small scales. The study of this cascade in a fully developed turbulence shows that the mixing frequency f_Z is a function of the characteristic length l_Z [195]:

$$f_Z(l_Z) \sim \left(\frac{\varepsilon}{\nu}\right)^{1/2} \left(\frac{\eta_k}{l_Z}\right)^{2/3}$$

  The speed at which Z is mixed increases when the characteristic length l_Z decreases, suggesting that the cascade mechanism is limited by the mixing frequency $f_Z(l_Z)$ of the largest scales. When the Schmidt number of Z is greater than unity ($\nu > D_i$), the impact of the molecular dissipation is less than the effect of viscous dissipation, then the smallest scales of Z are smaller than the Kolmogorov scales. For those small scales ($l_Z < \eta_k$) the mixing frequency is of the order of a constant $f_Z(l_Z) = (\varepsilon/\nu)^{1/2}$. This cascade process from large to small scale does not change the energy in the system and therefore does not affect $\widetilde{Z''^2}$.

- The molecular diffusion acting at smaller scales makes the gradients smoother and then induces **micromixing**, phenomenon required to put the reactants in contact with the reaction zone. When $\nu = D$, this process starts at the Kolmogorov scale, when $\nu \neq D$, the Batchelor scale becomes the relevant limiting length:

$$\lambda_B \sim (\nu D^2/\varepsilon)^{1/4} = Sc^{-1/2}\eta_k$$

All these approximations are given for non-reactive flows, to exactly quantify the effect of combustion is an arduous task. This difficulty is also encountered in flamelet or flame surface modeling, but appears in a different form.

In pdf modeling, the micromixing closure must estimate the term $(\overline{D\nabla^2 Y_i \mid \underline{Y} = \underline{Y}^*})$ describing the molecular diffusion of each chemical species, or mimic its impact on the pdf. Various techniques have been proposed [94].

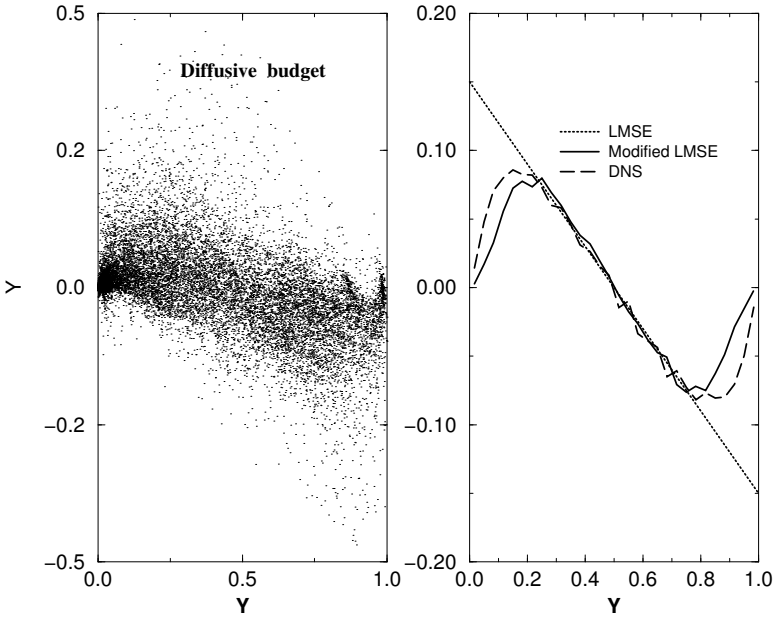

Figure 44: Left: Scatter plot of $D\nabla^2 Y$. Right: $\left(\overline{D\nabla^2 Y \mid Y(x,t) = Y^*}\right)$. These two terms were measured in DNS of an inert mixing layer. From [198].

9.8.2 Linear relaxation model, IEM/LMSE

In beta-pdf modeling (§ 9.2.2), the scalar dissipation rate of the mixture fraction was expressed as $\widetilde{\chi} = (\widetilde{Z''^2}/\tau_t)$. The extension of this linear relaxation to conditional diffusion provides the LMSE (Linear Mean Square Estimation) or IEM (Interaction by Exchange with the Mean) model. First proposed in the pdf context by Dopazo and O'Brien [196], IEM was also developed and used in chemical engineering applications by Villermaux [197]. Figure 44 shows the conditional mean of the diffusive budget of the mixture fraction Z measured in a DNS of a mixing layer. A quasi linear response is observed close to the mean, with a slope that can be approximated using the inverse of $\tau_t \simeq (k/\varepsilon)$. Since the gradient of Z must relax to zero for $Z = 0$ and $Z = 1$, this quasi linear response is combined with the conditions $(\overline{D\nabla^2 Z|Z=0}) = (\overline{D\nabla^2 Z|Z=1}) = 0$. For a "Gaussian type pdf" (no peaks at $Z = 0$ and $Z = 1$), the behavior at the edges of the sample space is not of premier importance to capture the major properties of micromixing, and a first approximation is given by:

$$\left(\overline{D\nabla^2 Z \mid \underline{Y} = \underline{Y}^*}\right) \approx \left(\frac{\overline{Z} - Z^*}{\tau_t}\right) \approx \left(\frac{\overline{Z} - Z^*}{k/\varepsilon}\right) \tag{243}$$

This simple model cannot capture the time evolution of the pdf in homogeneous mixing problems and has many shortcomings, for instance it relaxes the fluctuations without modifying the shape of the pdf [199, 93, 94, 95].

9.8.3 GIEM model

An improvement of the IEM model was recently discussed [200], a beta-pdf is used to reproduce the correct behavior of conditional diffusion. The mixture fraction is chosen as a shadow field to estimate

micromixing, this closure is also called a "Beta-Mapping-Closure". In an homogeneous field, the time evolution of the mixture fraction pdf is:

$$\frac{\partial \widetilde{P}(Z^*;\underline{x},t)}{\partial t} = -\frac{\partial}{\partial Z^*}\left[\left(\overline{D\nabla^2 Z \mid Z=Z^*}\right)\ \widetilde{P}(Z^*;\underline{x},t)\right]$$

since $\left(\overline{D\nabla^2 Z \mid Z=0}\right)=0$, one may write:

$$\left(\overline{D\nabla^2 Z \mid Z=Z^*}\right) = -\frac{1}{\widetilde{P}(Z^*;\underline{x},t)}\ \frac{\partial}{\partial t}\left(\int_0^{Z^*}\ \widetilde{P}(Z^+;\underline{x},t)\ dZ^+\right) \tag{244}$$

When $\widetilde{P}(Z^*;\underline{x},t)$ is given by a beta-function parameterized with $\widetilde{Z}$ and $\widetilde{Z''^2}$, this equation determines $\left(\overline{D\nabla^2 Z \mid Z=Z^*}\right)$.

The LMSE/IEM model leads to:

$$\left(\overline{D\nabla^2 Z \mid Z=Z^*}\right) \approx \frac{1}{\tau_t}\ \left(\widetilde{Z}-Z^*\right) \tag{245}$$

Making a direct analogy GIEM proposes:

$$\left(\overline{D\nabla^2 Z \mid Z=Z^*}\right) \approx C(Z^*,t)\ \left(B_Z(t)-Z^*\right) \tag{246}$$

Where $C(Z^*,t)$ is a pseudo-mixing frequency depending both on the position in mixture fraction space and time. It allows for reproducing the correct behavior at the edges $Z^*=0$ and $Z^*=1$ and its time dependence gives the correct behavior during the relaxation of the pdf. $B_Z(t)$ denotes the point where the diffusive flux is zero, relaxing the constraint $B_Z(t)=\widetilde{Z}$ of IEM, $C(Z^*,t)$ and $B_Z(t)$ are determined from Eq. (244) and Eq. (246).

The same treatment is applied to any reactive species Y_i, using the same pseudo-mixing frequency (assumption made in most micromixing models):

$$\left(\overline{D\nabla^2 Y_i \mid Y_i=Y_i^*,\ Z=Z^*}\right) = C(Z^*,t)\ \left(B_{Y_i}(t)-Y_i^*\right)$$

The parameter $B_{Y_i}(t)$ is then estimated from the fact that micromixing by itself should not change the mean:

$$\left(\overline{\frac{\partial Y_i}{\partial t}}\right) = \left(\overline{-D\nabla^2 Y_i}\right) \approx 0 \rightarrow B_{Y_i}(t) = \frac{\overline{C(Z,t)\ Y_i}}{\overline{C(Z,t)}}$$

This attractive model conserves the simplicity of linear relaxation modeling, but overcomes some of its drawbacks. As $\widetilde{Z''^2}$ is an input of the closure, the mean scalar dissipation rate $\widetilde{\chi}$ should be previously modeled. This approach has similarities with the estimation of the conditional values of χ in CMC using beta-pdf [186] and is not a full closure of micromixing per se.

9.8.4 Stochastic micromixing closures

Micromixing modeling may also be developed by choosing an ad-hoc stochastic process mimicking the relaxation of pdfs due to small scale diffusion. These closures are usually presented in the context of non-continuous interactions of volumes of fluid. When only diffusion is acting, the generic form of these models writes [93]:

$$\frac{\partial \widetilde{P}(Z^*;t)}{\partial t} = \frac{2\beta}{\tau_Z}\left(\int\int \widetilde{P}(Z^+,t)\widetilde{P}(Z^{++},t)\ T(Z^+,Z^{++}\rightarrow Z^*)\ dZ^+dZ^{++} - \widetilde{P}(Z^*)\right)$$

β is a parameter of the model and $T(Z^+, Z^{++} \rightarrow Z^*)$ is the probability that a volume of concentration Z^+ interacts with a volume at Z^{++} to evolve into Z^*. The difficult point lies in the choice of the transition probability T. Multiple choices are possible and have been made (see [94] for a review), the simplest one consists of writing:

$$T(Z^+, Z^{++} \rightarrow Z^*) = \delta\left(Z^* - \frac{Z^+ + Z^{++}}{2}\right) \tag{247}$$

meaning that the two volumes interact to generate a volume with $Z^* = (Z^+ + Z^{++})/2$. Eq. (247) was first proposed by Curl [201] to simulate the production of droplets of a given diameter by coalescence of two droplets of various sizes and re-dispersion of the two droplets.

These closures are clearly linked to a pure stochastic view of micromixing and are well suited to Monte Carlo simulations [92]. Their applications to flames can be disputed easily since mixing described via stochastic processes does not always account for the presence of reaction zones. However, much works have been done to improve these models which have then been quite successful in the calculations of jet flames [96]. Fig. 46 shows pdfs of the temperature calculated from Eq. (106) [204] using the coalescence-dispersion model [201] and the $k-\varepsilon$ closure for the velocity field [202]. For the same calculations, Fig. 45 illustrates the impact of micromixing modeling on temperature and CO concentrations predictions, the reduced chemical scheme of [203] has been utilized with the LMSE (IEM) and Curl's coalescence re-dispersion formulation.

Micro-mixing modeling is obviously one of the greatest challenges of turbulent combustion modeling, and strong efforts have been made in this direction. Many types of mixing models were proposed, a full review is out of the scope of this paper. Detailed discussion of mixing models in the context of pdfs may be found in the following list of references [201, 205, 206, 207, 208, 92, 209, 210, 211, 212, 213, 214, 215, 216, 217, 188, 96, 218, 219, 220, 221, 222, 223, 224, 94, 225, 103, 190, 226, 227, 95, 200, 202, 228, 198, 229, 230]. List which is far from being exhaustive.

9.8.5 Interlinks PDF / Flame surface modeling

The unclosed molecular diffusion term in the pdf balance equation (105) may be recast as:

$$\begin{aligned}
\overline{\left(\frac{1}{\rho}\left(\nabla\cdot(\rho D\nabla Z)\right) \mid Z=Z^*\right)} &= -\left(\overline{\frac{1}{\rho|\nabla Z|}\frac{\partial}{\partial n}\left(\rho D|\nabla Z|\right)|\nabla Z| \mid Z=Z^*}\right) \\
&- \left(\overline{D\nabla\cdot\mathbf{n}|\nabla Z| \mid Z=Z^*}\right) \\
&= -\left[\left\langle\frac{1}{\rho|\nabla Z|}\frac{\partial}{\partial n}\left(\rho D|\nabla Z|\right)\right\rangle_s + \langle D\nabla\cdot\mathbf{n}\rangle_s\right] \\
&\quad \left(\overline{|\nabla Z| \mid Z=Z^*}\right) \\
&= -\left[\langle w_n\rangle_s + \langle D\nabla\cdot\mathbf{n}\rangle_s\right]\left(\overline{|\nabla Z| \mid Z=Z^*}\right)
\end{aligned} \tag{248}$$

The molecular diffusion is decomposed into a normal contribution, that may be expressed in terms of a normal displacement speed w_n and a curvature term $D\nabla\cdot\mathbf{n}$, according to Eq. (38). The diffusion coefficient D is assumed constant and $\langle D\nabla\cdot\mathbf{n}\rangle_s = D\langle\nabla\cdot\mathbf{n}\rangle_s$. The flame surface averaged curvature may be modeled from geometrical considerations [118, 87] as in § 7.4.4 (Eq. 198):

$$\langle\nabla\cdot\mathbf{n}\rangle_s \approx -\frac{\overline{Z}-Z^+}{L_y} \tag{249}$$

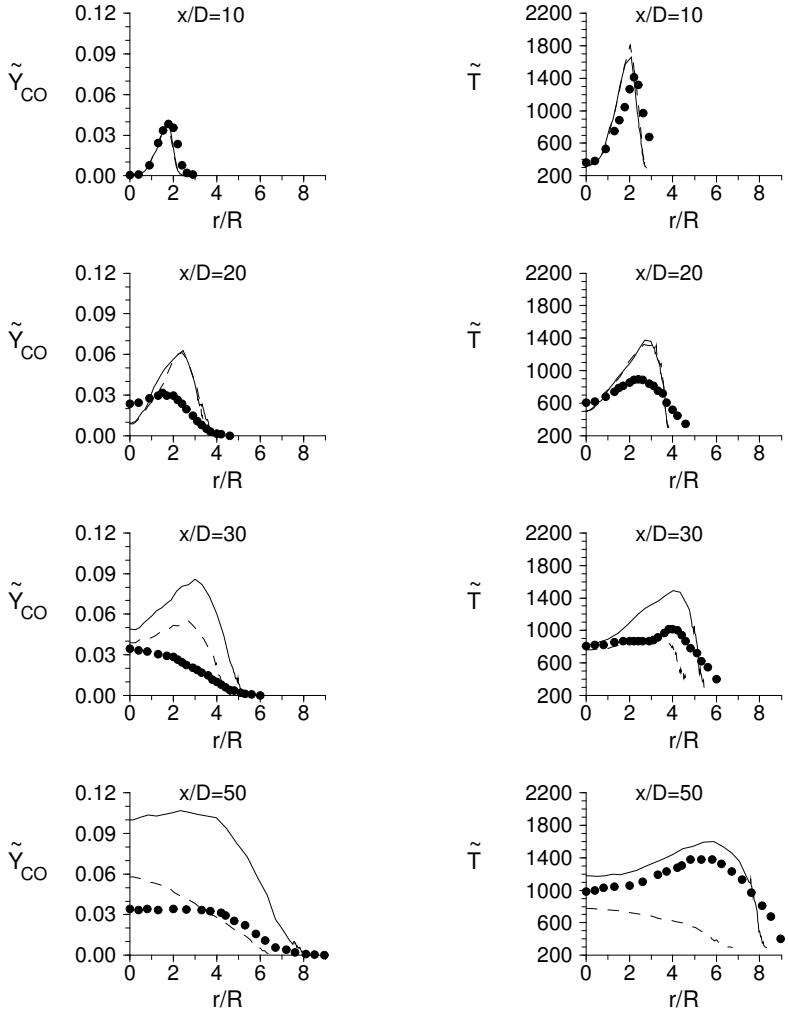

Figure 45: Radial profiles of CO mass fraction and temperature at different locations in Masri et al (1988) "B" jet flame, pdf calculations. From [202]. Two mixing models have been used: Filled circles: measurements; solid line: coalescence-dispersion micromixing Curl model [201]; dashed line: LMSE micromixing model (IEM). Reduced chemical scheme of Jones and Lindstedt [203].

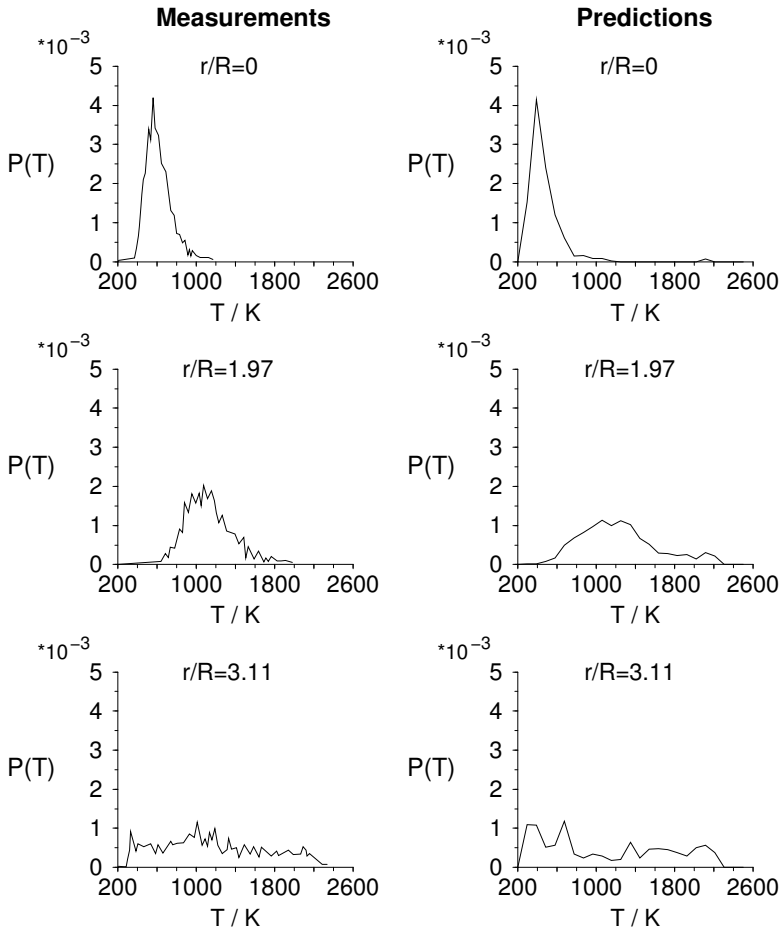

Figure 46: Comparison between measurements (left) and numerical predictions (right) of unweighted temperature Pdf at different locations in the Masri et al [204] "L" jet flame (location $x/D = 20$). Pdf calculations by Jones & Kakhi [202] using the Curl mixing model [201].

where L_y is a wrinkling length scale of the flame surface and Z^+ the $\overline{Z}$ level where mean curvatures are equal to zero. Mean curvatures are supposed positive (ie convex toward $\overline{Z}=0$ region) and negative for $\overline{Z}=1$. Comparing Eqs. (248) and (249) shows that the geometrical assumption used to model the mean curvature corresponds to an LMSE-IEM model of the molecular diffusion (§ 9.8.2).

$$\left(\overline{\frac{1}{\rho}\left(\nabla\cdot(\rho D\nabla Z)\right)\mid Z=Z^*}\right)=\frac{\overline{Z}-Z^*}{\tau_t} \tag{250}$$

It was shown in (§ 9.8.2) that for non reacting scalar, the IEM model provides an interesting estimation of the micromixing term around $\overline{Z}=Z^*$ when the turbulent mixing time is correctly calculated [198], but becomes deficient when Z^* tends towards 0 or 1, where $|\nabla Z|$ is expected to relax to zero. This shortcoming is attenuated in the flame surface density context where the surface averaged curvature $\langle\nabla\cdot\mathbf{n}\rangle_s$ is multiplied by the flame surface density (Eq. 87), ensuring zero values at either side of the flame brush. The turbulent mixing time τ_t and the flame wrinkling length scale, L_y, are then related as: $L_y\approx D(\overline{|\nabla Z|\mid Z=Z^*})\tau_t$, where $(\overline{|\nabla Z|\mid Z=Z^*})$ characterizes laminar flame elements.

Expressing the mixing time from linear relaxation hypothesis, $\tau_t\approx\widetilde{Z''^2}/\widetilde{\chi}$ and using Eq. (112) under a flamelet assumption yields $L_y\approx\widetilde{Z''^2}/\overline{|\nabla Z|}$. Wrinkling length scales depend on scalar fluctuations given by Eq. (216), evidencing, once again, the need for modeling scalar dissipation rates.

9.8.6 Joint velocity/concentrations pdf modeling

When the joint pdf of velocity and species enters the problem, one needs to model additional viscous and pressure terms related to velocity fluctuations (see Eq. 109). In turbulent non reactive flows, experiments have shown that the velocity fluctuations have pdfs that may be approximated with Gaussian functions. Closures for the velocity pdf may then be obtained using a Langevin type model, a simple stochastic model reproducing this velocity distribution, as done in [231].

Basic properties of stochastic methods [232] show that an equation with a diffusive term for a pdf $\overline{P}$:

$$\frac{\partial\overline{P}(Z^*)}{\partial t}=-\frac{\partial}{\partial Z^*}\left(A(Z^*,t)\overline{P}(Z^*)\right)+\frac{1}{2}\frac{\partial^2}{\partial^2 Z^*}\left(B(Z^*,t)\overline{P}(Z^*)\right)$$

is well reproduced by a stochastic process, $Z(t)$, similar to the Langevin process:

$$dZ(t)=A(Z(t),t)\,dt+\sqrt{B(Z(t),t)}\,dW(t)$$

where $dW(t)$ is a white noise (Wiener process). Using this equivalence, the Langevin model [231] for the pressure and viscous unclosed terms of Eq. (109) may be written:

$$\left[\left(\overline{\frac{1}{\rho}\frac{\partial p'}{\partial x_i}\mid\mathbf{u}=\mathbf{u}^*,Z=Z^*}\right)-\left(\overline{\nu\nabla^2u_i'\mid\mathbf{u}=\mathbf{u}^*,Z=Z^*}\right)\right]\overline{P}(\mathbf{u}^*,Z^*;\underline{x},t)=$$
$$G_{ij}(u_j^*-\overline{u}_j)\overline{P}(\mathbf{u}^*,Z^*;\underline{x},t)+C_o\varepsilon\frac{\partial}{\partial u_i^*}\left[\overline{P}(\mathbf{u}^*,Z^*;\underline{x},t)\right] \tag{251}$$

The physical properties of this closure are included in the tensor G_{ij}. The simplest model consider a linear relaxation for the velocity field, then $G_{ij}=(1/2+3C_o/4)(\varepsilon/k)\delta_{ij}$, where C_o is a constant. More sophisticated methods have been proposed [233], where a parallel is drawn between Reynolds Stress Closures (modeled equations for $\overline{u_i'u_j'}$) and the tensor G_{ij} [234].

As already indicated, numerical solution for pdf implies the development of accurate Monte Carlo solutions [92]. The pdf field is decomposed into a set of stochastic particles of which evolution simulate the turbulent flame. When a Lagrangian context is adopted [235], each particle n is characterized by

its position $\mathbf{x}_n^*(t)$, its velocity $\mathbf{u}_n^*(t)$ and concentration(s) $Y_n^*(t)$. The Langevin model given in Eq. (251) corresponds to the system for the discrete particles:

$$\begin{cases} \dfrac{dx_{in}}{dt} & = u_{in} \\ \dfrac{du_{in}}{dt} & = -\dfrac{1}{\overline{\rho}}\left(\dfrac{\partial \overline{p}}{\partial x_i}\right) + \nu\left(\dfrac{\partial^2 \overline{u}_i}{\partial x_j \partial x_j}\right) + G_{ij}(u_{j_n} - \overline{u}_j) + (C_o\varepsilon)^{1/2}\left(\dfrac{dW_i}{dt}\right) \\ \dfrac{dY_i^*}{dt} & = \dfrac{(\widetilde{Y}_i - Y_i^*)}{(k/\varepsilon)} + \dot{\omega}_i(Y_i^*) \end{cases} \tag{252}$$

The last difficulty is the determination of the mean pressure field $(\partial \overline{p}/\partial x_i)$. Methods have been proposed to calculate it from Monte Carlo simulations [100]. In most of Monte Carlo simulations, the Lagrangian simulation is coupled with an Eulerian calculations of means values providing the mean pressure field and the dissipation rate of the velocity fluctuations. However, full pdf methods including a model for the turbulent frequency following a fluid particle have also been developed with success [191].

10 Large eddy simulation

10.1 Introduction

As already described in § 2.4, large eddy simulation (LES) is a very attractive tool for numerical simulations of fluid flows. The objective is to explicitely compute the largest structures of the flow field (typically the structures larger than the computational mesh size) whereas only the effects of the small one are modeled. This technique is just at a very beginning stage for combustion modeling and this section is devoted to a brief summary of the various modeling approaches under developments. First, models for the unresolved turbulent fluxes (i.e. turbulence modeling) are briefly recalled.

10.2 Unresolved turbulent fluxes modeling

Our objective is not to provide a complete description of the subgrid scale models for the unresolved turbulent fluxes but just to recall some of the most popular formulations. The reader may found more details in several review papers [19, 20, 21, 22]. The following presentation is also limited to the modeling in the physical space. The unresolved momentum fluxes, corresponding to the Reynolds stresses in RANS, are:

$$\tau_{ij} = \overline{u_i u_j} - \overline{u}_i \overline{u}_j \tag{253}$$

Let us point out that the following models have been derived assuming constant density flows.

10.2.1 Smagorinsky model

The Smagorinsky model is the oldest one and is very popular because of its simple formulation. Unresolved momentum fluxes are expressed according to the Boussinesq assumption:

$$\tau_{ij} - \frac{\delta_{ij}}{3}\tau_{kk} = -\nu_t\left(\frac{\partial \overline{u}_i}{\partial x_j} + \frac{\partial \overline{u}_j}{\partial x_i}\right) = -2\,\nu_t\,\overline{S}_{ij} \tag{254}$$

where ν_t is a subgrid scale viscosity, modeled from dimensional analysis as:

$$\nu_t = C_S^2\,\Delta^{4/3}\,l_t^{2/3}\,\left|\overline{S}\right| \tag{255}$$

l_t is the turbulent integral length scale and C_S a model constant. Eq. (255) is simplified assuming $l_t \approx \Delta$:

$$\nu_t = (C_S \Delta)^2 \left|\overline{S}\right| \tag{256}$$

For an homogeneous and isotropic turbulence, the model constant is estimated as $C_S \approx 0.2$. Unfortunately, C_S seems to depend on flow configurations and, accordingly, its value is not universal. The Smagorinsky model is also known to be too dissipative.

10.2.2 Scale similarity model

The basic idea of this model is to assume that interactions between resolved and unresolved scales are mainly controled by the lowest resolved structures and the largest unresolved scales. This analysis leads to the following expression:

$$\tau_{ij} = \overline{\overline{u}_i \overline{u}_j} - \overline{\overline{u}_i}\,\overline{\overline{u}_j} \tag{257}$$

where all quantities are known filtering the resolved quantities.

Despite its qualities, this model is found to be unsufficiently dissipative. To overcome this difficulty, this model is generally coupled to the Smagorinski model (**mixed models**). The value, and the variability, of the Smagorinski model constant, C_S is then decreased.

10.2.3 Germano dynamic model

The objective of this very popular model is to improve the Smagorinski model by an automatic determination of the model constant C_S, depending on time and spatial location. A **test filter**, $\widehat{Q}$, having a larger size than the LES filter is introduced. The unresolved subgrid momentum fluxes are:

$$\tau_{ij} = \overline{u_i u_j} - \overline{u}_i \overline{u}_j \tag{258}$$

The unresolved fluxes at the test level are:

$$T_{ij} = \widehat{\overline{u_i u_j}} - \widehat{\overline{u}}_i \widehat{\overline{u}}_j \tag{259}$$

The two previous relations are combined to lead to the Germano identity:

$$\boxed{\underbrace{\widehat{\overline{u}_i \overline{u}_j} - \widehat{\overline{u}}_i \widehat{\overline{u}}_j}_{\mathcal{L}_{ij}} = T_{ij} - \widehat{\tau_{ij}}} \tag{260}$$

where the left hand side term is determined by filtering the resolved LES velocity field at the test level. Using the Smagorinski model to estimate the Reynolds stresses τ_{ij} et T_{ij} leads to:

$$\tau_{ij} - \frac{\delta_{ij}}{3}\tau_{kk} = -2\,C\,\overline{\Delta}^2 \left|\overline{S}\right| \overline{S}_{ij} = -2\,C\,\alpha_{ij} \tag{261}$$

$$T_{ij} - \frac{\delta_{ij}}{3} T_{kk} = -2\,C\,\widehat{\Delta}^2 \left|\widehat{\overline{S}}\right| \widehat{\overline{S}}_{ij} = -2\,C\,\beta_{ij} \tag{262}$$

where $\overline{\Delta}$ and $\widehat{\Delta}$ denote respectively the LES and test filter sizes. Two functions, α_{ij} and β_{ij} have been introduced for clarity.

Then, the Germano identity may be rewritten as:

$$\mathcal{L}_{ij} - \frac{\delta_{ij}}{3}\mathcal{L}_{kk} = -2\,C\,\alpha_{ij} + 2\,\widehat{C\,\beta_{ij}} \tag{263}$$

providing five independent equations for the unknown "model constant", C. C may be determined using optimization procedures.

This model seems to be very efficient in a large number of applications but may induce some numerical difficulties, for example when C becomes negative. In practical applications, C is not locally determined but averaged in homogeneous directions or along streamlines.

10.2.4 Structure function models

Developed by Lesieur and his coworkers [21, 22], these models are based on theoretical analysis in the spectral space (EDQNM modeling,...) and on subgrid scale viscosity concept.

In the structure function model, the subgrid scale dynamic viscosity is determined as:

$$\nu_t(\mathbf{x},\Delta) = 0.105\, C_K^{-3/2}\, \Delta \sqrt{F_2(\mathbf{x},\Delta)} \tag{264}$$

where $C_K = 1.4$ is the Kolmogorov constant and F_2 the structure function defined as:

$$F_2(\mathbf{x},\Delta) = \left[\overline{\mathbf{u}}(\mathbf{x}+\mathbf{r}) - \overline{\mathbf{u}}(\mathbf{x})\right]^2 \quad \text{with} \quad \sqrt{\mathbf{r}^2} = \Delta \tag{265}$$

estimated, in practical application from the six grid points in the vicinity of the location $\mathbf{x}$.

But, practical applications show that this model dissipates too rapidly the large structures. A **filtered structure function model** has been proposed by Ducros [21, 22]. The resolved velocity field is first high-pass filtered to eliminate the largest turbulent structures before the estimate of the structure function F_2. The model is then written:

$$\nu_t(\mathbf{x},\Delta) = 0.0014\, C_K^{-3/2}\, \Delta \sqrt{\overline{F}_2(\mathbf{x},\Delta)} \tag{266}$$

where $\overline{F}_2$ is the filtered structure function.

10.2.5 Unresolved scalar transport

In most cases, unresolved scalar fluxes are described from a gradient assumption:

$$\widetilde{u_i Y_k} - \widetilde{u}_i \widetilde{Y}_k = -\frac{\nu_t}{Sc_k} \frac{\partial \widetilde{Y}_k}{\partial x_i} \tag{267}$$

where Sc_k is a subgrid scale Schmidt number. The subgrid scale viscosity ν_t is estimated from the unresolved Reynolds stresses models (Smagorinsky, Germano, structure function models,...).

10.3 Simplest approaches for combustion modeling

10.3.1 Arrhenius law based on filtered quantities

A first rough model is to neglect subgrid scale contributions and to write the reaction rate as an Arrhenius law for filtered quantities:

$$\overline{\dot{\omega}}_F = A \overline{\rho}^2 \widetilde{Y}_F \widetilde{Y}_O \widetilde{T}^b \exp\left(-\frac{E}{R\widetilde{T}}\right) \tag{268}$$

Such simplified expression assumes a perfect mixing at subgrid scale level (perfectly stirred reactor) and implicitly suppose that turbulent time scales, τ_t, are shorter than chemical time scales τ_c ($\tau_t \ll \tau_c$). This assumption is generally used for reacting flows in atmospheric boundary layer [56] but is clearly not relevant in most combustion applications.

A more refined approach is to take into account the segregation factor, as already described in RANS modeling (§ 4):

$$\overline{\dot{\omega}}_F = A \overline{\rho}^2 \widetilde{Y}_F \widetilde{Y}_O \widetilde{T}^b \exp\left(-\frac{E}{R\widetilde{T}}\right) \left[1 + \frac{\widetilde{Y_F'' Y_O''}}{\widetilde{Y}_F \widetilde{Y}_O}\right] \tag{269}$$

The segregation factor $I_{sgs} = \widetilde{Y_F'' Y_O''} / \widetilde{Y}_F \widetilde{Y}_O$ is equal to 0 when the fuel and oxidizer are perfectly mixed at the subgrid level and $I_{sgs} = -1$ in a case of an infinitely fast reaction. I_{sgs} may be presumed or found from a balance equation for $\widetilde{Y_F'' Y_O''}$ [57]. Once again, such an approximation is quite rough but may be justified when temperature fluctuations are negligible (for example for the dispersion of pollutants in the atmospheric boundary layer).

10.3.2 Extension of algebraic Favre averaged approaches

A simple idea is to extent Favre algebraic models such as Eddy-Break-Up model (§ 7.2) for premixed combustion or Magnussen model (§ 9.3.1) for non premixed combustion to LES [236, 237]. For example, the subgrid scale Eddy-Break-Up model is simply written:

$$\overline{\dot{\omega}}_F = C_{EBU}\overline{\rho}\frac{1}{\tau_t^{SGS}}\frac{\widetilde{Y}_F}{Y_F^0}\left(1-\frac{\widetilde{Y}_F}{Y_F^0}\right) \tag{270}$$

where τ_t^{SGS} is a subgrid turbulent time scale, estimated as:

$$\tau_t^{SGS} = \frac{k^{SGS}}{\varepsilon^{SGS}} \approx C_D\frac{\Delta}{\sqrt{k^{SGS}}} \tag{271}$$

where k^{SGS} and ε^{SGS} are respectively the subgrid turbulent kinetic energy and its dissipation, C_D a constant and Δ the filter size. The turbulent kinetic energy k^{SGS} may be estimated from an algebraic model or a balance equation.

Such a simple formulation is quite attractive and has not been yet extensively tested. Nevertheless two drawbacks may be suspected. First, the Eddy-Break-up model has known deficiencies in Favre averaged context (reaction rate independent on chemical reaction, overestimation of the reaction rate in zones of strong shears...). In a LES context, the model constant C_{EBU} seems to be strongly dependent on various parameters (flow conditions, mesh size,...).

10.3.3 Simple extension of the Germano dynamic model

In a recent paper, Germano et al. [238] have proposed to extend the Germano dynamic model (§ 10.2.3) to reacting flows. Assuming a constant density flow without heat release, the filtered reaction rate $\overline{\dot{\omega}}_F$ is proportional to $\overline{Y_F Y_O}$ (Eq. 52). Assuming similarity between two filtering levels (respectively noted $\overline{Q}$ and $\widehat{Q}$), the unresolved reaction rate is expressed as:

$$\overline{Y_F Y}_O - \overline{Y}_F\overline{Y}_O = k_{fg}\left(\widehat{\overline{Y}_F\overline{Y}}_O - \widehat{\overline{Y}}_F\widehat{\overline{Y}}_O\right) \tag{272}$$

This analysis is attractive because of its simplicity and its similarity with the Germano dynamic model for unresolved Reynolds stresses $\overline{u_i u_j} - \overline{u}_i\overline{u}_j$. Nevertheless, a-priori tests against DNS data reveal a disappointing result: the similarity constant k_{fg} is found to strongly depend on the mesh size and on the Damköhler number (ratio between turbulent time scale and chemical time scale). In fact, an increase of the Damköhler number corresponds to a thinner reaction zone and the similarity filter $\widehat{Q}$ underestimates the unresolved production term (a large fraction of the chemical production occurs at the subgrid level scale), requiring a higher similarity constant. On the other hand, as the mesh size decreases, the reaction rate estimated from the similarity filter $\widehat{Q}$ increases (an increasing part of the reaction rate occurs between subgrid, $\overline{Q}$, and similarity, $\widehat{Q}$, filter levels) and, accordingly, the similarity constant decreases. Then, such a simple similarity model is not well suited to reacting flows. Length scales effects have to be incorporated (comparison between flame thickness, flame wrinkling and mesh size). The extension of this approach to non-constant density flows with heat release effects is also not obvious.

10.4 LES models for non premixed combustion

As previously described (§ 5), in non premixed flames, turbulent times τ_t may often be assumed to be quite longer than characteristic chemical times τ_c. Accordingly, such reacting flows are generally controlled by turbulent and molecular mixing processes. Two main ideas have been proposed to describe

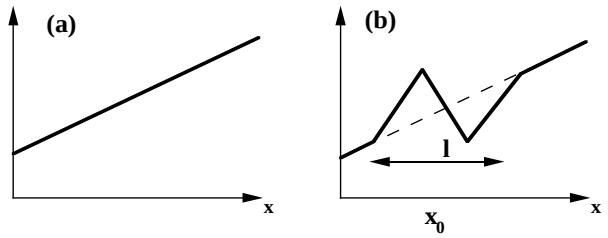

Figure 47: "Triplet map" used in the Linear Eddy Model developed by Kerstein to simulate a one-dimensional turbulent stirring process. (a) before mixing; (b) simulated mixing by a vortex of size l.

non premixed combustion flow fields with LES: the Linear Eddy Model (LEM) mainly developped by Kerstein [239, 240, 241, 242, 243] and the probability density function approach, initially proposed in [244] and developped further by various authors, such as Cook, Riley and their coworkers [245, 246].

10.4.1 Linear Eddy Model

The Linear Eddy Model (LEM) developed by Kerstein [239, 240, 241, 242, 243] is based on a one dimensional stochastic description of turbulent stirring processes. In a LES framework, this analysis is used to describe subgrid scale phenomena.

The **turbulent stirring mechanism** is modeled by a rearrangement process applied to the 1D scalar field. The initial scalar distribution (Fig. 47a) is rearranged on a given segment of size l according to Fig. 47b ("triplet map"). This process may be viewed as the effect of a single turbulent structure of size l located in x_0. Then, the turbulent mixing is simulated from a stochastic description where vortex locations x_0, vortex sizes l ($l_k \leq l \leq \Delta$, where l_k is the Kolmogorov length scale and Δ the LES filter size) and vortex frequencies λ are specified according to a given turbulence spectra (homogeneous turbulence in general).

Molecular diffusion and chemical processes are described by one dimensional balance equations:

$$\frac{\partial \rho Y_i}{\partial t} = \frac{\partial}{\partial x}\left(\rho D_i \frac{\partial Y_i}{\partial x}\right) + \dot{\omega}_i \tag{273}$$

To summarize, subgrid scale chemical reaction and turbulent mixing are analyzed from a one dimensional problem where a simple stochastic description of turbulence is achieved. Any complex chemistry or diffusion features may be easily incorporated in Eq. (273). This approach also provides a direct estimation of filtered mass fractions $\widetilde{Y}_i$ or temperature $\widetilde{T}$ without balance transport equations for these quantities. Nevertheless, mass fractions and temperature transports between adjacent mesh cells must be modeled. The LEM approach may also be quite time consuming because a one-dimensional calculation is required in each computational cell.

This approach is probably well suited for large eddy simulations of turbulent mixing [247] and non premixed combustion, at least when combustion phenomena are nearly mixing controled [248, 249, 250, 251]. But, despite some attempts [252, 253, 254], its extension to turbulent premixed combustion is more difficult. As pointed out in [63] and [65], viscous dissipation and flame front curvatures play an important role in flame / turbulence interactions and cannot be accounted for in LEM formulation.

10.4.2 Dynamic micro-mixing model

When simulating numerically the behavior of unsteady large scales in turbulent flames, subgrid diffusion of chemical species (turbulent micro-mixing) requires a closure. A dynamic model was proposed

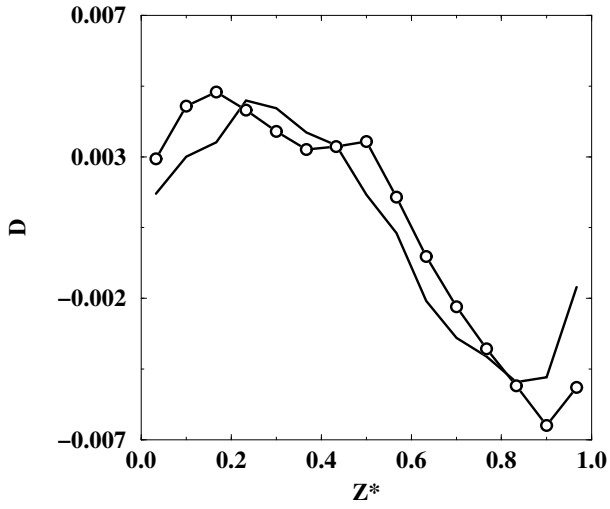

Figure 48: Conditional mean of the subgrid diffusion $D\nabla^2 Z$. The solid line was obtained from DNS and the line with symbols using the dynamic micromixing model proposed by Reveillon & Vervisch (1998).

to estimate micro-mixing from the known properties of the resolved large-eddy field. This dynamic procedure also provides a direct estimation of the micro-mixing time. A reference scalar field is invoked in the closure, and the physical model is based on basic properties of mass transfer by diffusion. The objective of this closure is to directly reproduce $\left(\overline{D\nabla^2 Z \mid Z^*}\right)$ used in pdf modeling (see § 6.4.3).

The Linear Eddy Model uses a 1D diffusive layer to reproduce subgrid turbulent mixing. A more direct approach consist of constructing a direct estimation of subgrid mixing from the knowledge of the resolved large eddy field. A reference scalar field is used to link subgrid diffusion at different filter sizes [198]. In the case of 3-D isotropic freely decaying turbulence including the mixing of an initially segregated mixture fraction field, the dynamic procedure reproduces the correct relaxation of the pdf and provides a direct estimation of the characteristic subgrid mixing time. For 2-D mixing layers, the comparison between direct numerical simulation results with those obtained from the closure indicates that dynamic procedure may be an alternative route to compute scalar mixing involving unsteady large eddies (see Fig. 48).

10.4.3 Probability Density functions

Under the assumption of fast chemistry, the species mass fractions Y_k and the temperature are functions of the passive scalar Z (see § 3). Then, the Favre filtered fuel mass fraction may be written as [244] :

$$\widetilde{Y}_f(x,t) = \frac{1}{\overline{\rho}} \int_{-\infty}^{+\infty} \rho(x',t)\, Y_f(Z(x',t))\, G(x-x')\, dx' \tag{274}$$

Introducing the Dirac δ-function, expression (274) may be recast as:

$$\widetilde{Y}_f(x,t) = \frac{1}{\overline{\rho}} \int_0^1 \int_{-\infty}^{+\infty} \rho(\Psi)\, Y_f(\Psi)\, \delta(Z(x',t)-\Psi)\, G(x-x')\, dx'\, d\Psi \tag{275}$$

leading to:

$$\widetilde{Y}_f(x,t) = \int_0^1 Y_f(\Psi) \underbrace{\frac{1}{\overline{\rho}} \int_{-\infty}^{+\infty} \rho(\Psi)\, \delta(Z(x',t) - \Psi)\, G(x-x')\, dx'}_{\text{filtered PDF } \widetilde{P}(\Psi,x,t)}\, d\Psi \tag{276}$$

Then:

$$\widetilde{Y}_f(x,t) = \int_0^1 Y_f(\Psi)\, \widetilde{P}(\Psi,x,t)\, d\Psi \tag{277}$$

where the sub-grid probability density function $\widetilde{P}(\Psi,x,t)$ has been introduced. The problem is now to determine this probability density function. As for Favre averaged models (§ 9.8), this PDF may be either presumed or found from a transport equation.

Presumed sub-grid PDF. This approach has been firstly proposed, and tested against DNS and experimental data, for reacting flow [245, 246]. The authors have found that a β function (§ 9.2), based on the filtered passive scalar $\widetilde{Z}$ and its unresolved fluctuations $\widetilde{Z''^2}$ is very accurate. They also discussed a similarity model to describe the variance $\widetilde{Z''^2}$ without an additive balance equation:

$$\widetilde{Z''^2} = C_Z \left(\widehat{\widetilde{Z}^2} - \widehat{\widetilde{Z}}^2 \right) \tag{278}$$

where $\widehat{Q}$ denotes a similarity filter.

Recent works [255, 256, 257] have proposed a dynamic procedure, similar to the Germano dynamic model to estimate C_Z leading to very promising results without solving a transport equation for the subgrid variance $\widetilde{Z''^2}$.

Transport equation for the sub-grid PDF. A transport equation for the subgrid scale PDF $\widetilde{P}(\Psi,x,t)$ may be derived [244] and is formally similar to Eq. (102). This formalism has not yet been extensively tested [257].

10.5 LES models for premixed combustion

10.5.1 Introduction

A difficult problem is encountered for large eddy simulations of premixed flames: the thickness δ_L of a premixed flame is about 0.1 to 1 mm and is generally smaller than the LES mesh size Δ as plotted in Fig. 49. The progress variable (i.e. non dimensionalized fuel mass fraction or temperature) is a very stiff variable and the flame front cannot be resolved in the computation, leading to numerical problems. To overcome this difficulty, two main approaches have been proposed: simulation of an artificially thickened flame or use of a flame front tracking technique (G-equation). A third one, based on the filtering of the c progress variable balance equation is developing.

10.5.2 Artificially thickened flames

The idea is to consider a flame thicker than the actual one, but having the same laminar flame speed S_L [258]. Following simple theories of laminar premixed flame [13, 14], the flame speed S_L and the flame thickness δ_L may be expressed as:

$$S_L \propto \sqrt{a\overline{W}} \qquad ; \qquad \delta_L \propto \frac{a}{S_L} \tag{279}$$

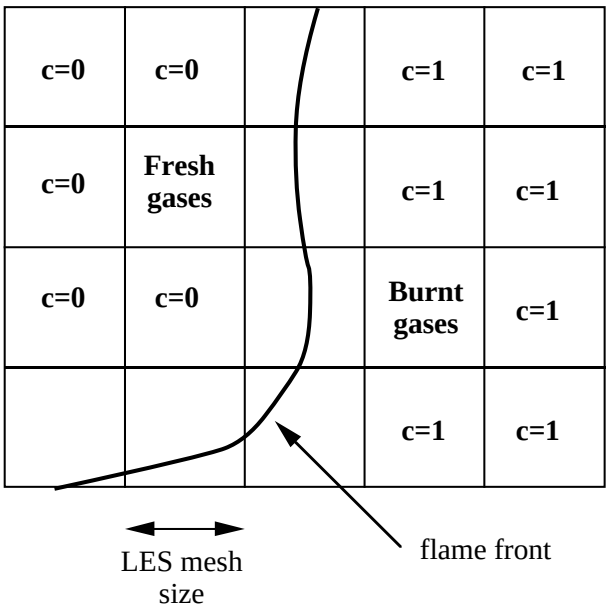

Figure 49: Comparison between premixed flame thickness δ_l and LES mesh size Δ. The flame front separates fresh gases (progress variable $c = 0$) from burnt gases ($c = 1$).

where a is the thermal diffusivity and $\overline{W}$ the mean reaction rate. Then, an increase of the flame thickness δ_L by a factor α with a constant flame speed S_L is easily achieved by replacing the thermal diffusivity a by $\alpha\, a$ and the reaction rate $\overline{W}$ by $\overline{W}/\alpha$. If α is sufficiently large (typically from 5 to 20), the thickened flame front may then be resolved on the LES computational mesh without subgrid modeling. The reaction rate is expressed using an Arrhenius law, as in direct numerical simulations.

This approach is very attractive:

- From a numerical point of view, the chemical reaction is described as in a direct numerical simulation on the LES computational grid, without subgrid scale model.
- Because of the use of an Arrhenius law, various phenomena are directly taken into account without requiring ad-hoc submodels (ignition, flame stabilization, flame/wall interactions...).
- Theoretically, this approach may be extended to complex chemistry.

This route has not been yet extensively tested in large eddy simulation [259] but seems to be very promising, at least when the flow motions are quite larger than the laminar flame thickness, as in combustion instabilities [260].

Unfortunately, when the flame is thickened from δ_l to $\alpha\delta_l$, the interaction between turbulence and chemistry may be modified because the Damköhler number, Da, comparing turbulent (τ_t) and chemical (τ_c) time scales:

$$Da = \frac{\tau_t}{\tau_c} = \frac{l_t}{u'}\frac{S_l}{\delta_l} \tag{280}$$

is decreased by a factor α and becomes Da/α.

Accordingly, the interaction between flame and turbulence may be altered. Poinsot et al. [77] have shown that when the length scale ratio between the turbulent length scale and the laminar flame thickness, l_t/δ_l, is decreased, the flame becomes more and more insensitive to turbulence motions. This ratio

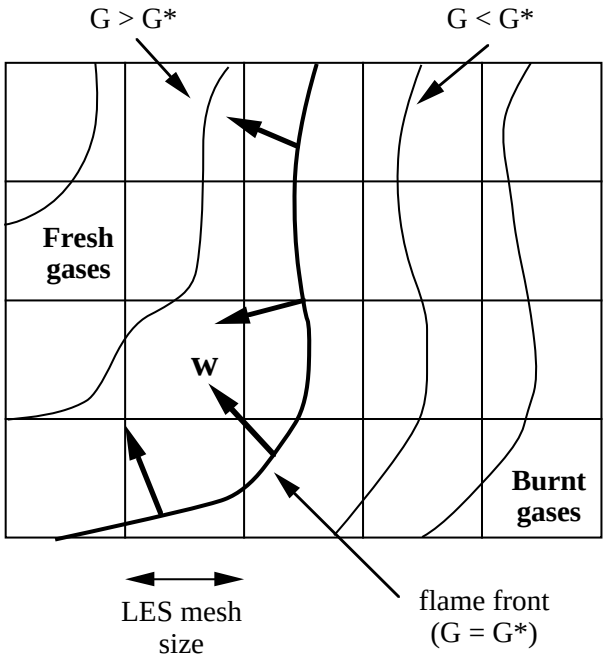

Figure 50: Flame front and G-field. w is the displacement speed, relatively to the local flow velocity, of the iso-level G.

is decreased by a factor α when the flame is thickened. This point have been investigated using DNS [261] and an efficiency function E, depending on velocity (u'/S_L) and length scale ($\Delta/\alpha\delta_l$), has been derived to counteract this effect. In practical applications, the thickened flame approach is implemented by changing the diffusivity and the reaction rate according to [261]:

$$\begin{array}{rccccc} \text{Diffusivity:} & a & \longrightarrow & \alpha\, a & \longrightarrow & E\,\alpha\, a \\ \text{Reaction rate:} & W & \longrightarrow & W/\alpha & \longrightarrow & E\,W/\alpha \\ & & \text{thickening} & & \text{wrinkling} & \end{array}$$

10.5.3 G-equation

In this approach, the flame surface is described as an infinitely thin propagating surface (flamelet). The key idea is to track the position of the flame front using a field variable G. The flame surface is associated to the isolevel $G = G^*$ as plotted on figure 50. The G-field does not have to follow the gradients of the progress variable c and can be smoothed out to be resolved on the LES mesh. The G-equation is written [76]:

$$\frac{\partial G}{\partial t} + u.\nabla G = w\,|\nabla G| \tag{281}$$

where w is the local displacement speed of the iso-surface G, relative to the flow field.

This kinematic description of the combusting flow field leads to various difficulties already summarized in section 6.3.1.

The application of a LES filter to the G-equation (Eq. 281) leads to:

$$\frac{\partial \overline{G}}{\partial t} + \overline{\mathbf{u}}.\nabla \overline{G} = \underbrace{-\left(\overline{\mathbf{u}.\nabla G} - \overline{\mathbf{u}}.\nabla \overline{G}\right)}_{\text{Unresolved turbulent transport}} + \underbrace{\overline{w\,|\nabla G|}}_{\text{Flame front displacement}} \tag{282}$$

where two unclosed terms, corresponding respectively to unresolved transport and to front displacement, should be modeled. To avoid this description, the G-equation is directly used for the resolved field $\overline{G}$, introducing a subgrid scale turbulent flame speed S_T:

$$\frac{\partial \overline{G}}{\partial t} + \overline{\mathbf{u}}.\nabla \overline{G} = \overline{S}_T \left|\nabla \overline{G}\right| \tag{283}$$

The challenge is then to propose a model for $\overline{S}_T$. This closure is generally based on Eq. (119):

$$\frac{\overline{S}_T}{S_L} = 1 + \alpha \left(\frac{\overline{u'}}{S_L}\right)^n \tag{284}$$

where $\overline{u'}$ is the subgrid scale turbulence level that may be estimated as:

$$\overline{u'} \approx \Delta \left|\overline{S}\right| = \Delta \sqrt{\left|2\overline{S}_{ij}\overline{S}_{ij}\right|} \tag{285}$$

where S_{ij} are the component of the resolved shear stresses. The constants α and n have to be specified. A dynamic determination for α has also been proposed when $n = 1$ [262].

Equation (283) is a simple formulation corresponding to a simple physical analysis (displacement of the resolved flame front with the displacement speed $\overline{S}_T$). Nevertheless, as already pointed out (§ 7.1), the turbulent flame speed is not a well defined quantity and no universal model is available. Despite these drawbacks, the G-equation approach is, up to know, the most advanced technique for large eddy simulations of premixed combusting flow fields [79, 263].

10.5.4 Filtering the progress variable balance equation

Assuming a single step chemistry and unity Lewis number (i.e. identical mass and thermal diffusivities), the mass fractions of the reactive species and the temperature are all linearly related and may be expressed in terms of a reaction progress variable c ($c = 0$ within fresh reactants and $c = 1$ within burnt products) as described in section 3.1, following the balance equation:

$$\frac{\partial \rho c}{\partial t} + \nabla \cdot (\rho \mathbf{u} c) = \nabla \cdot (\rho D \nabla c) + \dot{\omega}_c = \rho\, w\, |\nabla c| \tag{286}$$

Applying the LES filter F, the previous c-equation becomes:

$$\frac{\partial \overline{\rho}\widetilde{c}}{\partial t} + \nabla.\left(\overline{\rho}\widetilde{\mathbf{u}}\widetilde{c}\right) + \nabla.\left[\overline{\rho}\left(\widetilde{\mathbf{u}c} - \widetilde{\mathbf{u}}\widetilde{c}\right)\right] = \overline{\nabla.\left(\rho D \nabla c\right)} + \overline{\dot{\omega}}_c \tag{287}$$

$$= \overline{\rho w\, |\nabla c|} \tag{288}$$

where the three LHS terms in Eq. (287) correspond respectively to unsteady effects, resolved convective fluxes and unresolved transport. The two RHS terms in Eq. (287) denote respectively filtered molecular diffusion and filtered reaction rate. The RHS term in Eq. (288) corresponds to flame front displacement.

As already pointed out, the flame front (and the gradient of the progress variable c) is generally too thin to be resolved on the LES computational mesh. Nevertheless, the filtered progress variable $\widetilde{c}$ may

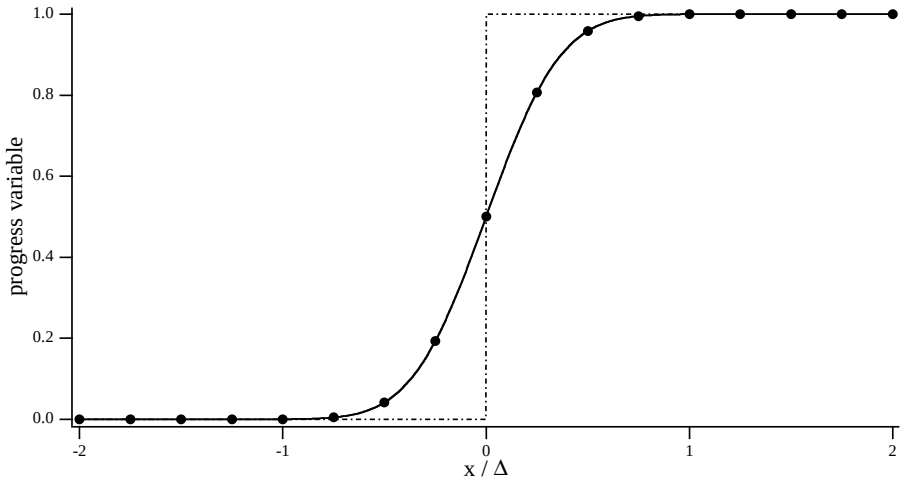

Figure 51: Effect of a spatial Gaussian filter (Eq. 24) having a size Δ larger than the mesh size Δ_m ($\Delta = 4\,\Delta_m$). The unfiltered progress variable c (—·—) and the filtered progress variable $\overline{c}$ (———) are plotted as a function of x/Δ where x is the spatial coordinate. The progress variable c is not resolved on the computational mesh denoted by (•) whereas the filtered progress variable $\overline{c}$ is resolved with about $2\,\Delta/\Delta_m = 8$ grid points in the filtered flame front ([264]).

be resolved using a physical space Gaussian filter F (Eq. 24) with a filter size Δ larger than the computational mesh size Δ_m as displayed on Fig. 51 [264]. Accordingly, the filtered flame front is numerically resolved with about $2\,\Delta/\Delta_m$ grid points. The $\widetilde{c}$-balance equation (288) is similar to a G-equation but, compared to an arbitrary G-field, the progress variable c has a main advantage: c and related quantities (Σ^*, Σ, $\langle \rho w \rangle_s$,...) are physically defined and may be extracted from DNS or experimental measurements.

Boger et al. [264] then propose a flame surface density formulation for subgrid scale modeling. The flame front displacement may be recast as [265]:

$$\begin{aligned}\overline{\rho w\,|\nabla c|} &= \int_{-\infty}^{+\infty} \rho w\,|\nabla c|\,F\,(\mathbf{x}-\mathbf{x}')\,d\mathbf{x}' = \int_{-\infty}^{+\infty}\int_0^1 \rho w\,|\nabla c|\,\delta\,(c-c^*)\,F\,(\mathbf{x}-\mathbf{x}')\;dc^*\,d\mathbf{x}' \\ &= \int_0^1 \langle \rho w\rangle_s^*\,\Sigma^*\,dc^* = \langle \rho w\rangle_s \Sigma = \langle \rho w\rangle_s \Xi\,|\nabla \overline{c}| \end{aligned} \tag{289}$$

where δ is the Dirac delta function. Σ^* is the subgrid surface density (i.e. the subgrid surface per unit volume) of the surface defined by $c = c^*$ and $\langle Q\rangle_s^*$ denotes the conditional averaging of Q along this surface c=c^*. These quantities are defined as:

$$\Sigma^* = \int_{-\infty}^{+\infty} |\nabla c|\,\delta\,(c-c^*)\,F\,(\mathbf{x}-\mathbf{x}')\;d\mathbf{x}' \tag{290}$$

$$\langle Q\rangle_s^*\,\Sigma^* = \int_{-\infty}^{+\infty} Q\;|\nabla c|\,\delta\,(c-c^*)\,F\,(\mathbf{x}-\mathbf{x}')\;d\mathbf{x}' \tag{291}$$

Σ and $\langle Q\rangle_s$, introduced in Eq. (289) may be viewed as generalized subgrid flame surface density and surface average, defined as:

$$\Sigma = \int_0^1 \Sigma^*\,dc^* = \overline{|\nabla c|} \qquad \text{and} \qquad \langle Q\rangle_s = \frac{1}{\Sigma}\int_0^1 \langle Q\rangle_s^*\,dc^* = \frac{\overline{Q\,|\nabla c|}}{\Sigma} \tag{292}$$

The flame front wrinkling Ξ, introduced in Eq. (289), compares the subgrid scale flame surface to its projection in the propagating direction:

$$\Xi = \frac{\int_0^1 \int_{-\infty}^{+\infty} |\nabla c| \, \delta\left(c - c^*\right) F\left(\mathbf{x} - \mathbf{x}'\right) \, d\mathbf{x}' \, dc^*}{\mathbf{n_p} \cdot \int_0^1 \int_{-\infty}^{+\infty} \mathbf{n} \, |\nabla c| \, \delta\left(c - c^*\right) F\left(\mathbf{x} - \mathbf{x}'\right) \, d\mathbf{x}' \, dc^*} \tag{293}$$

where $\mathbf{n}$ is the unit vector normal to the c-surface and $\mathbf{n_p}$ is the unit vector normal to the resolved propagating direction both pointing towards the fresh gases. They are defined by:

$$\mathbf{n} = -\frac{\nabla c}{|\nabla c|} \quad \text{and} \quad \mathbf{n_p} = -\frac{\nabla \overline{c}}{|\nabla \overline{c}|} \tag{294}$$

Eq. (293) is easily recast as:

$$\Xi = \frac{\overline{|\nabla c|}}{\frac{\nabla \overline{c}}{|\nabla \overline{c}|} \cdot \overline{\nabla c}} = \frac{\overline{|\nabla c|}}{|\nabla \overline{c}|} = \frac{\Sigma}{|\nabla \overline{c}|} \tag{295}$$

The previous relations may be used to recast the filtered c-balance equation (288) as a G-equation:

$$\frac{\partial \widetilde{c}}{\partial t} + \widetilde{\mathbf{u}} \cdot \nabla \widetilde{c} = \frac{1}{\overline{\rho}} \left(-\frac{\nabla . \left[\overline{\rho}\left(\widetilde{\mathbf{u}c} - \widetilde{\mathbf{u}}\widetilde{c}\right)\right]}{|\nabla \overline{c}|} + \langle \rho w \rangle_s \Xi \right) |\nabla \overline{c}| = \overline{S}_T \, |\nabla \overline{c}| \tag{296}$$

providing an expression for the subgrid scale turbulent flame speed S_T.

Assuming a thin flame front, the surface density Σ^* of the surface defined by $c = c^*$ does not depend on the chosen c^* level and $\Sigma \approx \Sigma^*$ corresponds exactly to the subgrid flame surface density (i.e. the subgrid flame surface per unit volume). In fact, the flame surface density description proposed in RANS (§ 7.4) may be easily extended to large eddy simulations.

$\langle \rho w \rangle_s$ and Ξ or Σ have now to be modeled. In a first step, the surface-averaged mass-weighted displacement speed $\langle \rho w \rangle_s$ may be estimated from the laminar flame speed S_L and the fresh gases density ρ_u as:

$$\langle \rho w \rangle_s \approx \rho_u \, S_L \tag{297}$$

As in RANS, the flame surface density Σ and the flame front wrinkling Ξ may be expressed from:

- **Algebraic expressions**, based, for example, on a BML-type approach [264] or from a fractal analysis. Dynamic formulations could be derived.
- **Balance equations**.

  Starting from Eq. (286) and using previous definitions, there is no difficulty to derive exact, but unclosed, balance equations for Σ^* or Σ. One easily obtains a balance equation for $|\nabla c|$. Then, using definitions (292) the equation becomes after LES filtering:

$$\frac{\partial \Sigma}{\partial t} + \nabla . \left[\langle \mathbf{u} \rangle_s \Sigma\right] = \langle \nabla . \mathbf{u} - \mathbf{n}\mathbf{n} : \nabla \mathbf{u} \rangle_s \Sigma - \nabla . \left[\langle w \mathbf{n} \rangle_s \Sigma\right] + \langle w \nabla . \mathbf{n} \rangle_s \Sigma \tag{298}$$

  $\nabla . \mathbf{n}$ denotes the iso-surface curvature. The two first terms on the right hand side correspond respectively to the strain rate acting on the c-surfaces and to the normal front displacement. The last term combines propagation and curvature effects. In fact, this equation is formally identical to the balance equation for flame surface density (Eq. 87) widely used in Reynolds averaged context [15, 86].

To our mind, this analysis is more promising than the simple use of a subgrid turbulent flame speed $\overline{S}_T$ in a G-equation (Eq. 283). In its simplest form, this approach is similar but may be easily refined taking benefits of the various studies conducted in a RANS context (§ 7.4).

10.6 Numerical costs

Large eddy simulations are a very promising tool for turbulent combustion and combustion instabilities. But such simulations have a numerical cost that may becomes prohibitive:

- LES are, by definition, unsteady simulations. Accordingly, some usual assumptions used in computation of averaged flows cannot be retained (symmetry, two-dimensional mean flows,...). A relevant description of the turbulent motions requires tri-dimensionnal simulations...
- The mesh size (i.e. the filter size) should be sufficiently small. Most models derived to describe the unresolved fluxes are based on similarity assumptions requiring that the cut-off scale between resolved and unresolved structures is in the inertial range of the turbulence spectrum. Accordingly, a given range of turbulence motions has to be resolved.
- The numerical precision of the code is a key point: as more precise phenomena are described, compared to RANS simulations (subgrid fluxes), the subgrid scale models have not to be blur by the code numerical diffusion...
- Initial and boundary conditions may be not obvious. For example, the numerical simulation of a turbulent flow in a channel requires to impose at the inlet an ad-hoc unsteady turbulent flow field. In non-reacting flows, numerical simulations generally assumed a periodic channel. With chemical reaction, or in a non-periodic configuration (obstacle, for example), a second simulation of a periodic channel may be used to provide the required instantaneous flow field...
- Relevant averaged and global quantities (mean, rms, correlation functions, energy spectra,...) may be extracted from large eddy simulations but require a long computational time and large databases.

Accordingly, LES developments have to be conducted together with numerical (algorithm precision,...) and computational (code vectorization and parallelism) studies. For example, it remains unclear today whether "industrial" codes (KIVA, FLUENT...), suited to complex flow geometries, may be used for large eddy simulations...

11 Conclusion

Modeling turbulent combustion is a challenging task. In turbulent flames, various difficulties (strong heat release, complex chemistry, large range of time and length scales, ...) are added to the complexity of constant-density turbulent flows.

A review of the most classical Reynolds (or Favre) averaged Navier-Stokes (RANS) models has been proposed. Three main ingredients must be modeled:

- Reynolds stresses: $\widetilde{u_i u_j} - \widetilde{u}_i \widetilde{u}_j$.
- Turbulent transport of species mass fractions: $\widetilde{u_i Y_k} - \widetilde{u}_i \widetilde{Y}_k$.
- Mean reaction rate of species: $\overline{\omega}_k$.

Most works have focus on refined descriptions of the mean reaction rate $\overline{\omega}_k$. To provide this reaction rate, tools have been proposed, which are based on a pure statistical or more oriented geometrical view of turbulent flames. All these various models are related via a scalar dissipation rate, a key quantity representing micromixing of the reactants occurring at the small scales where chemical reactions develop. The links and the similarities between combustion models have been evidenced here. The precise knowledge of these relations may be useful to understand the exact implications of the underlying physical hypothesis. Major models are then directly derived from the proposed expressions, which enlight unexpected links between well-known closure schemes.

Few studies have focussed on species turbulent transport, generally modeled using a gradient expression, whereas counter-gradient turbulent transport is known to appear in some situations. Reynolds stresses are generally described from well established turbulent models (mostly k, ε), simply re-written in terms of Favre averaged quantities. So far, combustion effects on the flow (flame induced turbulence generation, higher viscous dissipation...) are not intentionally included in the calculations.

There are many open questions and challenges left. One of them is the understanding of the coupling between spray and combustion including detailed chemistry. DNS with a two-way coupling between a dilute spray and a carrier phase were recently performed to progress in this direction [266] and closures exist [267, 268, 266], but more work is needed to reach a level where liquid atomization, vaporization together with flames are properly described.

RANS combustion models will remain useful for the next few years. However, Large Eddy Simulations (LES) stands as very promising for turbulent combustion:

- Combustion flow fields generally exhibit large scale motions [24].
- LES appear as a promising tool to capture combustion instabilities.
- Flames are mainly driven by mixing, LES is a good candidate to capture unsteady turbulent mixing.
- LES may directly provide part of the description of turbulence / combustion interactions, because zones of fresh and burnt gases, having different turbulence characteristics, are instantaneously identified at the level of the resolved grid.

LES is at a very early stage for combustion applications and only few works have been done in this direction, mainly devoted to feasibility tests (two dimensional simulations, constant density flows,...). Nonetheless, the results of these preliminary tests suggest that LES will rapidly become a complementary way to carefully simulate and understand turbulent combustion systems. So far LES modeling is essentially based on the same modeling strategies than the ones described here for RANS turbulent combustion modeling.

References

[1] A. Liñán and F. A. Williams. *Fundamental aspects of combustion*. Oxford University Press, 1993.

[2] P. Clavin. Premixed combustion and gasdynamics. *Annu. Rev. Fluid Mech.*, 26:321–52, 1994.

[3] J. Buckmaster and G. Ludford. *Theory of laminar flames*. Cambridge University Press, 1993.

[4] W.L. Roberts and J.F. Driscoll. A laminar vortex interacting with a premixed flame: measured formation of pockets of reactants. *Combust. Flame*, 87:245–256, 1991.

[5] C. J. Mueller, J. F. Driscoll, D. L. Reuss, M. C. Drake, and M. E. Rosalik. Vorticity generation and attenuation as vortices convect through a premixed flame. *Combust. and Flame*, 112, 1998.

[6] M. D. Smooke, R. E. Mitchel, and D. E. Keyes. Numerical solution of two-dimensional axisymmetric laminar diffusion flames. *Combust. Sci. and technology*, 67:85–122, 1989.

[7] P. Givi. Model free simulations of turbulent reactive flows. *Prog. Energy Combust. Sci.*, 15:1–107, 1989.

[8] T. Poinsot. Using direct numerical simulations to understand premixed turbulent combustion. In *Twenty-sixth Symposium (International) on Combustion*, pages 219 – 232. The Combustion Institute, 1996.

[9] T. Baritaud, T. Poinsot, and M. Baum. *Direct numerical simulation for turbulent reacting flows*. Editions TECHNIP, 1996.

[10] T. Poinsot, A. Trouvé, and S. Candel. Applications of direct numerical simulations of premixed turbulent combustion. *Prog. Energ. Combust. Sci.*, 21:531 – 576, 1996.

[11] L. Vervisch and T. Poinsot. Direct numerical simulation of non-premixed turbulent flame. *Annu. Rev. Fluid Mech.*, 30:655–692, 1998.

[12] M. Barrère and R. Prud'homme. *Equations fondamentales de l'aérothermochimie*. Masson, Paris, 1973.

[13] F.E. Williams. *Combustion Theory*. Addison-Wesley, 2 edition, 1985.

[14] K.K. Kuo. *Principles of Combustion*. John Wiley, New York, 1986.

[15] A. Trouvé and T. Poinsot. The evolution equation for the flame surface density. *J. Fluid Mech.*, 278:1–31, 1994.

[16] A. Favre. Statistical equations of turbulent gases. In SIAM, editor, *Problems of hydrodynamics and continuum mechanics*, pages 231–266. SIAM, Philadelphia, 1969.

[17] K.N.C. Bray, P.A. Libby, G. Masuya, and J.B. Moss. Turbulence production in premixed turbulent flames. *Combust. Sci. Technol.*, 25:pp 127 – 140, 1981.

[18] I.G. Shepherd, J.B. Moss, and K.N.C. Bray. Turbulent transport in confined premixed flame. In *19th Sympoisum (International) on Combustion*, pages 423 – 431. The Combustion Institute, Pittsburgh, 1982.

[19] U. Piomelli and J.R. Chasnov. Large eddy simulations: theory and applications. In H. Hallbäck, D.S. Henningson, A.V. Johansson, and P.H. Alfredsson, editors, *Turbulence and Transition Modelling*, pages 269 – 336. Kluwer Academic Publishers, 1996.

[20] J. Ferziger. Large eddy simulation: an introduction and perspective. In O. Métais and J. Ferziger, editors, *New tools in turbulence modelling*, pages 29 – 47. Les Editions de Physique - Springer Verlag, 1997.

[21] M. Lesieur. Recent approaches in large-eddy simulations of turbulence. In O. Métais and J. Ferziger, editors, *New tools in turbulence modelling*, pages 1 – 28. Les Editions de Physique - Springer Verlag, 1997.

[22] M. Lesieur and O. Métais. New trends in large-eddy simulations of turbulence. *Ann. Rev. Fluid Mech.*, 28:45 – 82, 1996.

[23] D. Veynante and T. Poinsot. Reynolds averaged and large eddy simulation modeling for turbulent combustion. In O. Métais and J. Ferziger, editors, *New Tools in Turbulence Modelling*, pages 105 – 140. Les Editions de Physique - Springer Verlag, 1997.

[24] C.M. Coats. Coherent structures in combustion. *Prog. Energ. Combust. Sci.*, 22:427 – 509, 1996.

[25] S. Menon and W.H. Jou. Large eddy simulations of combustion instability in an axisymmetric ramjet. *Combust. Sci. Technol.*, 75:53 – 72, 1991.

[26] S. Ghosal and P. Moin. The basic equations for the large eddy simulation of turbulent flows in complex geometry. *J. Comp. Phys.*, 118:24 – 37, 1995.

[27] N. Peters. The turbulent burning velocity for large-scale and small-scale turbulence. *J. Fluid Mech.*, 384:107–132, 1999.

[28] A. Liñán. The asymptotic structure of counterflow diffusion flames for large activation energies. *Acta Astronautica*, 1007(1), 1974.

[29] A. Liñán, P. Orlandi, R. Verzicco, and F. J. Higuera. Effects of non-unity lewis numbers in diffusion flames. In *Studying turbulence using numerical databases - V*, pages 5–18. CTR, Stanford U., 1994.

[30] R. S. Barlow, G. J. Fiechtner, C. D. Carter, and J.-Y. Chen. Experiments on the scalar structure of turbulent co/h2/n2 jet flames. *Combust. and Flame*, 120(4):549 – 569, 2000.

[31] K.N.C. Bray and N. Peters. Laminar flamelets in turbulent flames. In P.A. Libby and F.A. Williams, editors, *Turbulent Reacting Flows*, pages 63–113. Academic Press London, 1994.

[32] B. Cuenot and T.J. Poinsot. Asymptotic and numerical study of diffusion flames with variable lewis number and finite rate chemistry. *Comb. and Flame*, 104(1):111–137, 1996.

[33] S. P. Burke and T. E. W. Schumann. Diffusion flames. *Industr. Eng. Chem.*, 20:998–1004, 1928.

[34] J.S. Kim and F.A. Williams. Extinction of diffusion flames with nonunity lewis numbers. *J. of Eng. Math.*, 31:101–118, 1997.

[35] P. Clavin and A. Liñán. *Theory of gaseous combustion. An introductive course*. M.G. Verlarde, Non equilibrium cooperative phenomena in physics and related fields, Plenum Press, 1983.

[36] V. Favier and L. Vervisch. Edge flames and partially premixed combustion in diffusion flame quenching. *Combust. Flame*, In press.

[37] A. Liñán. Ignition and flame spread in laminar mixing layer. In J. Buckmaster, T. L. Jackson, and A. Kumar, editors, *Combustion in High Speed Flows*, page 461. Kluwer Academic Publishers, 1994.

[38] H. Phillips. Flame in a buoyant methane layer. In *Tenth Symposium (International) on Combustion*. The Combustion Institute, Pittsburgh, 1965.

[39] P. N. Kioni, B. Rogg, K. N. C. Bray, and A. Liñán. Flame spread in laminar mixing layers: the triple flame. *Comb. and Flame*, 95:276, 1993.

[40] T. Plessing, P. Terhoeven, N. Peters, and M. S. Mansour. An experimental and numerical study on a laminar triple flame. *Comb. and Flame*, 115(3):335–353, 1998.

[41] P. N. Kioni, K.N.C. Bray, D. A. Greenhalgh, and B. Rogg. Experimental and numerical studies of a triple flame. *Combust. Flame*, 116:192–206, 1998.

[42] J. W. Dold. Flame propagation in a nonuniform mixture: analysis of a slowly varying triple flame. *Comb. and Flame*, 76:71–88, 1989.

[43] L. J. Hartley and J. W. Dold. Flame propagation in a nonuniform mixture: analysis of a propagating triple-flame. *Combust. Sci. and Tech.*, 80:23–46, 1991.

[44] J. Buckmaster. Edge-flames and their stability. *Combust. Sci. Tech.*, 115:41–68, 1996.

[45] S. Ghosal and L. Vervisch. Theoretical and numerical investigation of a symmetrical triple flame using a parabolic flame tip approximation. *J. Fluid Mech.*, 415:227–260, 2000.

[46] A. Bourlioux, B. Cuenot, and T. Poinsot. Asymptotic and numerical study of the stabilization of diffusion flames by hot gas. *Combust. Flame*, 120(1/2), 2000.

[47] G.R. Ruetsch, L. Vervisch, and A. Liñán. Effects of heat release on triple flame. *Phys. Fluids*, 6(7):1447–1454, 1995.

[48] P. Domingo and L. Vervisch. Triple flames and partially premixed combustion in autoignition of nonpremixed mixtures. In *Twenty-Sixth Symposium (International) on Combustion*, pages 233–240. The Combustion Institute, Pittsburgh, 1996.

[49] P. Terhoeven and N. Peters. Basic flame structures of turbulent combustion for application in diesel engines. *Combust. and Flame*, page to appear, 1997.

[50] T. Echekki and J. H. Chen. Structure and propagation of methanol-air triple flames. *Comb. and Flame*, 114(1/2):231–245, 1998.

[51] V. Favier and L. Vervisch. Effects of unsteadiness in edge-flames and liftoff in non-premixed turbulent combustion. In *Twenty-Seventh Symposium (International) on Combustion*, pages 1239–1245. The Combustion Institute, Pittsburgh, 1998.

[52] S. Ghosal and L. Vervisch. Stability diagram for lioft-off and blowout of a round jet laminar diffusion flame. *Combust. Flame, submitted*.

[53] L. Vervisch. Using numerics to help understanding of nonpremixed turbulent flames. In *Topical review, twenty-eight Int. Symposium on combustion*, 2000.

[54] R. Borghi. *Réactions chimiques en milieu turbulent*. PhD thesis, Université Pierre et Marie Curie - Paris 6, 1978.

[55] R. Villasenor, R.W. Pitz, and J.Y. Chen. Interaction between chemical reaction and turbulence in supersonic non-premixed h2-air combustion. In AIAA, editor, *29th Aerospace Science Meeting*, Reno (Nevada), 1991. AIAA 91-0375.

[56] F.T.M. Nieuwstadt and J.P. Meeder. Large-eddy simulation of air pollution dispersion: a review. In *New tools in turbulence modelling*, pages 264 – 280. Les Editions de Physique - Springer Verlag, 1997.

[57] J.P. Meeder and F.T.M. Nieuwstadt. Subgrid-scale segregation of chemically reactive species in a neutral boundary layer. In J.P. Chollet, P.R. Voke, and L. Kleiser, editors, *Direct and Large Eddy Simulation II*, pages 301 – 310. Kluwer Academic Publishers, 1997.

[58] K.N.C. Bray. Turbulent flows with premixed reactants in turbulent reacting flows. In P.A.L.a.F.A. Williams, editor, *Topics in applied physics*, volume 44, page 115. Springer Verlag, New York, 1980.

[59] R. Borghi. On the structure and morphology of turbulent premixed flames. *Rec. Adv. Aerosp. Sci.*, pages 117–138, 1985.

[60] R. Borghi and M. Destriau. *Combustion and flames, chemical and physical principles*. Editions TECHNIP, 1998.

[61] N. Peters. Laminar flamelet concepts in turbulent combustion. In *Twenty-First Symposium (International) on Combustion*, pages 1231–1250. The Combustion Institute Pittsburgh, 1986.

[62] H. Tennekes and J.L. Lumley. *A first course in turbulence*. M.I.T. Press, Cambridge, 1972.

[63] T. Poinsot, D. Veynante, and S. Candel. Quenching processes and premixed turbulent combustion diagrams. *J. Fluid Mech.*, 228:561–606, 1991.

[64] D. Veynante, A. Trouvé, K.N.C. Bray, and T. Mantel. Gradient and counter-gradient scalar transport in turbulent premixed flames. *J. Fluid Mech.*, 332:263 – 293, 1997.

[65] W.L. Roberts, J.F. Driscoll, M.C. Drake, and L.P. Goss. Images of the quenching of a flame by a vortex: to quantify regimes of turbulent combustion. *Combust. Flame*, 94:58–69, 1993.

[66] R. W. Bilger. The structure of turbulent non premixed flames. In *Twenty-Second Symposium (International) on Combustion*. The Combustion Institute, Pittsburgh, 1988.

[67] R. Borghi. Turbulent combustion modelling. *Prog. Energy Combust. Sci.*, 14:245–292, 1988.

[68] Y. Y. Lee. *Nonpremixed reacting flows near extinction*. PhD thesis, Cornell University, 1994.

[69] B. Cuenot and T.J. Poinsot. Effects of curvature and unsteadiness in diffusion flames, implications for turbulent diffusion combustion. In *Twenty-Fifth Symposium (International) on Combustion*. The Combustion Institute, Pittsburgh, 1994.

[70] A. Cook and J. J. Riley. Direct numerical simulation of a turbulent reactive plume on a parallel computer. *J. Comp. Phys.*, 129(2):263–283, 1996.

[71] P. A. Libby and F. A. Williams. Turbulent combustion: Fundamental aspects and a review. In P.A. Libby and F.A. Williams, editors, *Turbulent Reacting Flows*, pages 2–61. Academic Press London, 1994.

[72] B. Cuenot, F. N. Egolfopoulos, and T. Poinsot. An unsteady laminar flamelet model for nonpremixed combustion. *Combust. Theory Modelling*, 4(1):77, 2000.

[73] S. Mahalingam, J.H. Chen, and L. Vervisch. Finite-rate chemistry and transient effects in direct numerical simulations of turbulent nonpremixed flames. *Comb. and Flame*, 102(3):285–297, 1995.

[74] K. N. C. Bray. The challenge of turbulent combustion. In *Twenty-Sixth Symposium (International) on Combustion*. The Combustion Institute, Pittsburgh, 1996.

[75] F. A. Williams. Turbulent combustion. In J. D. Buckmaster, editor, *The mathematics of combustion*, pages 116–151. SIAM, 1985.

[76] A.R. Kerstein, W. Ashurst, and F.A. Williams. Field equation for interface propagation in an unsteady homogeneous flow field. *Phys. Rev. A*, 37(7):2728–2731, 1988.

[77] T. Poinsot, T. Echekki, and M.G. Mungal. A study of the laminar flame tip and implications for premixed turbulent combustion. *Combust. Sci. Technol.*, 81(1-3):45, 1991.

[78] V. Smiljanovski, V. Moser, and R. Klein. A capturing-tracking hybrid scheme for deflagration discontinuities. *Combustion Theory and Modelling*, 1(2):183 – 215, 1997.

[79] A. Bourlioux, V. Moser, and R. Klein. Large eddy simulations of turbulent premixed flames using a capturing/tracking hybrid approach. In *Sixth International Conference on Numerical Combustion*, New Orleans, Louisiana, 1996.

[80] W.-W. Kim, S. Menon, and H. C. Mongia. Large-eddy simulation of a gas turbine combustor flow. *Combust. Sci. and Technology*, 143:25–62, 1999.

[81] J. Piana, D. Veynante, S. Candel, and T. Poinsot. Direct numerical simulation analysis of the g-equation in premixed combustion. In J.P. Chollet, P.R. Voke, and L. Kleiser, editors, *Direct and Large Eddy Simulation II*, pages 321 – 330. Kluwer Academic Publishers, 1997.

[82] F. Fichot, F. Lacas, D. Veynante, and S. Candel. One-dimensional propagation of a premixed turbulent flame with a balance equation for the flame surface density. *Combust. Sci. Technol.*, 90, 1993.

[83] F.E. Marble and J.E. Broadwell. The coherent flame model of non-premixed turbulent combustion. Project Squid TRW-9-PU, Project Squid Headquarters, Chaffee Hall, Purdue University, 1977.

[84] S. Candel and T. Poinsot. Flame stretch and the balance equation for the flame area. *Combust. Sci. Technol.*, 70:1–15, 1990.

[85] S.B. Pope. The evolution of surfaces in turbulence. *Int. J. Eng. Sci.*, 26(5):445–469, 1988.

[86] L. Vervisch, E. Bidaux, K.N.C. Bray, and W. Kollmann. Surface density function in premixed turbulent combustion modeling, similarities between probability density function and flame surface approach. *Phys. Fluids A*, 7(10):2496 – 2503, 1995.

[87] E. Van Kalmthout and D. Veynante. Direct numerical simulations analysis of flame surface density models for non premixed turbulent combustion. *Phys. Fluids A*, 10(9):2347 – 2368, 1998.

[88] N. Peters. *Turbulent Combustion*. Cambridge University Press, 2000.

[89] H.G. Weller, C.J. Marooney, and A.D. Gosman. A new spectral method for calculation of the time-varying area of a laminar flame in homogeneous turbulence. In *23rd Symposium (International) on Combustion*, pages 629–636. The Combustion Institute, 1990.

[90] H.G. Weller. The development of a new flame area combustion model using conditional averaging. Thermo-Fluids Section Report TF/9307, Imperial College of Science Technology and Medicine, 1993.

[91] E. E. O'Brien. The probability density function (pdf) approach to reacting turbulent flows. In *Turbulent Reacting Flows*, page 185. Academic Press London, 1980.

[92] S. B. Pope. Pdf method for turbulent reacting flows. *Prog. Energy Combust. Sci.*, 11:119–195, 1985.

[93] W. Kollmann. The pdf approach to turbulent flow. *Theor. and Comp. Fluid Dynamics*, 1:349–285, 1990.

[94] C. Dopazo. Recent developments in pdf methods. In P.A. Libby and F.A. Williams, editors, *Turbulent Reacting Flows*, pages 375–474. Academic Press London, 1994.

[95] C. Dopazo, L. Valino, and F. Fuego. Statistical description of the turbulent mixing of scalar fields. *International Journal of Modern Physics B*, 11(25), 1997.

[96] J. Y. Chen and W. Kollmann. Pdf modeling of chemical nonequilibrium effects in turbulent nonpremixed hydrocarbon flames. In *Twenty-Second Symposium (International) on Combustion*. The Combustion Institute, Pittsburgh, 1988.

[97] M. Abramowitz and I. A. Stegun. *Handbook of Mathematical Functions*. Dover publications, Inc., 1970.

[98] D. Bradley, M. Lawes, and M. J. Scott. *Combust. Flame*, 99:581–590, 1994.

[99] T.S. Lundgren. Distribution function in the statistical theory of turbulence. *Phys. Fluids*, 10(5):969–975, 1967.

[100] S.B. Pope. Computations of turbulent combustion: progress and challenges. In *Twenty-Third Symposium (International) on Combustion*. The Combustion Institute Pittsburgh, 1990.

[101] A. Y. Klimenko. *Fluid Dynamics*, 25:327, 1990.

[102] R. W. Bilger. Conditional moment closure for turbulent reacting flow. *Phys. Fluids*, 5(2):327–334, 1993.

[103] J.-Y. Chen and W. Kollmann. Comparison of prediction and measurement in non-premixed turbulent flames. In P.A. Libby and F.A. Williams, editors, *Turbulent Reacting Flows*, pages 213–308. Academic Press London, 1994.

[104] A. Y. Klimenko and Bilger R. W. *Prog. Energ. Combust. Sci.*, 25(6):595 – 687, 1999.

[105] N. S. A. Smith. Conditional moment closure of mixing and reaction in turbulent nonpremixed combustion. In *Annual Research Briefs*, pages 85–99. CTR, Standord U., 1996.

[106] N. Swaminathan and R. W. Bilger. Assessment of combustion submodels for turbulent nonpremixed hydrocarbon flames. *Combust. Flame*, 116(4):519–545, 1999.

[107] R. Borghi. Turbulent premixed combustion : further discussions on the scales of fluctuations. *Combust. Flame*, 80:304–312, 1990.

[108] R.G. Abdel-Gayed, D. Bradley, M.N. Hamid, and M. Lawes. Lewis number effects on turbulent burning velocity. In *20th Symposium (International) on Combustion*, pages 505–512. The Combustion Institute, 1984.

[109] R.G. Abdel-Gayed and D. Bradley. Combustion regimes and the straining of turbulent premixed flames. *Combust. Flame*, 76:213–218, 1989.

[110] V. Yakhot, C.G. Orszag, S. Thangam, T.B. Gatski, and C.G. Speziale. Development of turbulence models for shear flows by a double expansion technique. *Phys. Fluids*, 4(7):1510, 1992.

[111] F.C. Gouldin. Combustion intensity and burning rate integral of premixed flames. In *Twenty-sixth Symposium (International) on Combustion*, pages 381 – 388. The Combustion Institute, 1996.

[112] H.G. Im, T.S. Lund, and J.H. Ferziger. Large eddy simulation of turbulent front propagation with dynamic subgrid models. *Phys. Fluids A*, 9(12):3826 – 3833, 1997.

[113] D.B. Spalding. Mixing and chemical reaction in steady confined turbulent flames. In *13th Symposium (International) on Combustion*, pages 649–657, Pittsburgh, 1971. The Combustion Institute, Pittsburgh.

[114] R. Said and R. Borghi. A simulation with a "cellular automaton" for turbulent combustion modelling. In *Twenty-second Symposium (International) on Combustion*, pages 569 – 577. The Combustion Institute, 1988.

[115] J. B. Moss K. N. C. Bray. A unified statistical model of the premixed turbulent flame. *Acta Astronautica*, 4:291–319, 1977.

[116] T. Mantel and R. Borghi. A new model of premixed wrinkled flame propagation based on a scalar dissipation equation. *Combust. Flame*, 96(4):443, 1994.

[117] D. Veynante, J.M. Duclos, and J. Piana. Experimental analysis of flamelet models for premixed turbulent combustion. In *Twenty-fifth Symposium (International) on Combustion*. The Combustion Institute, 1994.

[118] D. Veynante, J. Piana, J.M. Duclos, and C. Martel. Experimental analysis of flame surface density model for premixed turbulent combustion. In *Twenty-sixth Symposium (International) on Combustion*, pages 413 – 420. The Combustion Institute, 1996.

[119] J.M. Duclos. *Etude théorique et expérimentale d'une flamme turbulente stabilisée par un barreau cylindrique*. PhD thesis, Ecole Centrale Paris, 1997.

[120] C. Martel. *Etude expérimentale de la combustion turbulente prémélangée. Analyse de modèles*. PhD thesis, Ecole Centrale Paris, 1998.

[121] K.N.C. Bray, M. Champion, and P.A. Libby. The interaction between turbulence and chemistry in premixed turbulent flames. In R. Borghi and S.N. Murphy, editors, *Turbulent Reacting Flows*, volume 40 of *Lecture Notes in Engineering*, pages 541 – 563. Springer, 1989.

[122] R.S. Cant, S.B. Pope, and K.N.C. Bray. Modelling of flamelet surface to volume ratio in turbulent premixed combustion. In *23rd Symposium (International) on Combustion*, pages 809–815, Orleans, 1990. The Combustion Institute, Pittsburgh.

[123] J.M. Duclos, D. Veynante, and T. Poinsot. A comparison of flamelet models for premixed turbulent combustion. *Combust. Flame*, 95(1/2):101–118, 1993.

[124] W.K. Cheng and J.A. Diringer. Numerical modelling of si engine combustion with a flame sheet model. In S.P. 910268, editor, *International Congress and Exposition*, Detroit, 1991.

[125] C.R. Choi and K.Y. Huh. Development of a coherent flamelet model for a spark ignited turbulent premixed flame in a closed vessel. *Combust. Flame*, 114(3/4):336–348, 1998.

[126] C. Meneveau and T. Poinsot. Stretching and quenching of flamelets in premixed turbulent combustion. *Combust. Flame*, 86:311–332, 1991.

[127] P. Bailly. *Contribution à l'étude de l'interaction turbulence - combustion dans les flammes turbulentes de prémélange à l'aide de modèles du second ordre*. PhD thesis, Université de Poitiers, 21 Mars 1996 1996.

[128] P. Bailly, D. Garréton, O. Simonin, P. Bruel, M. Champion, B. Deshaies, S. Duplantier, and S. Sanquer. Experimental and numerical study of a premixed flame stabilized by a rectangular section cylinder. In *Twenty-sixth Symposium (International) on Combustion*, pages 923 – 930. The Combustion Institute, 1996.

[129] H. Lahjaily, M. Champion, D. Karmed, and P. Bruel. Introduction of dilution in the BML model: application to a stagnating turbulent flame. *Combust. Sci. Technol.*, 135:153 – 173, 1998.

[130] K. N. C. Bray, M. Champion, and P. A. Libby. Premixed flames in stagnating turbulence part iv: A new theory for the reynolds stresses and reynolds fluxes applied to impinging flows. *Combust. and Flame*, 120(1/2):1–18, 2000.

[131] P. Domingo and K.N.C. Bray. Laminar flamelet expressions for pressure fluctuation terms in second moment models of premixed turbulent combustion. *Combust. and Flame*, 121(4):555–574, 2000.

[132] F.C. Gouldin, K.N.C. Bray, and J.Y. Chen. Chemical closure model for fractal flamelets. *Combust. Flame*, 77:241–259, 1989.

[133] R.O.S. Prasad and J.P. Gore. An evaluation of flame surface density models for turbulent premixed jet flames. *Combust. Flame*, 116(1-2):1 – 14, 1999.

[134] M.D. Checkel and A. Thomas. Turbulent combustion of premixed flames in closed vessels. *Combust. Flame*, 96(4):351–370, 1994.

[135] R.O.S. Prasad, R.N. Paul, Y.R. Sivathanu, and J.P. Gore. An evaluation of combined flame surface density and mixture fraction models for nonisenthalpic premixed turbulent flames. *Combust. Flame*, 117(3):514 – 528, 1999.

[136] C. Dopazo. On conditioned averages for intermittent turbulent flows. *J. Fluid Mech.*, 81:433 – 438, 1977.

[137] A. Trouvé. The production of premixed flame surface area in turbulent shear flow. *Combust. Flame*, 99:687–696, 1994.

[138] P.A. Libby and K.N.C. Bray. Countergradient diffusion in premixed turbulent flammes. *AIAA J.*, 19:pp 205 – 213, 1981.

[139] G. Masuya and P. Libby. Non gradient theory for oblique turbulent flame with premixed reactants. *AIAA J.*, 19:205 – 213, 1981.

[140] A. Trouvé, D. Veynante, K.N.C. Bray, and T. Mantel. The coupling between flame surface dynamics and species mass conservation in premixed turbulent combustion. In Center for Turbulence Research, editor, *Proceedings of the Summer Program*, pages p. 95 – 124, Stanford, 1994. Center for turbulence Research, Stanford.

[141] C. Rutland and R. S. Cant. Turbulent transport in premixed flames. In Stanford U. CTR, editor, *Studying turbulence using numerical databases - V*, pages 75–94, 1994.

[142] P.A.M. Kalt. *Experimenal investigation of turbulent scalar flux in premixed flames*. PhD thesis, University of Sydney, 1999.

[143] H. Boughanem. *Evaluation des termes de transport et de dissipation de surface de flamme par simulation numérique directe de la combustion turbulente*. PhD thesis, University of Rouen (France), 1998.

[144] H. Boughanem and A. Trouvé. The occurence of flame instabilities in turbulent premixed combustion. In *27th Symposium International on Combustion*, 1998.

[145] R. N. Paul and K. N. C. Bray. Study of premixed turbulent combustion including landau-darrieus instability effects. In *Twenty-Sixth Symposium (International) on Combustion*, pages 259–266. The Combustion Institute, Pittsburgh, 1996.

[146] K.N.C. Bray, J.B. Moss, and P.A. Libby. Turbulent transport in premixed turbulent flames. In J. Zierep and H. Oertel, editors, *Convective Transport and Instability Phenomena*. University of Karlsuhe, Germany, 1982.

[147] D. Veynante and T. Poinsot. Effects of pressure gradients on turbulent premixed flames. *J. Fluid Mech.*, 353:83–114, 1997.

[148] P.A. Libby. Theoretical analysis of the effect of gravity on premixed turbulent flames. *Combust. Sci. Technol.*, 68:15 – 33, 1989.

[149] J.Y. Chen, J.L. Lumley, and F.C. Gouldin. Modeling of wrinkled laminar flames with intermittency and conditional statistics. In *21st Symposium (International) on Combustion*, pages 1483–1491. The Combustion Institute, Pittsburgh, 1986.

[150] M. Boger and D. Veynante. Large eddy simulations of a turbulent premixed v-shape flame. In *Eighth European Turbulence Conference*, Barcelona, Spain, 2000.

[151] M. M. Koochesfahani and P. E. Dimotakis. Mixing and chemical reactions in turbulent liquid mixing layer. *J. Fluid Mech.*, 170:83–112, 1986.

[152] P. A. McMurty, J. J. Riley, and R. W. Metcalfe. Effects of heat release on the large-scale structure in turbulent mixing layer. *J. Fluid Mech.*, 199:297–332, 1989.

[153] J. C. Hermanson and P. E. Dimotakis. Effects of heat release in turbulent, reacting shear layer. *J. Fluid Mech.*, 199:333–375, 1989.

[154] H. Pitsh, M. Chen, and N. Peters. Unsteady flamelet modeling of turbulent hydrogen-air diffusion flames. In *Twenty-Seventh Symposium (International) on Combustion*, pages 1057–1064. The Combustion Institute, Pittsburgh, 1998.

[155] N. Peters. *Prog. Energy Combustion. Sci.*, page 319, 1984.

[156] F. Ravet and L. Vervisch. Modeling non-premixed turbulent combustion in aeronautical engines using pdf-generator. In *36st Aerospace Sciences Meeting and Exhibit AIAA paper 98-1027*, Reno, NV, 1998.

[157] W. P. Jones. Turbulence modelling and numerical solution methods for variable density and combusting flows. In P.A. Libby and F.A. Williams, editors, *Turbulent Reacting Flows*, pages 309–368. Academic Press London, 1994.

[158] B. F. Magnussen and B. H. Hjertager. On the mathematical modeling of turbulent combustion with special emphasis on soot formation and combustion. In *Sixteenth Symposium (International) on Combustion*, pages 719–729. The Combustion Institute, Pittsburgh, 1976.

[159] J. H. Ferziger and M. Perić. *Computational Methods for Fluid Dynamics*. Springer, 1996.

[160] J. Coupland and C. H. Priddin. Modelling of flow and combustion in a production gas turbine combustor. In F. Durst, B.E. Launder, J.L. Lumley, F.W. Schmidt, and J.H. Whitelaw, editors, *Turbulent Shear Flows 5th*, pages 310–323. Springer Verlag, 1987.

[161] R. S. Barlow, R. W. Dibble, J. Y. Chen, and R. P. Lucht. *Combust. and Flame*, (82), 1990.

[162] C.J. Montgomery, G. Kosaly, and J.J. Riley. Direct numerical simulation of turbulent h2-o2 combustion using reduced chemistry. In AIAA Paper 93-0248, editor, *31st Aerospace Sciences Meeting and Exhibit*, pages 1–10, Reno, NV, 1993.

[163] C. J. Sun, C. J. Sung, H. Wang, and C. K. Law. On the structure of nonsooting counterflow ethylene and acetylene diffusion flames. *Combust. and Flame*, 107(4):321–335, 1996.

[164] C. J. Sung, J. B. Liu, and C. K. Law. Structural response of counterflow diffusion flames to strain rate variations. *Comb. and Flame*, 102:481–492, 1995.

[165] B. Rogg. The cambridge universal laminar flamelet computer code. In N. Peters and B. Rogg, editors, *Reduced Kinetic Mechanisms for Applications in Combustion Systems, Appendix C,*. Springer Verlag, Berlin-Heidelberg, 1993.

[166] S. P. Nandula, T. M. Brown, and R. W. Pitz. Measurements of scalar dissipation in the reaction zones of turbulent nonpremixed h_2-air flames. *Combust. Flame*, 99:775–783, 1994.

[167] E.S. Bish and W.J.A. Dahm. A strained dissipation and reaction layer formulation for turbulent diffusion flames. In *Western States Section Fall Meeting*. The Combustion Institute, Pittsburgh, 1993.

[168] J. C. Ferreira. *Flamelet modelling of stabilization in turbulent non-premixed combustion*. PhD thesis, Swiss Federal Institute of Technology (ETH) Zurich, 1996.

[169] D. C. Haworth, M. C. Drake, S. B. Pope, and R. J. Blint. The importance of time-dependent flame structures in stretched laminar flamelet models for turbulent jet diffusion flames. In *Twenty-Second Symposium (International) on Combustion*, pages 589–597. The Combustion Institute, Pittsburgh, 1988.

[170] H. Pitsch, Y. P. Wan, and N. Peters. *SAE Paper*, 952357, 1995.

[171] Y. Zhang, B. Rogg, and K.N.C. Bray. 2-d simulation of turbulent autoignition with transient laminar flamelet source term closure. *Combust. Sci. and Tech.*, 105:211–227, 1995.

[172] N. Darabiha. Transient behaviour of laminar counterflow Hydrogen-Air diffusion flames with complex chemistry. *Combust. Sci. Technol.*, 86:163–181, 1992.

[173] F. Mauss, D. Keller, and N. Peters. A lagrangian simulation of flamelet extinction and re-ignition in turbulent jet diffusion flames. In *Twenty-Third Symposium (International) on Combustion*, pages 693–698. The Combustion Institute, Pittsburgh, 1990.

[174] W. E. Mell, V. N. Nilsen, G. Kosály, and J. J. Riley. Direct numerical simulation investigation of the conditional moment closure model for nonpremixed turbulent reacting flows. *Combust. Sci. and Technology*, 91:179–186, 1991.

[175] B. Delhaye. *Etude des flammes de diffusion turbulentes. Simulations directes et modélisation*. PhD thesis, Ecole Centrale Paris, 1994.

[176] B. Delhaye, D. Veynante, and S. Candel. Simulation and modeling of reactive shear layers. *Theoretical and Computational Fluid Dynamics*, 6:67–87, 1994.

[177] C.H.H. Chang, W.J.A. Dahm, and G. Trygvason. Lagrangian model simulations of molecular mixing, including finite rate chemical reactions, in a temporally developing shear layer. *Phys. Fluid*, 3(5):1300–1311, 1991.

[178] Y. Y. Lee and S. B. Pope. Nonpremixed turbulent reacting flow near extinction. *Comb. and flame*, 101:501–528, 1995.

[179] B. Cuenot, F. N. Egolfopoulos, and T. Poinsot. An unsteady laminar flamelet model for nonpremixed combustion. *Submitted*, 1998.

[180] C. M. Müller, H. Breitbach, and N. Peters. Partially premixed turbulent flame propagation in jets flames. In *Twenty-Fifth Symposium (International) on Combustion*, pages 1099–1106. The Combustion Institute, Pittsburgh, 1994.

[181] F. Fichot, B. Delhaye, D. Veynante, and S. Candel. Strain rate modelling for a flame surface density equation with application to non-premixed turbulent combustion. In *25th Symposium (International) on Combustion*. The Combustion Institute, 1994.

[182] E. van Kalmthout, D. Veynante, and S. Candel. Direct numerical simulation analysis of flame surface density equation in non-premixed turbulent combustion. In *Twenty-Sixth Symposium (International) on Combustion*. The Combustion Institute, Pittsburgh, 1996.

[183] E. Van Kalmthout and D. Veynante. Analysis of flame surface density concepts in non-premixed turbulent combustion using direct numerical simulation. In *Eleventh Symposium on Turbulent Shear Flows*, Grenoble, France, 1997.

[184] M. Obounou, M. Gonzalez, and R. Borghi. A lagrangian model for predicting turbulent diffusion flames with chemical kinetic effects. In *Twenty-Fifth Symposium (International) on Combustion*, pages 1107–1113. The Combustion Institute, Pittsburgh, 1994.

[185] J. E. Broadwell and A. Lutz. A turbulent jet chemical reaction model: no_x production in jet flames. *Comb. and Flame*, 114, 1998.

[186] S. S. Girimaji. *Phys. Fluids*, 4:2529, 1992.

[187] N. S. A. Smith, G. R. Ruetsch, J. Oefelein, and J. H. Ferziger. Simulation and modeling of reactive particles in turbulent nonpremixed combustion. In *Studying turbulence using numerical databases - VII*, pages 39–60. CTR, Stanford U., 1998.

[188] A. R. Kerstein. A linear-eddy model for turbulent scalar transport and mixing. *Combust. Sci Tech.*, 60:391–421, 1988.

[189] R. O. Fox. The lagrangian spectral relaxation model for differential diffusion in homogeneous turbulence. *Phys. Fluids*, 11(6):1550–1571, 1999.

[190] R. O. Fox. The spectral relaxation model of the scalar dissipation rate in homogeneous turbulence. *Phys. Fluids*, 7(5):1082–1094, 1995.

[191] P. R. Van Slooten Jayesh and S. B. Pope. Advances in pdf modeling for inhomogeneous turbulent flows. *Phys. Fluids*, 10(1):246–265, 1998.

[192] L. A. Spielman and O. Levenspiel. A monte carlo treatment for reacting and coalescing dispersed phase systems. *Chemical Engineering Science*, 20:247–254, 1965.

[193] L. Valino. A field monte carlo formulation for calculating the probability density function of a single scalar in turbulent flow. *Flow, Turbulence and Combustion*, 60(2):157–172, 1998.

[194] R. O. Fox. Computational methods for turbulent reacting flows in the chemical process industry. *Revue de L'Institut Français du Pétrole*, 51(2), 1996.

[195] S. Corrsin. The isotropic turbulent mixer : Part ii. arbitrary schmidt number. *AIChE J.*, 10:870–877, 1964.

[196] C. Dopazo. *Non-isothermal turbulent reactive flows: stochastic approaches*. PhD thesis, University of New York, Stony Brook, 1973.

[197] J. Villermaux. Micromixing phenomena in stirred reactors. *Encyclopedia of Fluid Mechanics*, 707, 1986.

[198] J. Réveillon and L. Vervisch. Subgrid mixing modeling: a dynamic approach. *AIAA Journal*, 36(3):336–341, 1998.

[199] V. Eswaran and S. B. Pope. Direct numerical simulation of the turbulent mixing of a passive scalar. *Phys. Fluids*, 31(3):506–520, 1988.

[200] K. Tsai and R. O. Fox. The bmc/giem model for micromixing in non-premixed turbulent reacting flows. *Ind. Eng. Chme. Res*, 6, 1998.

[201] R. I. Curl. Dispersed phase mixing. theory and effects in simple reactors. *AIChEJ*, 175(9), 1963.

[202] W. P. Jones and M. Kakhi. Pdf modeling of finite rate chemistry effects in turbulent nonpremixed jet flames. *Combust. Flame*, 115(1/2):210–229, 1998.

[203] W. P. Jones and R. P. Lindstedt. Global reaction schemes for hydrocarbon combustion. *Combust. Flame*, 73:233–249, 1988.

[204] A.R. Masri, R.W. Bilger, and R.W. Dibble. Turbulent non-premixed flames of methane near extinction. *Comb. and Flame*, 73:261–258, 1988.

[205] C. Dopazo. Relaxation of initial probability density functions in the turbulent convection of scalar fields. *Phys. Fluids*, 22(20), 1979.

[206] J. Janicka, W. Kolbe, and W. Kollmann. Closure of the transport equation for the probability density function of turbulent scalar fields. *J. Non-Equilib. Thermodyn.*, 4(47), 1979.

[207] S. B. Pope. An improved turbulent mixing model. *Combust. Sci. and Tech.*, 28:131–135, 1982.

[208] S. B. Pope. Consistent modeling of scalars in turbulent flows. *Phys Fluids*, 26:404–408, 1982.

[209] A. Leonard and J. Hill. Direct numerical simulation of turbulent flows with chemical reaction. *J. Scientific Computing*, 3(1):25–43, 1988.

[210] R. H. Kraichnan. Closures for probability distributions. *Bull. Am. Phys. Soc.*, 34:2298, 1989.

[211] A. Dutta and J. M. Tarbell. Closure models for turbulent reacting flows. *AIChE Journal*, 35(12), 1989.

[212] F. Gao. An analytical solution for the scalar probability density function in homogeneous turbulence. *Phys. Fluids*, 3(4):511–513, 1991.

[213] L. Valino and C. Dopazo. A binomial sampling model for scalar turbulent mixing. *Physics of Fluids A*, 2(7):1204–1212, 1990.

[214] A. T. Norris and S. B. Pope. Turbulent mixing model based on ordered pairing. *Comb. and Flame*, 83:27–42, 1991.

[215] L. Valino and C. Dopazo. A binomial langevin model for turbulent mixing. *Physics of Fluids A*, 3(12):3034–3037, 1991.

[216] L. Valino, J. Ros, and C. Dopazo. Monte carlo implementation and analytic solution of an inert-scalar turbulent-mixing test problem using mapping closure. *Physics of Fluids A*, 3(9):2191–2198, 1991.

[217] S. B. Pope. Mapping closure for turbulent mixing and reaction. *Theoret. Comput. Fluid Dyncamics*, 2:255–270, 1991.

[218] F. Gao. Mapping closure and non-gaussianity of the scalar probability density functions in isotropic turbulence. *Phys. Fluids A*, 3(10):2438–2444, 1991.

[219] F. Gao and E. E. O'Brien. Joint probability density function of a scalar and its gradient in isotropic turbulence. *Phys. Fluids*, 3(6), 1991.

[220] F. Gao and E. E. O'Brien. A mapping closure for multispecies fickian diffusion. *Phys. Fluids*, 3(3), 1991.

[221] A. R. Kerstein. Linear-eddy modelling of turbulent transport, part 6. microstructure of diffusive scalar mixing fields. *J. Fluid Mech.*, 231:361–394, 1991.

[222] J.-Y. Chen and W. Kollmann. Pdf modeling and analysis of thermal no formation in turbulent nonpremixed hydrogen-air jet flames. *Combust. Flame*, 88:397–412, 1992.

[223] T.-L. Jiang, P. Givi, and F. Gao. Binary and trinary scalar mixing by fickian diffusion - some mapping closure results. *Phys. Fluids A*, 4(5):1028–1035, 1992.

[224] A. R. Kerstein. Linear-eddy modelling of turbulent transport. part 7. finite rate chemistry and multi-stream mixing. *J. Fluid Mech.*, 240:289–313, 1992.

[225] R. O. Fox. Improved fokker-planck model for the joint scalar, scalar gradient pdf. *Phys. Fluids*, 1(6):334–348, 1994.

[226] A. R. Masri, S. Subramaniam, and S. B. Pope. A mixing model to improve the pdf simulation of turbulent diffusion flames. In *Twenty-Sixth Symposium (International) on Combustion*. The Combustion Institute, Pittsburgh, 1996.

[227] R. O. Fox. On velocity-conditioned scalar mixing in homogeneous turbulence. *Phys. Fluids*, 8(10):2678–2691, 1996.

[228] R. O. Fox. On the relationship between lagrangian micromixing models and computational fluid dynamics. *Chemical Engineering and Processing*, 37:521–535, 1998.

[229] S. Subramaniam and S. B. Pope. A mixing model for turbulent reactive flows based on euclidean minimum spanning trees. *Combust. Flame*, 115(4):487–514, 1998.

[230] S. Subramaniam and S. B. Pope. Comparison of mixing model performance for nonpremixed turbulent reacting flows. *Combust. Flame*, 117(4):732–754, 1998.

[231] D. C. Haworth and S. B. Pope. A generalized langevin model for turbulent flows. *Phys. of Fluids*, 29:208–128, 1986.

[232] C. W. Gardiner. *Handbook of Stochastic Methods*. Springer, 1997.

[233] S. B. Pope. On the relationship between stochastic lagrangian models of turbulence and second-moment closures. *Phys. Fluids*, 6:973–985, 1994.

[234] H. A. Wouters, T. W. J. Peeters, and D. Roekaerts. On the existence of a stochastic lagrangian model representation for second-moment closures. *Phys. Fluids*, 8(7):1702–1704, 1996.

[235] S. B. Pope. Lagrangian pdf methods for turbulent flows. *Annu. Rev. Fluid Mech.*, 26:23, 1994.

[236] C. Fureby and C. Löfström. Large eddy simulations of bluff body stabilized flames. In *Twenty fifth Symposium (International) on Combustion*, pages 1257 – 1264. The Combustion Institute, 1994.

[237] C. Fureby and S.I. Möller. Large eddy simulations of reacting flows applied to bluff body stabilized flames. *AIAA J.*, 33(12):2339, 1995.

[238] M. Germano, A. Maffio, S. Sello, and G. Mariotti. On the extension of the dynamic modelling procedure to turbulent reacting flows. In J.P. Chollet, P.R. Voke, and L. Kleiser, editors, *Direct and Large Eddy Simulation II*, pages 291 – 300. Kluwer Academic Publishers, 1997.

[239] A.R. Kerstein, W. Ashurst, and F.A. Williams. Field equation for interface propagation in an unsteady homogeneous flow field. *Phys. Rev. A*, 37(7):2728–2731, 1988.

[240] A.R. Kerstein. Linear-Eddy modeling of turbulent transport: Part II. Application to shear layer mixing. *Combust. Flame*, 75(3 - 4):397 – 413, 1989.

[241] A.R. Kerstein. Linear-eddy modelling of turbulent transport. Part 3. Mixing and differential molecular diffusion in round jets. *J. Fluid Mech.*, 216:411 – 435, 1990.

[242] A.R. Kerstein. Linear-eddy modelling of turbulent transport. Part 6. Microstructure of diffusive scalar mixing fields. *J. Fluid Mech.*, 231:361 – 394, 1991.

[243] A.R. Kerstein. Linear eddy modeling of turbulent transport. Part 4: structure of diffusion flames. *Combust. Sci. Technol.*, 81:75 – 96, 1992.

[244] F. Gao and E.E. O'Brien. A large-eddy simulation scheme for turbulent reacting flows. *Phys. Fluids A*, 5(6):1282–1284, 1993.

[245] A.W. Cook and J.J. Riley. A subgrid model for equilibrium chemistry in turbulent flows. *Phys. Fluids A*, 6(8):2868 – 2870, 1994.

[246] A.W. Cook and J.J. Riley. Subgrid scale modeling for turbulent reacting flows. *Combust. Flame*, 112:593 – 606, 1998.

[247] P.A. McMurthy, T.C. Gansauge, A.R. Kerstein, and S.K. Krueger. Linear eddy simulations of mixing in a homogeneous turbulent flow. *Phys. Fluids A*, 5(4):1023 – 1034, 1993.

[248] P.A. McMurthy, S. Menon, and A.R. Kerstein. A subgrid mixing model for non premixed turbulent combustion. In *AIAA 30th Aerospace Science Meeting*, pages Paper 92–0234, Reno, Nevada, 1992.

[249] S. Menon, P.A. McMurthy, A.R. Kerstein, and J.Y. Chen. Prediction of NOx production in a turbulent hydrogen-air jet flame. *J. Prop. Power*, 10:161–168, 1994.

[250] W.H. Calhoon and S. Menon. Subgrid modeling for large eddy simulations. In *AIAA 34th Aerospace Science Meeting*, Reno, Nevada, 1996. AIAA Paper 96-0516.

[251] F. Mathey and J.P. Chollet. Subgrid-scale model of scalar mixing for large eddy simulation of turbulent flows. In J.P. Chollet, P.R. Voke, and L. Kleiser, editors, *Direct and Large Eddy Simulation II*, pages 103 – 114. Kluwer Academic Publishers, 1997.

[252] S. Menon and A.R. Kerstein. Stochastic simulation of the structure and propagation rate of turbulent premixed flames. In *24th Symposium (International) on Combustion*, pages 443 – 450. The Combustion Institute, Pittsburg, 1992.

[253] S. Menon, P.A. McMurthy, and A.R. Kerstein. A linear eddy mixing model for large eddy simulation of turbulent combustion. In B. Galperin and S.A. Orzag, editors, *Large eddy simulation of complex engineering and geophysical flows*, pages 87 – 314. Cambridge University Press, 1993.

[254] T. Smith and S. Menon. Model simulations of freely propagating turbulent premixed flames. In *Twenty-sixth Symposium International on Combustion*. The Combustion Institute, Pittsburgh, 1996.

[255] J. Réveillon. *Simulation dynamique des grandes structures appliquée aux flammes turbulentes non-prémélangées*. PhD thesis, Université de Rouen, 1996.

[256] J. Réveillon and L. Vervisch. Response of the dynamic LES model to heat release induced effects. *Phys. Fluids A*, 8(8):2248 – 2250, 1996.

[257] J. Réveillon and L. Vervisch. Dynamic subgrid pdf modeling for non premixed turbulent combustion. In J.P. Chollet, P.R. Voke, and L. Kleiser, editors, *Direct and Large Eddy Simulation II*, pages 311 – 320. Kluwer Academic Publishers, 1997.

[258] T.D. Butler and P.J. O'Rourke. A numerical method for two-dimensional unsteady reacting flows. In *Sixteenth Symposium (International) on Combustion*, pages 1503 – 1515. The Combustion Institute, 1977.

[259] D. Thibaut and S. Candel. Numerical study of unsteady turbulent premixed combustion: application to flashback simulation. *Combust. Flame*, 113:53 – 65, 1998.

[260] D. Veynante and T. Poinsot. Large eddy simulation of combustion instabilities in turbulent premixed burners. In *Annual Research Briefs*. Center for Turbulence Research, 1997.

[261] C. Angelberger, D. Veynante, F. Egolfopoulos, and T. Poinsot. Large eddy simulation of combustion instabilities in turbulent premixed flames. In *Proceedings of the Summer Program*, pages 61–82. Center for Turbulence Research, 1998.

[262] H.T. Im. Study of turbulent premixed flame propagation using a laminar flamelet model. In *Annual Research Briefs*, pages 347 – 360. Center for Turbulence Research, 1995.

[263] S. Menon. Large eddy simulation of combustion instabilities. In *Sixth International Conference on Numerical Combustion*, New Orleans, Louisiana, 1996.

[264] M. Boger, D. Veynante, H. Boughanem, and A. Trouvé. Direct numerical simulation analysis of flame surface density concept for large eddy simulation of turbulent premixed combustion. In *Twenty-seventh Symposium (International) on Combustion*, pages 917 – 925. The Combustion Institute, 1998.

[265] J. Piana, F. Ducros, and D. Veynante. Large eddy simulations of turbulent premixed flames based on the g-equation and a flame front wrinkling description. In *Eleventh Symposium on Turbulent Shear Flows*, Grenoble, France, 1997.

[266] J. Reveillon and L. Vervisch. Spray vaporization in non-premixed turbulent flames: a single droplet model. *Combust. Flame to appear*, 2000.

[267] C. Hollmann and E. Gutheil. Modeling of turbulent spray diffusion flames including detailed chemistry. In *Twenty-Sixth Symposium (International) on Combustion*, pages 1731–1738. The Combustion Institute, Pittsburgh, 1996.

[268] X. Calimez. *Simulation à petite échelle par une méthode VOF d'écoulement diphasiques réactifs*. PhD thesis, Ecole Centrale Paris, 1998.